UNIVERSITY "POLITEHNICA" OF TIMIŞOARA, ROMANIA
FACULTY OF ELECTRICAL ENGINEERING
DEPARTMENT OF ELECTRIC MACHINES, DRIVES,
LIGHTING AND TECHNOLOGIES

"NEW ELECTRICAL GENERATORS FOR AUTOMOBILES"

Ph. D. Thesis

by Sever SCRIDON

Supervisor: Prof. Ion BOLDEA

January 2003

CONTENT

	Page
Abstract, Acknowledgments	**I**
List of Figures	**III**
Index of Symbols	**IX**
Introduction	**1**
Résumé in Romanian Language	**3**
Chapter 1. Variable Speed Electrical Generators for Automobile Industry	
1.1.Electrical Generators in Use	**9**
1.2. New Modern Variable Speed Vehicle Generators	**12**
1.2.1. Rice-Lundell Modified Alternators (R-L MA)	**16**
1.2.2. Induction Machine as Car Generator (IM)	**19**
1.2.3. Synchronous Generator with Interior Permanent Magnets (SG-IPM)	**20**
1.2.4. Axial Flux Circumferential Current Permanent Magnet Generator (AFCC-PMG)	**24**
1.2.5. Torus and Transverse Flux Generators (TFG)	**26**
1.2.6. Switched Reluctance Generator (SRG)	**27**
1.2.7. Hybrid Generator with Variable Reluctance (HG-VR)	**27**
1.2.8. Flux Reversal Generator (FRG)	**30**
1.2.9. Double Salient Machine with Permanent Magnets (DSM-PM)	**30**
1.2.10. Dynamic Double Salient Generator with Permanent Magnets (D-DSM-PM)	**34**
1.3. Conclusion	**37**
References	**41**

Chapter 2. The two phase Switched Reluctance Generator 2P - SRG

2.1.Introduction **46**

2.2.Two Phase Topology **53**

2.3.Conceptual Design for 2P-SRG **54**

2.3.1. Electromagnetic Power and Torque **54**

2.3.2. Rotor Diameter and Stack Length **55**

2.3.3. Stator and Rotor Poles, the Air-gap **56**

2.3.4. Coil m.m.f. **57**

2.3.5. Stator Slot Sizing **58**

2.3.6. Number of Turns per Coil **58**

2.3.7. Wire Gauge **59**

2.3.8. Phase Resistance and Slot Resizing Attempt **60**

2.3.9. Stator Yoke **60**

2.3.10. Phase Flux Linkage vs. Current and Position $\lambda(i, \theta_r)$ **60**

2.3.11. Core Losses Model **62**

2.3.12. The Efficiency **64**

2.3.13. Active Materials Weight **64**

2.3.14. Simplified Thermal Verifications **65**

2.4. Sample Design Results **67**

2.5.Numerical Analysis of the Electromagnetic Field for the 2P-SRG

Through Finite Element Method (FEM) **70**

2.6. The Model for Transients **81**

2.7. A Sensor-less Control Solution **83**

2.8.Conclusion **86**

References **87**

4.3.2. Geometrical Pre-optimisation Using FEM – Analysis for the First Prototype **151**

4.3.3. BEGA - Geometrical Pre-optimisation through FEM – the Second Prototype **159**

4.4.Optimal Design - The Method **173**

4.4.1. Mathematical Formulation of the Optimization Problem **173**

4.4.2. Exploratory Moves **174**

4.4.3. Pattern Moves **174**

4.4.4. Variables, Constraints and the Objective Function **175**

4.5.Conclusion **181**

References **183**

Chapter 5. BEGA Car Generating System Simulation

5.1.Introduction **185**

5.2.Model Construction **188**

5.3.Model Implementation **190**

5.4.Simulation Results **191**

5.4.1. BEGA Generator – Steady-State Digital Simulation Results **191**

5.4.2. BEGA Generating System – Transients Digital Simulation Results **197**

5.5.Conclusion **201**

References **202**

Chapter 6. BEGA – the Prototype and Test Results

6.1.Introduction **203**

6.2.Summary of the Results for the First Prototype **204**

6.3.Tests Results for the Final Prototype **208**

6.3.1. Static Tests **210**

6.3.1.1.Resistances **210**

Chapter 3. The Flux Reversal Generator - FRG

3.1.Introduction **92**

3.2.Theory **93**

3.3.Basis Equations of the Three Phase FRG **97**

3.3.1. Air-gap Flux Density **98**

3.3.2. Stator Geometry **99**

3.3.3. Rotor Core Geometry **101**

3.3.4. Stator Electrical Parameters **103**

3.3.5. Copper and Core Losses **104**

3.3.6. Efficiency Verification **105**

3.3.7. Number of Turns per Coil **105**

3.3.8. Stator Coil Wire Gauge **106**

3.3.9. Temperatures **106**

3.3.10. Sample Design Results **108**

3.4.Three Phase FRG Geometry Pre-Optimization Using FEM-Analysis **110**

3.5.FRG Car Generating System Simulation **122**

3.6.Conclusion **131**

References **134**

Chapter 4. BEGA - A New Variable Speed Electrical Generator for Automobile Industry

4.1.Introduction **135**

4.2.Theory **136**

4.2.1. Principle of Operation **136**

4.2.2. Configuration; The First Prototype **138**

4.3. Conceptual Design **141**

4.3.1. Basic design - example **141**

6.3.1.2.Fill Factors **210**

6.3.1.3.Inductance & Resistance Measurements **211**

6.3.1.4.Standstill d-axis Tests **214**

6.3.1.5.Standstill d-axis and q-axis a.c. Tests **219**

6.3.2. Dynamic Tests **222**

6.3.2.1.Setup and the No-Load Tests **224**

6.3.2.1.1. Determination of THF **224**

6.3.2.1.2. No-Load Test With and Without Excitation Current **226**

6.3.3. Setup and the Load Tests **228**

6.3.3.1.Load Tests With Load Resistor (With and Without Excitation) **228**

6.3.3.2.Load Tests With 3 Batteries (With and Without Excitation) **232**

6.3.3.3.Load Tests With 3 Batteries and Load Resistor (With and Without Excitation) **236**

6.3.4. Generating System Tests **237**

6.3.5. Temperature Measurements **240**

6.4.Final FEM Improvements **241**

6.5.Conclusion **244**

References **246**

Chapter 7. Contribution & Conclusion

7.1.FEM of Analysis **247**

7.2.Summary **251**

7.3.Personal Contributions **253**

7.4.Future Work **255**

Thesis References **256**

Appendixes **267**

A. Publications

B. BEGA –Optimal Design - Program Listing

C. Prototype Drawings

D. Matlab™ & PSpice™ Program Listings

E. Results From the "BEGAProject.exe" Computer Program

F. Other Test Results

Abstract. Acknowledgements

The work for the present thesis started in 1997, in Timisoara, at University "Politehnica"- the Electrical Engineering Faculty, having Prof. Ion Boldea as scientific supervisor.

The first main idea was to choose a proper subject for my future research field, based on my skills, work field and knowledge. The variable speed generators being a subject with many applications, we decided to focus my future work on this subject.

Anyway, we concluded that, because of its generality, it would be proper to approach only the small electrical generators, with direct application in automobiles and aerospace industries, a field not sufficiently treated by Romanian researchers.

For the next two years I put all my efforts searching, reading and studying the literature dedicated to this subject. The tremendous number of papers and researches on this subject, the interest shown by important companies (Daimler-Chrysler, Ford, Toyota etc) and prestigious universities (like MIT, University of Berlin etc), the big number of special meetings and conferences related to this subject and at last, but not at least, the huge variety of electrical generators and power converters already proposed to be applied on cars or airplanes generating systems, made me concentrate all my efforts in order to enter deeply into this subject and searching for new solutions with simple and effective application.

Having the chance of working in a professional stimulating environment, with very well prepared researchers, Ph.D. students and electrical engineers, from the "Politehnica" University of Timisoara and Bee Speed Automatizari SRL company, and being one of the first beneficiaries of the Maxwell™ program facilities (from Ansoft Corporation), a finite element analysis program from the Electrical Engineering Faculty, gave me the strength, confidence and certitude of a well work, with good results, drawing as final result the erection of a new electrical generator, the biaxial excitation generator for automobiles (BEGA).

I express my gratitude to all my colleagues from "Politehnica" University of Timisoara and from Bee Speed Automatizari SRL, for offering me outstanding technical information and support during all these years.

Special thanks to professor Frede Blaabjerg and professor Ewen Ritchie, for their support in building the BEGA prototype and making tests using the facilities and the laboratories from the Institute of Energy Technology, from Aalborg University, Denmark.

I would like to express my gratitude to my entire family and all my friends, for understanding me and supporting me all this time and to professor Ion Boldea for giving me the chance of working under his supervision, for sharing with me his knowledge and offering me useful advices.

Sever Scridon
M. of App. Sc. in Electrical Engineering *December 2002, Timisoara, Romania*

List of figures

Chapter 1

Figure 1.1. The claw-poles generator 9
Figure 1.2. New generating system with improved efficiency, proposed in [1.54] 10
Figure 1.3. The Permanent Magnets (PM) inside claw-pole generator rotor: a) on the shaft b) on the claw-pole; c) between the claw-pole 11
Figure 1.4. Additional ferromagnetic sheet stacks and rotor permanent magnets 18
Figure 1.5. The synchronous machine with pole permanent magnets 23
Figure 1.6. The generator with disk rotor (after [1.31]) 24
Figure 1.7. The torus generator 26
Figure 1.8. The electromagnetic field from 2D-finite element analysis 28
Figure 1.9. The air-gap magnetic flux density (upper picture), magnetic flux (middle) and the cogging torque variation (down) vs. rotor position (from 2D-FEA) 29
Figure 1.10. The repartition of the electromagnetic field produced by the permanent magnets (with an excitation role), from 2D-FEA 31
Figure 1.11. The DSM-PM variation of the magnetic flux and flux density from the air-gap (from 2D-FEA) 32
Figure 1.12. The cogging torque vs. rotor position [Nmx100/u.l.] (from 2D-FEA) 32
Figure 1.13. The electromagnetic field and the magnetic flux [Wb/u.l.] on the air-gap (from 2D-FEA) 33
Figure 1.14. The magnetic flux density [Tx10^6] and the cogging torque [Nm/u.l.] in the air-gap (from 2D-FEA) 34
Figure 1.15. The distribution of the electromagnetic field produced by the permanent magnets for different rotor positions (from FEA) 34
Figure 1.16. The variation of the flux [Wb/u.l.] and flux density [Tx10^6] in the air-gap (from 2D-FEA) 35
Figure 1.17. The cogging torque [Nm/u.l.] of the D-DSM-PM vs. rotor position (from 2D-FEA) 35
Figure 1.18. The manufacturing costs for different electric machines (for 6kW power), in comparison with data from [1.38] 39

Chapter 2

Figure 2.1. The structure of a four phase Switched Reluctance generator 46
Figure 2.2. The structure of SRG for high speed operation 47
Figure 2.3. Control strategies for the switched reluctance machine, with position sensors (a) or without position sensors (b) 48
Figure 2.4. Phase flux versus current for different positions 51
Figure 2.5. The phase flux variation vs. rotor position and the phase current waveform for a switched reluctance machine [2.48] 52
Figure 2.6. Phase inductance vs. rotor position 53
Figure 2.7. The heat transmission in the stator 65
Figure 2.8. The electromagnetic field of the proposed SRG, first geometrical structure 70
Figure 2.9. The resulting phase torque [Nm/u.l.] vs. rotor position 71
Figure 2.10. The electromagnetic field of the SRG after second changes 71
Figure 2.11. The air-gap flux waveform [Wb/u.l.] 72
Figure 2.12. The air-gap magnetic flux density variation [Tx10^6] 72

Figure 2.13. The phase torque [Nm/u.l.] vs. position 72
Figure 2.14. The electromagnetic field distribution for the third geometrical structure 73
Figure 2.15. The air-gap flux waveform [Wb/u.l.] 73
Figure 2.16. The air-gap magnetic flux density variation [Tx10^6] 74
Figure 2.17. The phase torque [Nm/u.l.] vs. rotor position 74
Figure 2.18. The electromagnetic field distribution for the fourth geometrical structure 74
Figure 2.19. The air-gap flux waveform [Wb/u.l.] 75
Figure 2.20. The air-gap magnetic flux density variation [Tx10^6] 75
Figure 2.21. The phase torque [Nm/u.l.] vs. rotor position 75
Figure 2.22 The 2P-SRG grid for numerical analysis using the finite element method 76
Figure 2.23 The electromagnetic field distribution for the not-aligned poles position 77
Figure 2.24. Torque variation [Nm/u.l.] against rotor position for a machine having an over-saturated area in the stator yoke 78
Figure 2.25. Torque variation [Nm/u.l.] against rotor position for a machine without an over-saturated area 78
Figure 2.26. The fringing magnetic flux variation as function of rotor position and phase excitation current 79
Figure 2.27. Torque [Nm] vs. rotor position waveforms for different Aturns on phase coils 80
Figure 2.28. The model of the control system for a 2P-SRG 82
Figure 2.29. The basic scheme of a generating system for 14 V d.c. bus, using the 2P-SRG 83
Figure 2.30. The OULTON scheme 85

Chapter 3

Figure 3.1. Flux Reversal generator topologies: a) the existing single phase; b) the proposed one, with three phase; 92
Figure 3.2. The principle of operation of the flux reversal machine (single phase topology) 93
Figure 3.3. The phase e.m.f. wave form for a three phase generator, N_s/N_r=6/8 poles 94
Figure 3.4. Three phase Flux Reversal generator with N_s/N_r=6/8 95
Figure 3.5. The flux reversal machine: a)Stator magnetic flux, b) Back e.m.f. c) Internal angle θ_r 97
Figure 3.6. FRG's electrical equivalent circuit 98
Figure 3.7. Three phase FRG stator topology for the virtual prototype (AutoCad ™ drawing) 101
Figure 3.8. Three phase FRG rotor topology for a virtual prototype (AutoCad ™ drawing) 103
Figure 3.9. The magnetic field produced by the PM, through FEA: a) zero magnetic flux in phase A; b) maximum magnetic flux in phase A 110
Figure 3.10. The cogging torque vs. rotor position for a three phase FRG with the indicated topology 111
Figure 3.11. The magnetic flux variation through a stator pole vs. rotor position [Wb/u.l.] for a three phase FRG with the indicated topology 111
Figure 3.12. The cogging torque variation [Nm/u.l.] vs. rotor position for a three phase FRG with the geometrical topology indicated above 112
Figure 3.13. The magnetic flux variation [Wb/u.l.] vs. rotor position for a three phase FRG with the geometrical topology indicated above 112
Figure 3.14. The cogging torque vs. rotor position for a three phase FRG with the geometrical topology as indicated above 113
Figure 3.15. The magnetic flux through the stator pole vs. rotor position for a three phase FRG with the geometrical topology as indicated above 113
Figure 3.16. The cogging torque vs. rotor position [Nm/u.l.] for a three phase FRG having the following geometrical topology: stator pole width / rotor pole width = 1/3, PM thickness = 2 mm, air-gap = 0.5 mm 114
Figure 3.17. The stator pole magnetic flux vs. rotor position for a three phase FRG

having the following geometrical topology: stator pole width / rotor pole width = 1/3, PM thickness = 2 mm, air-gap = 0.5 mm 114
Figure 3.18. The new cogging torque vs. rotor position (after changes indicated above) 115
Figure 3.19. The magnetic flux through a stator pole vs. rotor position (with the geometrical changes indicated above) 115
Figure 3.20. The cogging torque variation vs. rotor position 116
Figure 3.21. The magnetic flux through stator pole vs. rotor position 116
Figure 3.22. The electromagnetic field for the aligned position of the rotor poles with the corresponding stator poles for the new PM configuration 117
Figure 3.23. The cogging torque vs. rotor position 118
Figure 3.24. The air-gap magnetic flux vs. rotor position 118
Figure 3.25. The magnetic flux density vs. rotor position 118
Figure 3.27. The electromagnetic field distribution for the new configuration 119
Figure 3.28. The air-gap magnetic flux waveform 119
Figure 3.29. The air-gap magnetic flux density waveform 120
Figure 3.30. The total cogging torque waveform for the 4 stacks of rotor sheets 121
Figure 3.31. The generating system structure 124
Figure 3.32. Phase currents at 2100 rpm, 42 V d.c., R_{load}=1.16Ω, 1.5kW 124
Figure 3.33. Phase currents and d.c. voltage (42 V d.c.) at 4000 rpm, power P=3 kW (R_{load}=0.58 Ω) 125
Figure 3.34. D.C. voltage and phase currents at 18000 rpm if R_{load} changes from 0.58 Ω to 1.16 Ω 125
Figure 3.35. Zoom of generator currents at R_{load} = 0.58 W, d.c. voltage V = 42 V, at 18000 rpm 126
Figure 3.36. The dual 42 / 14 V d.c. generating system 127
Figure 3.37. Details of the controller 127
Figure 3.38. Digital simulation results for n_b = 1800 rpm 128
Figure 3.39. Digital simulation results for n = 9000 rpm 129
Figure 3.40. Digital simulation results for n = 18000 rpm 129
Figure 3.41. Details from a 3 kW Flux Reversal Machine prototype 133

Chapter 4

Figure 4.1. Four poles rotor with multiple flux barriers filled with PM's 136
Figure 4.2. The four poles rotor topology of biaxial excitation generator 138
Figure 4.3. rotor PM magnetization 139
Figure 4.4. The phasor diagram for cos φ_1 = 1 140
Figure 4.5. The resulted stator slot opening 145
Figure 4.6. Details of the BEGAProject.exe – the design program developed for the biaxial excitation generator for automobiles 150
Figure 4.7. The first bi-dimensional geometric structure of the biaxial generator studied with help of finite element method of analysis (drawn with help of AutoCAD™) 151
Figure 4.8. The electromagnetic field produced by the permanent magnets from the rotor barriers (drawn by FEM analysis using ANSOFT™) 152
Figure 4.9. The radial air-gap magnetic flux because of PM's vs. position for u.l. 153
Figure 4.10. The air-gap magnetic flux density because of PM's vs. position 153
Figure 4.11. The air-gap magnetic flux density fundamental vs. position (from FEM analysis) 154
Figure 4.12. The cogging torque vs. position 154
Figure 4.13. The resulted air-gap flux after q axis 155
Figure 4.14. The q axis flux density 155
Figure 4.15. The q axis flux density fundamental (from FEM analysis) 155
Figure 4.16. The d axis magnetic flux [Wb/u.l.] vs. rotor position 156

Figure 4.17. The d axis magnetic flux density [T] vs. rotor position 156
Figure 4.18. The d axis magnetic flux density fundamental (after FEM analysis) 157
Figure 4.19. The electromagnetic field distribution on a d axis magnetisation (after 2D-FEM analysis) 159
Figure 4.20. The d axis magnetic flux [Wb/u.l.] vs. rotor position (after 2D-FEM analysis) 160
Figure 4.21. The d axis magnetic flux density [T] vs. rotor position (after 2D-FEM analysis) 160
Figure 4.22. The q-axis magnetic flux [Wb/u.l.] vs. rotor position (after 2D-FEM analysis) 161
Figure 4.23. The q-axis magnetic flux density [T] vs. rotor position (after 2D-FEM analysis) 161
Figure 4.24. The d-axis magnetic flux [Wb/u.l.] vs. rotor position (after 2D-FEM analysis) 162
Figure 4.25. The electromagnetic field through a new geometrical topology of BEGA (after 2D- FEM analysis) 163
Figure 4.26. The d-axis magnetic flux [Wb/u.l.] vs. rotor position (after FEM analysis) 163
Figure 4.27. The q-axis magnetic flux density [T] vs. rotor position (after 2D-FEM analysis) 164
Figure 4.28. The q-axis magnetic flux [Wb/u.l.] vs. rotor position (after 2D-FEM analysis) 164
Figure 4.29. The electromagnetic field for the new configuration of BEGA rotor (after 2D-FEM analysis) 165
Figure 4.30. The d-axis magnetic flux [Wb/u.l.] vs. rotor position (after 2D-FEM analysis) 165
Figure 4.31. The q-axis magnetic flux density [T] vs. rotor position (after 2D-FEM analysis) 166
Figure 4.32. The rotor of the second prototype of BEGA 167
Figure 4.33. The electromagnetic field for the second prototype of BEGA (after 2D-FEM analysis) 168
Figure 4.34. The air-gap PM magnetic flux [Wb/u.l.] vs. rotor position (FEM analysis) 168
Figure 4.35. The air-gap PM magnetic flux density [T] vs. rotor position (FEM analysis) 169
Figure 4.36. The air-gap d-axis magnetic flux [Wb/u.l.] vs. rotor position (FEM analysis) 169
Figure 4.37. The air-gap d-axis magnetic flux density [T] vs. rotor position (FEM analysis) 169
Figure 4.38. The air-gap q-axis magnetic flux [Wb/u.l.] vs. rotor position (FEM analysis) 170
Figure 4.39. The air-gap q-axis magnetic flux density [T] vs. rotor position (FEM analysis) 170
Figure 4.40. The air-gap q-axis magnetic flux [Wb/u.l.] vs. rotor position (FEM analysis) 171
Figure 4.41. The air-gap q-axis magnetic flux density [T] vs. rotor position (FEM analysis) 171
Figure 4.42. The electromagnetic field for q-axis situation on two situations: for one sense of the windings current and then for the opposite sense of the current while keeping the same values (FEM analysis) 172
Figure 4.43. The criterions for the optimal design of the biaxial excitation generator, using the BEGAProject.exe computer program 177
Figure 4.44. The help menu for the BEGAProject.exe computer program to design the biaxial excitation generator 177
Figure 4.45. The evolution of the main parameters during the optimisation process using the BEGAProject.exe computer program (following the maximum efficiency) 179
Figure 4.46. The evolution of the main parameters during the optimisation process using the BEGAProject.exe computer program (following the minimum weight) 180

Chapter 5

Figure 5.1. The low cost regulation of the biaxial excitation generator for automobiles 190
Figure 5.2. Simulation results for: Stator flux (λ_s) vs. power; d axis current (i_d) vs. power; q axis current (i_q) vs. power; Excitation current (i_F) vs. power (where: 1-50Hz; 2-100Hz; 3-300Hz) 191

Figure 5.3. The no-load digital simulation results for the BEGA generator 192
Figure 5.4. The short-circuit digital simulation results for the BEGA generator 193
Figure 5.5. The external characteristics, digital simulation results for the BEGA generator 194
Figure 5.6. The electromagnetic torque vs. stator phase current, digital simulation results for the BEGA generator 195
Figure 5.7. The output power vs. phase current, digital simulation results for the BEGA Generator 196
Figure 5.8. Batteries and resistor load voltage at 9000 rpm, 42 V d.c., R_{load}=1Ω 197
Figure 5.9. Batteries and resistor load current at 9000 rpm, 42 V d.c., R_{load}=1Ω 198
Figure 5.10. Phase current at 9000 rpm, 42 V d.c., R_{load}=1Ω 198
Figure 5.11. Transients when adding the load resistor at 3000 rpm, 42 V d.c., R_{load}=0.7Ω, field current I_f = 1.5A 199
Figure 5.12. Details of the transients during the add of the load resistor at 3000 rpm, 42V d.c., R_{load}=0.7Ω 199
Figure 5.13. Transients when adding the load resistor at 3000 rpm, 42 V d.c., R_{load}=0.7Ω, the field current is I_f= 3A 200
Figure 5.14. Transients for adding the load resistor at 9000 rpm, 42 V d.c., R_{load}=0.7Ω, the field current is I_f= 1.5A 201

Chapter 6

Figure 6.1. Details of the first prototype of BEGA 205
Fig. 6.2. The induced voltage vs. speed for different excitation currents 206
Fig. 6.3. The *d* axis and *q* axis inductances vs. current 207
Fig. 6.4. The short-circuit current vs. speed for 0A and 1.9A excitation currents 208
Figure 6.5. Details of the final prototype of BEGA 209
Figure 6.6. Other details of the rotor of BEGA final prototype (with PM's only - left image and together with field coils – right image) 210
Figure 6.7. Details of the main setup for testing of the generating system 210
Figure 6.8. Details of the LCR meter during tests 212
Figure 6.9. The direct axis inductance versus frequency 213
Figure 6.10. Direct axis resistance versus frequency 213
Figure 6.11. The quadrature axis inductance versus frequency 214
Figure 6.12. Quadrature axis resistance versus frequency 214
Figure 6.13. Details of the setup during d.c. decay tests 215
Figure 6.14. The scheme of the setup for the d axis d.c. decay tests 216
Figure 6.15. The measured current (left side) and the offset (right side) for the d-aligned position 217
Figure 6.16. The measured current (yellow) and the calculated one (red) for different times of the tests 217
Figure 6.17. The final two d-aligned d.c. decay test with the measured current (yellow/light color) and the calculated one (red/dark color), the current initial value: 2.9A 218
Figure 6.18. The d.c. decay test with the measured current, the field current has a value of 1.3A, the stator windings are opened 218
Figure 6.19. The d-aligned d.c. decay test with the measured current (yellow/light color) and the calculated one (red/dark color), the field current has a value of (-1.3)A 219
Figure 6.20. The d-aligned d.c. decay test with the measured current (yellow/light color) and the calculated one (red/dark color), the field current has a value of (+1.3)A 219
Figure 6.21. The q-aligned a.c. test with the i_q measured current waveform (M) and the field current waveform (3) 220
Figure 6.22. The results for the d-axis a.c. test, the stator (M) and the field current (3)

Waveforms 221
Figure 6.23. Details from the setup used for standstill a.c. tests using the California Instruments a.c. power source of 5kVA 222
Figure 6.24. Details from the running tests for the final prototype of BEGA 223
Figure 6.25. Details from the setup used for running tests 225
Figure 6.26. The scheme of the setup used for dynamic tests 226
Figure 6.27. The e.m.f. and the FFT for 1000rpm and 4000rpm wit zero excitation current 227
Figure 6.28. The e.m.f. vs. speed for different field currents 228
Figure 6.29. The load current (2) and line voltage (1) for 1000 rpm, no excitation current 229
Figure 6.30. The load current (2) and line voltage (1) for 3000 rpm, no excitation current 230
Figure 6.31. The load current (2) and line voltage (1) for 6000 rpm, no excitation current 230
Figure 6.32. The load current (2) and line voltage (1) for 8000 rpm, no excitation current 231
Figure 6.33. The load current (2) and line voltage (1) for 1500 rpm, 1,5A the field current 231
Figure 6.34. The load current vs. speed for different values of the field current, for rectifier plus resistive load (0.7Ω) 232
Figure 6.35. The load voltage vs. load current, for different values of the field current 232
Figure 6.36. The load current (2) and line voltage (1) for 6000 rpm, no field current 233
Figure 6.37. The load current (2) and line voltage (1) for 3000 rpm, 1,5A the field current 233
Figure 6.38. The load current (2) and line voltage (1) for 39 rpm, 2A the field current 234
Figure 6.39. The load current (2) and line voltage (1) for 7000 rpm, 2,5A the field current 234
Figure 6.40. The load current (2) and line voltage (1) for 3000 rpm, 3A the field current 235
Figure 6.41. The load current (2) and line voltage (1) for 6000 rpm, 3A the field current 235
Figure 6.42. The load current vs. speed for different field current values 236
Figure 6.43. The load (battery) voltage vs. load current for different field current values 236
Figure 6.44. The load current (4) load voltage (5) and the current through the load resistor (6) for 6000 rpm generator speed, 2A - the field current (7) 237
Figure 6.45. Starting the charging process of the three batteries at 3000 rpm, excitation current 2,5A (left image) and sudden disconnection of the batteries (right image): batteries load current (4 - green) and voltage (5 - turquoise), field current (7 - red) 238
Figure 6.46. Introducing the load resistance (of 0,7Ω) during the charging process of the three batteries, at 3000 rpm, excitation current 2,5A (left image) and sudden disconnection of the resistance (right image): batteries load current (4 - green) and voltage (5 - turquoise), field current (7 - red), resistance current(6 - blue) 239
Figure 6.47. Charging start of the three batteries at 6000 rpm, excitation current 2,5A: batteries load current (4 - green) and voltage (5 - purple), field current (7 - red) 239
Figure 6.48. Charging of the three batteries at 3000 rpm, excitation current 1,7A and sudden change of the field current sign: batteries load current (2 - blue) and voltage (1 - green), field current (3 - red) 240
Figure 6.49. Charging of the three batteries at 3000 rpm, excitation current 3A and sudden change of the field current sign: batteries load current (4 - blue) and voltage (6 – green), field current (5 - red) 240
Figure 6.50. Charging of the three batteries at 3000 rpm, excitation current -3A and sudden change of the field current sign: batteries load current (4 - blue) and voltage (6 – cyan), field current (5 - red) 241
Figure 6.51. The electromagnetic field for the new configuration of the BEGA 242
Figure 6.52. The magnetic flux (left) and flux density (right) waveforms for the new configuration of the BEGA on d-axis 243
Figure 6.53. The q-axis magnetic flux (left) and flux density (right) waveforms for $I_q>0$ and $I_d=0$ 243

Index of Symbols

2D-FEA	two dimension finite element analysis
2P-SRG	two phase - switched reluctance generator
a	exponent that describes how fast the cost increases with increasing the diameter
A, A`	stator coil areas
A_s	stator external area
a.c.	alternate currrent
A_{co}	copper area
ANSOFT™	digital simulation software using the finite element method of analysis
A_{slot}	slot area
AutoCad ™	designing Cad software
A_W	area of the rotor slot opening
A_{wire}	wire cross-section
β	between-poles interval
B	magnetic flux density
b_{cr}	rotor pole width
b_{cs}	stator back iron thickness
B_{cs}	average flux density in the rotor back core
BEGA	biaxial excitation generator for automobiles
B_{g0}	air-gap magnetic flux density for no load operation
B_{gF} (B_{g1})	air-gap flux density
B_{gPM}	air-gap flux from the premanent magnets
B_{gs}	saturated value for the local (pole shoe) flux density
B_i	amplitude of flux density variation.
BLDCM	machine
B_m	flux density
B_n	normal component of the magnetic flux
B_{PM}	radial flux density
B_{PMg}	permanent magnet to air-gap flux density
B_{pr}	space average flux density in the rotor poles
B_{ps}	pole flux density
B_r	remanent flux density
B_{rpm}, B_{spm}	rotor (stator) pole flux density
B_{rym}, B_{sym}	rotor (stator) yoke flux density
b_s	slot and wire insulation thickness
B_s	stator back iron flux density
b_{s1}	stator slot base width
b_{s2}	stator slot top width
B_t	tangential component of the magnetic flux density
C_{act}	cost of active parts
c_{Cu}	cost of copper
C_e	eddy current coefficient (Steinmetz formula)
C_f	filtering capacitor
c_{Fe}	cost of back iron

C_h	hysteresis current coefficient (Steinmetz formula)
c_{pm}	cost of permanent magnets
CPRG	claw-pole rotor generators
c_{struct}	cost of a reference structure
C_{struct}	structure costs
C_{tot}	total costs
δ	machine internal angle
d	the direct axis of the electrical machine
D_o	external rotor diameter
d.c.	direct current
d_{co}	wire gauge
d_{cos}	stator coil conductor diameter
D-DSM-PM	dynamic double salient machine with permanent magnets
D_e	stator external diameter
d_F	field coil conductor diameter
D_i	stator bore diameter
d_{os}	stator outer diameter
D_{pe}	external pole diameter
d-q	d and q axes reference
D_r	rotor outer diameter
d_{ref}	reference diameter
D_{shaft}	rotor shaft diameter
D_{se}	external stator diameter
E	electromotive force (e.m.f.)
$e_{a,b,c}(t)$	phase e.m.f.
E_1 (E_{01})	phase e.m.f. - fundamental
E_3	phase e.m.f. - third harmonic
E_e	eddy current function (Steinmetz formula)
E_h	hysteresiy function (Steinmetz formula)
F	objective function
$\vec{F}$	force vector
f_0 f_n f_r	rated tangential force
FEA	Finite Element Analysis
FEM	Finite Element Method
FFT	Fast Fourier Transformed
fig.	figure
FRG	flux reversal generator
FRM	flux reversal machine
f_x	tangential specific force on the rotor surface;
γ_{co}	copper
$\gamma_{core}(\gamma_{iron})$	iron
g	air-gap
G_i	constraint function
H_o	coercive force
h_c	stator pole height
h_{cs}	stator yoke height
hfbt	ratio between the flux barrier thickness and the air-gap
h_m	radial height of the PM
h_{pm}	permanent magnet height

h_{pr}	rotor pole height
h_{ps}	stator pole height
h_{pso}, h_{ps1}	stator pole heights
h_{su}	useful slot (pole) height
h_{tps}	top stator pole height
h_{yr}	rotor yoke heitght
i	electrical current
I_0	output current
$i_{a,b,c}$	phase current
$I_{1,2,3}$	controllers output currents
IAS	Industry Automation Society
I_b	base current
I_d (i_d, I_{d0})	direct axis current
I_D	diode current
ID	bore diameter
I_{dc}	d.c. bus rated current
I_{dcmin} (I_{dcm})	d.c. current at n_{min}
Ie (i_f, I_f)	excitation current
IEEE	Institute of Electrical and Electronic Engineers
IGBT	Insulate Gate Bipolar Tranzistor
$I_{L1,L2}$	line current
$I_{Lf1,Lf2}$	filtering inductance current
IM	induction machine
i_{max}	maximum current
I_n (i_n, I_r, I_{rated})	rated current
I_{nmin}	electrical current for minimum speed
I_{peak}	peak current
IPM	interior permanent magnets
i_q	q-axis current
I_{qr} (I_{qrated})	q-axis rated current
I_s	load current
I_{sc}	short-circuit current
J	inertia moment
j_{co}	current density
j_{cob}	base current density
j_{cod}	design current density
j_{cof}	field current density:
j_{cos}	stator rated current density
K	set of constraints (secondary parameters)
K_σ (K_{fringe})	fringing factor
$K_{\sigma min}$	minimum fringing factor
K_1	coefficient, depends on the core material and on lamination thickness.
K_c	Carter coefficient
K_{dm}	d-axis magnetizing coefficient
K_{fill}	slot-filling factor
k_{fill}	global filling factor
K_i	ratio between peak current and RMS current
K_t	ratio of even three between the peak and the average torque value
K_r	resultant coefficient
K_s	global magnetic saturation factor

K_V	voltage coefficient
K_{W1} K_W	coiling coefficient
Λ	permeance
Λ_{ec}	end connection specific permeance
Λ_s	slot specific permeance
λ	flux
λ_a (λ_b)	phase a (phase b) flux
λ_d	d-axis flux
λ_{max}	maximum flux
λ_n	the share factor for the frequency corresponding to the n – order harmonic.
λ_{PM}	real max. PM flux
λ_{Pmi}	ideal max. phase flux
λ_{PMq}	PM magnetic flux across q axis.
λ_q	q-axis flux
λ_s	stator flux
L	stack length
L_A	phase A inductance
L_B	phase B inductance
l_c (l_{coil})	coil length
l_{cF}	field coil length
LCR	LCR meter
l_{cs}	stator turn length
L_d	d-axis inductance
L_{dm}	d-axis magnetizing inductance
L/D_r	the stack length per rotor diameter ratio
Ld,q	d (q) axis inductance
l_{ec}	coil ends length
L_f	filtering inductance
L_F	field total inductance
L_l	leakage inductance
Lm	magnetic inductance
L_{mf}	mutual inductance
L_q	q-axis inductance
l_s	stator length
L_s	stator phase inductance
L_{sl}	stator stack length
L_{stack}	the stack length.
L_u	phase inductance (useful inductance)
L_{ua}	un-aligned phase inductance value
L_{uag}	linkage inductance air-gap component
L_{ual}	leakage inductance (self-inductance)
l_{wc}	stator coil length
L_{wel}	stator length
l_{wi}	slot lower length
μ_0	absolute permeability
μ_{rec}	relative permeability
m	phase number
max.	maximal

m.m.f.	magneto-motive force
m_{rec}	relative permeability
M_r	rated electromagnetic torque
η_b	base efficiency
η_{el}	total electrical efficiency
η_{min}	efficiency for idle speed operation
η_n	rated efficiency
n	rotor speed
n_b	base speed
N	number of turns
N_c	number of turns/coil
N_cI_n	rated Ampere-turns
N_cI_{peak}	peak Ampere-turns
NdFeB	Neodymium-Iron-Borom
n_{max}	maximal generator speed
n_{min}	idle speed
Nr	rotor poles
Ns	stator poles
ω	speed
ω_b	base speed
ω_r (Ω_r)	rotor speed
OD	outer diameter
φ_l	machine angle
p	pole number
P	number of pole pairs;
P_a	d.c. link power
P_b	base power
p_{co}	copper losses
p_{cof}	field coil dissipated power
p_{cop}	copper losses per pole
p_{copper}	copper losses
p_{core} (p_{fe})	core loss
p_{cos}	stator coil rated losses
p_{diode}	diode losses
P_e	electromagnetic power
P_{elm}	electromagnetic power (average value)
PEC	power electronics converter
p_{iron}	core (iron) losses.
pL_s	reactance
PM	permanent magnets
p_{mec}	mechanical losses
P_n	nominal power
P_{out}	output power
p_{rpe}	rotor pole eddy current losses
p_{rph}	rotor pole hysteresis losses
p_{rye}	rotor yoke eddy current losses
p_{spe}	stator pole eddy current losses
p_{sph}	stator pole hysteresis losses
PSpice™	digital simulation software

p_{sye}	stator yoke eddy current losses
p_{syh}	stator yoke hysteresis losses
p_{ryh}	rotor yoke hysteresis losses
PWM	pulse width modulation
q	the q axis of the electrical machine
q	number of paths
ρ_{co}	the copper resistivity
R_c	Resistance fig 4.4
r_{co}	copper resistivity
R_D	diode equivalent resistance
R_F (R_f)	field coil resistance
R_{load} (r_s)	load resistance
r.m.s.	root main square
rpm	rotation per minute
R_q	quadrature axis resistance
R_s	stator phase resistance
S_0	single power switch for voltage control
$S_{1,2}$	switches
SPM	surface permanent magnets
SRG	switching reluctance generator
SRM	switching reluctance machine
θ	angle
θ_0	zero torque position
θ_{ca}	over-temperature of the stator core with respect to surrounding air
θ_{co}	main temperature gradients conductor to iron through the insulation
$\Delta\theta_{co}$	temperature difference
θ_{coa}	main temperature gradients cooling air to the ambient
θ_{cos}	main temperature gradients iron to the cooling air
θ_{er}	rotor position
θ_p	pole angle
θ_r	the geometrical angle.
θ_s	Temperature
θ_u	conducting (useful) angle
t	time
τ	tangential force
τ (τ_p)	polar shoe
τ_{load}	load torque
τ_{ref}	reference torque
τ_s	stator pole span
τ_s	slot pitch
τ_{total}	total torque
T_e	electrical time constant
T_{ek}	critical electromagnetic torque
T_{elm}	electromagnetic torque
THF	telephonic harmonic factor
T_{peak}	peak torque
T_{ua}	electrical time constant for unaligned position
U/f control	voltage per frequency control
u.l.	unit of length

v	virtual displacement factor
V	volume
V	measured output voltage of the generator
V_0	rectifier output voltage
$V_{1,2}$	switches
V_1	voltage, for $\cos\varphi_1=1$
V_{12}	difference voltage
V_a (V_b, V_c)	phase a (b, c) voltage
V_{dc}	d.c. voltage
V_D	diode residual voltage
V'_n	value of the n - order harmonic;
VRM	variable reluctance machine
vs.	versus
ψ_q	zero magnetic flux in q axis
W_1	number of turns for one path
W_c	number of turns in slot opening
W_{coil}	coil thickness
W_{Cu}	weight of copper
W_{Fe}	weight of active iron
W_{copper}	copper weight
W_{cr}	rotor back core weight
W_{cs}	stator back core weight
W_F	number of field turns
W_{lam}	lamination weight
W_p	pole width
W_{pm}	weight of permanent magnets
W_{ps}	stator pole weight
W_{pr}	rotor pole weight
W_{rpt}	total rotor pole weight
W_{ry}	rotor yoke weight
W_{ryt}	total rotor yoke weight
W_{so}	stator slot opening
W_{s0}	slot opening
W_{s1}	slot width, interior
W_{s2}	slot width, exterior
W_{spt}	total stator pole weight
W_{sp}	stator pole weight
$W_{statiron}$	stator iron weight
W_{sy}	stator yoke weight
W_{syt}	total stator yoke weight
W_t	stator tooth (pole) width
W_{ts}	the pole width
X	a vector of N real variables (primary parameters)
X_d	synchronous reactance
X_d	direct axis reactance
X_d',X_d''	direct axis transient and sub transient reactance
$X^{(K-1)}$	previous base point;
$X^{(K)}$	current base point;
$X^{(K+1)}$	pattern point, the point obtained after the pattern move.
$X^{(K+2)}$	new pattern point

X_q	quadrature axis reactance
y	the coil opening
Y	star connection
Z_b	base impedance

INTRODUCTION

In today's vehicles, the combustion engine directly drives many of accessories. When the engine is cut off, during driving, also these accessories stop to operate. But systems like power steering, vacuum brake or air conditioning compressor must be available permanently. So it is mandatory to find alternatives to power these components.

One possibility is to power those electrically; this allows an operation of the accessories independently of engine or vehicle speed following their real demands. The components can always operate with best efficiency. But electrical operation of the accessories also increases the demand for electrical power in the vehicle.

As is already known, a substantial part of the energy consumption is caused by the operation of accessories like fuel pump, water pump, oil pump, power steering pump, air conditioning compressor and alternator which are estimated to cause up to 24% of the fuel consumption of today's vehicles. Increasing the efficiency of permanently operating accessories reduces their part of the total fuel consumption.

To ensure a sufficient charging balance, engine-driven alternator has to produce this increased average during vehicle running time and the batteries for the vehicle operation time. An increased power demand for the alternator by a factor of about 4 compared to today's design is required, as long as no additional consumers are introduced.

Anyway, additional electrical safety (like on-board diagnosis systems) and comfort reasons (air conditioning) consumers are expected to be introduced.

Improving alternators efficiency will allow producing more electric power with limited increase of the engine load and with minimal increase of their weight.

Today's 14 V electrical systems are not able to cover the demands of these consumers, which often exceeds 50 or 100 A. For this, 42 V electrical power generation and distribution systems are on their way to replace the existing 14 V systems in automobiles.

A 42 V power system would allow at least some of the functions provided now by propulsion engine, through a variety of belts and chain drives, to be driven by independent

electric motors. Eliminating the need for belts and pulleys would bring some benefits in terms of saving space and simpler mechanical design. The real gain would be the greater overall efficiency in terms of energy efficiency a good example is to provide steering assistance with an electric motor that operates only as and when required.

Considering the maximum rated power of today's alternators: 2 kW with an efficiency of 55%, and the expected increase of electric power demand, a mechanical power of 5.5 kW would be necessary to generate an electrical power of 3 kW, alternator losses would reach 2.5 kW, unacceptable from both commercial viability and technical solution points of view.

The 12 V lead-acid batteries accept the 14 V output of the generator as its charging voltage. Multiplied by three, a battery of 36 V needs a power rail voltage of 42 V if it is to be charged close to 100% of its capacity.

To sum up: 14 V / 42 V is the working voltage of the electrical network (engine/generator running); 12 V / 36 V is the unloaded average battery voltage (engine/generator off).

There is also the possible scenario of local zero emission zones within city entries or environmentally sensitive areas, a hybrid vehicle with its relatively small traction batteries will be able to traverse them only in an electric mode.

This subject of hybrid vehicles is introduced only as a remark for actual research subject trends in automobiles industry and it will be not treated here.

A synthesis regarding electrical generators already integrated in automotive generator system and batteries charging, together with the new electrical generator and generating system topologies proposed or under studies, constitute the ground of the present dissertation.

Finding new prototypes and designing new low cost generator types and low voltage regulation generating system, in order, to improve the efficiency of the actual car generating systems are the main declared scopes.

Résumé in Romanian Language

Generatoarele electrice care să funcționeze eficient în aplicațiile cu turație de antrenare variabilă, prezintă un interes deosebit în planul cercetării la nivel mondial, pornind de la cele de mică şi medie putere, cu aplicații directe în industria automobilelor, cea aerospațială sau cea a computerelor dar şi în cea energetică (mori de vânt în locuri izolate, sisteme generatoare autonome etc) şi continuând cu cele de mare putere, întâlnite indeosebi în majoritatea aplicațiilor din industia energetică.

Interesul manifestat față de acest tip de generatoare electrice se datorează în special din punct de vedere tehnic: al creşterii randamentului acestora la funcționarea în plaje de turații tot mai mari, simplificarea părții mecanice - de antrenare, cât şi din punct de vedere economic, respectiv: reducerea costurilor întregului sistem de generare a energiei electrice, obținerea de energie electrică la un preț mai scăzut etc.

Funcționarea eficientă a acestora, pe domenii de turații cât mai extinse implică însă şi utilizarea electronicii de putere, în diferite topologii, care duce însă la o mărire a prețului de ansamblu a sistemului de generare.

Industria automobilelor constituie una dintre marile utilizatoare de generatoare electrice de mică - medie putere, tendințele actuale impunând găsirea de noi soluții viabile care să ducă în final la un consum mai mic de combustibil şi la o reducere cât mai mare a noxelor eliminate prin arderea combustibililor, cu efecte negative asupra mediului înconjurător.

După cum este deja cunoscut, o parte substanțială din consumul de energie la automobile, este cauzat de funcționarea unor accesorii cum sunt: pompa de injecție, pompa de apă, pompa hidraulică, sistemele de frânare, compresorul pentru aer condiționat, alternatorul; care duc la un consum cumulat de circa 24% din consumul total de combustibil la un automobil modern.

Creşterea eficienței accesoriilor aflate în regim de funcționare permanentă, reduce partea acestora din consumul de combustibil însă creşterea continuă a numărului acestora în cadrul întregului sistem ce dotează automobilele moderne, cu scopul declarat de a spori gradul de securitate al pasagerilor dar şi confortul acestora în timpul călătoriilor, nu rezolvă decât parțial reducerea consumului de combustibil necesar producerii de energie electrică.

Astfel, pentru asigurarea unei balanțe energetice optime, la încărcarea bateriei acumulatoare, alternatorul (generatorul) trebuie să producă energie electrică mai multă pe durata de funcționare a sistemului de antrenare a acestuia decât este consumată în timpul în care energia necesară bunei funcționări a sistemelor electrice din dotare este preluată doar din bateria acumulatoare.

Sistemul electric de 14V c.c. din prezent, nu este capabil să acopere eficient cererea de energie din partea consumatorilor existenți la bordul autovehiculelor, din acest motiv, un sistem de generare – distribuire la 42 V c.c. este propus a fi utilizat. Mai mult, în cazul în care este necesară o funcționare a autovehiculului cu emisie de gaze zero, de exemplu în centrul unor localități, dotarea cu motoare electrice pentru tracțiune este obligatorie, deci utilizarea unui sistem de generare/distribuție de putere mai mare decât cel existent se impune.

Generatoarele utilizate in aplicatii de acest gen trebuie sa functioneze avand o sursa de putere mecanica instabila, care variaza cu turatia la care este angrenat generatorul si trebuie sa genereze energia electrica produsa pe un sistem izolat

„Generatoare electrice noi pentru automobile" - rezumat

Prezenta lucrare este structurată pe şapte capitole principale, fiecare având o parte finală de concluzii, din care un capitol teoretic - în care este prezentat pe scurt modul de aplicare al metodei elementului finit (MEF) pentru analiza câmpului electromagnetic şi propuneri privind posibilitatea de continuare a activităţii de cercetare în subiectul generatoarelor electrice cu funcţionare la turaţie variabilă.

Capitolul I – structurat în trei părţi – cuprinde o analiză sintetică, din punct de vedere constructiv, al randamentului, dar şi al costurilor, asupra celor mai cunoscute tipuri de generatoare electrice existente sau propuse pentru aplicaţiile din industria automobilelor.

Prima parte introduce noile tipuri de generatoare electrice utilizate în industria automobilelor, în speţă generatorul cu poli ghiară şi propune un mod simplu de calcul al costurilor aferente unei structuri de generator, ţinând cont de dimensiunile geometrice şi materialele componente. Partea a doua include o analiză, prin metoda elementului finit, pentru o serie de generatoare în scopul evidenţierii unelor mărimi caracteristice ale acestora, comparând aceste noi topologii cu avantajele şi dezavantajele care le prezintă atât pentru maşina electrică în sine cât şi pentru electronica de putere şi metodele de control aferente. Astăzi, înainte de a include o maşină electrică într-un sistem, studii şi analize, în special utilizând MEF, sunt asteptate şi uşor de implementat. Partea a treia este destinată discuţiilor şi concluziilor.

Capitolul II – transpune maşina pas cu pas de putere într-o variantă mai simplă, propusă ca generator în industria automobilelor.

Tinând cont atât de avantajele cât şi de dezavantajele maşinii pas cu pas (dublu reluctantă) de putere, utilizarea acesteia pe scară tot mai largă, inclusiv în cadrul automobilelor hibride existente deja pe piaţa mondială, a făcut necesară includerea ei ca studiu în cadrul prezentei teze de doctorat.

Capitolul III – este dedicat în întregime studiului asupra maşinii cu reversare de flux, recent prezentata şi propusă ca un candidat serios pentru postul de generator electric cu aplicaţie directă în sistemele de generare a energiei la bordul autovehiculelor. Pornind de la proiectarea conceptuală a acesteia, continuând cu analize prin metaoda elementului finit

(MEF) şi terminând cu simulări digitale pentru întreg sistemul de generare, inclusiv electronica de putere şi partea de control, capitolul III descrie într-un mod concis, practic modalitatea de desfăşurare a următoarelor trei capitole din teza de doctorat, anticipând paşii ce vor fi urmaţi în acest sens.

Capitolul IV – introduce în premieră un nou tip de maşină electrică sincronă, cu excitaţie biaxială, concepută pentru a substitui cu succes actualele alternatoare. Un model de proiectare analitic, împreună cu mai multe studii efectuate prin metoda elementului finit şi un procedeu de proiectare optimizată – cu rezultate directe privind realizarea unui prototip de 3 kW, sunt componentele de bază pentru noul tip de generator electric

Capitolul V – prezintă simulări extinse pentru un sistem de generare – distribuţie de 42 V c.c. care are în componenţă un generator BEGA.

Capitolul VI – include rezultatele obţinute pentru o serie de măsurători făcute pentru a dovedi eficacitatea utilizării generatorului BEGA în aplicaţiile specifice industriei automobilelor. Sunt prezentate atât rezultate ale testelor efectuate pe acest tip de maşină dar şi pentru întreg sistemul de generare a energiei electrice pe noul sistem de 42 V c.c. propus spre aplicare.

Capitolul VII – are un conţinut teoretic, prezentând, pe scurt, modul de utilizare a MEF în calculul anumitor mărimi electromagnetice, cu aplicare directă în studiul maşinilor electrice. De asemenea sunt incluse şi contribuţiile personale ale autorului alături de unele perspective şi propunerea de activităţi viitoare care să continue studiul în cadrul acestui vast domeniu de cercetare.

Contribuții personale

Fiecare capitol al prezentei lucrări conține contribuții originale, astfel:

© utilizarea analizei bi-dimensionale, prin MEF, pentru efectuarea de comparații simple, cu efecte directe, pentru diferite tipuri de mașini electrice;

© propunerea de aplicare a unor formule simple de calcul al costurilor;

© prezentarea unei structuri bifazate, cu cost redus, a unei mașini pas cu pas (dublu reluctante) de putere, pornind de la o mașină de inducție la care sunt modificate înfașurările statorice și respectiv rotorul;

© utilizarea analizei prin metoda elementului finit (MEF) pentru a putea trage unele concluzii asupra unei structuri geometrice optime a mașinii pas cu pas de putere propuse spre studiu;

© proiectarea, pe baza unor relații simplificate, a unei mașini pas cu pas de putere cu aplicație directă în funcționarea ca generator în industria auto;

© introducerea a două noi tipuri de generatoare electrice cu preț redus: – generatorul cu reversare de flux – prezentat doar teoretic și, în premieră mondială – generatorul cu excitație biaxială – prezentat prin două prototipuri realizate la scară;

© proiectarea unui prototip virtual al generatorului cu reversare de flux, utilizând o serie de formule de bază, caracteristice mașinilor electrice cu magneți permanenți;

© propunerea și simularea a doua sisteme de generare a energiei electrice ce pot fi utilizate în industria automobilelor, unul dual – cu două magistrale de tensiune diferită, 14 V c.c. și 42 V c.c. – și unul pentru o magistrală de 42 V c.c.;

© efectuarea de analize cu MEF pentru a îmbunătăți cuplul pulsatoriu, caracteristic mașinilor electrice cu magneți permanenți;

© prezentarea metodei de proiectare conceptuală a generatorului cu excitație biaxială pentru automobile (BEGA) și propunerea unei metode de optimizare eficiente în proiectarea finală a acestuia;

© efectuarea de simulări pentru regimurile statice şi dinamice pentru un sistem ce include noul tip de generator, BEGA şi prezentarea rezultatelor acestor simulări;

© realizarea a două prototipuri la scară reală şi supunerea evaluării experimentale, unul dintre ele fiind optimizat şi studiat în detaliu.

© principalele contribuţii aduse în aceasta lucrare au fost publicate, astfel:

- I.Boldea, S. Scridon, L. Tutelea: *"BEGA – a biaxial excitation generator for automobiles"* – Conferinţa Internaţională "OPTIM 2000", Brasov, Romania, May 2000;

- Boldea, S. Scridon, L. Tutelea, C. Lascu, N. Muntean - *"The flux reversal machine (FRM) as an automotive alternator with 42/14 v d.c. dual output"* - Conferinţa Internaţională "OPTIM 2000", Brasov, Romania, May 2000;

- I. Boldea, E. Ritchie, F. Blaabjerg, S. Scridon, L. Tutelea – *"Characterization Of Biaxial Excitation Generator For Automobile"*- Conferinţa Internaţională "OPTIM 2002", Brasov, Romania, May 2002.

CHAPTER I

VARIABLE SPEED ELECTRICAL GENERATORS FOR AUTOMOBILE INDUSTRY

1.1. Electrical Generators in Use

Electric machines used in automobile applications usually are custom made in accordance with guidelines for: frame size, costs, quantities, noise, lifetime and ambient conditions.

The synchronous electrical machines have shown a lot of advantages so by their geometry and also by their reliability in working in good conditions at variable speeds. From those, the claw-pole machine is mostly used as electrical power generator in the automobiles industry to supply the electrical and electronic equipment from those and to charge the power batteries too.

The claw-pole generator is an electric machine with radial flux which has the stator build with two electrical phase having rotor poles of claw type, shifted with a pole pitch and the rotor is robust, hetero-poles magnetized through continuous current windings or with permanent magnets (figure 1.1).

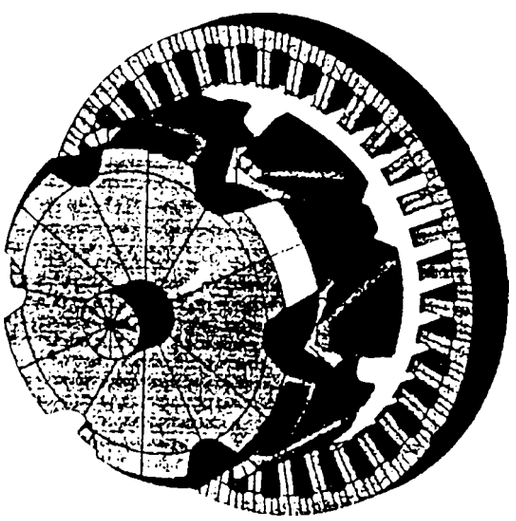

Figure 1.1. The claw-poles generator (after [1.4])

Through the phase excitation, thanks to the rotor motion, electric alternating voltage will be induced in the stator windings, and through the use of a diode rectifier it will be transformed into direct voltage for the supply of the existing consumers from the vehicle dashboard and for charging the power batteries.

A generator of such a type with a rectifier, is generally composed of: a stator stack of sheets with a three-phase winding together with a rotor and slip rings, collecting brushes and claw poles, an excitation winding, a rectifying bridge with diodes, a voltage regulator (chopper) with transistor (for the hybrid technique - with permanent magnets), a shield for the motor and of the slip rings, an iron sheet fan. [1.4]

The a.c. voltage produced in the stator windings is rectified and the output voltage will be kept constant through the excitation current regulator on a speed range of 1:10. [1.5]

At the claw pole generator, the mechanical limits were already reached (given by the centrifugal forces at high speed and the efficiency limits caused by the eddy current losses from the claw poles, made of massive iron, and the stator teeth tighter with the excitation losses. The principal advantage of the excitation of claw-pole (known also as Lundell type of generator) alternator is the generation of a big magnetic poled field with just one field coil. [1.7]

New generating systems with improved output power efficiency, using the claw-pole generators, were already proposed (fig.1.2). The improvement is provided for low speed with help of an additional active rectifier, synchronized with the alternator and for high speed by changing the number of turns of the stator winding, realized by taping the winding and using two rectifiers and two switches. [1.54]

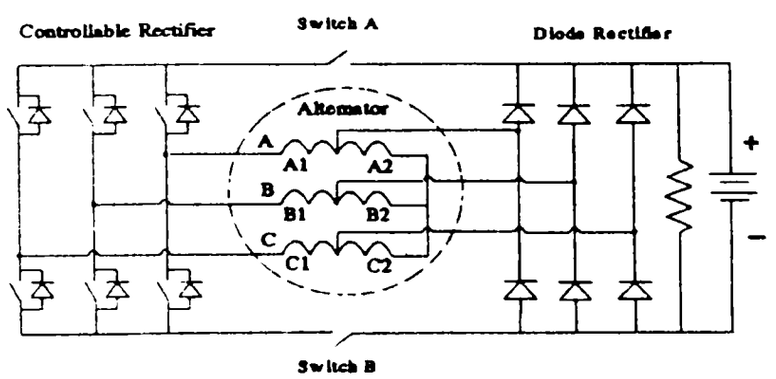

Figure 1.2. New generating system with improved efficiency, proposed in [1.54]

The system efficiency is in this way increased by 21% (from 47% to 57%) but the cost associated with the semiconductors switches is a serious issue, which has to be considered.

So, new types of variable speed generators have been proposed, a part of these new modern generators designed to operate efficiently at variable speed will be presented and briefly compared in what follows.

1.2. New Modern Variable Speed Vehicle Generators

The efficiency of the classic generators with claw poles tends to be reduced up to 60% at maximal speed and charge.

The aspects which has to be taken into consideration for increasing the efficiency of the generator systems which equip the vehicles in the automotive industry are:

- The excitation - to prolong their life time, the high speed generators should have the field without collecting brushes (for example with permanent magnets - to reduce the rotor losses - but which needs power electronic devices to regulate the given voltage on the storage battery);
- The rotor - because of the high centrifugal forces that appear at high speeds, the generators should be even with longer rotor, with a radial magnetic field, or with a disc rotor with axial magnetic field. The space limits show us an advantage for disc rotor generators.
- The stator - using a stator with small slots, to reduce the losses into the stator iron;
- The cooling unit - the cooling method of the generator: with air or with liquid (for wide speed range);
- The acceleration energy - the mass of the generator must be linearly accelerated with the vehicle while the rotor must be rotationally accelerated, according with the speed of the internal combustion engine that equips the vehicle.

Taking all formerly mentioned aspects into account there were proposed measurements to increase the discharged power of a classic alternator (with claw-poles) by attaching (clueing) permanent magnets on the rotor, using controlled power rectifier [1.6] or through the use of a double rotor topology.

Those solutions have not solved the efficiency problems and neither system dynamic behave for consumer voltage recovery.

It is, however, difficult to compare the generator types based on data given in the papers since the generators are designed for different specifications, using different methods and since all data are not present.

Anyway, as it will be presented in what follows, using the finite element method and effective cost comparison formulas, simple comparisons between different types of electrical generators can be done to have a perspective image for those.

The goal of this chapter is to investigate part of those electrical generators, especially the new types and drawing out the advantages and disadvantages of various generators based on cost and torque densities comparisons.

Comparing the total cost of the different alternatives we can choose the generator system for automobiles. The total cost includes more than the cost of purchasing or manufacturing the generator. It includes both direct costs and indirect costs.

Some of the costs are:

- Material costs (direct);
- Manufacturing costs (direct);
- Cost of maintenance (indirect);
- Cost of availability (indirect).

The material and manufacturing cost of the active part of the generator is estimated from the weights of the active materials. The cost of the supporting structure is determined from the diameter and length of the generator structure and the cost of the losses is calculated from the average losses of the system. Because the maintenance required for a generator is very limited, the cost of maintenance is neglected.

Moreover, the cost of the availability is neglected since the availability is assumed to be very close to 100% for all generator systems.

Apart from the total cost of the generator system, a comparison can include other aspects that cannot be easily be economically evaluated. For instance the noise of the generator can

be crucial tot the acceptance of the system. Such aspects have not been included in this study.

The cost of the active parts of the generator is based on the assumption that the cost of both, the material and the manufacturing can be expressed as a specific cost per weight of the different materials. The cost of the active parts is:

$$C_{act} = c_{Cu} W_{Cu} + c_{Fe} W_{Fe} + c_{pm} W_{pm} \quad (1.1)$$

Where W_{Cu}, W_{Fe}, W_{pm} are the weight of the copper, the active iron and respectively of the permanent magnets. The specific costs of the different materials (c_{Cu}, c_{Fe}) and c_{pm} are given in table 1.1.

The cost of the structures has not been detailed analyzed in this dissertation. Only an appropriate model is used, without any mechanical details, it is evident that the amount of material used and the difficulty in manufacturing the structure of the generator increase as the diameter and length increase.

The structural cost is a function of the stator outer diameter, d_{os}, and stator length, l_s, including the end windings.

In this chapter, the cost of the structure is simplified because for the comparison analysis, the 2D-FEA is used. So, the stator length is considered being the same for all types of generators. So, the structure costs approximated as:

$$C_{struct} = c_{struct} \left(\frac{d_{os}}{d_{ref}} \right)^a \quad (1.2)$$

Where: c_{struct} – the cost of a reference structure with the diameter d_{ref};

a – the exponent that describes how fast the cost increases with increasing the diameter (a=2);

Of course, this model is only approximate. The real cost function will be much more complicated and include terms which depend on both the diameter and length as well as terms which are functions of other variables than the outer dimensions.

The total cost function used in this chapter includes the cost of the active parts and the cost of the structure:

$$C_{tot} = C_{act} + C_{struct} \tag{1.3}$$

Table 1.1. The cost function parameters and their nominal values

Cost parameter		Nominal value
Cost of copper	c_{Cu}	4 EURO/kg
Cost of iron	c_{Fe}	3 EURO/kg
Cost of permanent magnets	c_{pm}	100 EURO/kg (NdFeB) 15 EURO/kg (Ferrite)
Reference diameter	d_{ref}	0.8 m
Structure exponent	a	2
Cost of reference structure	c_{struct}	550 EURO

The torque density of a machine can be defined as the rated electromagnetic torque divided by the machine volume:

$$\tau = \frac{T_{elm}}{V}, \tag{1.4}$$

where:

$$T_{elm} = Ni\frac{\partial \varphi}{\partial \theta} \tag{1.5}$$

So, it is clear that the torque density is related to the machine operating current (Ampere-turns). When evaluating a machine's torque producing capability, excluding external factors, it will be meaningful to eliminate the influence of the current.

1.2.1 Rice-Lundell Modified Alternators (R-L MA)

To use the claw-pole generator for a large speed bandwidth, field-weakening domain, with effective conditions, some constructive changes were made, the result is known as the Rice-Lundell modified alternator. [1.6]

This new alternator has the rotor split in two parts, a magnetic one and a non-magnetic second part.

The magnetic part consists in two claw poles separated with a non-magnetic material, which fill the space between poles creating a barrier to prevent pole flux trespassing the space from one claw pole to the next one (from the other pole), without crossing the stator core.

The toroidal field coils from stator are placed coaxially with the shaft, fixed on the motor cage (making together a solid magnetic circuit), where the currents are passing the same direction through rotor longitudinal axis.

The cage, stator core and coils are as usual for a synchronous machine, main flux path being three-dimensional.

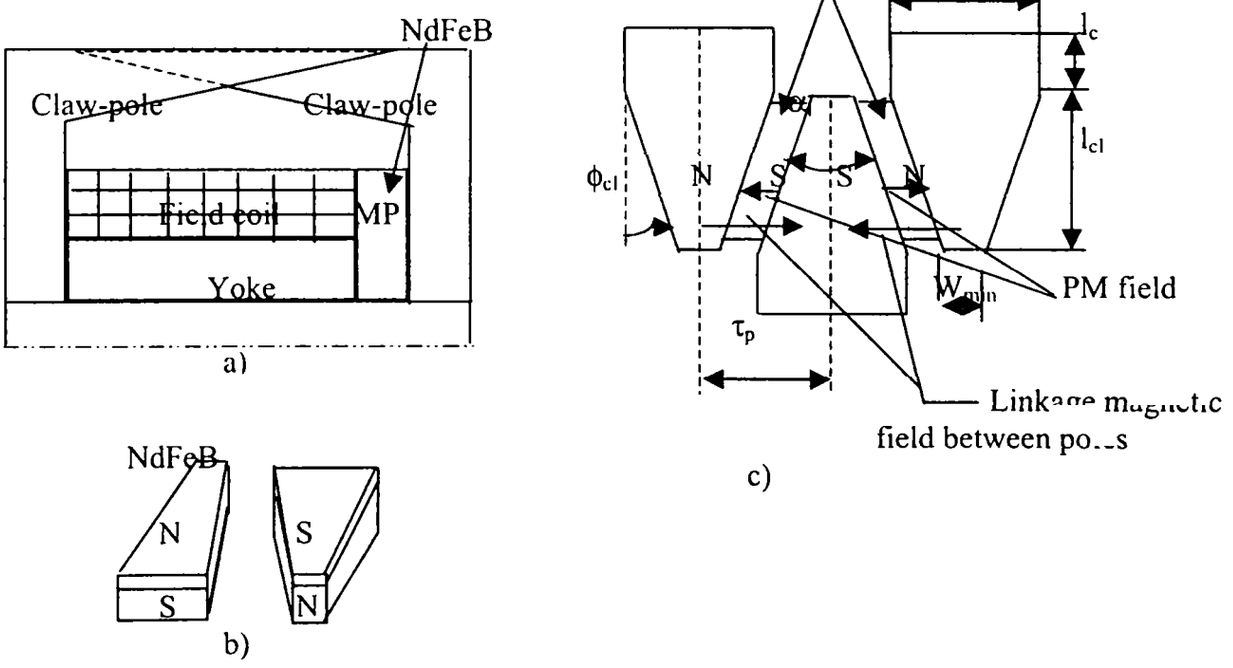

Figure 1.3. The Permanent Magnets (PM) inside claw-pole generator: a) on the shaft; b) on the claw-pole; c) between the claw-poles.

The permanent magnets are placed in different configurations [1.5] (as shown in the previous figure):

- on the rotor shaft of the generator (at one side of the field coil);

- on claw-pole surface, with a radial magnetization;

- between the claw-poles.

Adding of permanent magnets in the rotor to provide a better useful flux and to decrease fringing flux, some changes on the excitation system were made.

One of the variants consists in the placement of the permanent magnets in a ring form, which are axially magnetized, in the rotor between the rotor iron and the flywheel with claw poles. The effect is the appearance of a magnetization for low speed operation, when the excitation winding is not supplied sufficiently through the battery (if the battery is not charged), but the effect decreases in the same time with the excitation of the rotor coil.

A new variant is based on the fact that if the magnets should be placed so near as it can be by the stator air-gap, a higher flux should be induced into the stator windings, therefore the magnet placement between the rotor poles with this end in view, could reach the increase of the main flux in low speed operation, without the coil excitation in the rotor.

The third variant is based on the decrease of the magnetic leakage flux between the rotor poles, which increases in the same time with the reach of the saturation level, thus, the permanent magnets are placed between the claw poles to force the leakage flux to return into the poles and to transform it into an useful flux which is necessary to induce the voltage in the stator windings. [1.8]

All three solutions lead to an increase of the output current at a constant voltage, for all the speed range, solution c), with PM of ferrite placed between the poles (to reduce the leakage flux and thus the main flux from the air-gap to be increase), had produced the highest increase in current at idle speed (or a decrease of the speed from 940 rpm to 815 rpm) and an increase with 20% of the output power for all the range of speed. [1.5]

But, from thermal and mechanical points of view, the fixing of the magnets between the claw poles is not an efficient solution. Anyway a standard controller can be used to prevent significant rising of the no-load voltage appearance.

Another way to improve the output power is through the elongation of the stator sheet packet, extending the claw poles at the ends and introducing the PM's at the ends, by increasing a little the air-gap, also on all the rotor length (figure 1.4).

The enlargement of the sheet pack length is justified just if a substantial increase of the output power is obtained and if the efficiency is higher for a large gamut of speeds, anyway we have to take into account the space limitations.

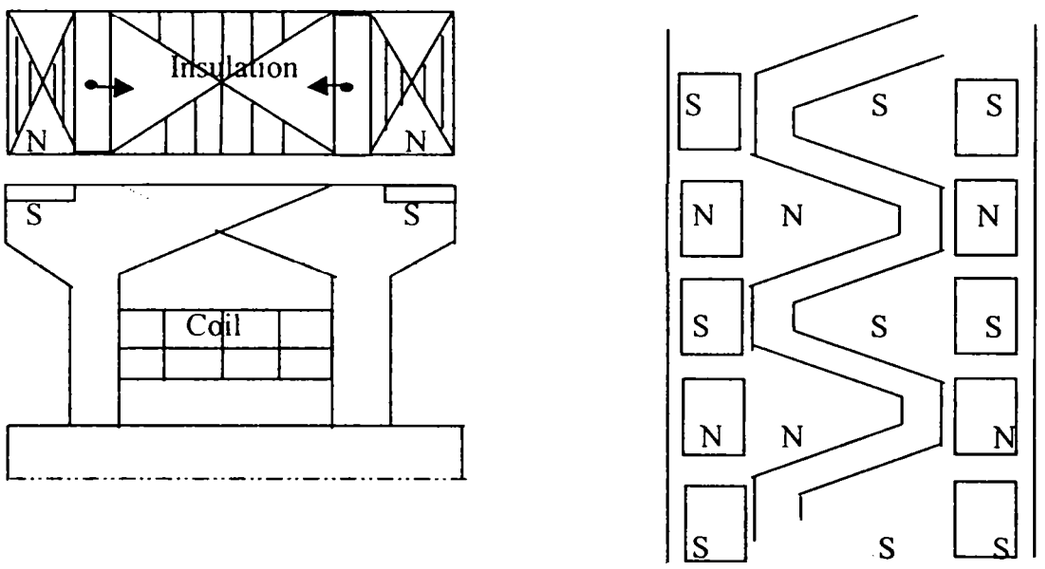

Figure 1.4. Additional ferromagnetic sheet stacks and rotor permanent magnets

The increase of the air-gap will reduce the losses through eddy current from the stator claw poles in the same time as the harmonics of the e.m.f. voltage will be reduced (for a given winding and a field current); the no-load voltage and the number of turns remain the same (including the thickness of the winding wire).

The machine reactance will be lower (because the air-gap is higher in presence of PM's) thus the output current will increase.

For high speeds, the reducing of the field current could be interesting, thus, the losses in the stator iron and those through the turbulent currents from the rotor claw poles are significantly reduced.

To avoid the over-voltage, at small loads and high operating speeds, it should be necessary to produce a negative excitation current. This can be done with the help of a four quadrant chopper.

An increase of the output power of the generators seems a good solution if it is made with low costs but this solution must be demonstrated practically.

Other variants of the Lundell alternator were studied and applied to increase their discharged power. Thus, because the speed at which the alternators are running can be reduced, they will have to assure an output voltage at these speeds, too. The variants with magnets placed between the poles are efficient but hard to realize because of the mechanical problems regarding their fastening and because of the fact that at high speeds the induced voltages cannot be reduced.

Considering the standard Lundell generator as a base for the cost comparison, we will have for the above modified structures a cost increase of about 10% because of the PM's insertions plus another 10% for the manufacturing process and of course other 30% for the power electronic cost (if a 4 quadrant chopper is needed).

1.2.2. Induction Machine as Car Generator (IM)

Mainly used in power generating systems, the induction generator has two different topologies:

- Induction generator with squirrel cage rotor, very popular due its rotor mechanical simplicity.

The main drawback of the squirrel cage induction generator is the overheating and torque pulsation when it runs at low speeds but which can be handled using a proper power converter (with negative effect on the entire system cost).

- Induction generator with wounded rotor, used especially for constant speed solution. The output power of the generator can be controlled and optimized, solutions of this kind were already proposed.

Here, the disadvantage is represented by the wounded rotor, which implies more production costs and can affect the machine lifetime, depending on the operating conditions. Anyway, a good solution for variable speed operation is using slip/rated power converter, which is placed in the rotor of the electrical generator.

Induction machines have a relatively high power density, are durable and require little maintenance (especially for squirrel cage induction generator).

It has been shown that using different sizes for the induction generator, the efficiency of a starter-generator system is changing and so a system using a larger machine is more effective. [1.47] This means, of course, a higher direct cost of the system but with positive effect on system reliability and a reduce of the indirect costs.

The induction generator remains a solid solution for automobiles generating system, many models and simulations being already done. [1.40, 1.46]

A 75,3% efficiency at 4kW load for idle speed, which is about 20 percentile points more than the current production Lundell machine based system has been proved and the system efficiency increases to 85% from 2000rpm to 3000rpm and decreases to 76% at maximum speed of 6000rpm. [1.48]

1.2.3. Synchronous Generator with Interior Permanent Magnets (SG-IPM)

In contrast to the asynchronous machine, the synchronous generator is much more expensive. The rotor comprises the pole shoes, the poles lying beneath and the exciter windings. The stator consists of the stator core and a.c. windings. Higher frictional losses, brush and slip ring erosion and higher maintenance costs, are serious drawbacks for the synchronous generators.

Synchronous generators can be either electrically excited or excited by permanent magnets. The question of which type of excitation is the best is determined mainly by comparing the cost of the permanent magnets with the total cost of the rotor pole, the field winding and the field winding losses.

The cost and the losses of an electrically excited generator depend on the pole pitch. A simplified way of showing this is to look into the required field current at no-load operation.

The m.m.f. required of the field pole is determined by the required air-gap flux density and the magnetic air-gap. The m.m.f. required for the iron has been neglected. For the electrically excited generator, the magnetic air-gap is the distance between the pole shoe and the stator teeth.

Even when the pole pitch is reduced, the no-load m.m.f. required of each pole remains the same for given air-gap flux density, although there is less room for the field winding. To allow constant no-load field m.m.f., the field pole radial height has to be larger as the pole pitch is decreased.

Permanent magnets are expensive but they eliminate the excitation losses and allow smaller pole pitches to be used than electrical excitation does. The pole pitch of a generator with permanent magnets can be very small. It is only limited by the leakage flux between the magnets.

Just as for the electrically excited generator, the no-load m.m.f. required of the magnet does not depend on the pole pitch. The m.m.f. produced by a permanent magnet is the magnet height times the coercive force of the permanent magnet material.

Therefore, the magnet height can be constant as the pole pitch decreases. For electrically excited generators the magnetic air-gap is small and as a consequence, the armature reaction will be important if the pole pitch is large.

For rotors with surface-mounted permanent magnets, the magnetic air-gap is much larger since the permeability of the permanent magnets is almost equal to that of air. So, the armature reaction is much smaller for a permanent magnet generator with surface magnets than in electrically excited generators.

Even though the permanent magnets are very expensive, the losses of the field winding make the permanent magnet excitation better than electrical excitation for small pole pitches. Besides, by reducing the losses, the permanent magnets lead to a lighter design.

The induction generators are electrically excited, too, but in contrast to the electrically excited synchronous generators, the magnetizing current flows in the stator winding.

The induction generator has the same problem as the pole pitch is reduced.

The magnetizing m.m.f. is constant, but as the pole pitch is reduced a larger part of the stator current will be needed to magnetize the air-gap.

This effect causes the power factor to decrease as the pole pitch decreases. Another reason why the induction generator cannot be made with a small pole pitch even if the air-gap can be made small is that the stator winding should be made with at least two slots per pole and phase to keep the space harmonics of the air-gap flux-wave low.

With a large constructive and configuration variety, the synchronous machines with interior Permanent Magnets are used as generators, basically for small and medium power.

In permanent magnet generators, the magnetization can either be achieved by the magnets directly on the rotor surface or by magnets inside the rotor.

The magnets on the rotor surface have to have a remanent flux density higher than the required air-gap flux density, so, it is necessary to use expensive magnets, like Neodymium-Iron-Boron (NbFeB), with a remanent flux density of 1.2T, or Samarium-Cobalt (SmCo) with a remanent flux density of 1.3T.

If the air-gap flux density has to be close to remanent flux density, the amount of permanent magnets will be large.

Anyway, surface-mounted magnets lead to a very simple rotor design with a low weight and from the costs point of view an advantage can be observed (gluing the PM's on the rotor surface is cheaper than manufacturing a wounded rotor with slip rings and brushes).

The PM synchronous machine geometrical structure looks similar to the classical synchronous machine structure, figure 1.5.

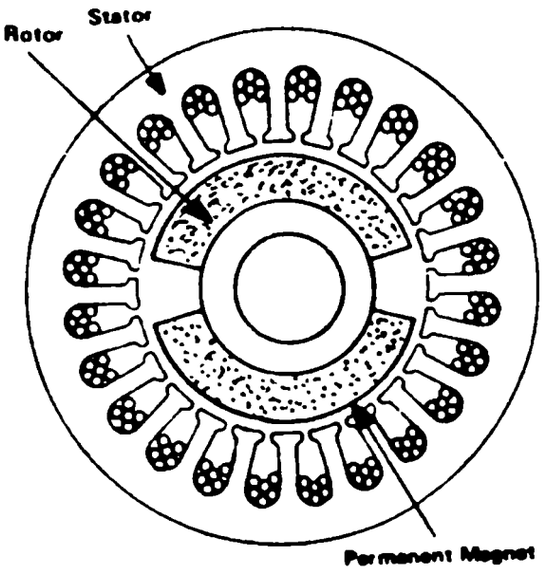

Figure 1.5. The synchronous machine with pole permanent magnets

The stator is composed of a sheet stack with slots in with the multi-phase stator windings are placed. The rotor has placed permanent magnets that have to excite the machine. The magnet placement in the rotor is realized in two variants, generally looking to optimize the rotor structure from the weight and costs point of view.

Thus the magnets can be placed between the poles, in this case the magnetic reluctance after d axis is smaller than that from q axis, or they can be polar placed, in this case the magnetic reluctance is considered same on both axes. [1.2]

An efficient rotor should have to maximize the flux density in the air-gap and to minimize the magnetic leakage between the magnets, to contribute at the energy conversion process. [1.3, 1.49]

Flux concentration can be used to utilize cheap low-energy permanent magnets and still obtain high air-gap flux density. [1.61]

The magnets are then placed inside the rotor and the flux is guided through magnetic circuits that are narrower at the air-gap than to the magnets. A common low-energy magnet material is ferrite that has a remanent flux density of about 0.4T.

A more complicated rotor is required for flux concentration than for surface mounted and it would also normally be heavier, while the cost for magnets can be much lower than for

surface mounted magnets, but considering the enlargement for the speed range operation it might be good advantage. Today, NdFeB magnets cost about 8 times more than ferrite magnets and their maximum magnetic energy product is about 10 times higher than it is for ferrite.

1.2.4. Axial-Flux Circumferential Current Permanent Magnet Generator (AFCC-PMG)

In parallel with different studies made to achieve maximum power density for the traditional claw-pole generators, a new solution regarding a new alternator solution with permanent magnets in rotor and axially air-gap has been proposed (IEEE-IAS 1994), it works at high speed (3kW, 3000 – 30,000 rpm) and solve partially the energetic efficiency problems but still the demagnetisation effect of permanent magnets, together with rotor large inertia moment are a real problem. [1.31]

So, to avoid the use of sleep rings that are necessary for field coils, the excitation has been moved on the stator.

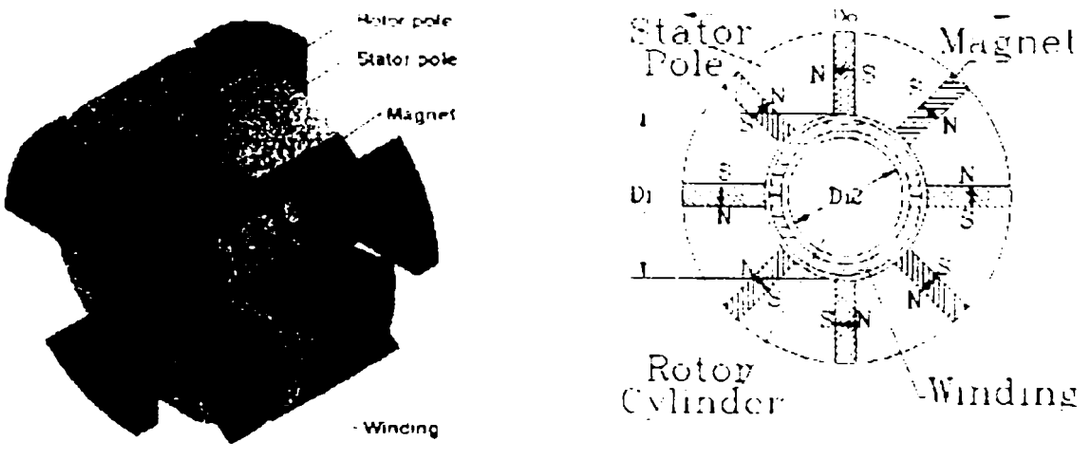

Figure 1.6. The electrical generator with disk rotor (after [1.31])

This new solution of generator system with high efficiency is given by a synchronous generator with excitation with permanent magnets with a high magnetic energy and disk rotor, together with a chopper with IGBT's.

As shown in figure 1.6, the stator of this type of an electrical generator is with prominent ferromagnetic poles with permanent magnets and with a circumferential winding, the rotor being compound of two prominent parts placed in the exterior. The main magnetic flux is provided by two neighboring permanent magnets having axially orientation and passing through the air-gap, the rotor pole and yoke.

The stator winding designed in this way, leads to the reduction of the losses at the coil ends. The rotor rotation provokes the production of a coupling flux through a winding that is periodically reversed to generate an induced electromotor voltage.

Axial-flux generators can be designed in a way similar to radial-flux machines. One important restriction for axial-flux machines is that the amount of windings in the air-gap is limited by the available space at the inner diameter. [1.50]

The air-gap at larger radius cannot be fully utilized because of this and the utilization of the iron core and magnets is slightly less efficient in axial-flux machines than in radial-flux machines. While for the radial-flux machines, the length of the stator and the air-gap diameter can be made with a small diameter by using a long stator, to reduce the diameter of the axial-flux machine, while keeping the rated torque constant, the difference between the inner and outer diameter has to be increased. The maximum torque of an axial-flux machine is achieved when the inner diameter is about 0.6 times the outer diameter. [1.51]

A smaller inner diameter will only decrease the rated torque, so, the diameter of the axial-flux machines cannot be reduced as much as for the radial-flux machines. One way of avoiding a large diameter is to stack a number of axial-flux machines with a small diameter on the same shaft, thus, the rated power can be increased without increasing the diameter but it will increase the price, too.

Another disadvantage of this type of generator, beside the large inertia moment is the torque ripple. If the axial-flux machine is made with a double-sided stator, the need for a rotor yoke as a return path for the flux will be eliminated.

Subsequently, the active weight of the generator can be reduced. Nevertheless, the rotor has to be made of magnetic powders to handle, without considerable losses, the three dimensional a.c. field occurring from stator during motion. A more complex non-magnetic stator structure has to be used instead to hold the magnets.

The double-sided stator also allows the winding to be divided into two, half as thick parts. In a radial-flux machine an equivalent electromagnetic design can be achieved by doubling the stator length instead of using two stator halves. Such a solution will lead to a lower amount of end windings than the double-sided stator.

If the machine length is not restricted, the axial-flux machine with a double-sided stator will not be better than a radial-flux one, with a long stator, from an electromagnetic point of view. Three dimensional distribution of the magnetic main flux impose a careful pole core structure cutting, which implies, beside permanent magnets cost, high manufacturing costs.

1.2.5. Torus and Transversal Flux Generators (TFG)

A special type of axial-flux generator is the toroidal stator machine (figure 1.7). Beside the above-mentioned advantages and disadvantages, the toroidal stator winding leads to simple end windings but it becomes more difficult to fix the stator to the generator structure.

This new solution is a synchronous generator with field winding and PM, having a disc rotor. The main disadvantages of the axial flux generator are it's manufacture difficulty and it's high inertia.

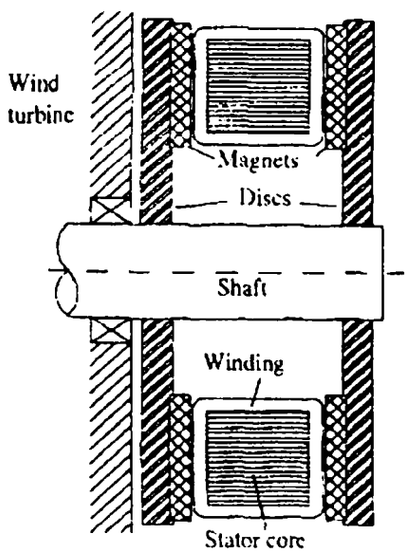

Figure 1.7. The torus generator

With a wounded toroidal stator, without slots but with PM's, this type of generator was already proposed as a solution for generating systems.

Many studies were done for such kind of electric machine on small power applications, where the power electronics configuration is predominant, there are known as small electronically-commutated permanent magnet motors. [1.59 - 1.61]

The transversal-flux generator is rather different from the other machines and it is difficult to make any simple comparisons between it and radial-flux generators. The major difference is that the transversal-flux concept allows an increase in the space for the windings without decreasing the available space for the main flux; this allows for very low copper losses.

The transversal-flux machine can also be made with a very small pole pitch compared with the other types. Unfortunately the electromagnetic structure is more complicated than for conventional generator types, which may consider it more expensive from manufacturing point of view.

1.2.6. Switched Reluctance Generator (SRG)

Proposed for generating applications, the switched reluctance machine proof it's simplicity, low cost, rugged configuration and most of all its fault tolerance but also it's dependency on power electronics (from the control point of view). [1.21-1.25]

A lot of improvements were made for the switched reluctance machine, in order from the starting capability, [1.57], to new power converter topologies, [1.15-1.19], but the wide speed constant power and voltage recovery under sudden load variation are still to be demonstrated.

A more detailed study for the switched reluctance generator is included in this dissertation in chapter two.

1.2.7. Hybrid Generator with Variable Reluctance (HG-VR)

It was found that for higher power the Lundell alternators are no more practical because of the worth cooling, the high leakage flux and because of the losses in the air-gap, too. [1.9]

For a good operation on a large domain of constant power a new type of electrical hybrid machine, double prominent with permanent magnets in the rotor, a machine which can be used also as electrical generator, has been proposed. [1.32]

This proposed new machine has a similar structure with that of the switched reluctance machine; the difference consists in the existence of the permanent magnets placed inside its rotor.

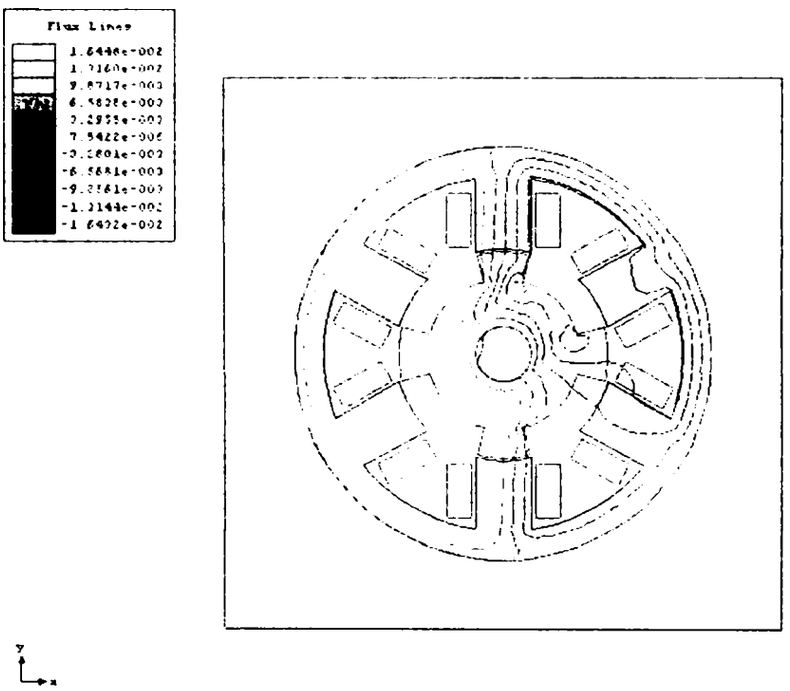

Figure 1.8. The electromagnetic field from 2D-finite element analysis

As it was demonstrated in several papers in which it was treated, this machine is mostly unique from the energy conversion point of view, the only problem being the current switching-over to assure a good energy conversion, for both, as generator or as motor operation.

When the machine is loaded, the bulk of the armature reaction flux is forced to circulate through another overlapped pole pair because the existence of PM constitutes a high reluctance path for the flux.

In figure 1.8, the electromagnetic field, resulted from 2D-FEA, created by permanent magnets for the aligned position for one phase, is presented for one of the machine topologies.

The magnetic flux from the air-gap (fig. 1.9) has a high value, this being concentrated to a great extent on the superposition zone of the stator poles with the rotor ones, the good energy conversion being emphasized.

However, it can be observed a leakage that appears because of the placement manner of the permanent magnets in the rotor.

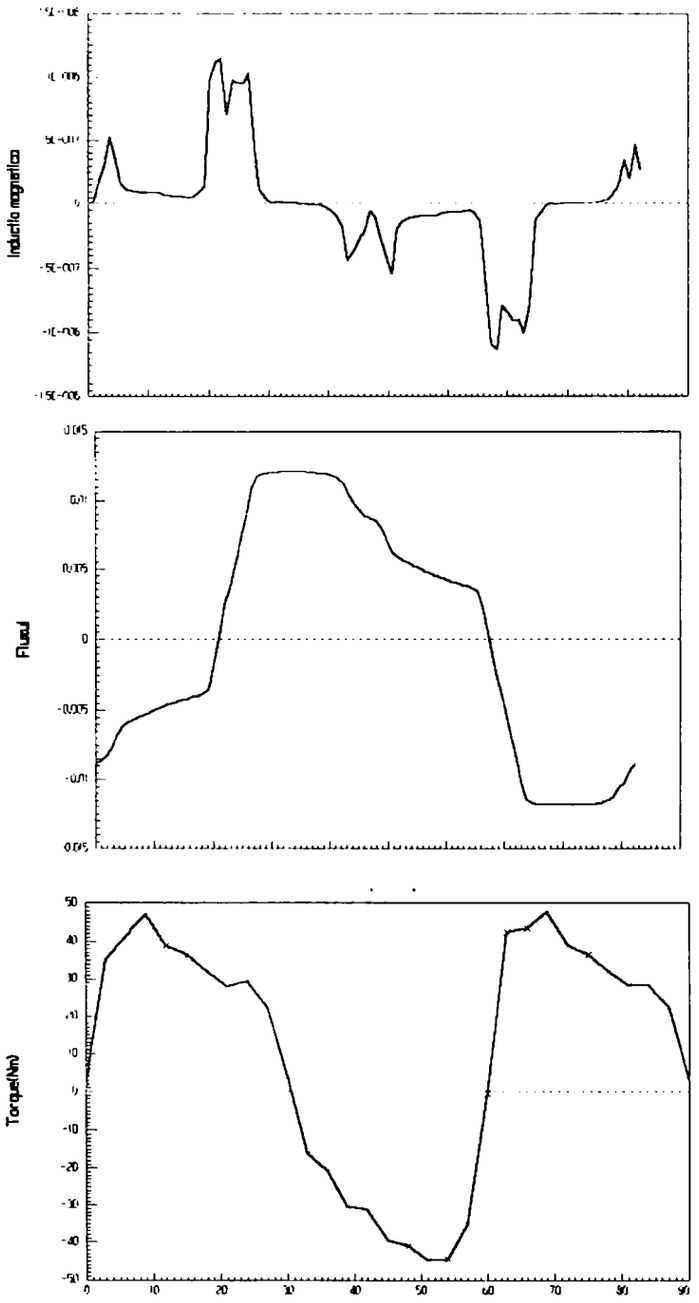

Figure 1.9. The air-gap magnetic flux density (upper picture), magnetic flux (middle) and the cogging torque variation (down) vs. rotor position (from 2D-FEA)

In figure 1.9, the flux density and the cogging torque for this topology of the hybrid machine with variable reluctance, are shown. It is found the existence of a large cogging torque, constitutes a serious disadvantage for this type of machine.

It can be observed from figure 1.9 that the flux is mainly concentrated at the overlapped pole area.

This variant of hybrid machine, with variable reluctance, has the following advantages: the inductance reduction thanks to the presence of the permanent magnets, the high efficiency and the high energy conversion, the reduced inertia moment, the simple structure.

1.2.8. Flux Reversal Generator (FRG)

Recently introduced, this type of electric machine can be easily used as a generator because it's simplicity and cost.

This machine is a doubly salient permanent magnet machine having low cost permanent magnet placed on the stator pole shoes.

A detailed study for this generator is presented in chapter three of the dissertation, including a generating system proposal using the flux reversal generator.

1.2.9. Double Salient Machine with Permanent Magnets (DSM-PM)

Beside the enumerated reasons in the introductory part of this chapter regarding the imposed restrictions, by the demands of the automotive construction domain and from the aeronautics industry, we must take into consideration the general accepted fact that about 60% from the produced electric energy is consumed by the electric machines, and this is an enough reason to study the efficiency increase of these machines.

Double salient generators with stator PM's and pulsating (homopolar) flux linkage have been proposed long ago.

With the same rotor topology like switched reluctance machine but having stator PM's for excitation purpose, the cogging torque for these machines is an important factor which has to be consider in the designing process. [1.39]

In fact, through the placement of these permanent magnets in the stator, the simplification of the supply/excitation converter structure of the switched reluctance machine was desired.

To try a reduction of the cogging torque and a standardizing of the flux repartition from the air-gap, a change was made in the structure of the previous presented hybrid generator with variable reluctance, through the modification of the permanent magnets position that is their passing from the rotor in the stator of the machine.

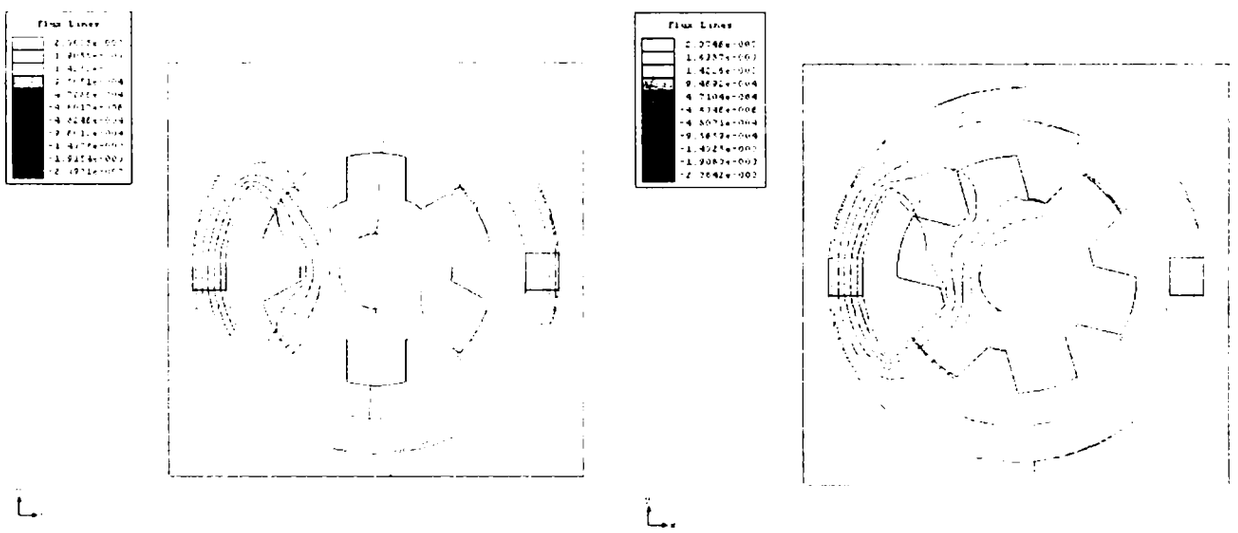

Figure 1.10. The repartition of the electromagnetic field produced by the permanent magnets (having an excitation role), from 2D-FEA

In figure 1.10, the repartition of the electromagnetic field produced by the permanent magnets through this machine can be watched, so for the aligned position of the stator poles with the rotor ones as for the un-aligned position.

To prove the high leakage that appears for the poles overlapping, the use of the finite element method is evident for this case. The desired effect from the permanent magnets is considerable reduced and the power conversion of the generator being reduced, too.

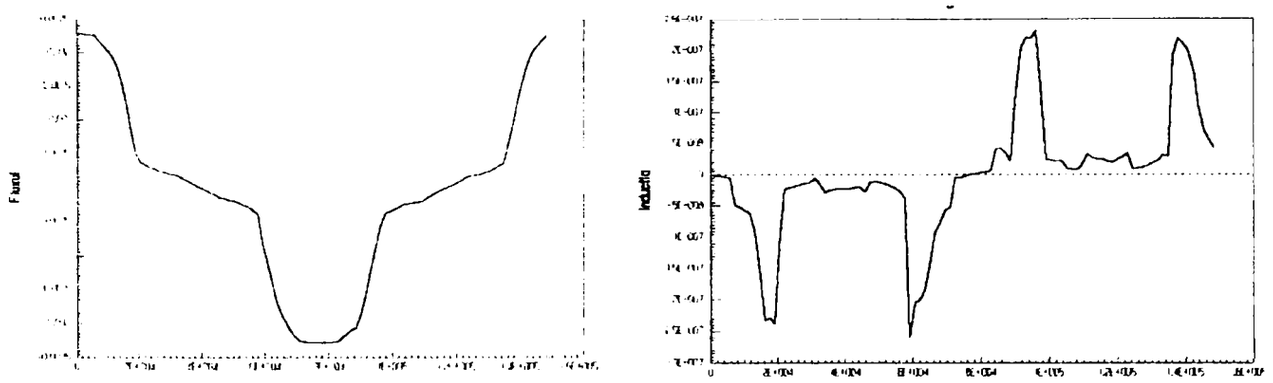

Figure 1.11. The DSM-PM variation of the magnetic flux and flux density from the air-gap (from 2D-FEA)

In figure 1.11, the variation of the flux and the magnetic flux density in the air-gap are presented.

In the specialized papers dedicated to this type of machine, the forms of the phase inductance and the saturation effects above the machine behaviour were studied also, showing that thanks to the impossibility of starting the machine in every position, it is more favourable to use it as a generator. [1.32]

The cogging torque that appears because of the presence of the permanent magnets has the shape as indicated in figure 1.12.

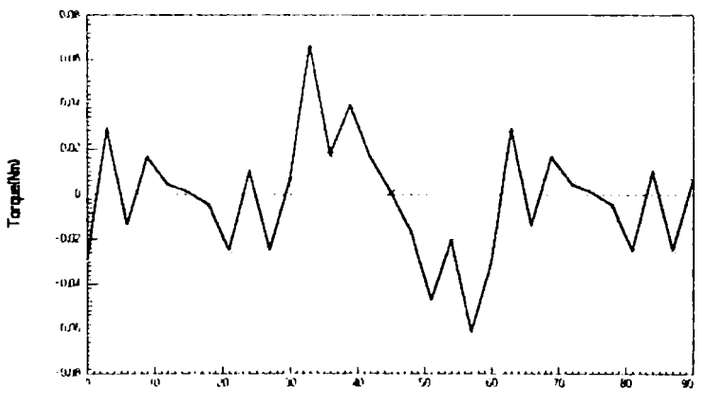

Figure 1.12. The cogging torque vs. rotor position [Nmx100/u.l.] (from 2D-FEA)

A relative high variation for the cogging torque can be observed.

In the following, another structure of this type of generator is presented, as it can be observed in figure 1.13, where the lines of the electromagnetic field and of the flux from the air-gap for a new structure are presented.

A standard repartition of the electromagnetic field lines is realized, the part from the stator yoke, where a permanent magnet is placed, is more narrow thus it is required a standardized saturation of this. The air-gap flux has a higher value than in the previous case, although for the analysis, the same type of permanent magnet is used (NdFeB).

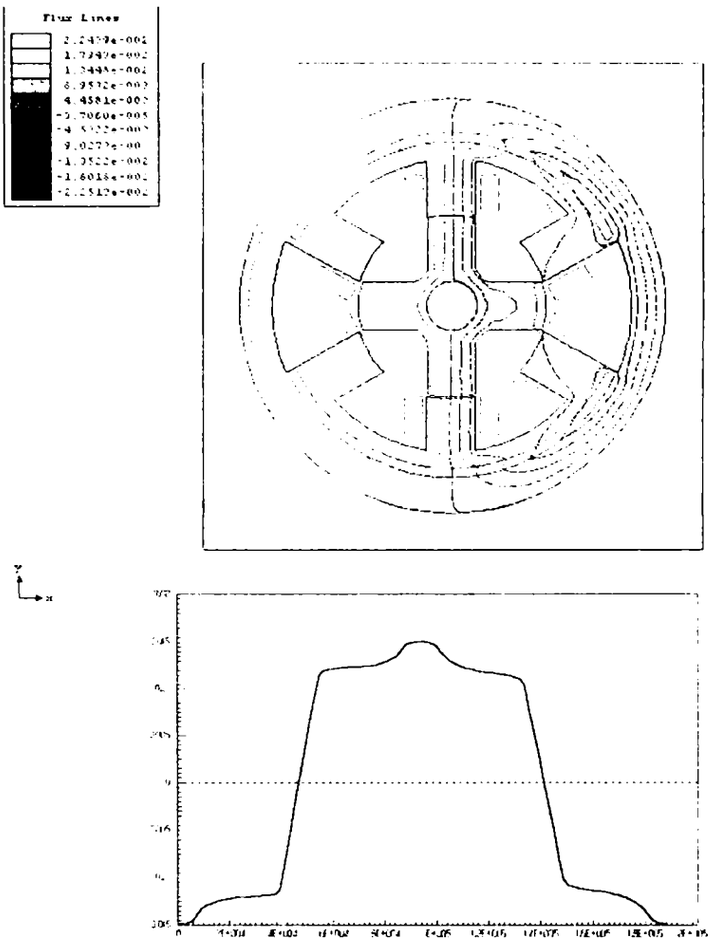

Figure 1.13. The electromagnetic field and the magnetic flux [Wb/u.l.] on the air-gap (from 2D-FEA)

This time, the magnetic flux in the air-gap is much bigger and this due to the PM size from the stator yoke.

Also, as a consequence of the change of the permanent magnets placement is the increase of the cogging torque, as it can be observed in figure 1.14.

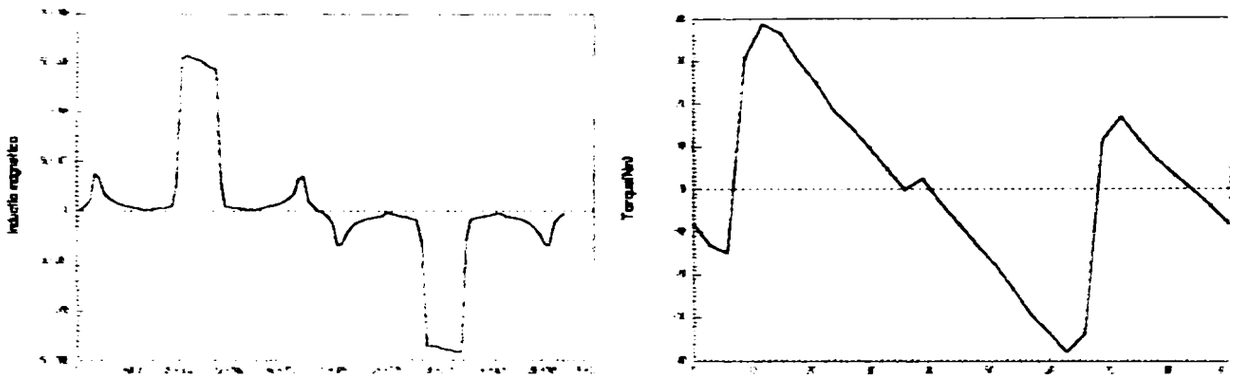

Figure 1.14. The magnetic flux density [Tx10^{6}] and the cogging torque [Nm/u.l.] in the air-gap (from 2D-FEA)

The leakage flux has higher values, too, so, a change in machine structure must be made, even making smaller the rotor poles thickness or increasing the air-gap, both solutions with negative aspects from electromagnetic point of view.

1.2.10. Dynamic Double Salient Generator with Permanent Magnets (D-DSM-PM)

The presence of the permanent magnets contributes to the appearance of a way with high reluctance, forcing the flux to circulate through another pair of super-positioned poles, as result: the active phase of the stator will have low inductances in the aligned and un-aligned position, the maximum value being obtained at the 1/2 superposition of the stator poles with the rotor ones (figure 1.15).

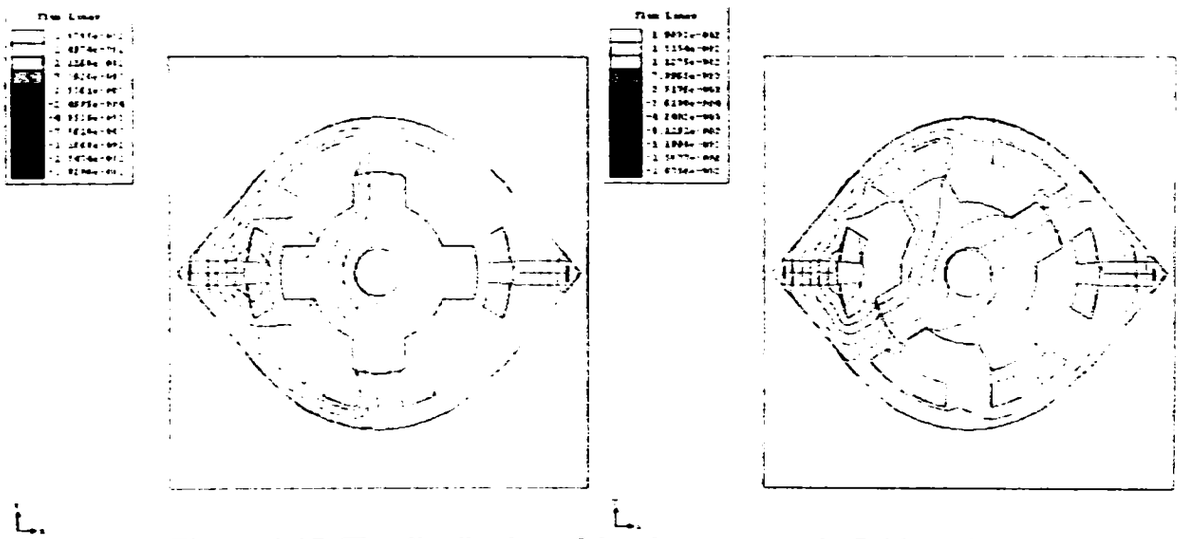

Figure 1.15. The distribution of the electromagnetic field produced by the permanent magnets for different rotor positions (from FEA)

The proposed configuration is based on the use of some permanent magnets placed in the stator, with low setting costs, but which must have a marked effect above the machine function. [1.34]

The mechanical design of the machine ensures that the total overlapped pole area is kept constant at any position of the rotor.

The power electronic for this type of machine is made according the used method at the switching reluctance machine, too, the converter structure being similarly.

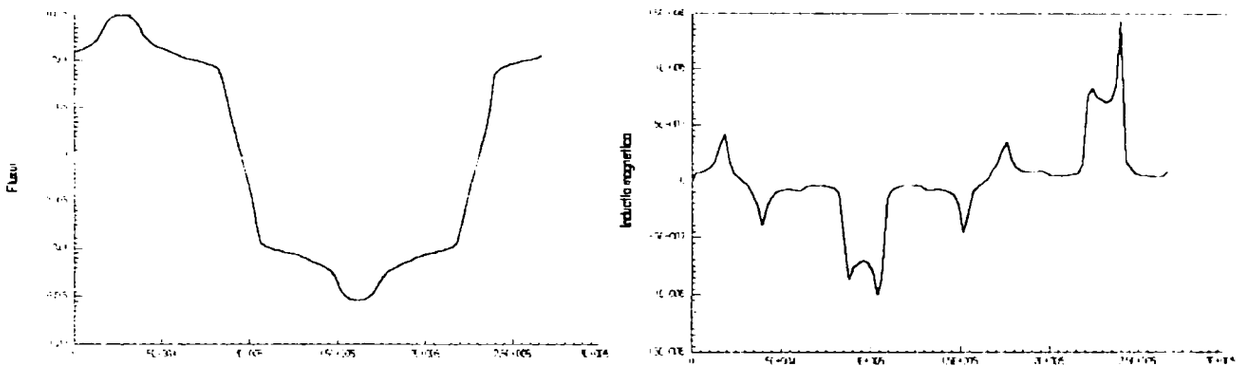

Figure 1.16. The variation of the flux [Wb/u.l.] and flux density [Tx10^6] in the air-gap (from 2D-FEA)

Observing the obtained results through the analysis with the finite element method (fig. 1.15 and fig. 1.16) we can draw the conclusion that despite of the simplification of the manufacturing technological process of this machine, that is the reduction of the afferent costs and the good dynamic behavior, we must find other solutions which have as result a generator which equips the vehicles and which fulfils the most of the demands imposed by the new function conditions.

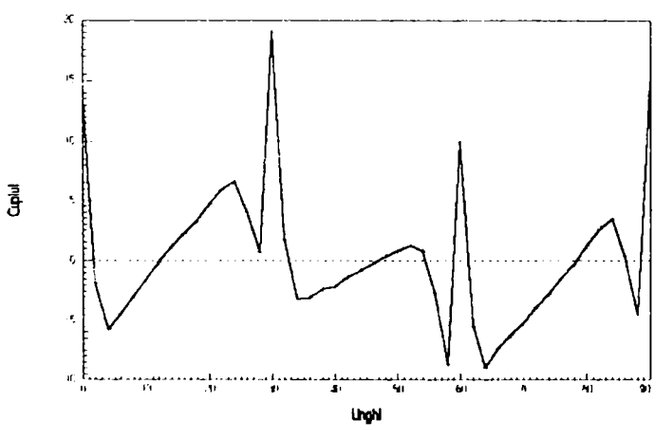

Figure 1.17. The cogging torque [Nm/u.l.] of the D-DSM-PM vs. rotor position (from 2D-FEA)

Recent studies show us that a 8/6-pole configuration of the D-DSM-PM take advantages over the 6/4-pole counter-part, namely higher power density, wider speed range, less torque ripple and lower current magnitude are obtained.

These advantages can well outweigh its drawbacks on relatively more complex in structure and, of course, in control (when necessary). [1.55]

Many other types of electric machines were studied and can be proposed for applications where are operating as generators, starting with the axially laminated machine, [1.20], and continuing with special hybrid synchronous machines. [1.56], [1.58-1.60]

Besides the manufacturing cost of those, their efficiency and wide speed operation capability are the most important factors to be considered but, of course, the manufacturing cost reductions can be achieved by changing the structure of the power electronic converters, together with proper control strategies, too.

Anyway, including the power converter cost for the generating system cost optimisation, a significant impact appears on machine design, either by exchanging a larger and more expensive machine for a lower power electronics costs by reducing the current for the power converter or designing the machine with a large power factor and so reducing the apparent power of the requested power converter.

1.3. Conclusion

The electric machines presented in this chapter constitute only a part of the most indicated variants to use as electrical alternators that has to equip the generator systems of the modern cars.

We can draw the following conclusions:

- The claw-pole (Lundell) generators efficiency is up to 50% for maximum load and speed, so, new solutions to improve their efficiency or to find other alternatives are requested.

- Instead of the changes made to improve the efficiency by placing the permanent magnets with different geometric topologies, the modified Rice-Lundell generators are not offering the expected results.

  The positive effect of the permanent magnet presence is obtained just for low speed range and constitutes anyway an advantage for idle speed automobile operation.

- The synchronous generators with interior permanent magnets are a viable solution but for high-speed operation, the permanent magnets disadvantage because of detachment tendency.

- Disc rotor generators are solving the energetic performance problem but the permanent magnets demagnetization and detachment effects, together with the high moment of inertia of the disc rotor, are a real problem.

- The hybrid generators with variable reluctance show us a good energy conversion but the high value of the fringing flux, mainly because of the permanent magnets placing.

  Beside their high efficiency and small inductances (small electrical constant), this type of electric machine needs to be optimized.

- The double salient permanent magnets generators have a geometrical configuration similar to the hybrid generators but the permanent magnets are placed in the stator to expand the speed range.

Placing the permanent magnets in the stator was choose to simplify the power electronic converter structure (consequently it's price, too) for the switching reluctance machine. The leakage effect is high so, the power conversion of the machine is reduced.

The second alternative is more efficient, but the cogging torque and the air-gap flux density are bigger, anyway the manufacturing costs are a little bit higher, too

- The dynamic double salient permanent magnets generators, with a similar topology, have bigger permanent magnets inserted in the stator yoke, to reduce more the electrical time constant, so for a better dynamic behavior with a relative small increase of the manufacturing and PM's costs.

  The beneficial effect of the large permanent magnets is partially reduced by their placing mode (not expensive to realize but with a high fringing effect) but this type of electric machine deserve to be considered from both manufacturing costs and dynamic behavior.

- The switched reluctance machines are from the constructive point of view the most redundant, using simple numerical analysis (by finite element method) can be geometrically optimized.

  Beside its simplicity, the switched reluctance machine has not a spread use, at least as generator and that because of the power converter complexity and high costs.

- The flux reversal machines, to be introduced and studied in the 3rd chapter of this dissertation, are more reliable and relatively easy to manufacture, placing the permanent magnets in the stator poles eliminates the detachment tendency for high-speed operation.

  Because the bi-polar variation of the stator magnetic flux, so, of the good usage of the stator iron, and because of the low rotor induced currents and small electrical time constant, caused by the presence of the permanent magnets, this machine imposes itself as a good one especially for generator operating mode.

Recently, a cost study was done for a 6kW starter/generator system, built in four variants: with an induction machine (IM); with a synchronous machine with rotor surface permanent

magnets (SPM); with a hybrid machine with interior permanent magnets (IPM); respectively with a variable reluctance machine (VRM); each of them with the appropriate power converter topology. [1.38]

The results of this study was expanded taking into account all the generator structures presented in this chapter, together with the afferent power electronic devices, using the cost formulas from 1.1 to 1.2 and table 1.1, and considering the de results from [1.38], are completing the above conclusion.

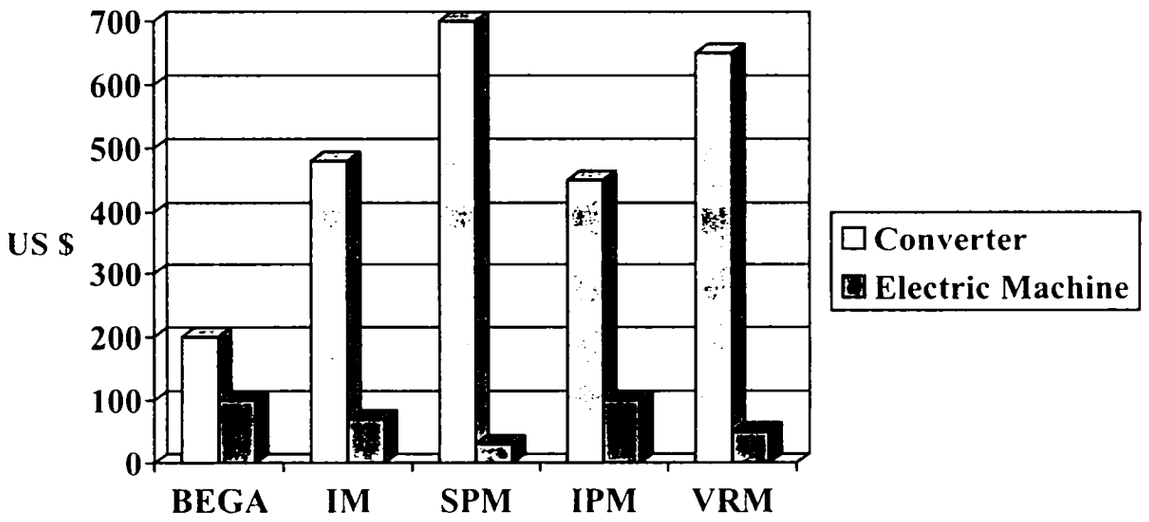

Figure 1.18. The manufacturing costs for different electric machines (for 6kW power), in comparison with data from [1.38]

Beside these results we have considered the case of a new kind of generating system that includes new types of generators, the two phase switched reluctance generator (2P-SRG), the flux reversal generator (FRG) and the biaxial excitation generator for automobiles (BEGA), together with their power converters.

The costs for the last new system was calculated considering the results from the designing program from chapter four, from the present dissertation, where this new type of generator, together with its power converter will be studied in detail.

One direct observation: to be integrated efficiently in automobiles industry, the costs for a starter/generator system may go up to 500$ for the present systems, having 14V d.c. bus voltage. This is a rather large amount of money.

As known, the main manufacturing costs are those for the power electronic converter, each system being built for a four quadrants operation for the electric machines.

As can be observed, only for the systems with induction machine and those with a biaxial excitation generator or flux reversal generator and even those with internal permanent magnet machines, the manufacturing costs requirements are mostly accomplished.

Mainly, the manufacturing cost reductions can be achieved by the power electronic converters but also, for the internal permanent magnets machines, choosing the right configuration and type for the magnets can give us supplementary cost reductions.

The continuous development of the electronic industry together with new semiconductor devices and permanent magnets appearances are the main factors that will lead us to prices drop of the starting/generating system in the near future.

Anyway, low power control for the converters, for maximum voltage and current operation, will give us important manufacturing cost reduction.

References

[1.1] P. P. Acarnley, P.G. McLaren - "*Optimum Magnetic Circuit Configurations For Permanent Magnet Aerospace Generators*"- IEEE Transactions on Aerospace and Electronic Systems, vol. AES 21, no. 2, March 1985;

[1.2] I. Boldea -"*Transformatoare si masini electrice*"- Ed.D.P.Bucureşti 1994;

[1.3] I. Boldea, S.A. Nasar, L.E. Unnewehr -"*Permanent Magnet Reluctance and Self Synchronous Motors*"- CRC Press Boca Raton Ann Arbor London Tokyo;

[1.4] Gerhard Henneberger -"*Elektrische Motorausrüstung*"- Bosch GmbH;

[1.5] M. Hecquet, P.Brochet -"*Validation of Coupled Electric Permeance Net-work Model on a Claw-Pole Alternator*"- Ecole Centrale de Lille, France;

[1.6] G.Barakat, A.Foggia, M.Ivanes, A.Masson, R.Periot -"*Three Dimensional Computation of a Claw-Pole Synchronous Machine Performance*" Laboratoire d'Electrotechnique de Grenoble, France;

[1.7] G. Henneberg, S. Küppers, I. Ramesohl -"*Numerical Calculation, Simulation and Design Optimization of Claw-Pole Alternators for Automotive Application*"- Institute for Electrical Machines, University of Technology Aachen;

[1.8] G. Henneberger -"*Improvement of the output performance of claw pole alternators by additional permanent magnets*"- D10 Special machines and actuators;

[1.9] G. Henneberger, S. Küppers, I. Ramesohl -"*The Influence of the Number of Poles on the Output Performance of a Claw-Pole Alternator*"- Institute for Electrical Machines, University of Technology Aachen;

[1.10] S. Andersen - "*Flux Reversal Machine*"- Master thesis project, September 22 1996;

[1.11] Rajesh P. Deodhar, I. Boldea, T.J. Miller -"*The Flux-Reversal Machine: a New Brushless Doubly-Salient Permanent Magnet Machine*"- IEEE Transactions;

[1.12] Miller T.J.E. -"*Switched Reluctance Motors and Their Control*"- Magna Physics Publishing and Clarendon Press, Oxford 1993;

[1.13] A. Radun -"*Generating With the Switched Reluctance Motor*"- University of Kentucky, USA;

[1.14] I. Boldea, E. Serban, R. Babau -"*Flux Reversal Stator PM Single Phase Generator With Controlled D.C. Output*"- OPTIM '96;

[1.15] D. E. Cameron, J. H.Lang -*"The Control of High-Speed Variable Reluctance Generators In Electric Power Systems"*- IEEE Transactions on Industry Aplications, Vlo.29, No.6, Nov.-Dec.1993;

[1.16] P. Materu, R. Krishan -*"Estimation of Switched Reluctance Motor Losses"*- IEEE Transactions, Reprinted, 1988;

[1.17] P. C. Kjaer, T.J.E. Miller, J.J. Gribble -*"High-Grade of Switched Reluctance Machines"*- University of Glasgow, SPEED Laboratory, Scotland, U.K.;

[1.18] S. R. McMinn, W.J. Rzesos, P.M. Szczesny, T.M. Jahns -*"Application of Sensor Integration Technique to Switched Reluctance Motor Drives"*- IEEE Transactions on Industry Applications, Vol.28, No.6, Nov.-Dec. 1992;

[1.19] Iqbal Husain, M. Ehsani -*"Rotor Position Sensing in Switched Reluctance Motors Drives by Measuring Muttualy Induced Voltages"*- IEEE Transactions on Industry Applications, Vol.30, No.3, May-June 1994;

[1.20] R. Lagerquist, I. Boldea, T.J.E. Miller -*"Sensorless Control of the Synchronous Reluctance Motor"*- IEEE Transactions on Industry Applications, Vol.30, No.3, May-June 1994;

[1.21] P. P. Acarnley, R.J. Hill, C.W. Hooper -*"Detection of Rotor Position in Stepping and Switched Motors by Monitoring of Current Waveforms"*- IEEE Transactions on Electronics, Vol.IE-32, No.3, August, 1985;

[1.22] P. C. Kjaer, G. Gallegos-Lopez -*"Single Sensor Regulation in Switched Reluctance Motor Drives"*- University of Glasgow, SPEED Laboratory, Scotland, U.K.;

[1.23] A. Lumsdaine, J.H. Lang -*"State Observers for Variable-Reluctance Motors"*- IEEE Transactions on Industrial Electronics, Vol.37, No.2, April, 1990;

[1.24] P. Laurent, B. Multon -*"Sensorless Position Measurement Based on PWM Eddy Current Variation for SRM"*- EPE '95 Sevilla;

[1.25] W. F. Ray, M.T. Ebrahim -*"A Novel High Speed Switched Reluctance Generator"*- EPE'95 Seville;

[1.26] Sabonnadiere J.C., Konrad A. -*"Computing EM Fields"*- IEEE Spectrum, November 1992, pp. 52 – 56;

[1.27] A. G. Jack, J.W. Finch, J.P. Wright -*"Adaptive Mesh Generation Applied to Switched Reluctance Motor Design"*- IEEE Transactions on Industry Applications, Vol.28, No.2, March-April 1992;

[1.28] R. P. Deodhar -"*The flux-MMF Diagram Technique and Its Applications in Analysis and Comparative Evaluation of Electrical Machines*"- University of Glasgow, October 1996;

[1.29] Jung-Chien Li -"*A Saturation Model for the Switched Reluctance Motor to Maximize the Torque with Minimum Ripple*"- Department of Electrical Engineering, National Taiwan Ocean University, Keelung, Taiwan;

[1.30] G. Henneberger, S. Küppers –"*Field Calculation and Dynamic Simulation of a Claw Pole Alternator*"- Electrical Machines and Drives 11-13 Sept. 1995 Conference Publication No.412, IEE, 1995;

[1.31] H. J. Gutt, J. Mueller – "*New Aspects for Developing and Optimizing Modern Motorcar Generators*" – Record of IEEE 1994;

[1.32] Y. Liao, Th. A. Lipo – "*A New Doubly Salient Permanent Magnet Motor for Adjustable Speed Drives*" – Record of IEEE, 1992;

[1.33] X. Luo, D. Qin, Th. A. Lipo – "*A Novel Two Phase Doubly Salient Permanent Magnet Motor*" – Record of IEEE, 1996;

[1.34] P. Pedersen, L. Christensen, F. Blaabjerg, L. Oestergaard – "*A New Dynamic Model for a Doubly Salient Permanent Magnet Motor*" – Record of IEEE, 1996;

[1.35] E. C. Lovelace, T. M. Jahns, J. L. Kirtley Jr., J. H. Lang – "*An Interior PM Starter/Generator for Automotive Applications*" – Record of IEE 1998;

[1.36] F. Caricchi, F. Crescimbini, F. Giulii Capponi, L. Solero – "*Permanent-Magnet, Direct Drive, Starter/Alternator Machine with Weakened Flux for Constant-Power Operation Over Extremely Wide Speed Range*" – Record of IEEE, 2001;

[1.37] Yanhong Xue, Shaotang Chen – "*Instability Issues for Control System in Induction Generator*" – Record of IEEE, 2001;

[1.38] Klaus Bolenz – "*Design Modifications of the Electrical System to use Intermittent Engine Operation*"- Record of IEE, 1996;

[1.39] A. Manzone, A. Pincetti, D. de Costantini – "*Fault Tolerant Automotive Systems: an Overview*" – Record of IEEE, 2001;

[1.40] H. Thiemer – "*Influence of Automotive 42V Power-net on Small PM DC Motors*" – Record of IEEE, 2001;

[1.41] Z. John Shen, S.P. Robb, F.Y. Robb, M. Fuchs, D. Berels, K. Hampton – "*Load Dump Protection in 42V Automotive Electrical Distribution Systems*" – Record of IEEE, 2001;

[1.42] T. M. Jahns, Wen L. Soong – *Pulsating Torque Minimization Techniques for Permanent Magnet AC Motor Drives – A Review"* - Record of IEEE, 1996;

[1.43] P. J. McCleer, J.M. Miller, A.R. Gale, M.W. Degner, F. Leonardi – *" Nonlinear Model and Momentary Performance Capability of a Cage Rotor Induction Machine Used as an Automotive Combined Starter-Alternator"* – Record of IEEE, 2001;

[1.44] R. D. Schultz – *"Performance Model of an Automotive Starter-Generator"*- Record of IEEE, 2000;

[1.45] M. Naidu, J. Walters – *"A 4 kW, 42 V induction machine based automotive power generation system with a diode bridge rectifier and a PWM inverter"* – Record of IEEE, 2001;

[1.46] K. Yoshida, K. Kesamaru, Y. Hita – *"Eddy Currents Analysis of Surface Mounted PMSM by Finite Element Method"* – Record of IEE, 1999;

[1.47] J. Luo, S. Huang, S. Chen, T.A. Lipo – *"Design and Experiments of a novel Axial Flux Circumpherential Current Permanent Magnet (AFCC) Machine with Radial Airgap"* – Record of IEEE, 2001;

[1.48] F. Caricchi, F. Crescimbini, E. Santini, L. Solero – *"High-Efficiency Low-Volume Starter/Alternator for Automotive Applications"* – Record of IEEE, 2000;

[1.49] N. A. Demerdash, R. Wang, R. Secunde – *"Three Dimensional Magnetic Fields in Extra High Speed Modified Lundell Alternators Computed by a Combined Vector-Scalar Magnetic Potential Finite Element Method"* – Record of IEEE, 1992;

[1.50] R. Wang, N.A. Demerdash – *"Extra High Speed Modified Lundell Alternator Parameters and Open/Short –Circuit Characteristics from Global 3D-FE Magnetic Field Solutions"* – Record of IEEE, 1992;

[1.51] F. Liang, J. Miller, X. Xu – *"A Vehicle Electric Power Generation System with Improved Output Power and Efficiency"* – Record of ELECTROMOTION International Conference, 1998;

[1.52] K. T. Chau, M. Cheng, C.C. Chan – *"Performance Analysis of 8/6-Pole Doubly Salient Permanent Magnet Motor"* – Record of IEEE, 1996;

[1.53] A. Mutter – *"Elektrische Antriebe mit kombinierter elektrischer und Dauermagneterregung"* – Deutsches Patent und Markenamt, Patentschrift DE 4139843C2;

[1.54] G. E. Horst – *"Auxiliary starting switched reluctance motor"* – European Patent Application, EP 0695020A2;

[1.55] C. E. Stille – *"Exciting arrangement for homopolar machine"* – UK Patent Application, GB2247362A;

[1.56] K. K. Meidensha – *"Hybrid excitation type permanent synchronous motor"* – European Patent Application, 0620634A1;

[1.57] Syverson et all – *"Hybrid Alternator with Voltage Regulator"* – United States Patent, 5502368;

[1.58] E. C. Lovelace, T.M. Jahns, J.H. Lang – *"Impact of Saturation and Inverter Cost on Interior PM Synchronous Machine Drive Optimization"* – Record of IEEE, 1999;

[1.59] C. Martis, M.M. Radulescu, K. Biro – *"Dynamic Analysis of a Switched Variable Reluctance Permanent Magnet Small Motor"* – Record of ELECTROMOTION, 1999;

[1.60] M.M. Radulescu, Z. Biro, C.M. Pop – *"Two-Phase Electronically-Comutated Permanent-Magnet Small Motor without Position Sensor"* - Record of ELECTROMOTION, 1999;

[1.61] G. Cimuca, M.M. Radulescu, B. Robyns, S. Brisset – *"Back-EMF Approach for Sensorless Operation of Small Electronically-Commutated Permanent-Magnet Motors"* – Record of OPTIM-2002, International Conference, Brasov, Romania;

CHAPTER II

TWO PHASE SWITCHED RELUCTANCE GENERATOR (2P-SRG)

2.1. Introduction

In chapter one, a relatively comprehensive review of various types of electric machines has been presented. The reason for doing this is that the novel electric machines, for variable speed generating operation mode, proposed and presented in this dissertation are closely related to some of the existing types of electric machines.

The switched reluctance generator is an electrical generator at which the conversion of the energy relies on the reluctance variation, has so the stator as the rotor with seeming poles topology, the field winding being placed in the stator.[2.12] [2.13]

In the figure 2.1, a structure of a four phase switched reluctance machine, with eight stator poles and six rotor poles is represented.

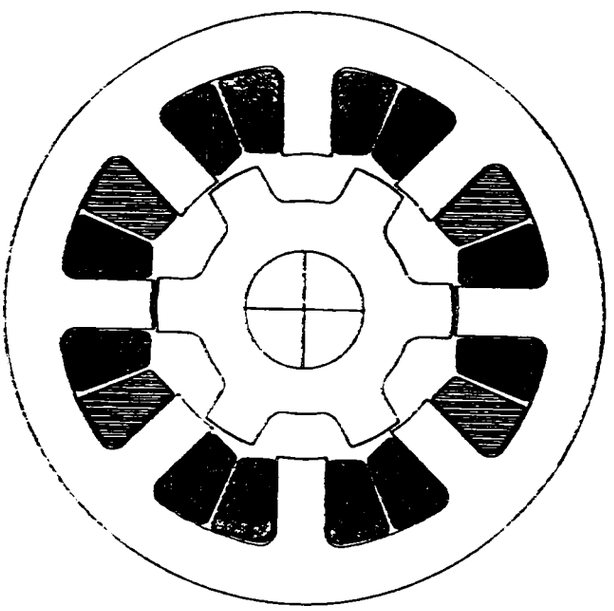

Figure 2.1. The structure of a four phase switched reluctance generator

Each phase is made up of two coils that are placed on the opposite poles.

In the present, this imposes itself through its constructive simplicity, through the absence of the permanent magnets, the independence of the phases, through the robust rotor, and through the good work at high temperatures conditions. [2.7]

Switched Reluctance machines had a continuously request as electrical generators in aerospace industry but in other applications, too, where the robustness, high speed operation and fault tolerance are of major priority.

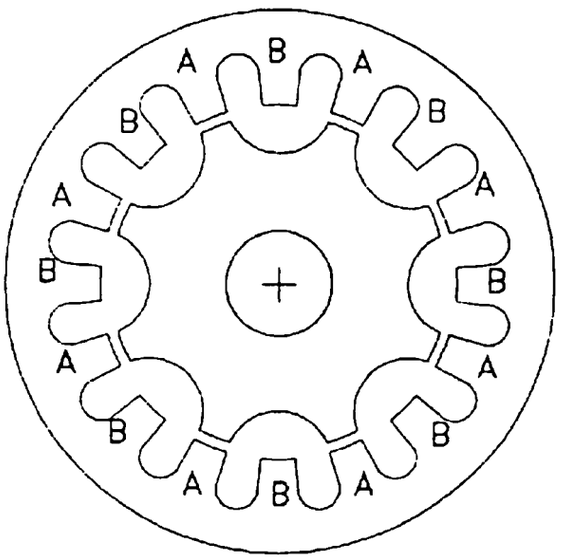

Figure 2.2. The structure of SRG for high-speed operation

SRG direct control methods, especially those for small power applications, increase the drive delivery price over acceptable limits and, in addition, reduce the system reliability by making it environmental sensitive.

Substituting the position transducer from the shaft and using other control techniques, these drawbacks were eliminated:

- rotor position sensing by transducers placed between stator poles;
- rotor position detection by current or voltage waveforms monitoring;
- indirectly rotor position detection by phase inductance variation (or through other machine parameters).

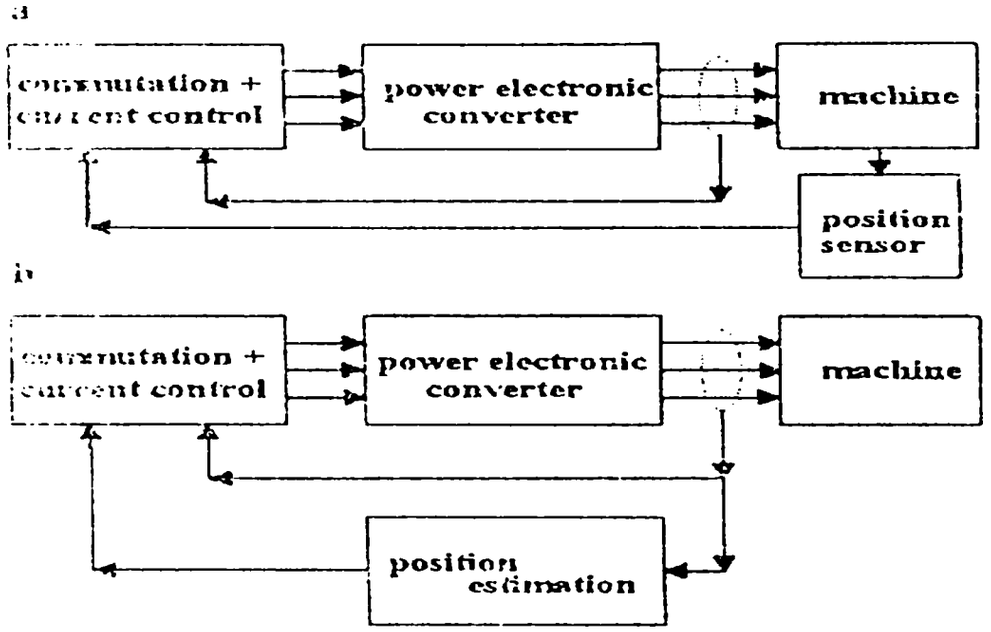

Figure 2.3. Control strategies for the switched reluctance machine, with position sensors (a) or without position sensors (b)

The most frequently methods used for Switched Reluctance machine sensor-less control can be classify, considering estimator location, in two major groups:

- rotor position estimation methods through measuring and calculation of parameters from the not supplied phase;
- rotor position estimation methods through the measuring and calculation of parameters from the supplied phase.

From the first group, make part:

- the method of the phase inductance measurement, through the modulation in amplitude or the frequency, with the disadvantage of the influence above the sensibility of the machine parameters, specially, thanks to the saturation; [2.17]
- the method of diagnose pulses injection, in the not-supplied phase and the measurement of the current ripple, with the disadvantage for high speed operation; [2.18]
- the method of the armature voltage line measurement, which needs a significant phase coupling; [2.19]

- the flux valuation method through the agency of voltage integration and of inductance calculation with help of a simple machine model, with the given disadvantage of the chosen machine model. [2.20]

From the second group can be mentioned:

- the method of the current wave form monitoring, with difficulties in the influence of the armature voltage and of the magnetic saturation; [2.21]
- the method of the current gradient measurement, with motor starting difficulties, when an self-synchronization is necessary; [2.22]
- methods based on the state observers, the complicated mathematical model having influence above the speed and accuracy in the calculation; [2.23]
- the method of the rotor position valuation, through the agency of the eddy current losses measurement, which can be considered independent of the magnetic saturation and whose variation with the rotor position is similar with that of the phase inductance. [2.24] The problem that could appear is in connection with the influence of the hysteresis losses, which depend on the saturation level of the machine, that is why this method can be applied just considering that the eddy current losses are prevalent.

The sensor-less control imposes itself because of the following reasons: the manufacturing cost diminishing, also, the reliability increase and the motor adaptation for hard conditions operating modes. In this way, the Hall sensors or the resolvers are the most used.

The estimator has to deduce the instantaneous position of the rotor, using measurements of the stator voltage and currents and also, of the electric machine parameters. Physically, the position valuation function can be made through electronic circuits placed near the controller. [2.16]

The advantages are the followings: the remove of the costs regarding the position sensors and their concession; the remove of the function temperature limitation; positional signal lines are not necessary.

These valuations were applied for SRM controlled through a chopper. There appeared errors in the valuation because of e.m.f., the saturation and because of the natural coupling effects.

The mathematical model for the numeric simulations of the two-phase switched reluctance generator is given by the following equations.

$$\frac{d\lambda_a}{dt} = i_a R_s - V_a(\theta_r) \tag{2.1}$$

$$\frac{d\lambda_b}{dt} = i_b R_s - V_b(\theta_r) \tag{2.2}$$

$$\frac{d\omega_r}{dt} = (T_e - T_m) / J \tag{2.3}$$

$$\frac{d\theta_r}{dt} = \omega_r \tag{2.4}$$

$$T_e = \lambda_m \frac{1}{\theta_c} \frac{i_a^2}{2i_0} + \lambda_m \frac{-1}{\theta_c} \frac{i_b^2}{2i_0}; \quad \text{for } i_a, i_b \le i_0 \tag{2.5}$$

$$T_e = \lambda_m \frac{1}{\theta_c} (i_a - i_b); \quad \text{for } i_a, i_b \ge i_0 \tag{2.6}$$

The one-phase flux depends of a relative position of the rotor to the stator poles of the same phase, for phase A, we can write:

$$\lambda_a = L_{ua} i \quad \text{for the unaligned position;} \tag{2.7}$$

$$\lambda_a = \lambda_m i / i_0 + L_{ua} i ; \quad \text{for } i \le i_o \text{ and } \theta_{er} \le \theta_c \tag{2.8}$$

$$\lambda_a = \lambda_m + L_{ua} i ; \quad \text{for } i \ge i_0 \text{ and } \theta_{er} \le \theta_c \tag{2.9}$$

A similar function can be built also, for the decreasing zone of the flux. We proceed in the same way for phase B, the only difference is the choice of the angle. The flux on one phase depending on current and position, $\lambda(i, \theta_r)$, is precisely obtained from FEA.

Anyway, for the preliminary design, it is necessary only an approximate analytical solution, especially by the calculation of the permanent and dynamic system and of the driver. On the basis of the till present obtained results, through the finite element method, it seems that an estimation of the dependence $\lambda(i, \theta_r)$ through straight lines segments is practical.

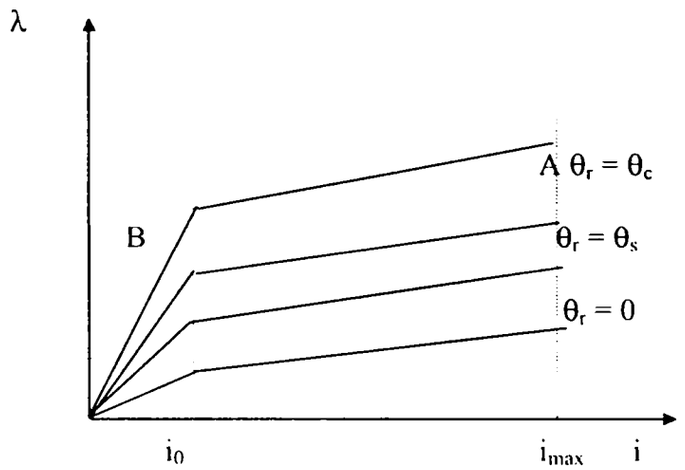

Figure 2.4. Phase flux versus current for different positions

The minimum flux is obtained for $\theta_r = 0$ and is given by:

$$\lambda = L_{ua}\, i \qquad [Wb] \tag{2.10}$$

The unaligned phase inductance value, L_{ua}, is composed from the leakage inductance (self-inductance), L_{ual} and the linkage inductance, L_{uag} from the air gap:

$$L_{ual} = L_{uals} + L_{uale} \tag{2.11}$$

However, for generator operating mode, the stator windings of the machine, must be excited on the angular side, between the align position of the stator poles with the rotor ones and that in which the poles do not overlap, reverse as by the excitation in the motor operating mode.

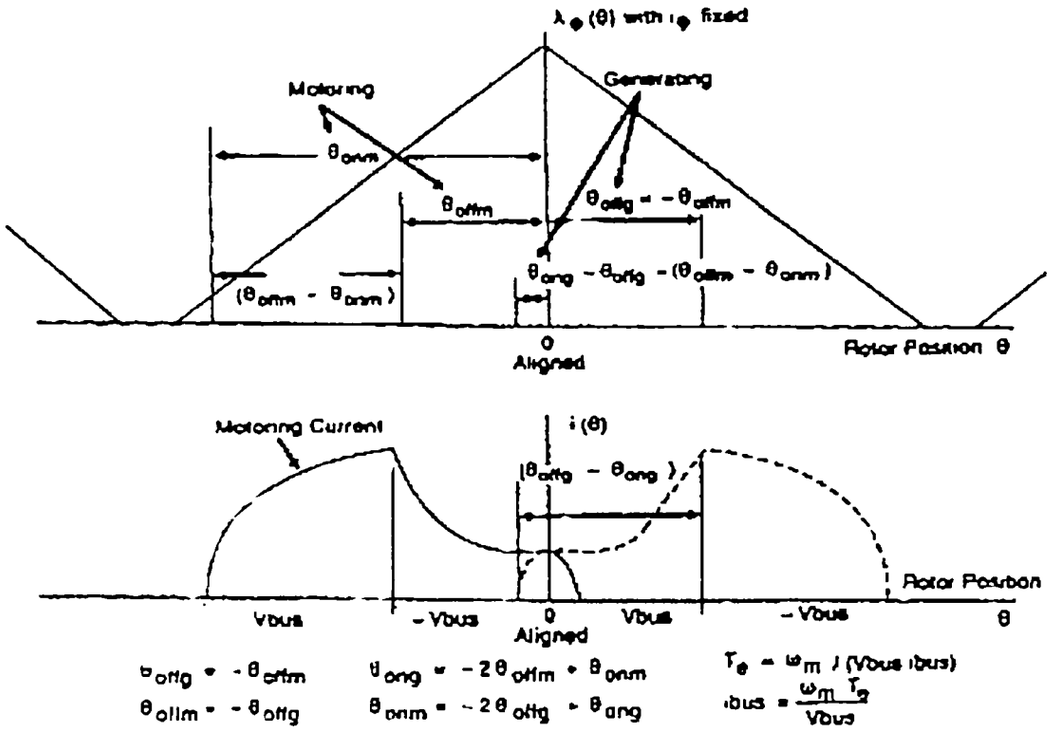

Figure 2.5. The phase flux variation vs. rotor position and the phase current waveform for a switched reluctance machine [2.48]

In the present, to reduce the costs, we have in view to realize systems with switched reluctance generators in sensor-less control.

A sensor-less generating system, with switched reluctance machine as generator, which had to lead to reduced costs for both manufacturing and exploiting, is made of the following components:

a) a machine which has to operate on the same principle as the switched reluctance one, with two phase (eventually single phase) and in whom structure can be introduced short circuited windings (with help of a Triac), for an adequate positioning before to start in one of the possible directions, if motor operating mode is desired, too;

b) a converter for excitation supply, built in a simple structure, and whose command for the generator drive is sensor-less; In its structure is included a current sensor (preferable) which is used just for protection and for giving information regarding the position of the rotor poles instead the stator poles in the starting moment.

2.2. Two Phase Topology

This machine has the structure of the classic switched reluctance machines, therefore, has salient rotor and stator poles, the number of the rotor poles Nr = 2, 4 or 6 and that of the stator poles: Ns = 2 x Nr, having the same width with the rotor ones.

In the 2xNr stator slots, 2xNr stator windings are introduced, Nr windings for each phase (series connected) each disposed around a stator pole, alternatively, for respecting the structure of a two-phase machine.

All the rotor poles simultaneously contribute to the increase of the electromagnetic torque; thus, a good torque density in the rotor is created.

We consider the case of one machine with this topology, having Nr=4 rotor poles and Ns=8 stator poles, the phase inductance variation as rotor position function will be as shown in next figure:

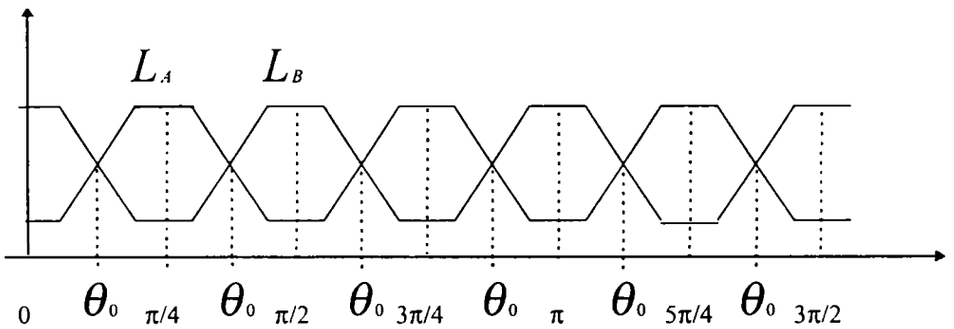

Figure 2.6. Phase inductance vs. rotor position

As can be observed, it exists a zero torque position and so, the resulted optimal starting position is for θ_0, where phase inductances are equal, so the starting is possible in both directions.

Considering the saturation effect, when both phases A and B are fed with the same high currents, there is a tendency (torque) to move the rotor from the axis of the phase A (or B) to the optimum (intermediate) starting position - θ_0.

2.3. Conceptual Design for 2P-SRG

For the design process of the two-phase switching reluctance generator, finding the useful torque using the geometry of the machine, so, an important role has the value and shape of the main magnetic flux or phase reluctance, as function of rotor position and field current.

The machine energy conversion capacity is presented through the closed area given by the operating trajectory on the flux - current plane from un-aligned to aligned positions.

A magnetic saturated machine has a bigger energy conversion area for the same peak current, so the machine has to be designed with a small air-gap for pole aligned position, a machine with a significant magnetic saturation has a power factor two times larger than a not-saturated one.

For variable reluctance machines classical design methods cannot be applied, because of complications that appears because of different number of poles.

The most important element, which introduces difficulties in the design process, is the power electronic converter, the power supply of the switched reluctance machine.

When this kind of machine has to be designed we have to consider the difference between constant speed motor, supplied with sinusoidal three phase current, design and one motor for variable speed and power electronic converter design. Finally we have to consider that the machine will work on a wide torque and speed range, with implications on proper design of the cooling system.

There are more intrinsic design methods:

- linear methods;
- non-linear methods;
- finite element method, applied to the magnetic field, method that guide us to a direct estimation of machine performance and parameter determination.

2.3.1. Electromagnetic Power and Torque

Sizing the SRM is a very difficult task, mainly due to magnetic saturation but also due to the involved dependence of phase inductances on rotor position (not only on current). So,

we have to start sizing with some initial educated guess of a few variables and after the complete sizing to make the necessary verifications and adjusting to obtain a satisfactory practical design.

Let us suppose for the beginning that the rotor losses are of mechanical, p_{mec} and core (iron), p_{iron}, type.

The electromagnetic power (average value), P_{elm}, is:

$$P_{elm}= P_n+ p_{mec}+ p_{iron}\ [W] \tag{2.12}$$

At this stage of the design we only can assign a value for $p_{mec}+ p_{iron}$ as a function of the nominal power, P_n.

For the case in point we assume that:

$p_{mec}+ p_{iron} = K_0P_n$, where $K_0=0.03$, consequently:

$$P_{elm}= P_n+ K_0P_n \tag{2.13}$$

The electromagnetic torque (average value), T_e, is:

$$T_e=P_{elm}/2\pi n \tag{2.14}$$

2.3.2. Rotor Diameter and Stack Length

A new design variable will be now introduced; this is crucial for the machine sizing, the rated tangential force (f_0):

$$f_0 = \frac{2}{D_r} \times \frac{Te}{\pi L_{stack} D_r} \tag{2.15}$$

where: D_r – the rotor diameter;

L_{stack} – the stack length.

Generally, for self-ventilated machines with good efficiency: f_0= 0.5 - 2 N/cm^2 for torque levels between 0.5 and 5 Nm.

These values are good for starting the design process and after efficiency, weight and temperature assessments they may be adjusted accordingly.

The aspect ratio L_{stack}/D_r = 0.6 - 1.5 in most cases.

Let us adopt L_{stack}/D_r = 1 and f_0= 1.5 N/cm^3. From (3) and (4) we get:

$$D_r = \sqrt[3]{\frac{2 \times T_e}{f_0 \times \pi \times (L_{stack}/D_r)}} \text{ [m]} \qquad (2.16)$$

2.3.3. Stator and Rotor Poles, the Air-gap

The number of rotor poles, N_r, has to be chosen first. Basically N_r = 4 or 6. We choose N_r = 4, in this case the stator will have $N_s = 2xN_r$ = 8 poles.

The air gap should be as small as possible, a value g = 0.2 mm would be a practical choice for this case.

The stator teeth (poles) and slots structure shall now be dealt with. The stator core looks like that of a low power induction motor with a low number of slots.

The slot opening, W_{s0}, should be carefully chosen to reduce notably the slot leakage flux. A value W_{s0}=(15 - 20) x g seems adequate for the case. A too high value would increase the no torque zone and is not allowed.

As we have the slot openings, the stator tooth (pole) width is:

$$W_t = \frac{\pi(D_r + 2g) - 2Nr \times W_{SO}}{2Nr} \qquad (2.17)$$

The rotor pole has the same width as the stator pole. The rotor shaft, d_{shaft}, may be chosen, for torque range envisaged.

With a rotor pole height of:

$$h_{pr} = 0.6 \times W_t \qquad (2.18)$$

the rotor yoke is:

$$h_{yr} = \frac{1}{2} \times (D_r - d_{shaft} - 2xh_{pr}) \qquad (2.19)$$

To reduce somewhat the influence of magnetic saturation in the rotor, the rotor poles width is kept constant along the radial direction.

As we can se from finite element analysis, the stator shoe and body will be most saturated.

2.3.4. Coil m.m.f.

The saturation of the stator pole (tooth) zone close to the air gap – local saturation – is required to obtain good performance (if flux density in the stator pole shoe does not vary with rotor position – due to saturation – the flux will vary linearly with position).

Even in this case, if no current chopping is assumed for rated speed, the current will reach a maximum and then will decrease as the motion induced voltage reaches the level of the input d.c. voltage and thus the torque versus position will not be a constant quantity.

Consequently, a part from average torque, as peak torque, T_{peak}, may be defined.

Design experience shows that a ratio of even three between the peak and the average torque value is practical for the two phase machine:

$$K_t = T_{peak} / T_e = 3 \tag{2.20}$$

The ratio between peak current and RMS current / phase is close to K_t value.

$$K_i = K_t \tag{2.21}$$

Now, we have to adopt a saturated value for the local (pole shoe) flux density: $B_{gs} = 1.7$ T

Consequently, the peak ampere-turns $N_c I_{peak}$ is related to the peak torque by:

$$N_c I_{peak} = \frac{T_{peak}}{B_{gs} \times L_{stack} \times N_r \times D_r/2} \quad [\text{Aturns}] \tag{2.22}$$

where: N_c- number of turns/coil

The RMS ampere-turns is:

$$N_c \times I_n = N_c \times I_{peak} / K_i \quad [\text{Aturns}] \tag{2.23}$$

2.3.5. Stator Slot Sizing

Stator slot sizing is related to the design current, j_{cod}. The RMS current per phase during its conduction stage has been defined above through RMS m.m.f. per coil $N_c i_n$.

We should also notice that only half of time one phase is conducting, so in fact, the RMS current per phase is still $\sqrt{2}$ times smaller.

However, targeting for good (high) efficiency we will define $j_{cod} = 6$ A / mm^2 and notice that $N_c i_n$ is the only m.m.f. active at any time like if the losses in the windings are produced by one (only) phase. This observation is important for thermal design and when calculating the winding losses.

Also the slot-filling factor has to be chosen $K_{fill} = 0.38$ only since there are two coils in one slot.

The slot area is:

$$A_{slot}=2 \times N_c I_n / j_{cod} \times K_{fill} \quad [m^2] \tag{2.24}$$

Let us assume a pole width, W_p and a useful slot (pole) height, h_{su}, the slot widths, interior and exterior are:

$$W_{s1} = \frac{\pi(D_r + 2g + 5) - 2N_r \times W_p}{2N_r} \quad [m] \tag{2.25}$$

respectively:

$$W_{s2} = \frac{\pi(D_r + 2g + 5 + 2h_{su}) - 2N_r \times W_p}{2N_r} \quad [m] \tag{2.26}$$

Consequently, the slot area would be:

$$A_{slot} = h_{su} \frac{W_{s1} + W_{s2}}{2} \quad [m^2] \tag{2.27}$$

2.3.6. Number of Turns per Coil

The pole angle is:

$$\theta_p = (2\pi/8) \times \frac{W_p}{W_p + W_{s0}} \quad [rad] \tag{2.28}$$

Let us assume that the conducting (useful) angle, θ_u, is:

$\theta_u = (2/3) \times \theta_p$ (18)

The peak phase flux will be reached after an angle θ_m:

$$\lambda_{\nu peak} = \frac{V_0 \theta_u}{\Omega_r} \quad [Wb] \tag{2.29}$$

where:

$$\Omega_r = 2\pi m \quad [rad/s] \quad \text{is rotor speed} \tag{2.30}$$

and V_0 – is the d.c. supply voltage

On the other hand, the peak phase flux is:

$$\lambda_{peak} = B_{gs} W_t L_{peak} N_c \frac{\theta_u}{\theta_p} N_r \quad [Wb] \tag{2.31}$$

Considering a value for V_0 (corresponding to a single phase power grid), the number of turns per coil, N_c, is obtained.

So, the peak and rated currents can be now calculated to make sure that the rated power at rated speed even with 10% reduction in the d.c. input voltage, are obtained.

2.3.7. Wire Gauge

The wire gauge, d_{co}, may be determined based on knowing the RMS current and corresponding design current, $j_{cod} = 3...6$ A/m.

$$d_{co} = \sqrt{\frac{4 i_n}{\pi j_{cod}}} \quad [m] \tag{2.32}$$

Now we have the wire gauge and each coil will be made using wire with F class of insulation.

2.3.8. Phase Resistance and Slot Resizing Attempt

Each phase is made of N_r coils connected in series. Consequently the phase resistance, R_s, is:

$$R_s = N_r \frac{\rho_{co} l_{coil}}{A_{co}} N_c \qquad [\Omega] \tag{2.33}$$

where: ρ_{co} - the copper resistivity

$$l_{coil} = 2L_{pac} + 2W_p + 2W_{s2} \qquad [m] \tag{2.34}$$

is the coil length.

The rms losses (for both phases) in the windings are:

$$p_{co} = R_s i_n^2 \qquad [W] \tag{2.35}$$

2.3.9. Stator Yoke

The stator yoke height, h_{ys}, has to be sized from both mechanical and magnetic considerations.

To avoid over-saturation in the yoke zone, we assume:

$$h_{ys} > W_p / 2 \qquad [m] \tag{2.36}$$

So, the external diameter – on the square lamination size is:

$$D_0 = D_r + 2g + 2h_{su} + 2h_{ys} \quad [m] \tag{2.37}$$

2.3.10. Phase Flux Linkage versus Current and Position $\lambda(i, \theta_r)$

This function is obtained through FEM analysis. However, an approximate analytical solution could be available for preliminary design purpose, especially in calculating the steady state and dynamics of the drive.

Based on many FEM and tests results it seems that is practical to approximate the $\lambda(i, \theta_r)$ by straight-line segments, as indicated in figure 2.3.

The minimum flux is obtained for $\theta_r = 0$:

$$\lambda = L_{ua}\, i \ \ [Wb] \tag{2.38}$$

The unaligned value of the phase inductance, L_{ua}, is composed of the leakage inductance, L_{ual} and the air-gap component, L_{uag}:

$$L_{ual} = L_{uals} + L_{uale} \ \ [H] \tag{2.39}$$

where:

$$L_{uale} = 2N_r\, N_c^2\, \mu_0\, p_e\, L_{stack} \tag{2.40}$$

with :

$$p_e = 0.34(l_{ec} - 0.64y) / L_{stack} \tag{2.41}$$

and

$$L_{uals} = 2N_r\, N_c^2\, \mu_0\, p_{slot}\, L_{stack} \tag{2.42}$$

with

$$p_{slot} = (l_{s0} / W_{s0}) + [2l_{s0} / (W_{s0} + W_{s1})] + [2h_{ss} / 3(W_{s1} + W_{s2})] \ [W] \tag{2.43}$$

where: y – coil width

$$y = W_p + (W_{s1} + W_{s2}) / 2 \ [m] \tag{2.44}$$

and l_{ec} – coil end connection length (on one side)

$$l_{ec} = W_p + W_{s2} \ \ [m] \tag{2.45}$$

The useful not saturated phase inductance is:

$$L_{uag} = N_r\, N^2 \mu_0 L_{cap}(W_{ps} + W_{s0}) \sum_n \frac{\left[\sin \frac{n\pi W_{s0}}{W_{s0} + W_{ps}} + \sin \frac{n\pi (W_{s0} - W_{ps})}{W_{s0} + W_{ps}} \right] \frac{1}{W_{s0}}}{(n\pi)^2 \tanh \frac{n\pi h_{ps}}{W_{s0} + W_{ps}}} \tag{2.46}$$

The ideal maximum flux for $\theta_r = \theta_c$ and $i = i_{max}$ (point A from figure 2.3) is:

$$\lambda_{max} = N_r\, N_c\, B_s\, W_p\, L_{pac}\, \theta_u / \theta_p \qquad [Wb] \tag{2.47}$$

For point B, we will have:

$$\lambda_B = \lambda_{max} - L_{ua}(i_{max} - i_0) \tag{2.48}$$

In the above mathematical expressions all dimensions are known and so, we can determine the magnetic flux for each point for a variation of the rotor angle, θ_r, from 0 to θ_c for both phase.

In this way, for phase A:

$$\lambda_A = \lambda_B (\theta_r i / \theta_c i_0) - L_{ua} i; \text{ for } i \leq i_0 \quad (2.49)$$

$$\lambda_A = \lambda_B (\theta_r / \theta_c) - L_{ua} i; \text{ for } i \geq i_0 \quad (2.50)$$

Those are valid for phase B, too, considering the firing angle, which is θ_c, so, $\theta_r = 0$ for phase A, means $\theta_r = \theta_c$ for phase B. We will obtain:

$$\lambda_B = \lambda_B (\theta_c - \theta_r) i / \theta_c i_0] - L_{ua} i; \text{ for } i \leq i_0 \quad (2.51)$$

$$\lambda_B = \lambda_B [(\theta_c - \theta_r) / \theta_c] - L_{ua} i; \quad \text{for } i \geq i_0 \quad (2.52)$$

These functions are recurrent, so, the θ_r angle can be maintained between 0 and θ_c limits by choosing the zero value any time it reaches the θ_c value.

The above flux/current/position curves should serve for the computation of the steady state waveform of current and flux versus time and for steady state and dynamic performances. The power electronic sizing is dependent on these aspects also.

The electrical time constant for unaligned position is:

$$T_{ua} = L_{ua} / R_s \text{ [s]} \quad (2.53)$$

2.3.11. Core Losses Model

To calculate the core losses, the time variation of flux density in the rotor and stator laminations – poles and yokes – has to be known.

As the magnetic saturation varies locally and is dependent also on the machine control (turn on and turn off angles, speed etc.) the flux density variation (in the core) with position and time is very difficult to calculate.

Two approximate models for core losses have been already introduced, requested for preliminary design purpose. [2.38]

They are based on Fourier series decomposition of flux density time variation or using directly the dB/dt values. In what follows we will adopt the last method to the case of the two-phase machine.

To simplify the computation process we will consider that the flux in the stator and rotor poles varies linearly up and down and only the peak values depend on speed (frequency in fact). Also we consider that there is no overlapping between the two phases.

We now proceed to develop expressions for the core loss, we can start using Steinmetz formula:

$$p_{core} = C_h f B_m^{a+bBm} + C_e f^2 B_m^2 \quad [W] \tag{2.54}$$

where: C_h and C_e are hysteresis and eddy current coefficients.

Let's change the dB/dt by $2\pi fB$, results: $C_{el} = C_e/(2\pi)^2$ - depends on the type of alloyed steel and lamination thickness.

The eddy current losses for the stator and rotor are spread as follows:

- for the poles:

$$p_{spe} = \frac{\omega_r}{2\pi} N_s N_r W_{sp} E(B_{spm}) \quad [W] \tag{2.55}$$

$$p_{rpe} = \frac{\omega_r}{2\pi} N_s N_r W_{rp} E(B_{rpm}) \quad [W] \tag{2.56}$$

Where: W_{sp}, W_{rp} – are the rotor and stator poles weights

$E = C_{el}(B_m)^2(2/T_r)$ and $T_r = 1/(2nN_r)$

Similar, we can obtain for the rotor and stator yokes:

$$p_{sye} = \frac{\omega_r}{2\pi} N_s N_r W_{sy} E_e(B_{sym}) \quad [W] \tag{2.57}$$

$$p_{rye} = \frac{\omega_r}{2\pi} N_s N_r W_{sy} E_e(B_{sym}) \quad [W] \tag{2.58}$$

The hysteresis losses can be divided similar for each component:

$$p_{sph} = \frac{\omega_r}{2\pi} N_s N_r W_{sp} E_h(0, B_{spm}) \quad [W] \tag{2.59}$$

$$p_{rph} = \frac{\omega_r}{2\pi} N_s N_r W_{rp} [E_h(0, B_{rpm}) + E_h(-B_{rpm}, B_{rpm})] \quad [W] \tag{2.60}$$

$$p_{syh} = \frac{\omega_r}{2\pi} N_s N_r W_{sy} [2E_h(B_{sym}) + E_h(-B_{sym}, B_{sym})] \quad [W] \tag{2.61}$$

$$p_{ryh} = \frac{\omega_r}{2\pi} N_s N_r W_{ry} [E_h(0, B_{rym}) + E_h(-B_{rym}, B_{rym})] \quad [W] \tag{2.62}$$

2.3.12. Efficiency

The rated efficiency of the machine is given as follows:

$$\eta_n = \frac{P_n}{P_n + \sum \text{losses}} \tag{2.63}$$

and it has maximum values between 0.86 and 0.87.

2.3.13. Active Materials Weight

For machine's stator and rotor core we have next components:

$$W_{lam} = W_{spt} + W_{rpt} + W_{syt} + W_{ryt} \quad [kg] \tag{2.64}$$

The copper weight is:

$$W_{copper} = N_s l_{coil} A_{co} \gamma_{co} \quad [kg] \tag{2.65}$$

We will add the accessories weights of the machine, bearings, frame etc.

2.3.14. Simplified Thermal Verifications

We will essentially verify the stator temperatures considering that no transmission of heat from stator to rotor (and vice versa) takes place.

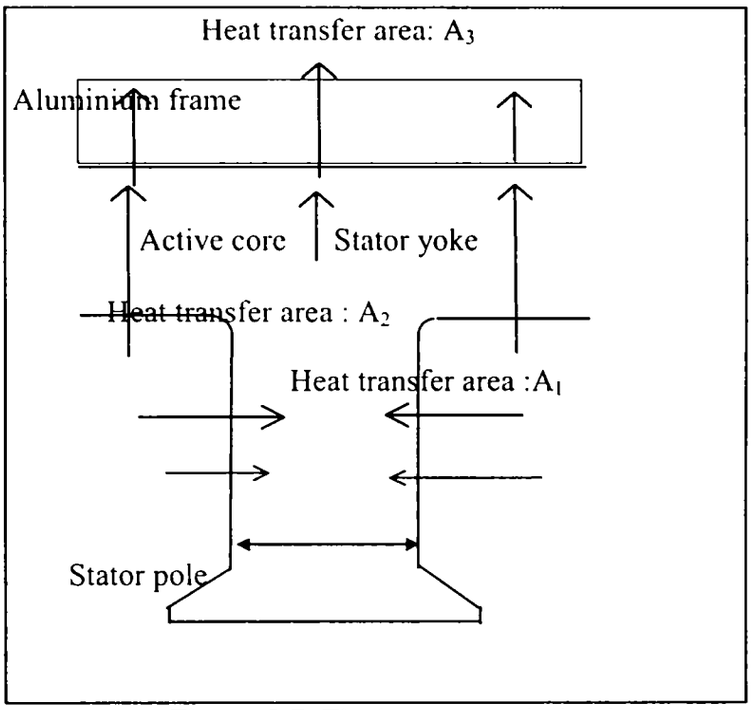

Figure 2.7. The heat transmission in the stator

Further on, we may investigate one pole zone only. The total copper losses will be considered in the heat transfer from slot to iron.

The copper losses per pole are:

$$p_{cop} = p_{co} / N_s \quad [W] \tag{2.66}$$

The core losses per stator pole are:

$$p_{Fep} = p_{Fe} / N_s \quad [W] \tag{2.67}$$

There are three main temperature gradients:

- conductor to iron through the insulation, θ_{co}
- iron to the cooling air, θ_{cos}
- cooling air to the ambient, θ_{coa}

For these gradients we have the calculation equations as follows:

$$\theta_{co} = p_{cop} \times b_s / [\lambda_{hs} 2(A_1 + A_2)] \tag{2.68}$$

$$\theta_{cos} = (p_{cop} + p_{Fep}) \times \frac{1}{\alpha A_3} \tag{2.69}$$

θ_{coa} = 10 [°C] for a ventilated air speed of v_s = 10 [m/s] (2.70)

So, the winding over-temperature above the ambient:

$$\Delta\theta_{co} = \theta_{co} + \theta_{cos} + \frac{\theta_{coa}}{2} \quad [°C] \tag{2.71}$$

We may consider the rotor loss contribution (mechanical and core losses) to the above over-temperature. Anyway, this is acceptable for a class F insulation wire.

A complete thermal model, or tests on a prototype are required for a more precise assessment of thermal behavior of 2P-SRG

2.4. Sample Design Results

Using the equations and presumptions from the previous paragraph, a numerical example data will be presented in what follows.

The basic specifications for the 2P-SRG virtual prototype are:

- Rated power: P_n = 1kW;
- Rated speed: n_n = 3000rpm;
- Maximum speed: n_{max} = 4500rpm (for an output power equal to the rated one);
- A.C. grid: single phase a.c. 50Hz, 220V;
- Variable speed range: (3000 – 4500)rpm;
- Motion sensors: none;
- Number of switches: minimum (2).

The output data are:

P_{elm} = 1030 [W]

T_e = 3.28 [Nm]

D_r = 0.052 [m] for f_0 = 1.5 [N/cm^2]

L_{stack} = 0.052 [m]

W_t = 16.56x10^{-3} [m] for g = 0.2x10^{-3} [m], W_{s0} = 15xg and N_r = 4

h_{pr} = 10x10^{-3}[m] for d_{shaft} =14 x10^{-3}[m]

h_{yr} = 9x10^{-3}[m]

T_{peak} = 9.84 [Nm] for K_t = 3

$N_c i_{peak}$ = 802 Ampere turns

$N_c i_n$ = 476 Ampere turns for K_i = 2.25

A_{slot} = 375x10^{-6}[m^2] for j_{cod} = 6.65 [A/mm^2]

W_{s1} = 10.5x10^{-3}[m] for W_p = 12x10^{-3}[m] and h_{su} = 20x10^{-3}[m]

W_{s2} = 26.22x10^{-3}[m] and so results a slot area of: A_{slot}' = 367.3x10^{-6}[m^2] (about the same as A_{slot});

θ_p = 0.6322 [rad]

Ω_r = 100π

λ_{peak} = 0.15597 [Wb]; for θ_u = 24^o

N_c = 51 turns/ coil (we choose N_c = 40); for V_0 =150 [V] d.c.

I_{peak} = 26.7 [A]

$I_n = 11.9$ [A]

$d_{co} = 1.5x10^{-3}$[m]

$R_s = 0.342$ [Ω]

$l_{coil} = 0.18046$ [m]

$p_{con} = 48.367$ [W]

$p_{copeak} = 137.85$ [W]

$h_{ys} = 9x10^{-3}$[m]

$D_o = 115.2x10^{-3}$[m]

$\lambda_{max} = 0.155$[Wb]

$L_{uag} = 8.768x10^{-4}$[H]

$y = 34.935x10^{-3}$[m]

$l_{ec} = 42.81x10^{-3}$[m]

$p_{slot} = 0.81$

$p_e = 0.1336$

$L_{ua} = 16.65\ x10^{-4}$[H]

$L_B = 0.1343$ [Wb]

$K_{speak} = 2.9527$

$K_{s0} = 1.0378$

$W_{pst} = 0.831$ [kg]

$W_{prt} = 0.261$ [kg]

$p_{spe} = 1.176$ [W]

$p_{rpe} = 0.741$[W]

$E_{esel} = 0.00312$ [J/kg]

$W_{sy} = 0.14$ [kg]

$W_{ry} = 0.06$ [kg]

$p_{sye} = 1.48$ [W]

$p_{rye} = 0.32$ [W]

$p_{sph} = 5.7638$ [W]

$p_{syh} = 16.48$ [W]

$p_{rph} = 12.71$ [W]

$p_{ryh} = 5.52$ [W]

$p_{Fe} = 44.19$ [W]

$\eta_n = 0.893$ for $p_{mec} = 27$ [W]

$W_{lam} = 2.4568$ [kg]

W_{copper} = 1.033 [kg]

W_{tot} = 3 [kg] that means we obtain a 2P-SRG with a 3 [kg/kW]

p_{cop} = 6.045 [W]

p_{Fep} = 2.64 [W]

θ_{co} = 7.045 [°C]

θ_{cos} = 67.74 [°C] for air speed of v_s = 10[m/s]

θ_{coa} = 10 [°C]

$\Delta\theta_{co}$ = 80 [°C]

Having all the above data, a virtual prototype, which may be used for analysis using the FEM and after some verification, a real prototype may be erected, too.

2.5. Numerical Analysis of the Electromagnetic Field for the 2P-SRG Through Finite Element Method (FEM)

The finite element method is a general numerical analysis method that belongs to the class of direct analysis and design methods, this provides an approximately solution for the field problem and with its help we can model complicate geometries and non-linear magnetic materials. [2.8]

The field outline is made from a finite number of triangles; the field inside each triangle is specified as a function of triangle nodes values. [2.9] This method is increasingly used for electric machine design, especially for electromagnetic field and its parameters determination studies.

With help of ANSOFT-MAXWELL© - finite element analysis program, from MIR (Movement Intelligent Regulation) laboratory, Department of Electrical Engineering, University "Politehnica" of Timisoara endowment, magnetic circuits for different geometrical structure of SRG were studied.

Starting from the structure of an existing standard three phase squirrel cage machine, with twelve stator poles, we change it's rotor by the way of making it as a rotor with six preeminent poles, characteristic for a switched reluctance machine. We proposed to analyze this new machine using the FEM.

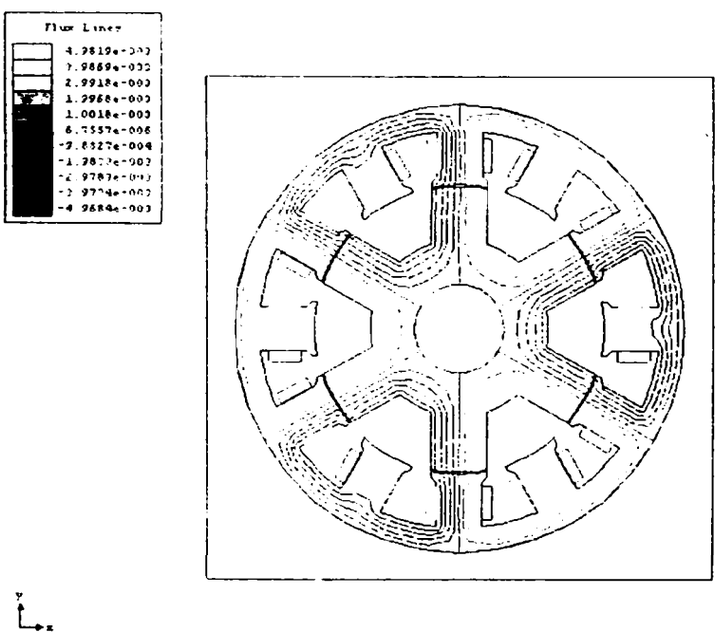

Figure 2.8. The electromagnetic field of the proposed SRG, first geometrical structure

Figure 2.9 shows us the electromagnetic field through finite element method of analysis for the resulted three phase switched reluctance machine, keeping the pole shoes for the stator poles and having the rotor poles width equal with the stator pole shoes.

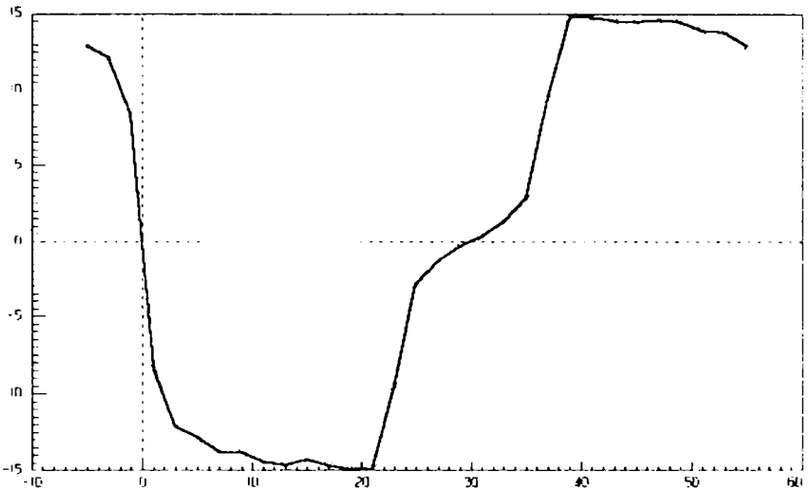

Figure 2.9. The resulting phase torque [Nm/u.l.] vs. rotor position

The result of this first analysis that the proposed geometrical structure is not the optimal one, the main reason is the existence of a high leakage flux, given by the presence of the stator pole shoes, and the small value of the torque through phase coil excitation.

As a direct consequence we decided to change the machine geometry by pulling out the pole shoes, keeping the rotor poles with the same width (see figure 2.10).

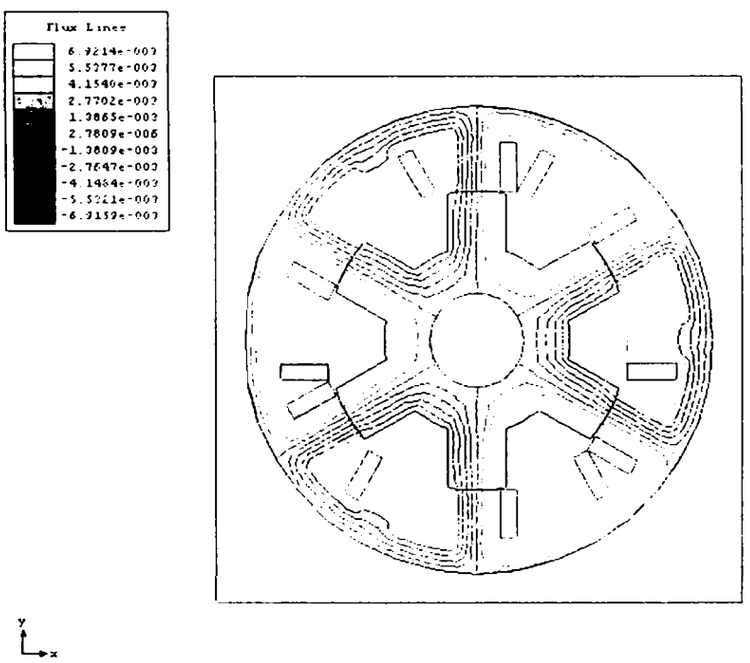

Figure 2.10. The electromagnetic field of the SRG after second geometric change

After this new analysis, the results became more encouraging and are presented in figure 2.11, 2.12, and figure 2.13:

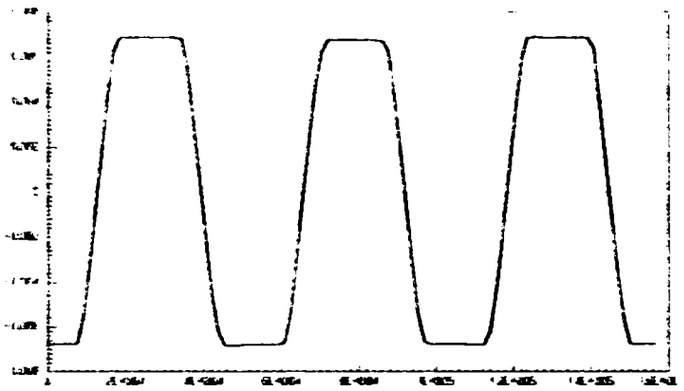

Figure 2.11. The air-gap flux waveform [Wb/u.l.]

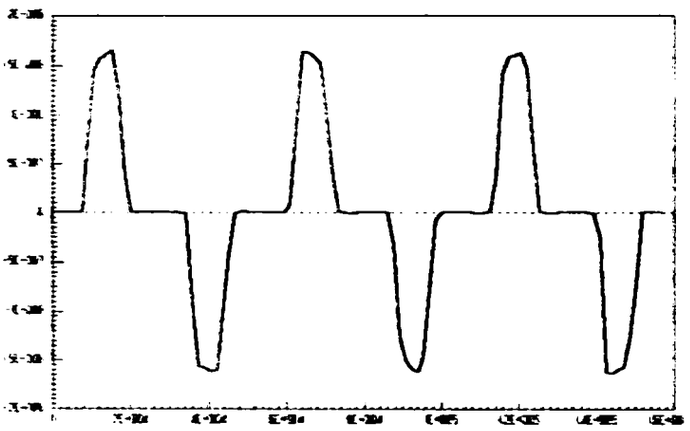

Figure 2.12. The air-gap magnetic flux density variation [Tx10^6]

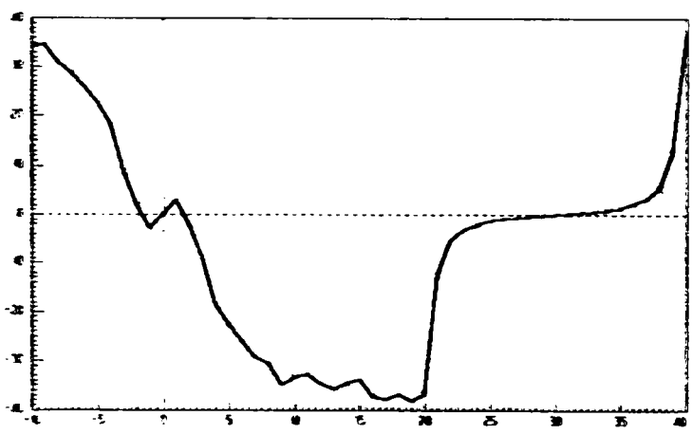

Figure 2.13. The phase torque [Nm/u.l.] vs. position

We can remark a better phase torque production, for the same ampere-turns in the phase coils (to respect the same conditions as in the previous case), much larger than before

(double), so, only by cutting out of stator pole shoes we obtained an improvement for both, the air-gap magnetic flux and the phase torque.

To have a complete image of this study, we did study the geometrical alternative where the rotor poles are re-sized to have the width equal to two times the stator pole width, like presented in figure 2.14.

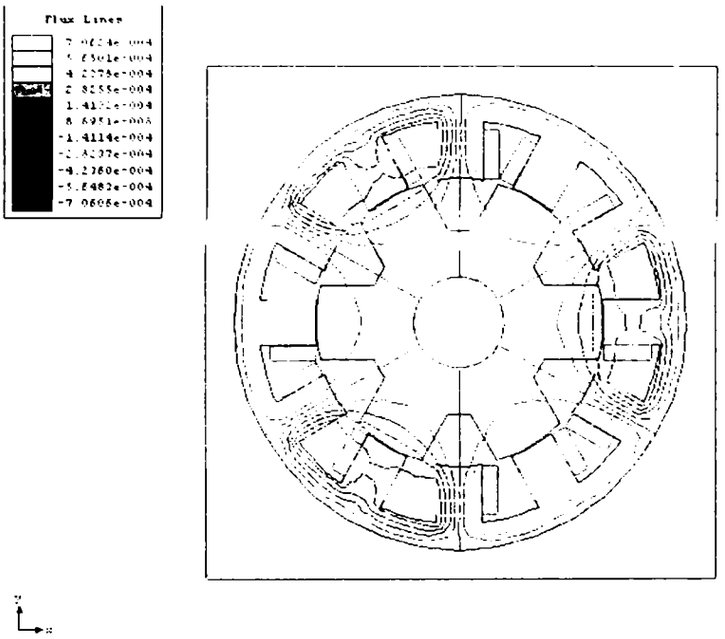

Figure 2.14. The electromagnetic field distribution for the third geometrical structure

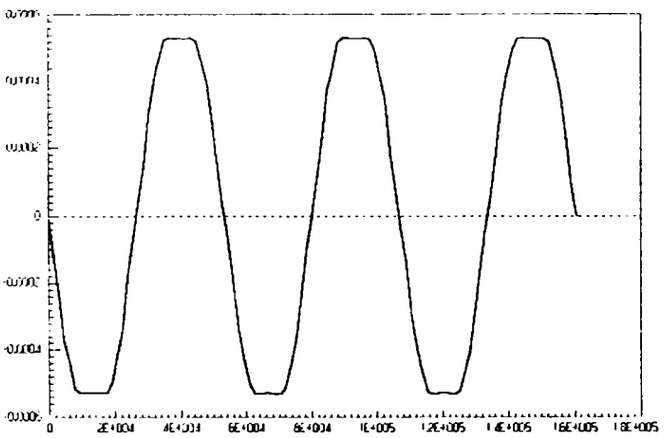

Figure 2.15. The air-gap flux waveform [Wb/u.l.]

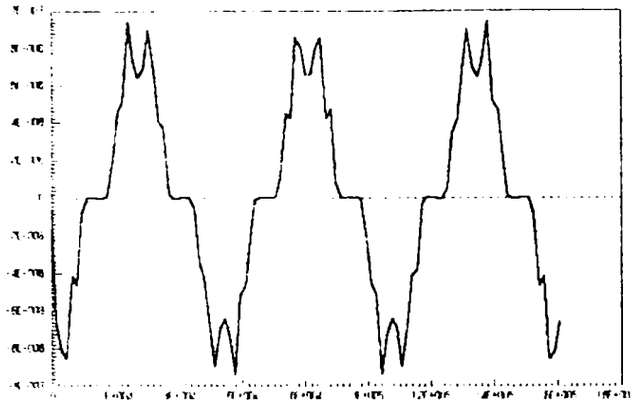

Figure 2.16. The air-gap magnetic flux density variation [Tx10^6]

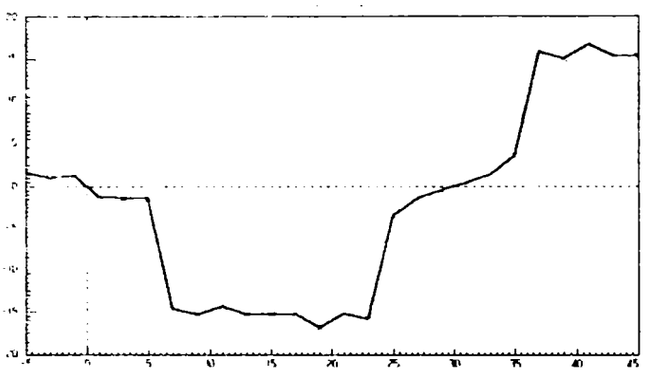

Figure 2.17. The phase torque [Nm/u.l.] vs. rotor position

Another alternative solution studied using the FEM analysis is that were the rotor poles width is modified to become equal to the stator poles width, in order to respect the classical SRM geometry. The new geometrical structure gives us the following results, figure 2.18, 2.19 and figure 2.20.

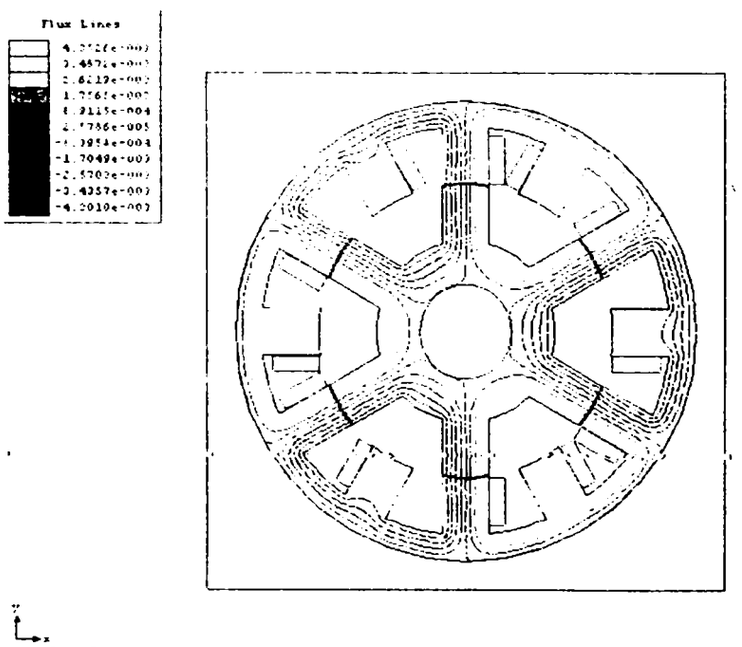

Figure 2.18. The electromagnetic field distribution for the fourth geometrical structure

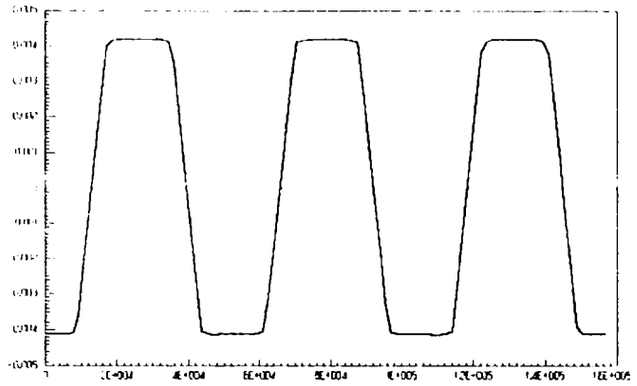

Figure 2.19. The air-gap flux waveform [Wb/u.l.]

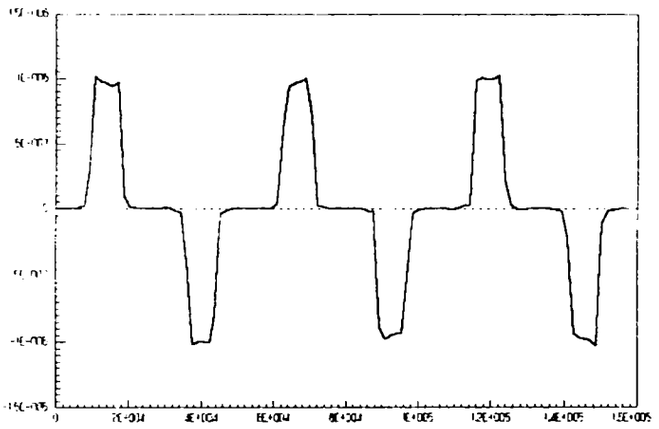

Figure 2.20. The air-gap magnetic flux density variation [Tx10^6]

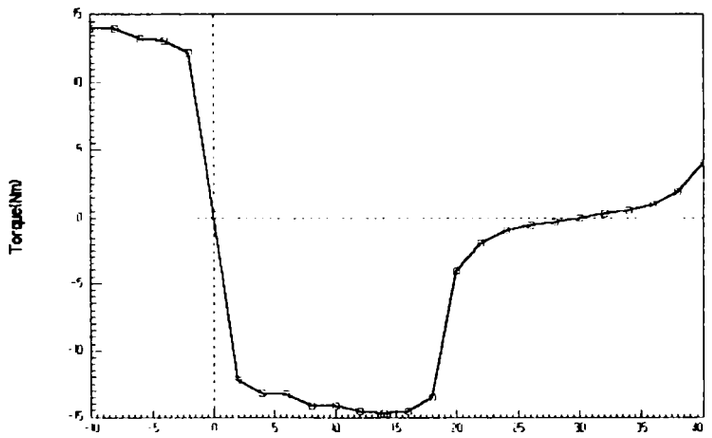

Figure 2.21. The phase torque [Nm/u.l.] vs. rotor position

One of the geometrical structure for a two phase Switched Reluctance Generator with shaded poles, having eight stator poles and four rotor poles was studied using the finite element method. The finite elements network is presented in next figure, each phase is

constituted from two coils placed on opposite stator poles, and al machine poles are straight.

For the new type of SRG, proposed as an alternative solution to the actual claw pole generators in automobile industry, numerical analysis based on the FEM were done to find the air-gap flux and torque, respecting the geometrical dimension resulted from the design procedure introduced in the previous part of the chapter.

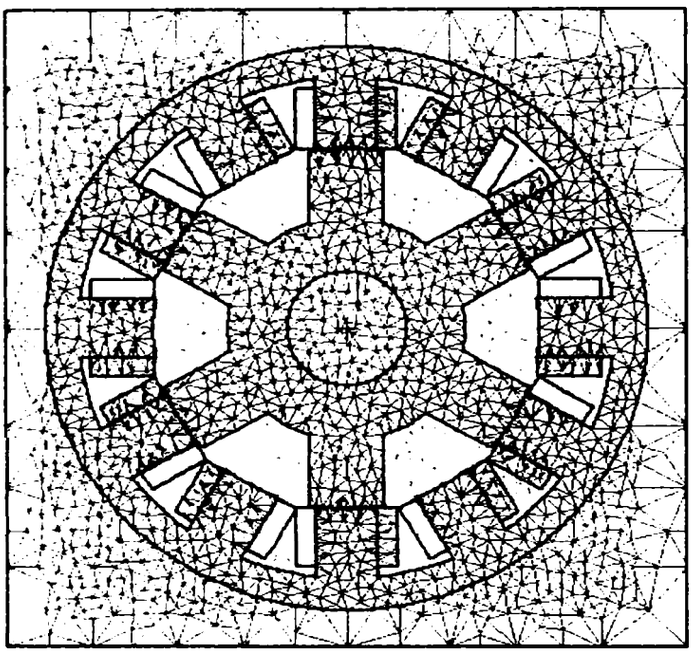

Figure 2.22 The 2P-SRG grid, for numerical analysis using the finite element method

It can be easily observed the finite element network symmetry and the changeable number of triangles, choose independently for each area, sufficiently high for a fast and correct result.

The electromagnetic field distribution is presented by magnetic flux lines like in the following figure, for the aligned position of the poles. The over-saturated area in the stator yoke can be emphasized.

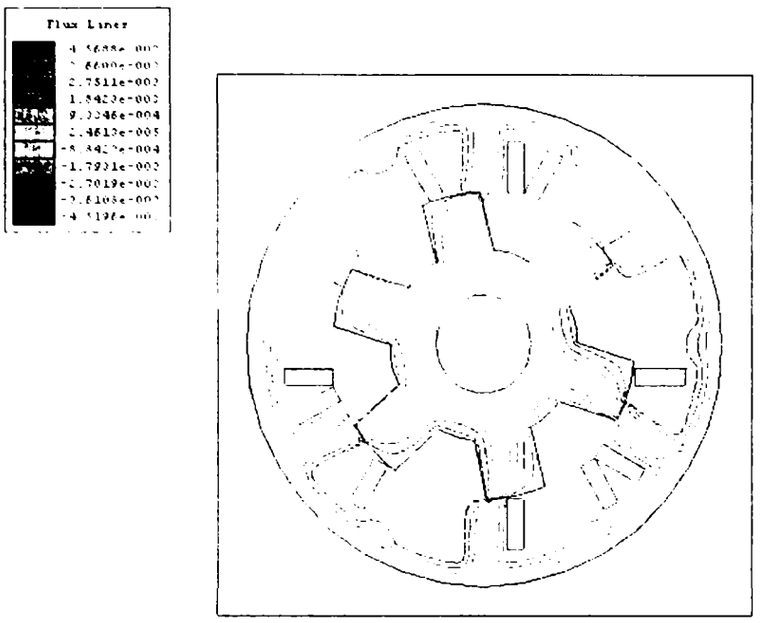

Figure 2.23 The electromagnetic field distribution for the not-aligned poles position

It can be observed, from the field lines, that for the not-align position of the rotor poles with the stator poles of the excited phase, a relative large leakage electromagnetic field appears which is closing through the stator poles of the other phase.

The align position of the rotor poles with the stator poles of the excited phase is not presented here, this time we consider a 2P-SRG having the stator poles without pole shoes and with a trapezoidal geometry, used to guide the electromagnetic field through the air-gap, so, to saturate locally the machine.

From the electromagnetic torque variation with rotor position for this type of trapezoidal stator poles (for flux concentration), it can be easily observed that the machine has a zero torque for the un-aligned poles position ($\theta_r = 22.5^0$).

Using the finite element method, we can compare the torque variation with position, as indicated in figures 2.24 and 2.25, if an over-saturated area is made in the stator yoke, or not.

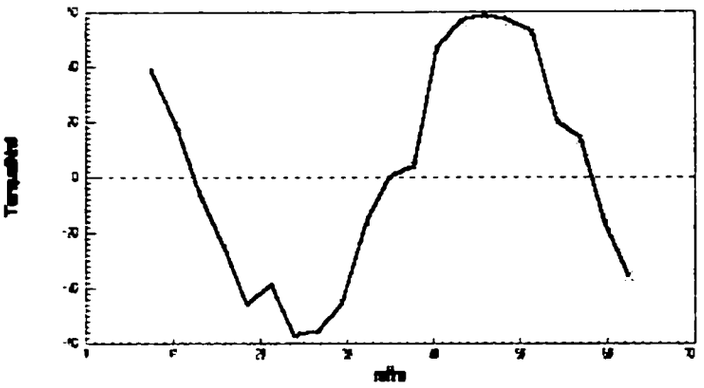

Figure 2.24. Torque variation [Nm/u.l.] against rotor position for a machine having an over-saturated area in the stator yoke

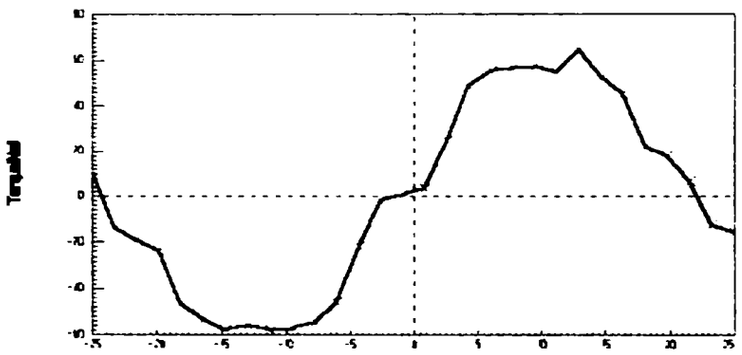

Figure 2.25. Torque variation [Nm/u.l.] against rotor position for a machine without an over-saturated area

An influence of the over-saturated area from the stator yoke in the way of obtaining a bigger value for the torque in the align position of the poles can be observed but with a high torque ripple.

The torque area is larger for the machine without an over-saturated area.

Because of their robustness, high-speed operation capability and fault tolerant characteristics, the need for the switched reluctance machines for special use like power generators for aeronautic industry or other applications, is continuously growing.

For the switched reluctance machine design, we need to calculate the produced torque using the selected geometrical size, so, an important contribution has the determination and plot of the magnetic flux or of the phase reluctance, as a function of the rotor position and the phase excitation current (fig. 2.26). [2.28]

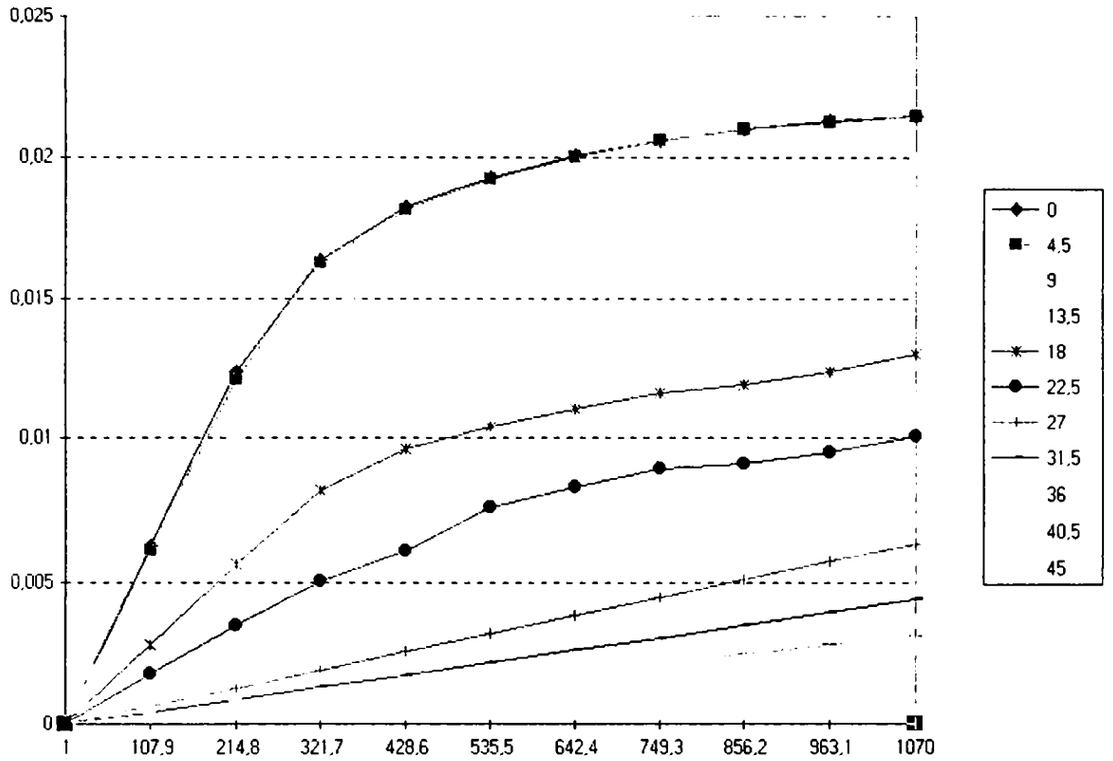

Figure 2.26. The phase magnetic flux [Wb] variation as function of rotor position and phase excitation m.m.f. [Aturns]

The saturated switched reluctance machine has a larger energy conversion area for the same excitation peak current, so, the switched reluctance machine must be designed with a small air-gap for the aligned poles overlapping position, the machine with a large magnetic saturation coefficient has a power factor two times bigger than a not-saturated one. [2.29]

The torque versus position variation is represented in figure 2.28 and is requested to define the control strategy of the machine.

Using the finite element method of analysis for a two phase switched reluctance generator with 6 rotor poles and 12 stator poles, the impact of different rotor geometries has been studied, a part of the most important results were presented.

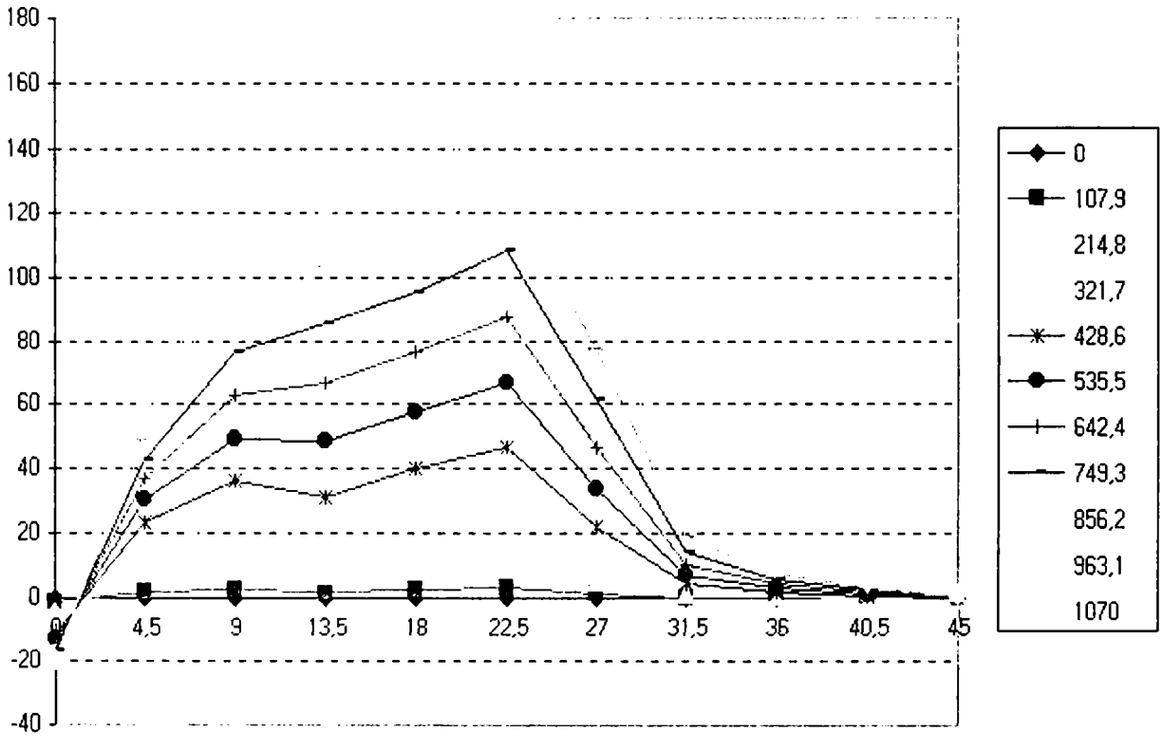

Figure 2.27. Torque [Nm] vs. rotor position waveforms for different Aturns on phase coils

For an easier network definition and a fast field and torque calculation for the first FEA studies, we used a straight structure for the stator poles.

2.6. Model for Transients

The mathematical model used for digital simulations of the SRG-2P is included in equations 2.1 to 2.6, as follows:

$$\frac{d\lambda_a}{dt} = i_a R_s - V_a(\theta_r)$$

$$\frac{d\lambda_b}{dt} = i_b R_s - V_b(\theta_r)$$

$$\frac{d\omega_r}{dt} = (T_e - T_m) / J$$

$$\frac{d\theta_r}{dt} = \omega_r$$

$$T_e = \lambda_m \frac{1}{\theta_c} \frac{i_a^2}{2i_0} + \lambda_m \frac{-1}{\theta_c} \frac{i_b^2}{2i_0} ; \qquad \text{for } i_a , i_b \le i_0$$

$$T_e = \lambda_m \frac{1}{\theta_c} (i_a - i_b) ; \qquad \text{for } i_a , i_b \ge i_0$$

The phase flux depends on rotor relative position against the stator poles of one phase, for phase A we can write:

$\lambda_a = L_{ua} i$ for the un-aligned position;

$\lambda_a = \lambda_m i / i_0 + L_{ua} i$; for $i \le i_o$ and $\theta_{er} \le \theta_c$

$\lambda_a = \lambda_m + L_{ua} i$; for $i \ge i_0$ and $\theta_{er} \le \theta_c$

A similar function may be assign for the decreasing area of the flux.

For phase B we proceed in the same way, the lonely difference is in choosing the angle.

The block diagram of the torque-controlled machine together with the transfer functions is included in next figure:

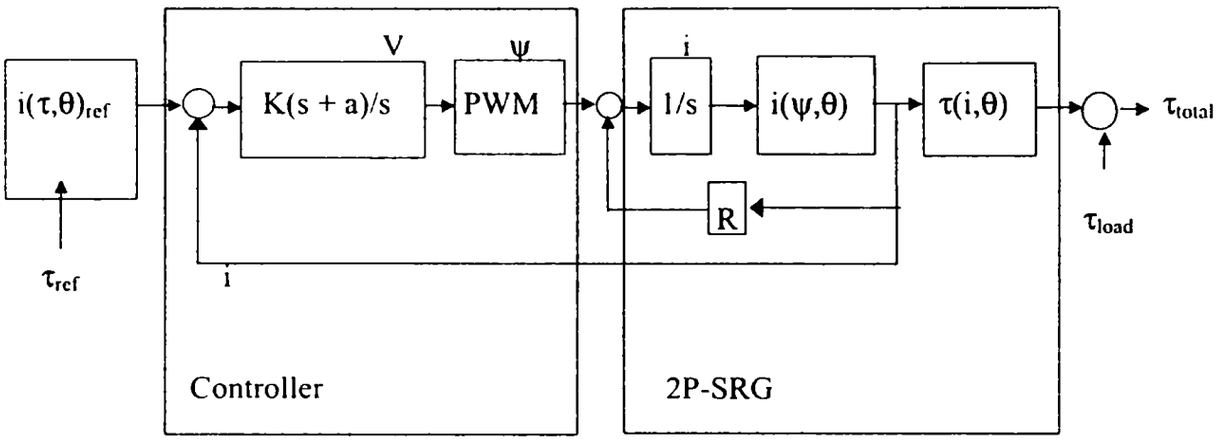

Figure 2.28. The model of the control system for a 2P-SRG

2.7. A sensor-less Control Solution

Because of the advantages offered by the sensor-less systems, such kind of a system is proposed for study.

The system is using for rotor position identification only one current Hall sensor, placed between the two phase of the machine.

With help of the gradient method, which uses the phase current derivate to determine the relative position of the rotor poles against the stator poles. So, knowing the poles structure, we can determine the rotor position.

The most important element of the generative system that introduces some design complications is the power electronic converter, the supplying/exciting source of the switched reluctance generator.

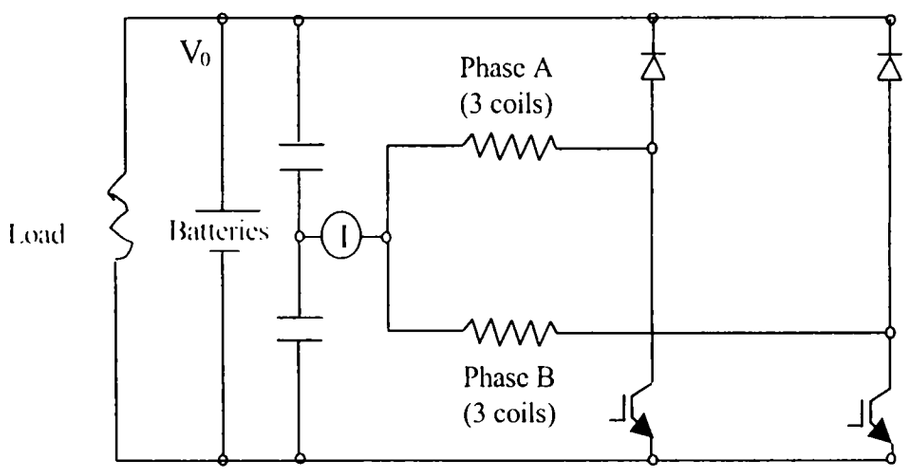

Figure 2.29. The basic scheme of a generating system for 14 V d.c. bus, using the 2P-SRG

When we design such a machine, we have to make the difference between the calculations for a three phase sinusoidal supplied machine that operates at constant speed and the calculations for a machine that operates at variable speed being supplied through a power converter.

For the last case, we will consider the fact that the machine is working on a large range of speeds and torques, fact that implies some considerations to take regarding the cooling aspect, which can be studied using the 2D-FEA.

Control Strategy

Each phase is supplied at a certain firing angle θ_{on} , which varies with the speed, and is disconnected at the angle θ_{out} - constant.

Phase A		Phase B	
θ_{on}	θ_{out}	θ_{on}	θ_{out}
$0 - \theta_{\omega}$	θ_{cr}	$45° - \theta_{\omega}$	$45° + \theta_{cr}$
$90° - \theta_{\omega}$	$90° + \theta_{cr}$	$135° - \theta_{\omega}$	$135° + \theta_{cr}$
$180° - \theta_{\omega}$	$180° + \theta_{cr}$	$225° - \theta_{\omega}$	$225° + \theta_{cr}$
$270° - \theta_{\omega}$	$270° + \theta_{cr}$	$315° - \theta_{\omega}$	$315° + \theta_{cr}$

$\theta_{\omega} = 0$ for speed up to $n < 1500$ rot/min.

$\theta_{\omega} = 4.5°(n - 1500)/1500$ for speed more than $n \geq 1500$ rot/min.

To produce a negative torque, for breaking capability, the control strategy is as follows:

Phase A		Phase B	
θ_{on}	θ_{out}	θ_{on}	θ_{out}
$45° - \theta_{\omega}$	$45° + \theta_{cr}$	$0° - \theta_{\omega}$	θ_{cr}
$135° - \theta_{\omega}$	$135° + \theta_{cr}$	$90° - \theta_{\omega}$	$90° + \theta_{cr}$
$225° - \theta_{\omega}$	$225° + \theta_{cr}$	$180° - \theta_{\omega}$	$180° + \theta_{cr}$
$315° - \theta_{\omega}$	$315° + \theta_{cr}$	$270° - \theta_{\omega}$	$270° + \theta_{cr}$

For the beginning, the torque control is done through current control instead of angle control.

In a subsequent stage, the firing angle control shall be used for an efficient optimization of the machine control.

The OULTON connection scheme is presented in the next figure. This circuit is used for the four phase drives, with IGBT transistors and GTO thyristors. It has the advantage of allowing the voltage reversing in order to reduce the magnetic flux and of operating with only one power device for each phase, without adding other passive component or sacrificing the flexibility of the control.

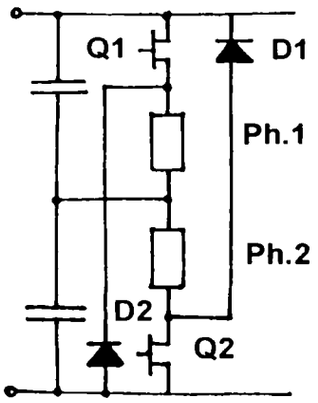

Figure 2.30. The OULTON scheme

The d.c. voltage from the battery is divided with the help of the capacitors. The main disadvantage of this scheme is that it doesn't allow a soft chopping and the balance between the two phase must be carefully maintained.

Any fault determines an increase of the capacitors voltage that's why we use only half of the supply voltage, $\frac{V_S}{2}$ for each phase.

Many control strategies are proposed or already used for the switched reluctance machine, starting from simple fuzzy-logic voltage control and continuing with other more complicated strategies.

Because the specialized literature offers us plenty of digital simulations and control strategies, no digital simulations will be done here, anyway this may be a proper subject for the further researches in this field of electric generators for automobile industry.

2.8. Conclusion

This chapter transposes the switched reluctance machine in a simple variant, proposed to be applied as an electrical generator for the automobile industry, where it is already used for some hybrid car configurations.

Considering both, the advantages and the disadvantages of this type of electric machine, the demanding use of it on a larger scale, including for the existing hybrid automobiles on the market, made the decision of studying it in this thesis easier.

This chapter shows a two-phase configuration, with low costs, of a switching reluctance machine, designed starting from the induction machine by modifying the windings in the stator and adapting a new structure for the rotor.

With help of the FEM analysis, some conclusion regarding the optimal geometry of the switching reluctance machine, which is proposed for study, were drawn.

A simple design method of a switched reluctance machine - proposed to operate as a generator, starting from a simplified analytical method is here detailed.

This simplified design procedure can be easily used and integrated for sizing the switched reluctance machine and so, having the possibility of making faster digital simulations.

Because of its simplicity, the switched reluctance machine can be easily studied and optimized only using the FEM of analysis, in this chapter, the use of 2D-FEA was very useful for the choose of a proper topology of the 2P-SRG.

Many control strategies of the switched reluctance machine are detailed and much more, a principia scheme for a generating system that includes a switched reluctance generator is than introduced.

The main conclusion is that the switched reluctance machine can become a strong candidate in automobile industry too, for both: the generating or the motoring use and so studying it carefully is mandatory.

References

[2.1] P.P. Acarnley, P.G. McLaren - "*Optimum Magnetic Circuit Configurations For Permanent Magnet Aerospace Generators*"- IEEE Transactions on Aerospace and Electronic Systems, vol. AES 21, no. 2, March 1985;

[2.2] I. Boldea -"*Transformatoare şi maşini electrice*"- Ed. D.P. Bucureşti 1994;

[2.3] I. Boldea, S.A. Nasar, L.E. Unnewehr -"*Permanent Magnet Reluctance and Self Synchronous Motors*"- CRC Press Boca Raton Ann Arbor London Tokyo;

[2.4] Gerhard Henneberger -"*Elektrische Motorausrüstung*"- Bosch GmbH;

[2.5] M. Hecquet, P. Brochet -"*Validation of Coupled Electric Permeance Network Model on a Claw-Pole Alternator*"- Ecole Centrale de Lille, France;

[2.6] G. Barakat, A. Foggia, M. Ivanes, A. Masson, R. Periot -"*Three Dimensional Computation of a Claw-Pole Synchronous Machine Performance*" Laboratoire d'Electrotechnique de Grenoble, France;

[2.7] G. Henneberg, S. Küppers, I. Ramesohl -"*Numerical Calculation, Simulation and Design Optimization of Claw-Pole Alternators for Automotive Application*"- Institute for Electrical Machines, University of Technology Aachen;

[2.8] G. Henneberger -"*Improvement of the output performance of claw pole alternators by additional permanent magnets*"- D10 Special machines and actuators;

[2.9] G. Henneberger, S. Küppers, I. Ramesohl -"*The Influence of the Number of Poles on the Output Performance of a Claw-Pole Alternator*"- Institute for Electrical Machines, University of Technology Aachen;

[2.10] Svante Andersson - "*Flux Reversal Machine*"- Master thesis project, September 22 1996;

[2.11] Rajesh P. Deodhar, I. Boldea, T.J. Miller -"*The Flux-Reversal Machine: a New Brushless Doubly-Salient Permanent Magnet Machine*"- IEEE Transactions;

[2.12] Miller T.J.E. -"*Switched Reluctance Motors and Their Control*"- Magna Physics Publishing and Clarendon Press, Oxford 1993;

[2.13] A. Radun -"*Generating With the Switched Reluctance Motor*"- University of Kentucky, USA;

[2.14] I. Boldea, E. Serban, R. Babau -"*Flux Reversal Stator PM Single Phase Generator With Controlled D.C. Output*"- OPTIM '96;

[2.15] D.E. Cameron, J.H. Lang -*"The Control of High-Speed Variable Reluctance Generators In Electric Power Systems"*- IEEE Transactions on Industry Applications, Vlo.29, No.6, Nov.-Dec.1993;

[2.16] P. Materu, R. Krishan -*"Estimation of Switched Reluctance Motor Losses"*- IEEE Transactions, Reprinted, 1988;

[2.17] P.C. Kjaer, T.J.E. Miller, J.J. Gribble -*"High-Grade of Switched Reluctance Machines"*- University of Glasgow, SPEED Laboratory, Scotland, U.K.;

[2.18] S.R. McMinn, W.J. Rzesos, P.M. Szczesny, T.M. Jahns -*"Application of Sensor Integration Technique to Switched Reluctance Motor Drives"*- IEEE Transactions on Industry Applications, Vol.28, No.6, Nov.-Dec. 1992;

[2.19] Iqbal Husain, M. Ehsani -*"Rotor Position Sensing in Switched Reluctance Motors Drives by Measuring Mutually Induced Voltages"*- IEEE Transactions on Industry Applications, Vol.30, No.3, May-June 1994;

[2.20] Rolf Lagerquist, I. Boldea, T.J.E. Miller -*"Sensorless Control of the Synchronous Reluctance Motor"*- IEEE Transactions on Industry Applications, Vol.30, No.3, May-June 1994;

[2.21] P.P. Acarnley, R.J. Hill, C.W. Hooper -*"Detection of Rotor Position in Steppping and Switched Motors by Monitoring of Current Waveforms"*- IEEE Transactions on Electronics, Vol.IE-32, No.3, August 1985;

[2.22] P.C. Kjaer, G. Gallegos-Lopez -*"Single Sensor Regulation in Switched Reluctance Motor Drives"*- University of Glasgow, SPEED Laboratory, Scotland, U.K.;

[2.23] A. Lumsdaine, J.H .Lang -*"State Observers for Variable-Reluctance Motors"*- IEEE Transactions on Industrial Electronics, Vol.37, No.2, April 1990;

[2.24] P. Laurent, B. Multon -*"Sensorless Position Measurement Based on PWM Eddy Current Variation for SRM"*- EPE '95 Seville;

[2.25] W.F. Ray, M.T. Ebrahim -*"A Novel High Speed Switched Reluctance Generator"*- EPE'95 Seville;

[2.26] Sabonnadiere J.C., Konrad A. -*"Computing EM Fields"*- IEEE Spectrum, November 1992, pp. 52 – 56;

[2.27] A.G. Jack, J.W. Finch, J.P. Wright -*"Adaptive Mesh Generation Applied to Switched Reluctance Motor Design"*- IEEE Transactions on Industry Applications, Vol.28, No.2, March-April 1992;

[2.28] R.P. Deodhar -"*The flux-MMF Diagram Technique and Its Applications in Analysis and Comparative Evaluation of Electrical Machines*"- University of Glasgow, October 1996;

[2.29] Jung-Chien Li -"*A Saturation Model for the Switched Reluctance Motor to Maximize the Torque with Minimum Ripple*"- Department of Electrical Engineering, National Taiwan Ocean University, Keelung, Taiwan;

[2.30] G. Henneberger, S. Küppers -*Field Calculation and Dynamic Simulation of a Claw Pole Alternator*"- Electrical Machines and Drives 11-13 Sept. 1995 Conference Publication No.412, IEE, 1995;

[2.31] N.N. Fulton, P.J. Lawrenson -"*Switched Reluctance Drives for Electric Vehicles*"- Intelligent Motion, June 1993, Proceedings;

[2.32] E. Kokornaczyk, M. Stiebler -"*Substitution of Measuring Hardware in Sensorless SR-Motors by Software*"- Intelligent Motion, June 1997 Proceedings;

[2.33] Fulton N.N., Stephenson J.M. -"*A Review of Switched Reluctance Machine Design*"- Proceedings ICEM '88, Sept. 12-14, Pisa, Italy, pp.423 – 428;

[2.34] Faiz J. -"*Prediction of Static Magnetization Characteristics of Switched Reluctance Motors for General Rotor Positions*"- EPE - Firenze, vol.1, 1991, pp.355 - 359;

[2.35] Ray W.F., Lawrenson P.J., Davis R.M., Stephenson J.M., Fulton N.N., Blake R.J. - "*High Performance Switched Reluctance Brushless Drives*" - IEEE Transactions on Industry Applications, Vol IA-22, No.4, July - August 1986, pp.722 – 729;

[2.36] Harris M.R., Finch J.W., Mallick J.A., Miller T.J.E. -"*A Review of the Integral - Horsepower Switched Reluctance Drive*"- IEEE Transactions on Industry Applications, vol. IA-22, No.4, July - August 1986, pp. 716 – 721;

[2.37] Kwon Y.A., Reichert K. -"*Chopping-less Operation of a Nonlinear Switched Reluctance Motor*"- Proceedings, Part 2, International Conference on the Evolution and Modern Aspects of Synchronous Machines; 27 - 29 August 1991, Zürich, Switzerland, pp.465 – 468;

[2.38] Chai J., Yao R., Chen P. -"*Principles for Switched Reluctance Motors Design*"- Proceedings, Part 2, International Conference on the Evolution and Modern Aspects of Synchronous Machines; 27 - 29 August 1991, Zürich, Switzerland, pp.445 – 448;

[2.39] Jufer M., Crivii M., Poffet P. -"*Conception du moteur reluctant à comutation electronique*"- Proceedings MOP – 1990;

[2.40] Chan S., Bolton H.R., -"*Development of sub-KW single phase switched reluctance motor drives*";

[2.41] Jufer M., Crivii M., Hatefi K., Poffet P., Osseni, R., -"*Synchronous electronically comutated motors - design and comparison*"- Proceedings ICEM '90;

[2.42] Verma S.P. -"*Design and Performance of Special Reluctance Motors with Regard to Torques, Vibration and Noise*"- Proceedings, Part 2, International Conference on the Evolution and Modern Aspects of Synchronous Machines; 27 - 29 August 1991, Zürich, Switzerland, pp. 494 – 499;

[2.43] Zaim M.E., Tahi S., Laporte B. -"*Calculation and Performances of Smooth Stator Reluctance Machines*"- Proceedings, Part 2, International Conference on the Evolution and Modern Aspects of Synchronous Machines; 27 - 29 August 1991, Zürich, Switzerland, pp.500 – 505;

[2.44] Lawrenson P.J. -"*A brief status review of Switched Reluctance Drives*"- EPE, vol.2, nr.3, October 1992;

[2.45] Hava A.M., Blasko V., Lipo T.A. -"*A modified C-dump Converter for Variable Reluctance Machines*"- IEEE Transactions on Industry Aplications, vol.28, nr.5, Sept./Oct. 1992;

[2.46] C.A. Ferreira, Eike Richter -"*Detailed Design of a 250kW Switched Reluctance Starter/Generator for an Aircraft Engine*"- SAE Technical Paper Series, April, 1993;

[2.47] W.J. Bonwick -"*Voltage waveform distortion in synchronous generators with rectifier loading*"- IEEE Proceedings, Vol.127, No.8, January 1980;

[2.48] T.J.E. Miller -"*Faults and Unbalance Forces in the Switched Reluctance Machine*"- IEEE Transactions on Industry Applications, Vol.31, No.2, March-April 1995;

[2.49] Longya Xu, Th.A. Lipo -"*Analysis of a New Variable Motor Utilizing Only Two Transistor Switches*"- IEEE Transactions on Industry Applications, Vol.26, No.2, March-April 1990;

[2.50] Kimmo Tolsa, Pertti Silventoinen, Jussi Salo, Juha Pyrhönen -"*Torque Control of the Switched Reluctance Motor Minimizing Copper Losses*"- Department of Energy Technology, Lappeenranta University of Technology, Finland;

[2.51] B.K. Bose, T.J.E. Miller, P.M. Szczesny - *"Microcomputer Control of Switched Reluctance Motor"*- General Electric Company, Corporate Research And Development, Schenectady, New York;

[2.52] P.C. Kjaer, T.J.E. Miller, J.J. Gribble - *"Dynamic Testing of Switched Reluctance Motors for High-Bandwidth Actuator Applications"*- University of Glasgow, SPEED Laboratory, Scotland, U.K.;

[2.53] A.V. Radun - *"Design Considerations for the Switched Reluctance Motor"*- University of Kentucky, USA;

[2.54] R.C. Becerra, M. Ehsani, T.J.E. Miller - *"Commutation of SR Motors"*- IEEE Transactions on Power Electronics, Vol.8, No.3, July 1993;

[2.55] M. Moallem, Chee-Mun Ong, L.E. Unnewehr - *"Effect of Rotor Profiles on the Torque of a Switched Reluctance Motor"*- IEEE Transactions on Industry Applications, vol.28, No.2, March-April 1992;

[2.56] P.C. Kjaer, G. Gallegos-Lopez, T.J.E. Miller - *"Active Clamp Resonant DC Link Inverter for Current Controlled Switched Reluctance Motors"*- SPEED Laboratory, University of Glasgow, Scotland, U.K.;

[2.57] M.J. DeBortoli, S.J. Salon - *"Computation of Forces and Torque in Electromagnetic Devices Using the Finite Element Method"*- Department of Electric Power Engineering Rensselaer Polytechnic Institute Troy, N.Y., USA;

CHAPTER III

THE FLUX REVERSAL GENERATOR (FRG)

3.1. Introduction

The flux reversal machine is a doubly salient permanent magnet machine, with the permanent magnets placed on the stator poles. It has two magnets with opposite polarity on each salient stator pole with wounded coil and a salient variable reluctance rotor (like switched reluctance machine rotor). By putting two magnets with opposite polarity on each stator pole, both the flux and the current were made bipolar in almost the whole machine. Thus the new machine, the Flux Reversal machine, uses both the cooper and the iron better than the Switched Reluctance machine. It combines some features from the brushless d.c. machine and the Switched Reluctance machine, it behaves mainly like a brushless d.c. machine as its currents and voltages are ideally square-wave shaped and both current and flux are bipolar in nature.

This machine can be built in diverse configurations with different combinations of pole and phase numbers. In figure 3.1 are shown cross-section of the Flux Reversal machine. [3.1]

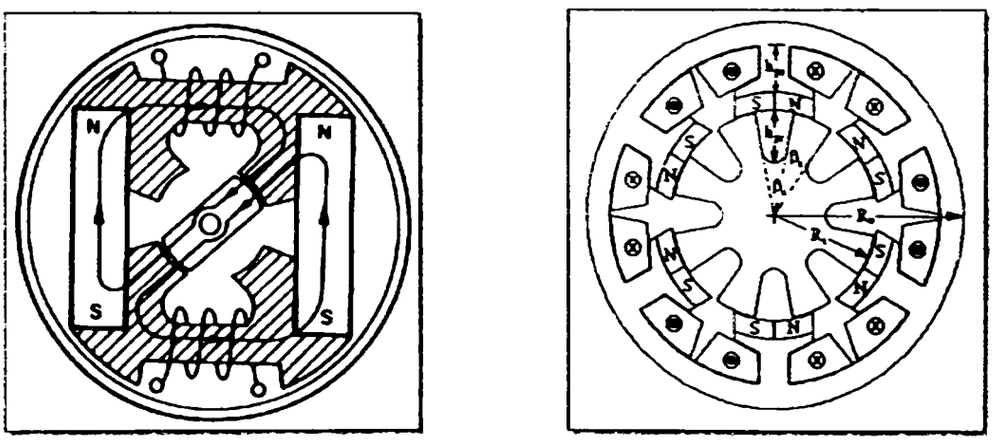

a) b)

Figure 3.1. Flux Reversal generator topologies:
a) the existing single phase;
b) the proposed one, with three phase;

3.2. Theory

This kind of machine was promoted as a result of many researches regarding the speed limitation of the synchronous machines with variable reluctance, the complex control of those and the excitation ways for those.

The principle of operation is based on magnetic reluctance variation due by the rotor rotation and machine structure (topology). As the rotor rotates, the reluctance in the magnetic path of the magnets varies. A rotor pole covering a magnet offers a low reluctance flux path and so the rotor poles is varying the value and direction of the flux-linkage as the rotor rotates.

For a better understanding of the principle of operation follow the indication from the next figure and the text bellow.

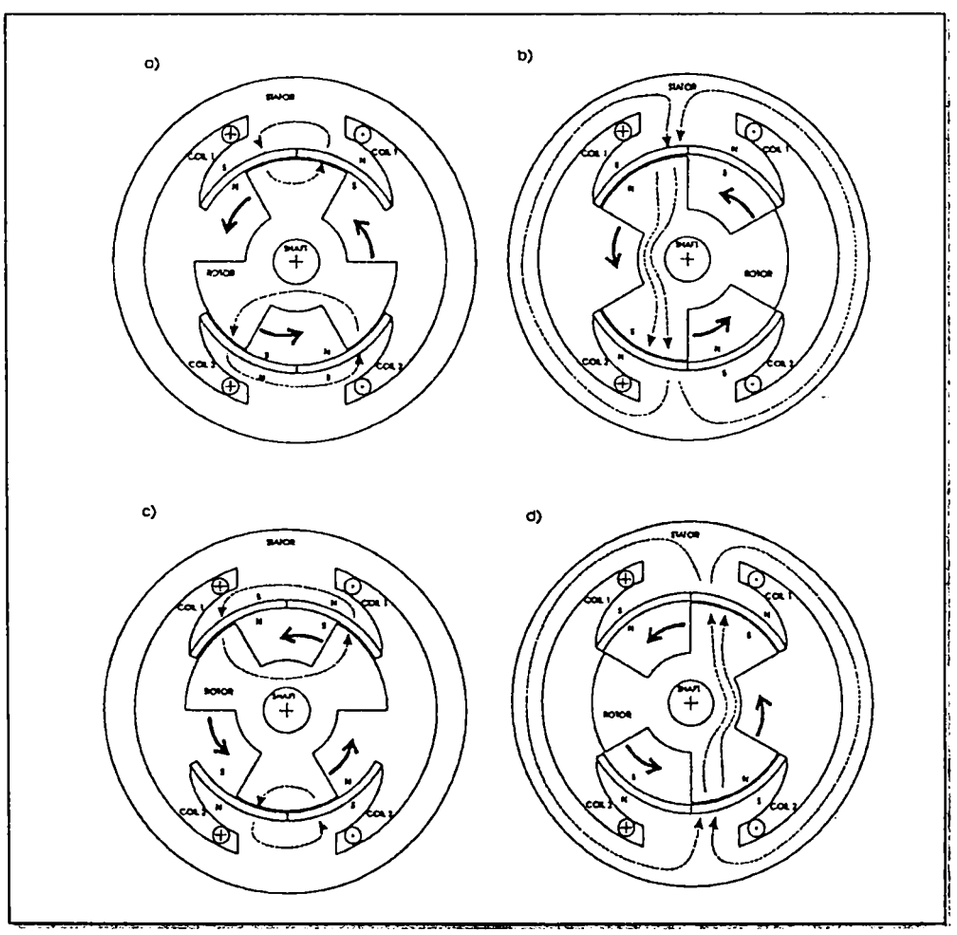

Figure 3.2. The principle of operation of the flux reversal machine (single phase topology)

Starting in the middle position (fig.3.2.a), where the rotor poles "short-circuit" the magnets from the stator poles, there is no net flux linking the coils from the stator poles. The flux parts that are going in the stator core in either direction are canceling each other.

If the rotor rotates so that the rotor poles are covering the magnets on one side of the stator poles (fig.3.2.b), offer a path for the flux from the magnets through the rotor. The flux returns via the stator core and thus link the coils. The magnet from the other halves of the stator poles have a high reluctance flux path, so they are not contributing to the net flux apart from a small amount of fringing flux.

As the rotor is rotated further, the same rotor pole (considered above as being aligned with the left part of stator poles) will reaches the position between stator poles (fig.3.2.c and 3.2.d) and after that will cover the magnets on the right side of the stator poles, offering a path for the flux from the magnets through the rotor. Than will came another position in which it "short-circuiting" the magnets and so on.

The back e.m.f. will be as in figure 3.3.[11]

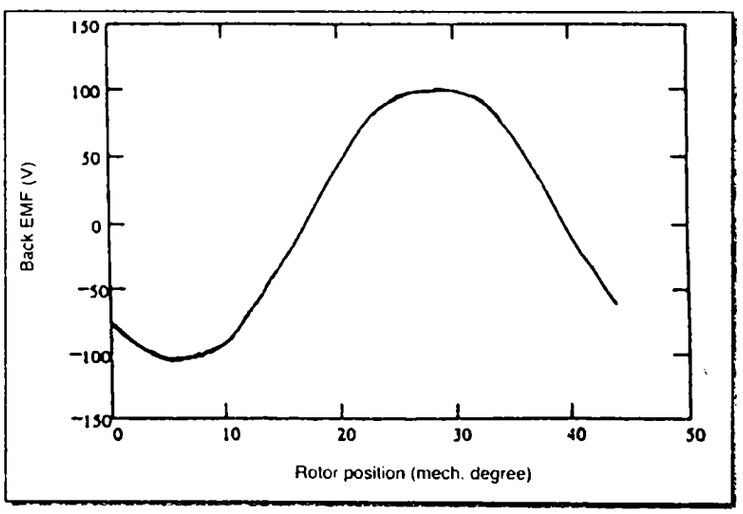

Figure 3.3. The phase e.m.f. wave form for a three phase generator, N_s/N_r=6/8 poles

There are several possible configurations of the Flux Reversal machine, the inductance is most of all determined by the length and width of the air-gap which is constant in this case because the same pole area is covered by the rotor poles regardless of the rotor position.

The three phase configuration machine has the advantage of having total electrical and magnetic isolation between the phase and hence it is fault tolerant by nature.

Even if is not the same electric machine with salient structure and permanent magnets in stator, it proved itself as being the first one having a bipolar flux and current, with a lower inductance because of the permanent magnets, with advantages on high speed and working as a generator in places were the influence of load fast changes can be efficiently observed.

The peak to peak flux linkage variation depends on the PM remanent flux density, coercive force and some geometrical parameters: the ratio of the PM radial thickness and stator pole span, the ratio between stator pole span and rotor pole span and the ratio of PM thickness over rotor pole height; as will be demonstrated in this chapter.

The stator and rotor poles can be either straight or with flux concentrating design. The benefit of the flux concentrating design of the poles is that so it makes a better use of the iron. If the PM are mounted as small pieces, as shown in the following figure (fig. 3.4), the eddy currents losses will be reduced.

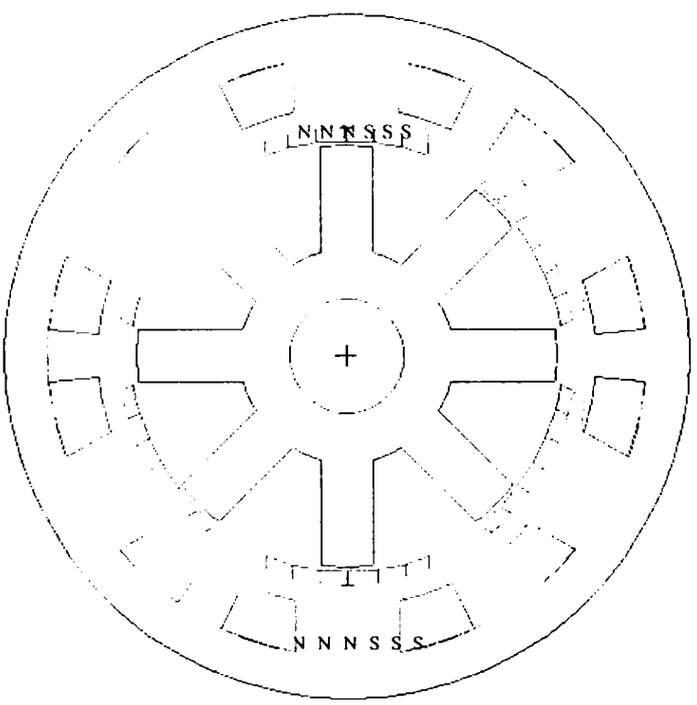

Figure 3.4. Three phase Flux Reversal generator with $N_s/N_r=6/8$

Usually, the desired flux density in the iron is higher than what can be produced in the magnets. As high flux density as possible, taking into account the iron losses, because the less iron can give the same flux. In the rotor poles, flux-concentrating design leads to higher saliency and therefore lower fringing.

In a generator operation, this means higher voltage for the same speed. The straight stator poles have the advantage of being able to accept the use of pre-wound coils, which are desirable for fast and economical manufacturing.

3.3. Basis Equations of the Three Phase FRG

By conceptual design, we design a machine (for given specifications) through making use of analytical electromagnetic and thermal models.

In order, to make a good an real analysis of the FRG using the FEM and afterwards to simulate a real generating system, a topology of the machine has to be achieved. For this, considering the application domain, automobiles industry, a three phase FRG, which has to operate for a very wide speed domain (from 1800 rpm to 18000 rpm) giving an output voltage in d.c. link of 42 V has to be designed, at least as basic design.

The phase back e.m.f. waveform is like in the following picture (fig. 3.5) and can be approximated using relation (3.1):

$$e_{a,b,c}(t) = E_1 \sin\left(\omega_r t - (i-1)\frac{2\pi}{3}\right) + E_3 \sin \omega_r t\,; \qquad i = 1,2,3 \tag{3.1}$$

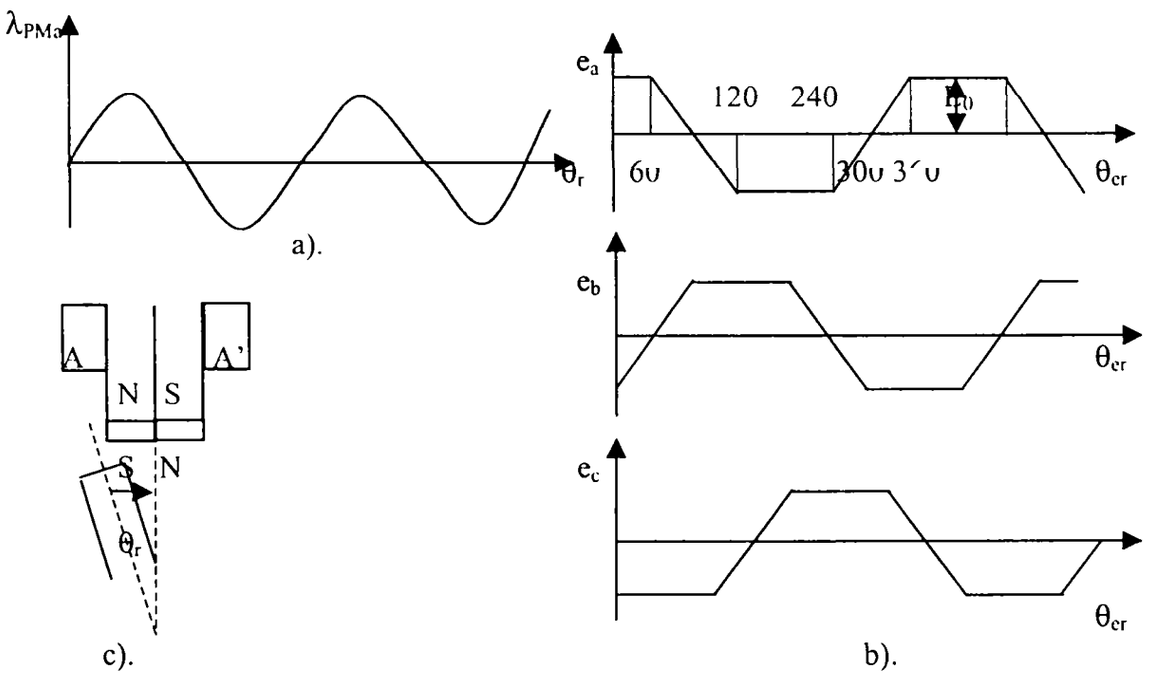

Figure 3.5. The flux reversal machine: a)Stator magnetic flux; b) Back e.m.f.; c) Internal angle θ_r

$$\omega_r = 2\pi M_r n\,; \qquad \text{n - rotor speed, in rps.} \tag{3.2}$$

With: L_s, R_s, phase inductance and resistance and considering the mutual inductance $L_{ij} = 0$, the equations for generator operating are:

$$\frac{di_a}{dt} = \left(e_a(t) - v_a(t) - i_a R_s\right) / L_s \tag{3.3}$$

$$\frac{di_b}{dt} = \left(e_b(t) - v_b(t) - i_b R_s\right) / L_s \tag{3.4}$$

$$\frac{di_c}{dt} = \left(e_c(t) - v_c(t) - i_c R_s\right) / L_s \tag{3.5}$$

The electromagnetic power, P_e, and torque, T_e, are:

$$P_e = e_a(t)i_a(t) + e_b(t)i_b(t) + e_c(t)i_c(t) \tag{3.6}$$

$$T_e = P_e / 2 \cdot \pi \cdot n \tag{3.7}$$

The electrical equivalent circuit of FRG is:

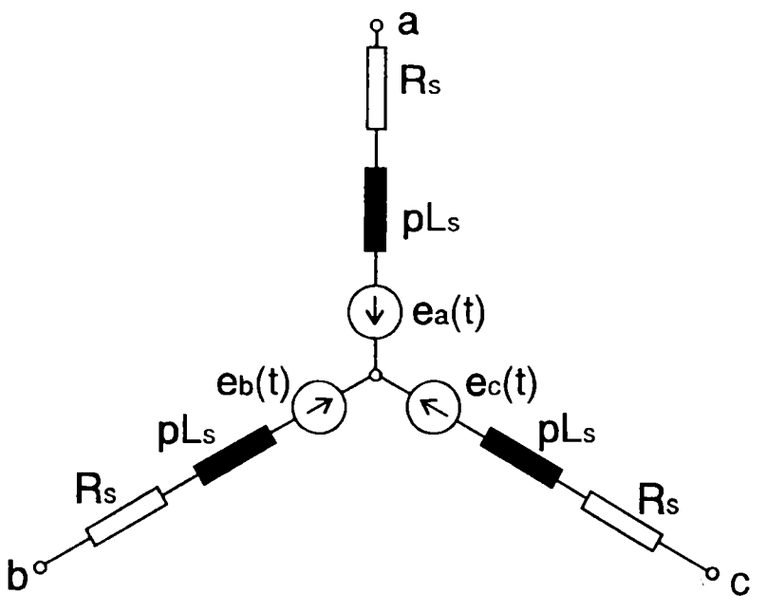

Figure 3.6. FRG's electrical equivalent circuit

3.3.1. The Air-gap Flux Density

Ideally, PM flux density, B_m, (on the air-gap side) and air-gap flux density, B_{gi}, are the same. So, for a linear PM magnetization curve, we have:

$$B_m = B_r / [\ 1 + m_{rec} \cdot g(1 + K_s) / H_0 \cdot h_m] \tag{3.8}$$

The influence of iron path is considered using a global magnetic saturation factor, k_s.

A problem is the radial height of the PM, h_m, to have a small inductance (small electrical constant) a PM with a thin thickness is recommended, this means that a FEM study is indicated, a rotor pole height / PM height ratio is to be around 2.5 for a good compromise between costs and performance. So, as the rotor pole is choose, the PM height will results.

The PM material can be NeFeB, or any other type having $B_r \sim 1.2T$.

For high-speed operation, an air-gap: g = 0.5 mm seems to be OK.

On the other hand:

$$d\lambda_{PM} / d\theta_r = (D_r/2) \cdot d\lambda_{PM} / dx \tag{3.9}$$

where θ_r is the geometrical angle.

The phase back e.m.f., E, for two windings in series connection (one phase), is:

$$E = \frac{-d\lambda_{PM}}{d\theta_r} \cdot 2Nc \cdot \frac{d\theta_r}{dt} \tag{3.10}$$

Where the rotor speed is in rotations per second.

Generator output power:

$$P_e = 2 \cdot E \cdot I \tag{3.11}$$

3.3.2. Stator Geometry

Stator slot opening is $W_{so} = (2/3)\tau$. The slots may be considered as half-closed.

First we have to calculate the slot area. To do so, we must adopt the slot filling factor. As we intend to leave two spaces for axial air circulation, we feel that a global filling factor $k_{fill} = 0.38$ may be acceptable. Now, in terms of flux density, there are two options: we may call them the generator option and the drive option.

For the generator option, we use axial air self-ventilation while for the drive option we envisage forced liquid cooling of stator either indirect (around the stator frame) or direct (through the electric wires directly).

For both cases the choosing of base design current density is a matter of compromise. A higher current density reduces the machine time constant and thus improves the commutation process in the converter at high speed (for instance 18000 rpm means 2.4 kHz) but it also reduces the efficiency. Finally, it reduces the size of the machine. On top of this 2.4 kHz, the skin effect may not be neglected as it may double the stator copper losses, at least.

Again, there are two options: first is to use standard (Litz-type) wire, which is more expensive or bear the consequence of high skin effect and eventually counteract it by reducing the design current density which means an increase in stator slot area and thus of stator external diameter and finally an increase in the motor weight. Also, for the generating option, we recommend axial air self ventilation and the base current density is:

$$j_{cob} = 12 \text{ A/mm}^2 \tag{3.12}$$

Consequently, the slot area is:

$$A_{slot} = 2(N_c \cdot I)_b / j_{cob} \cdot k_{fill} \tag{3.13}$$

By now we have to define more precisely the stator core geometry. As the air-gap flux density (max.) is reflected in the stator pole only partly due to the circumferential fringing, the maximum pole PM flux is:

$$\lambda_{PPMax} \cong N \cdot B_{gPMax} \cdot \Lambda \cdot \tau \cdot (1+K_{fringe}) / 2 \tag{3.14}$$

where:

$$\tau = \pi (D_r+2g)/2 \cdot N_r \tag{3.15}$$

Choosing a pole flux density B_{ps}=1.2T, the pole width is:

$$W_{ts} = \lambda_{PPMax} / L \cdot B_{ps} \tag{3.16}$$

The slot lower length is:

$$l_{wi} = p (D_r + 2g + 2h_{PM} + 2h_{tps}) / N_s - W_{ts} \tag{3.17}$$

Now, to produce the slot area we need at least a useful height, h_{ps}. Finally, the external pole diameter is:

$$D_{pe} = (D_r + 2g + 2h_{PM} + 2h_{tps}) + 2h_{ps} \tag{3.18}$$

The stator back iron thickness is :

$$b_{cs} = B_{gPMi} \cdot \tau \cdot k_{fill} / 2B_{cs} \tag{3.19}$$

For mechanical reasons we always adopt a bigger value for the back iron thickness. Consequently, the external stator diameter is:

$$D_{se} = D_{pe} + 2b_{cs} \tag{3.20}$$

With help of the stator topology resulted from the start data using the above formulas, shown in figure 3.7, a stator virtual prototype was "built" with help of dedicated software AutoCad ™ in order to be use for numerical analysis using the FEM.

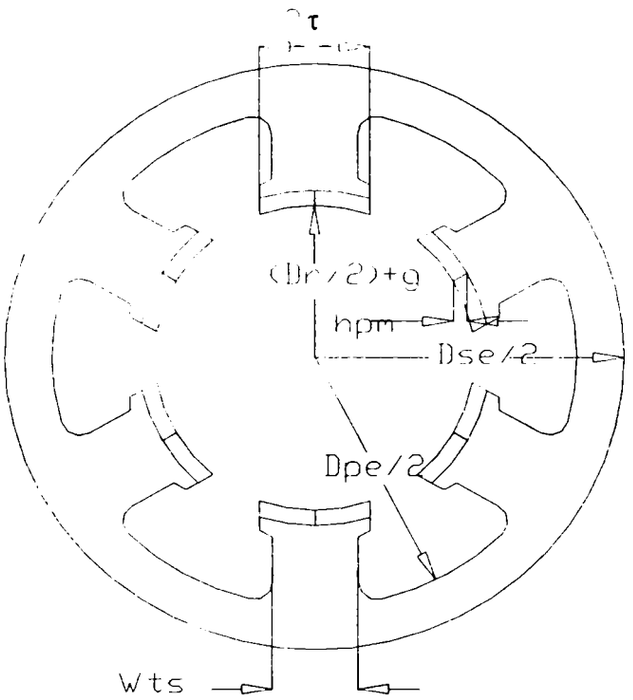

Figure 3.7. Three phase FRG stator topology for the virtual prototype (AutoCad ™ drawing)

3.3.3. Rotor Core Geometry

For the three phase FRG adopted topology, the rotor core contains 8 poles and a back-core. The rotor core is placed on the shaft.

The rotor pole tips span and the between-pole air intervals are:

$$\alpha = \beta = 2p / 2N_r \tag{3.21}$$

To keep the rotor core loss within reasonable limits while also reducing the between-pole flux fringing the pole sided are rounded. This way the poles on the rotor have stronger (wider) lower zone and thus are more rugged.

The space average flux density in the rotor poles may be considered as:

$$B_{pr} \sim B_{gPMi}(1+K_{fring}) / 2 \tag{3.22}$$

We have to notice that, as in the stator back core, the rotor pole flux density reverses sign. This fact is to be accounted for when calculating the rotor core loss.

The rotor shaft diameter, D_{shaft}, should be calculated in relation to the peak torque.

The rotor back core radial thickness is taken equal to that in the stator, consequently, the pole height is:

$$h_{pr} = (D_r - D_{shaft} - 2b_{cr}) / 2 \tag{3.23}$$

If the mechanical ruggedness is considered to be a problem, the pole height can be reduced while increasing the rotor back core.

The average flux density in the rotor back core is:

$$B_{cr} = B_{gPMi} \cdot K_{fring} \cdot \tau / 2b_{cr} \tag{3.24}$$

Again, B_{cr} changes polarity (sign) and this is important for core loss calculation .

For FEM-analysis, using the initial data, the above formulas and with help of AutoCad ™ software, a rotor virtual prototype was created, figure 3.8.

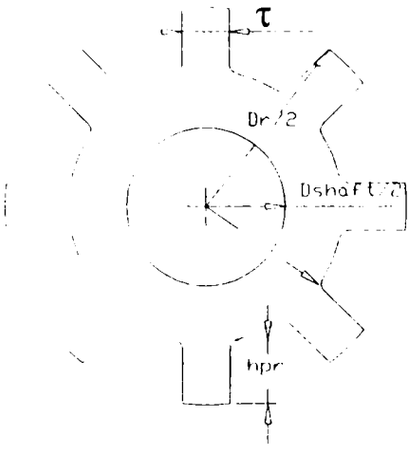

Figure 3.8. Three phase FRG rotor topology for a virtual prototype (AutoCad ™ drawing)

3.3.4. Stator Electrical Parameters

The stator phase resistance (two coils in series) is:

$$R_s = r_{co} \cdot l_c \cdot 2N_c^2 \cdot j_{co} / N_c \cdot I_b = K_r \cdot N_c^2 \tag{3.25}$$

Coil length:

$$l_c = 2L_s + 2 \cdot 1.3[W_{ts} + (l_{wc} + l_{wi}) / 4] \tag{3.26}$$

The phase inductance (useful and fringing inductances):

$$L_u = 2N_c^2 [\mu_0 / (g + h_m \cdot \mu_{rec} / \mu_0)] \cdot L \cdot \tau \cdot (1 + k_{fring}) \tag{3.27}$$

The leakage inductance has two components: the slot leakage and coil end connection leakage.

The slot specific permeance, Λ_s, is:

$$\Lambda_s = \frac{h_{ps0}}{w_{s0}} + \frac{2h_{ps1}}{(l_{wi} + w_{s0})} + \frac{2h_{ps}}{3(l_{we} + l_{wi})} \tag{3.28}$$

To be on the safe side we may consider that the end connection specific permeance is:

$\Lambda_{cc} = \Lambda_s / 2$; consequently the total leakage inductance is:

$$L_l = 2N_c^2 \cdot \mu_0 \cdot \lambda_s \cdot l_c \tag{3.29}$$

The total phase inductance, which is practically independent of rotor position is:

$$L_s = C_l \cdot N_c^2 \tag{3.30}$$

Now, the machine electrical time constant (there seems to be no coupling between phases) is:

$$T_e = L_s / R_s \tag{3.31}$$

In case of doubling R_s by using normal (not Litz-type) wires through skin effect at high speed, the losses will be doubled but the time constant will be reduced.

The e.m.f. may be written as:

$$E = 2N_c \cdot 2 \cdot \pi \cdot n \cdot (d\lambda_{PM} / d\theta_r) \tag{3.32}$$

3.3.5. Copper and Core Losses

The copper losses at base speed (1800 rpm) with two phases conducting at any time, are:

$$p_{copper} = 2R_s \cdot I_b^2 = 2K_R(N_c \cdot I)_b^2 \tag{3.33}$$

The copper weight:

$$W_{copper} = l_c \cdot \gamma_{co} \cdot 6N_c \cdot I / j_{co} \tag{3.34}$$

To calculate the core loss, the weight of various core parts with constant flux density amplitude has to be determined.

The stator pole weight is:

$$W_{ps} = 6[w_{ts} \cdot h_{ts} + 2 \cdot \tau \cdot h_{ps0} + h_{ps1}(2\tau + w_{ts}) / 2] \cdot L \cdot \gamma_{core} \tag{3.35}$$

The rotor pole weight is :

$$W_{pr} = [D_r^2 - (D_r - 2h_{pr})^2]L \cdot \gamma_{core} \cdot \pi / 2 \cdot 4 \quad (3.36)$$

The stator back core weight is:

$$W_{cs} = (\pi / 4) \cdot (D_{se}^2 - D_{pe}^2)\, L \cdot \gamma_{core} \quad (3.37)$$

The rotor back core weight is:

$$W_{cr} = (\pi / 4) \cdot [(D_r - 2h_{pr})^2 - D_{shaft}^2] \cdot L \cdot \gamma_{core} \quad (3.38)$$

To a first approximation we may consider sinusoidal flux density variations for calculating the core loss (eddy current mainly):

$$p_{core} = 96\, K_l \cdot f^{1.7} \cdot B_i^2 \quad (3.39)$$

The coefficient K_l depends on the core material and on lamination thickness.

For 0,5 mm M19 material K_l=0,11 but for 0,1 mm thick laminations, K_l=0,0076.

B_i is the amplitude of flux density variation.

3.3.6. Efficiency Verification

With help of the initial efficiency value, the total losses would be:

$$\Sigma p = P_b / \eta_b - P_b \quad (3.40)$$

As copper losses (using Litz wires) and core losses are already known, the mechanical losses, Σp_{mec}, could not be high as:

$$\Sigma p_{mec} = \Sigma p - p_{copper} - p_{core} \quad (3.41)$$

3.3.7. Number of Turns per Coil

We already decided that the rectifier output voltage is V_0 = 42 V.

At this stage we notice both the inductance voltage drop (due to overlapping angle) and the resistance voltage drop.

Consequently: $$2E - 2R_s \cdot I_b - (3 / \pi)\omega_b \cdot L_s \cdot I_b = V_o \quad (3.42)$$

The no load voltage at 1800 rpm is two time the e.m.f., this might seem too high since the speed is rather low but, despite the low electrical time constant, the frequency is already high.

The generator current value is the average value due to commutation overlapping, thus the active power circulation is given by:

$$V_0 \cdot I_0 = (2E - 2R_s \cdot I_b) \cdot I_b \quad (3.43)$$

The current on d.c. link is:

$$I_0 = P_a / N_c \quad (3.44)$$

3.3.8. Stator Coil Wire Gauge

The wire cross-section of the stator coil is:

$$A_{wire} = I_b / j_{cob} \quad (3.45)$$

3.3.9. Temperatures

Temperature, θs, is divided between the windings in the slot and stator iron core as follows:

$$\theta_s = p_{cos} \cdot b_s / \lambda_{hs} (A_1 + A_2 + A_3) \quad (3.46)$$

where: $$p_{cos} = (p_{copper})_{phase} / 2 (L / l_c) \quad (3.47)$$

Let us assume the slot and wire insulation thickness, b_s=0,3 mm, and λ_{hs} = 0.5 W/m^{0}C.

The areas are: $$A_1 + A_2 + A_3 = [h_{ps} + L_{wel} + (\tau - w_{ts} / 2)] \cdot L \quad (3.48)$$

Finally, the temperature.

The over-temperature of the stator core with respect to surrounding air, is:

$$\theta_{ca} = (2/3p_{copper} + p_{core}) / 6 \cdot \alpha \cdot A_5 \quad (3.49)$$

where:

α is the heat convection transfer coefficient, for zero air speed $\alpha = 1.33x10^{-3}$ W/cm^2 ^{0}C

The stator external area is: $A_5 = \pi \cdot D_{se} \cdot L / 6$ (3.50)

If the over-temperature is not acceptable, too high, to protect the PMs, the over-temperature must not exceed 75^{0}C so we have to consider two new factors:

- the first is the duty-cycle at base speed and power, this duty-cycle is max. 33% ;
- the second factor is the factor introduced by the presence of a self ventilator on the machine's shaft.

For this reason a fan has to be mounted on the shaft to increase the value of coefficient and to obtain the desired over-temperature, a fan able to redirect the air through the holes between coils and to "wash" the external side of the stator.

At high speed, self-ventilation seems to be more efficient and for machines with power over 10 KW forced ventilation with liquid is required.

Some of the advantages of the FRG are:

- unlike the SRG, the FRG has a bipolar alternating flux linking the windings. Thus it can produce current on both the positive and negative slopes of the flux variation;
- there are no magnets on the rotor, so it is well suited for high speed;
- it has low inductance because of the magnets;
- it has low inertia.

The main drawback is the cogging torque.

The control is quite simple working as a generator, because is no need for excitation, the generator can give an a.c. current which can be easily transformed in a d.c. current by a diode rectifier and so battery charging or any type of d.c. loads (in some cases - using an inverter – a.c. loads) can be fed. In order, to keep the voltage from the rectifier exit at a

constant value, independently from the generator speed and the load, a voltage regulator might be useful. [3.14]

3.3.10. Sample Design Results

Following the conceptual design equations, we will size a machine for a set of given specifications for the FRG:

- Output power at base speed: P_b = 1500 [W] for 30 [rps]
- Maximum power P_{max} =3000 [W] for n_{max} = 300 [rps]
- Output d.c. voltage: V_o =56 [V] d.c.
- Speed range from 150 [rps] to 300 [rps]
- Efficiency: above 75%

The output data, obtained with help of above equations, are:

Electromagnetic power	P_b=1848 [W]
Voltage	V_{dc}=56 [V]
Rotor external diameter	D_r=0.067 [m]
Stack length	L_s =0.081 [m] for λ = 1.2
Electromagnetic torque	T_{eb}=8.40 [Nm]
PM remanent flux density	B_r= 1.2 [T]
Pole m.m.f.	N_cI_c= 638 [Aturns]
PM coercive force	H_c=0.65 [MA/m]
PM radial thickness	h_{PM}=4x10^{-3} [m]
Stator core radial depth	b_{cs}=2.24x10^{-3} [m]
Rotor core radial depth	b_{cr}=2.24x10^{-3} [m]
External stator core diameter	D_{se}=0.105 [m]
Weights	

Copper weight	W_{Cu} =1.116 [kg]
Stator poles weight	W_{ps}= 0.366 [kg]
Stator core weight	W_{cs} = 0.347 [kg]
Rotor poles weight	W_{pr}= 0.516 [kg]
Rotor core weight	W_{cr}= 0.108 [kg]
Aluminum frame weight	W_{Al}= 1.65 [kg]
Total weight	W_{total}= 4.11 [kg]
Loses	
Copper loss at base speed	p_{Cu}= 315 [W]
Core loss at base speed	p_{core}= 3.65 [W]
Calculated efficiency	η_b = 81.13%

3.4. Three Phase FRG Geometry Pre-Optimization Using FEM-Analysis

In this chapter, FEA is carried out for the three-phase FRG (virtual prototype with the geometrical data given by using the relations from previous chapter). The cogging torque and magnetic flux linkage are obtained through extensive FEA calculation. Based on the results, an equivalent circuit model of the three-phase FRG will be than used for digital simulations. For simplicity, the effect of the losses is not considered.

The main scope in FRM analysis is the optimal determination of the optimal geometric structure; especially of the poles in order to obtain the useful magnetic flux is possible, taking into account of the saturation and of the core losses.

In figure 3.9, a cross-section of a three phase FRG with the geometrical dimensions analytically calculated, is presented. The ratio between the stator and rotor poles width being 1/2, the PM thickness is 6mm and the air-gap is 0.5mm.

The field lines from the figure are because of the stator PM's, with radial magnetization.

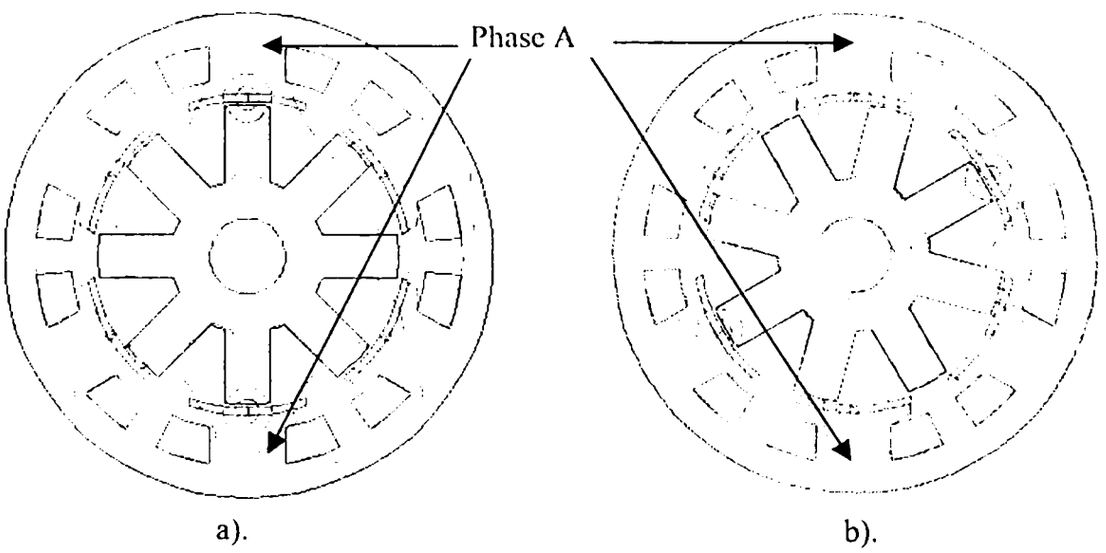

Figure 3.9. The magnetic field produced by the PM, through FEA:
a) zero magnetic flux in phase A
b) maximum magnetic flux in phase A

For this geometrical topology of the three phase FRG – stator pole width / rotor pole width = 1/2, PM thickness = 6mm, air-gap = 0.5mm - the cogging torque and the magnetic flux through one stator pole (the electro-magnetically most solicited part for this kind of machine) were calculated, simulating a rotational movement of the rotor using the FEM program.

The results of the simulation using FEM are presented in figure 3.10 and figure 3.11: the cogging torque variation and the magnetic flux through one of the stator pole, both versus the rotor position.

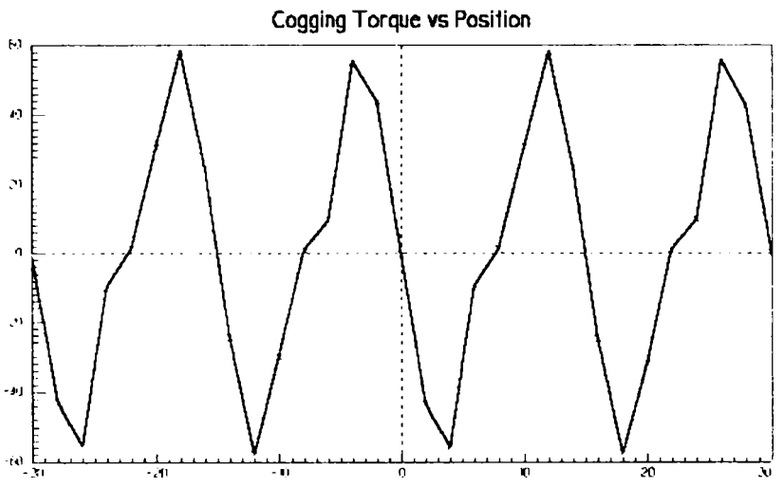

Figure 3.10. The cogging torque vs. rotor position for a three phase FRG with the indicated topology

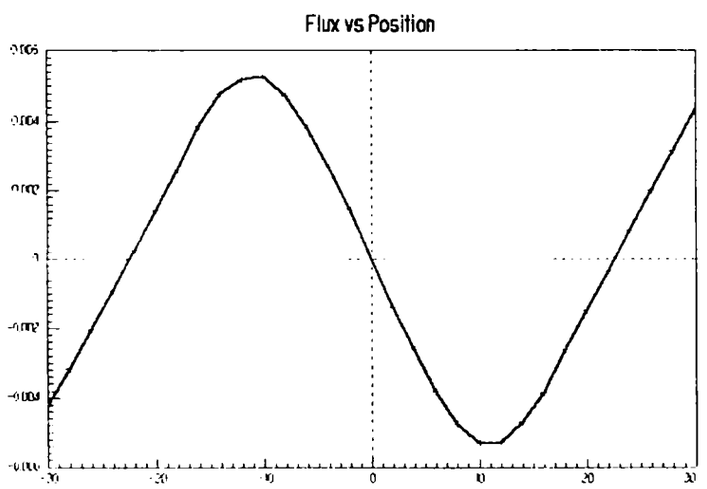

Figure 3.11. The magnetic flux variation through a stator pole vs. rotor position [Wb/u.l.] for a three phase FRG with the indicated topology

As it can be observed, the cogging torque variation vs. rotor position is large, with a peak value of 50 Nm/u.l., this variation is influenced, as it will be shown, by the geometrical dimensions of the poles, the air-gap and the PM thickness, so generally by the geometrical topology of the generator.

First step to decrease the cogging torque was to decrease the effect of the PM's by making thinner. For this we decided to use the following geometrical configuration: stator pole width / rotor pole width = 1/2, PM thickness = 2mm, air-gap = 0.5mm. In figure 3.12 and 3.13 the results of this change are presented.

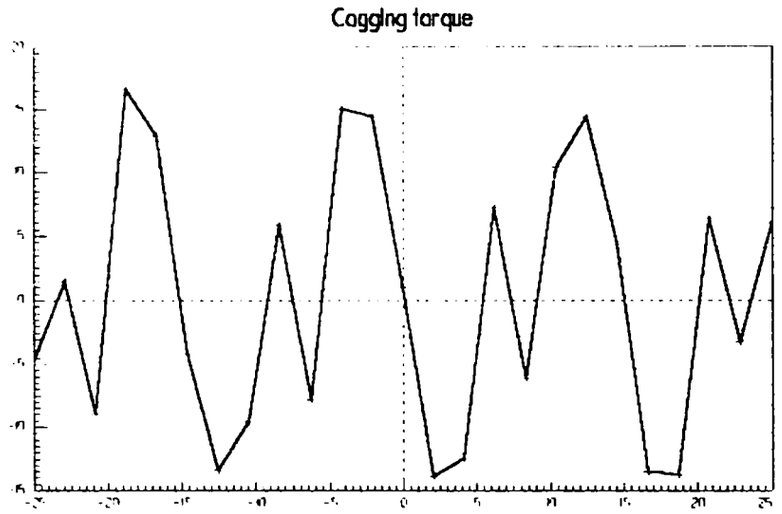

Figure 3.12. The cogging torque variation [Nm/u.l.] vs. rotor position for a three phase FRG with the geometrical topology indicated above

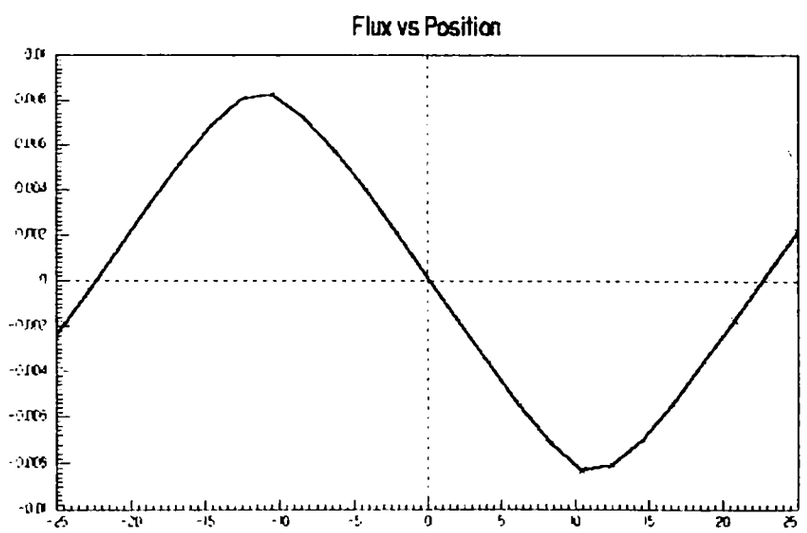

Figure 3.13. The magnetic flux variation [Wb/u.l.] vs. rotor position for a three phase FRG with the geometrical topology indicated above

As it was expected, the cogging torque variation decreases, the peak value is now approximately 17 Nm/u.l., and the maximum value of the magnetic flux through the stator pole is increasing at 0.0082 Wb/u.l., from 0.0058 Wb/u.l., previously.

To study the effect of rotor poles dimensions against generator characteristics, the width of rotor poles was decrease, from a stator pole width / rotor pole width ration of 1/2 to a new one of 1/3, the PM thickness is again 6 mm and the air-gap of 0.5 mm. The results of this change are presented in the characteristics from figure 3.14 and figure 3.15.

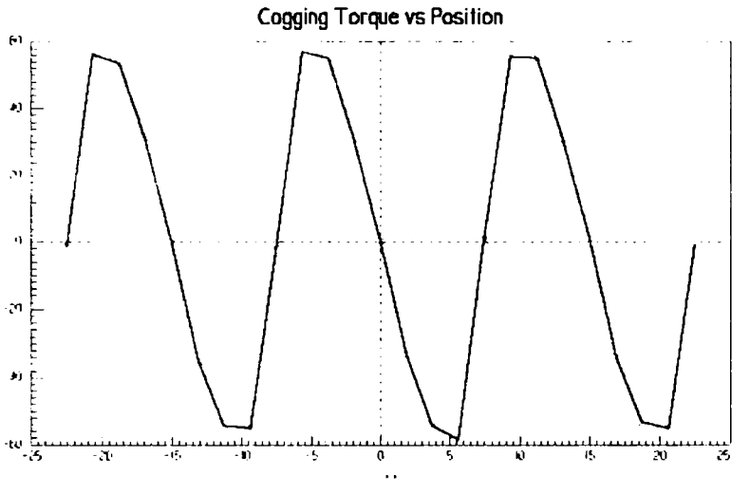

Figure 3.14. The cogging torque vs. rotor position for a three phase FRG with the geometrical topology as indicated above

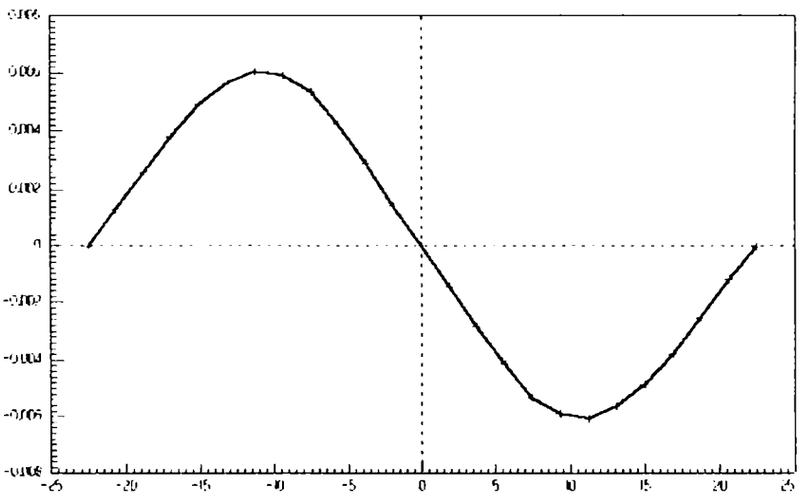

Figure 3.15. The magnetic flux through the stator pole vs. rotor position for a three phase FRG with the geometrical topology as indicated above

In this way, keeping the same air-gap and the same PM thickness, the cogging torque peak value is reduced with 10% and the magnetic flux maximum value increases with

approximately same percent of 10%, so the effects are similar with those obtained in the case of PM's thickness decrease.

Making the both changes simultaneously – decreasing the PM's thickness and the rotor poles width, a cumulated effect is expected, a decrease of the cogging torque peak value – because of PM's – and an increase of the useful magnetic flux – because of the rotor poles width. As shown in figure 3.16 and figure 3.17, the expected results

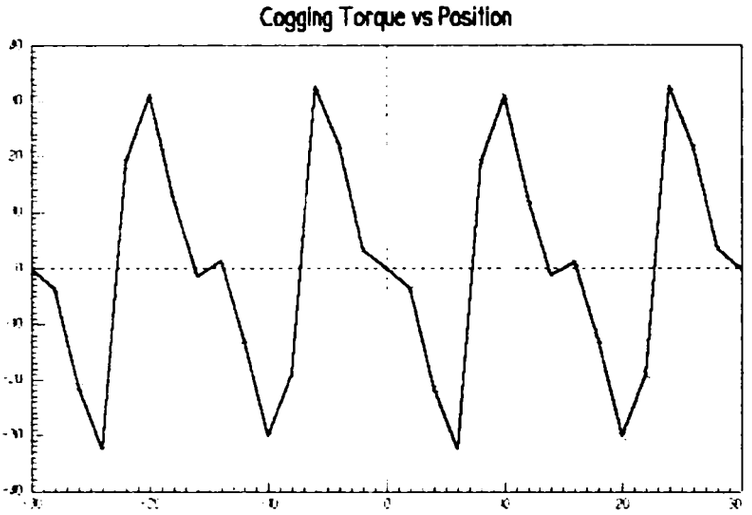

Figure 3.16. The cogging torque vs. rotor position [Nm/u.l.] for a three phase FRG having the following geometrical topology: stator pole width / rotor pole width = 1/3, PM thickness = 2 mm, air-gap = 0.5 mm

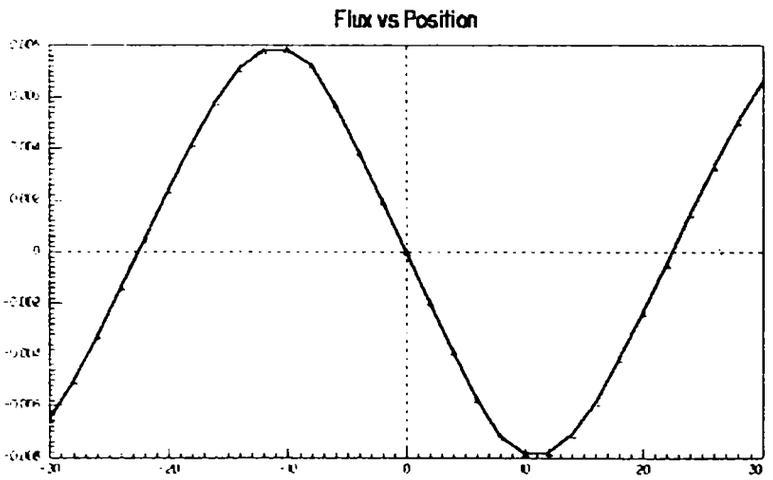

Figure 3.17. The stator pole magnetic flux vs. rotor position for a three phase FRG having the following geometrical topology: stator pole width / rotor pole width = 1/3, PM thickness = 2 mm, air-gap = 0.5 mm

Now, the cogging torque has a peak value of 32 Nm/u.l. and the magnetic flux maximum value is 0.008 Wb/u.l.

Considering the previous changes and their effects from the main generator characteristics point of view, the air-gap is modified in the way of increasing it from 0.5mm to 1mm.

The first result in modifying the air-gap, without any numerical analysis, will be the costs for stator and rotor sheets manufacturing process, high requirements are not necessary, so the production costs are minimized.

As will be shown in figure 3.18 and figure 3.19, for both geometrical topologies of rotor iron, the effects of air-gap increase are positives, of course to obtain this conclusion, many changes of the air-gap dimension were made, always looking for the optimal solution.

The geometrical topology of the machine changes as follows: stator pole width / rotor pole width = 1/2, PM thickness = 2 mm, air-gap = 1 mm.

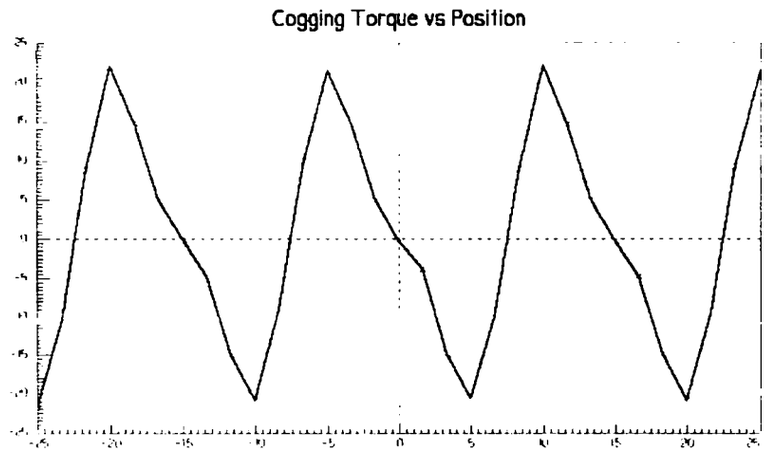

Figure 3.18. The new cogging torque vs. rotor position (after changes indicated above)

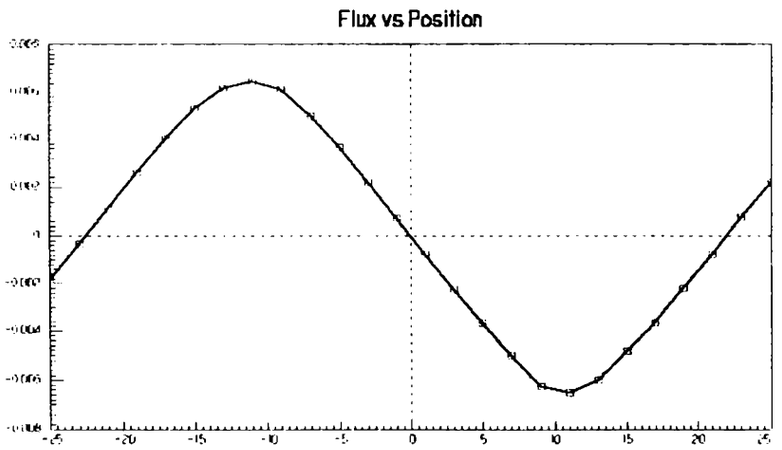

Figure 3.19. The magnetic flux through a stator pole vs. rotor position (with the geometrical changes indicated above)

The new peak values are: 23 Nm/u.l for the cogging torque and 0.0063 Wb/u.l. for the flux.

By making the next changes in geometrical topology: stator pole width / rotor pole width = 1/3, PM thickness = 2 mm, air-gap = 1 mm, the results will be as indicated in next figures.

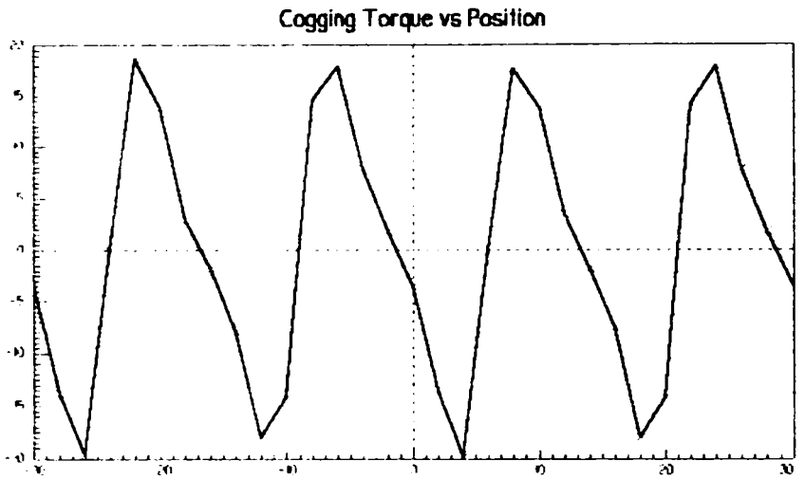

Figure 3.20. The cogging torque variation vs. rotor position

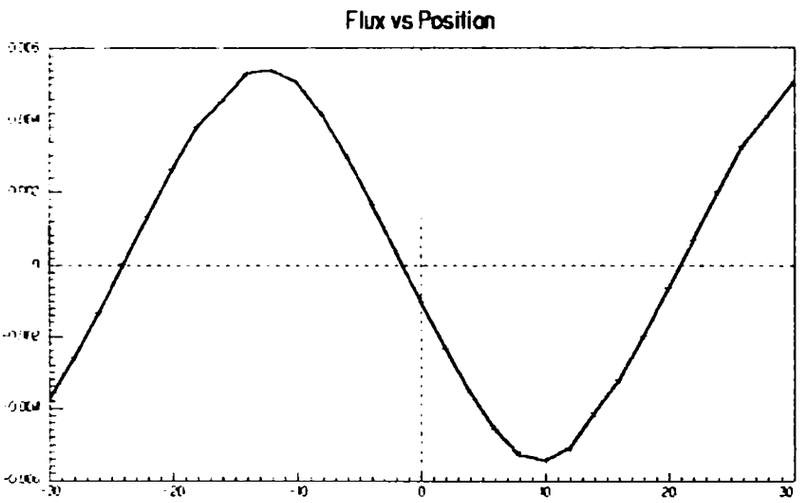

Figure 3.21. The magnetic flux through stator pole vs. rotor position

After these changes, the peak values are: 20 Nm/u.l. for the cogging torque and 0.0056 Wb/u.l. for the magnetic flux.

Generally speaking, optimizing the geometrical topology for an electric machine, in this case of the FRG, it is one of the main problems in the designing process, which has to be treated with responsibility, to reach the optimum for the production costs, the efficiency and working conditions.

The numerical analysis through FEM of an electric machine for the geometrical structure and configuration is a modern, efficient and fast method of analysis who is imposing both, from the easy to use and the good results point of view.

In challenge, to improve the performances of the FRG, to concentrate the magnetic flux through the rotor poles in the align position; changing the PM position in the stator pole plate has been done.

By introducing them inside the stator pole, the immediate influence will be on the manufacturing costs.

We have to mention that in rest, the FRG topology remains the same: same outer and inner diameters, same rotor topology, only the stator poles topology is changing in order to offer the possibility of introducing the PMs in this new positions.

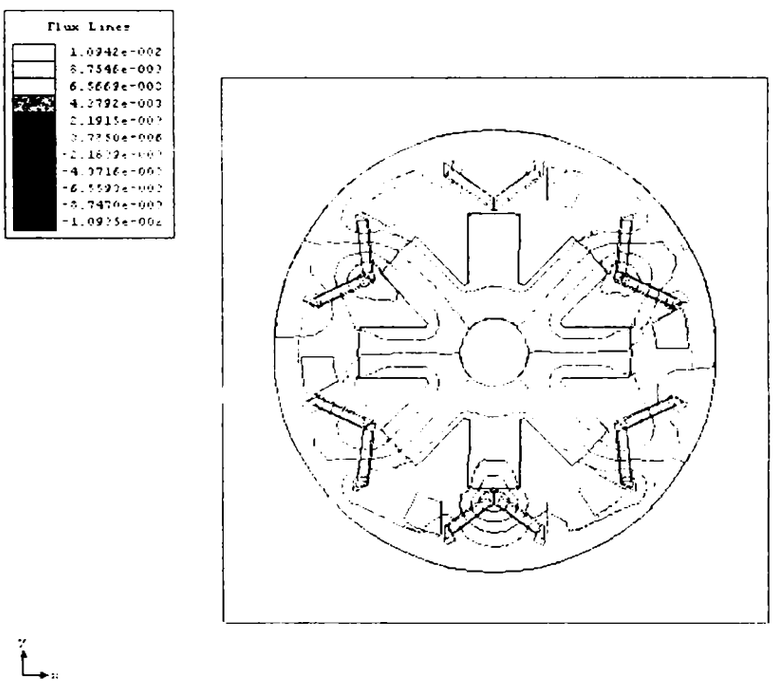

Figure 3.22. The electromagnetic field for the aligned position of the rotor poles with the corresponding stator poles for the new PM configuration

As expected, the useful space between the stator poles is reducing with consequences on machine output power (smaller space for windings). Maybe, using bigger PM's this effect will be reduced.

Figures 3.23, 3.24 and 3.25 show us the first results of the study using the FEM for this new topology of the three phase FRG.

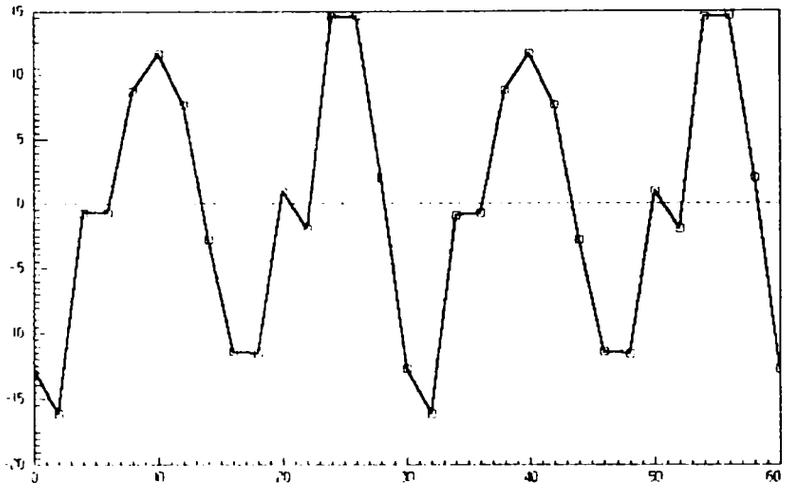

Figure 3.23. The cogging torque vs. rotor position

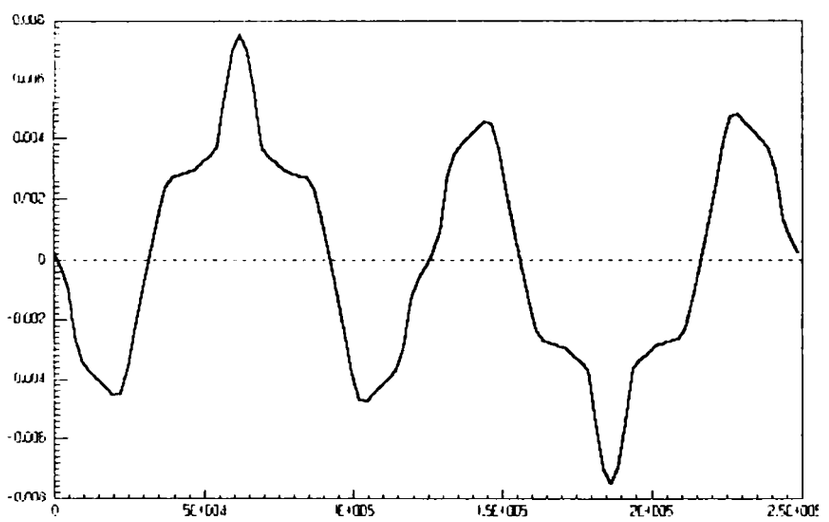

Figure 3.24. The air-gap magnetic flux vs. rotor position

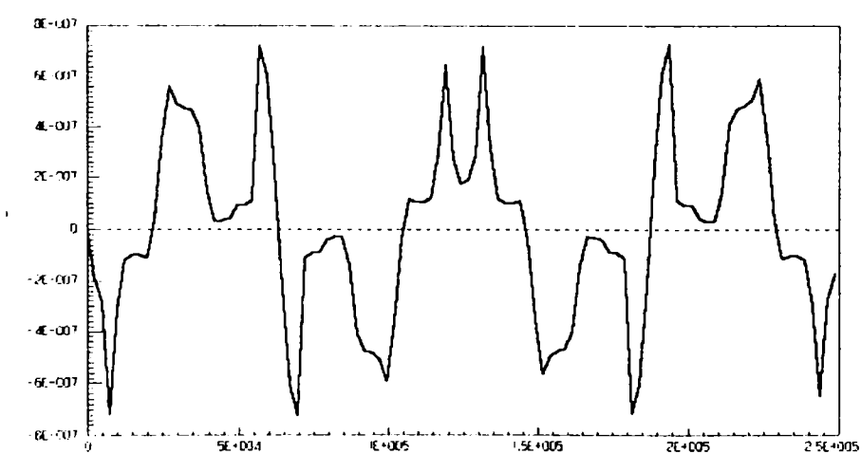

Figure 3.25. The magnetic flux density vs. rotor position

A decrease of the cogging torque (now a peak value of just 16.5 Nm/u.l.) with good effects on high speed behavior of the machine, but it can be observed that the magnetic flux and flux density waveforms (and peak values) are not promising for this new topology a good future.

Making the rotor poles width smaller (figure 3.27), the air-gap magnetic flux is larger on the align position (figure 3.28), as was expected.

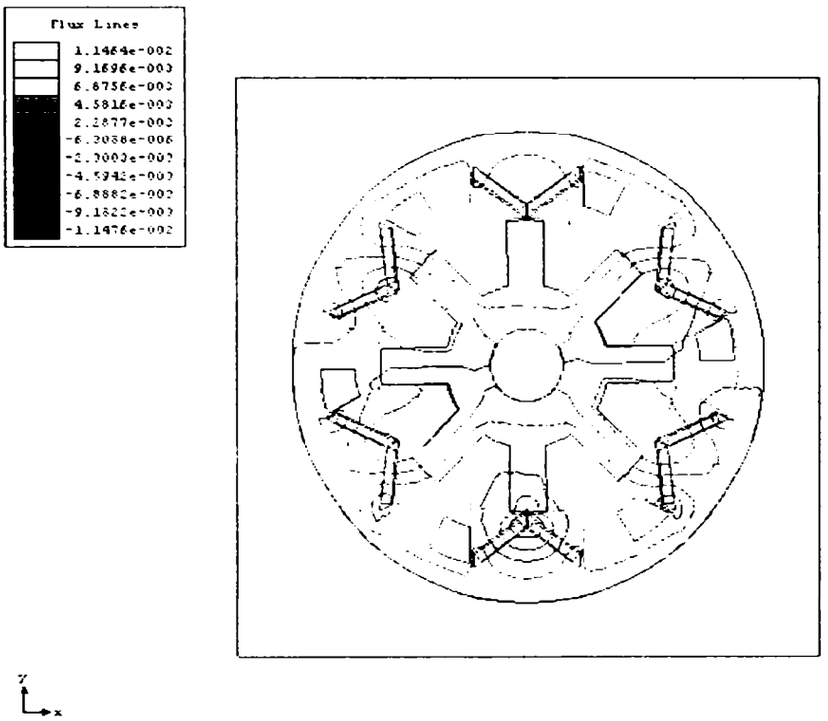

Figure 3.27. The electromagnetic field distribution for the new configuration

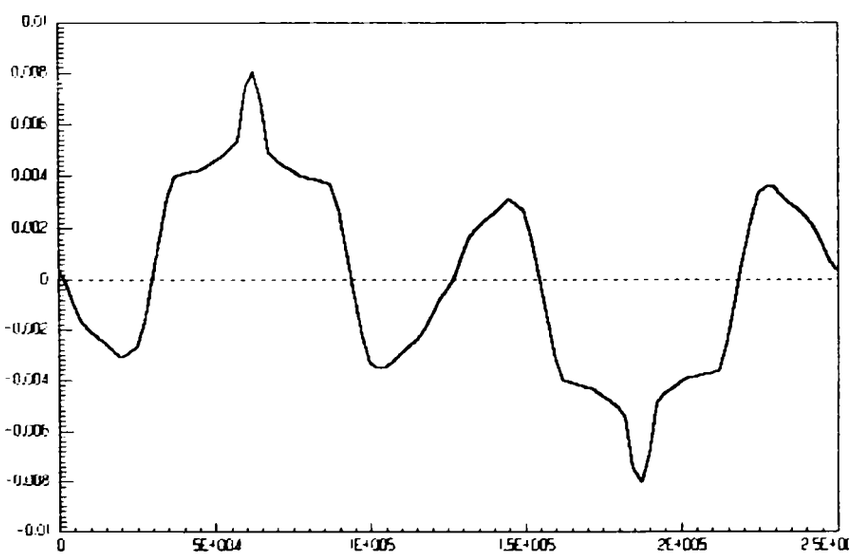

Figure 3.28. The air-gap magnetic flux waveform

Unfortunately, the waveform of the magnetic flux and the air-gap flux density waveform (figure 3.29) demonstrate us that with this configuration we will not have the expected results.

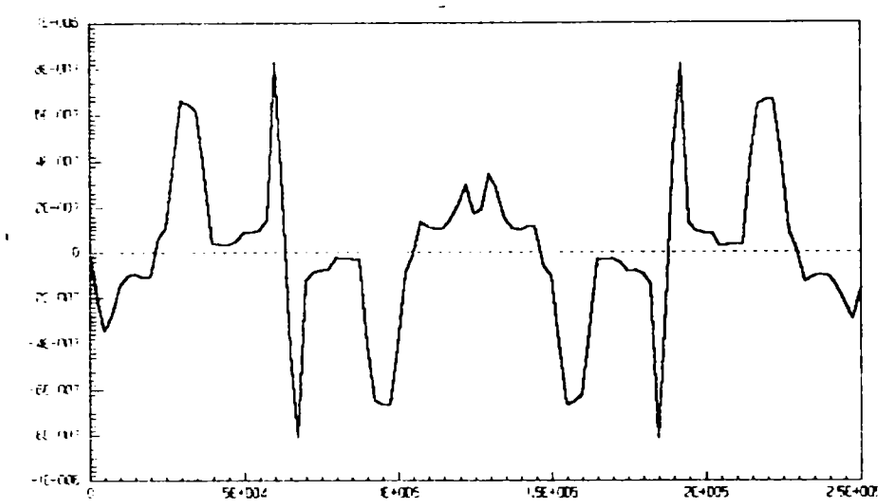

Figure 3.29. The air-gap magnetic flux density waveform

Studying the Flux Reversal generator with the Finite Element Method brought us some remarkable results regarding its geometrical structure.

As preliminary analysis shown, skewing the rotor can do a substantial minimization of the cogging torque, the result for the model under study will be presented in what follows.

Analyzing the effects against the cogging torque by skewing the rotor, built as small number of rotor sheets stacks, we observe that the resulting cogging torque waveform is smaller so a good behavior of the machine at high speeds is expected.

For the generator under study, having the stator pole width/ rotor pole width ratio of , the PM thickness of and an air-gap of 0.5mm, by skewing the rotor (4 rotor sheets stacks) with 15^0 mechanical degrees (from the first one up to the last one), 120^0 electrical degrees, results a cogging torque waveform as indicated in the figure 3.30 (comparing with the previous waveform from figure 3.10).

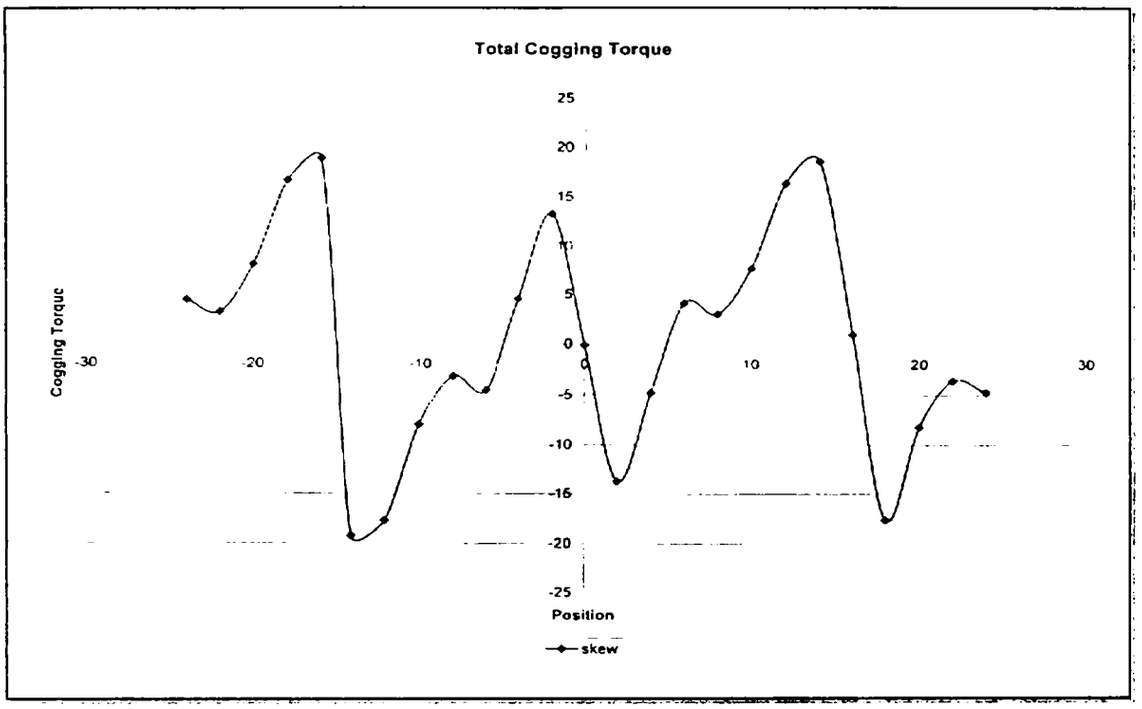

Figure 3.30. The total cogging torque waveform [Nm/u.l.] vs. position [mechanical degrees] for the 4 stacks of rotor sheets

3.5. FRG Car Generating System Simulation

The following features of the FRG make it a favorable choice for next generation of automobile alternators:

- Stator has a concentrated winding;
- Rotor is winding-less;
- Robust and easy to build;
- The simple structure of stator and rotor – manufacture low costs;
- High performance of PM's and flux reversal feature make high power density and high efficiency possible;
- Radial flux path allows more flexibility in scaling up and down the design to meet specific power requirements;
- The absence of the field coil, slip rings, brushes makes the machine easy to maintain;
- Wide speed range is a generic capability of the FRG;

A three-phase equivalent circuit model will be obtained, in order to get a constant and stabilized voltage output, a controller will be presented. Combining the circuit model with the proposed control circuit, PSpice™ simulations will be carried out.

Analytical design together with some FEM back up has lead to the following data:

- stator bore diameter D_i= 0.07 m
- stator external diameter D_e= 0.129 m
- stack length L= 0.08 m
- stator/rotor poles N_s/N_r = 6/8
- phase inductance L_s= 0.67 mH

- phase resistance $R_s = 0.19\ \Omega$
- phase e.m.f. fundamental $E_1 = 1.6n$ (n = rotor speed in rps)
- phase e.m.f. third harmonic $E_3 = 0.3\ n$

For the system's digital simulations we do require the mathematical model of the generator, power electronics converter (PEC) and for the voltage controllers.

The generator model for constant speed reduces itself to the phase voltage equations:

$$L\frac{d}{dt}\begin{vmatrix} i_a \\ i_b \\ i_c \end{vmatrix} = \begin{vmatrix} V_a \\ V_b \\ V_c \end{vmatrix} - R_s \begin{vmatrix} i_a \\ i_b \\ i_c \end{vmatrix} + \begin{vmatrix} e_a(\theta_r) \\ e_b(\theta_r) \\ e_c(\theta_r) \end{vmatrix} \tag{3.51}$$

$$\theta_r = 2\pi \int n dt + \theta_0 , \tag{3.52}$$

with $e_a(\theta_r)$, $e_b(\theta_r)$ and $e_c(\theta_r)$.

We have to add to this model the PEC equations. Based on the PEC configuration its model is easy to obtain in Pspice™. Finally, the voltage controllers are added.

To produce controlled d.c. output, the FRM a.c. output is rectified, filtered and than chopped at constant frequency (10 kHz) as triggered by a hysteresis voltage controller, and filtered again (figure 3.31).

For the beginning, a simple generating system for a 42 V d.c. battery charging with a rectifier and chopper, using a single power switch for voltage control (S_0), was designed.

Load damping is handled easily unless the power switch remains open. In this latter case the FRM high no load voltage reaches the load and special means of protection might be necessary.

In reality, considering the presence of the battery, which behaves like a "huge" capacitor, special means of protection are not necessary.

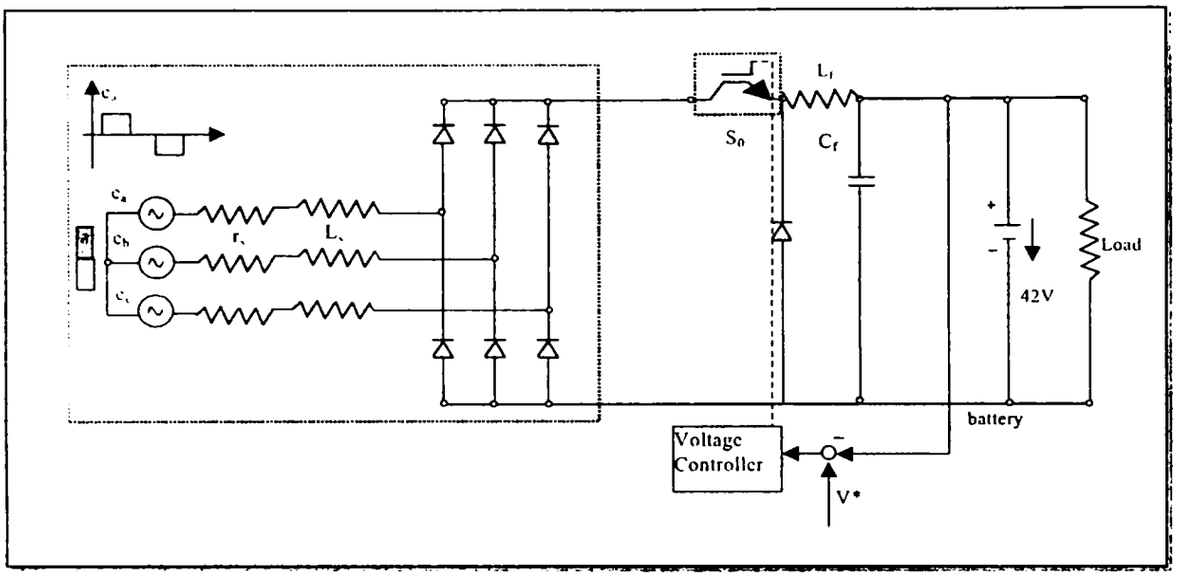

Figure 3.31. The generating system structure

The primary goal of the controller is to regulate the output voltage to the required level with a fast response.

The output voltage of the FRG varies quasi linearly with speed. The controller has to regulate faster the output voltage to the reference voltage. For this, the switch can be controlled by a PWM signal, which comprises the output voltage feedback loop and a feed-forward loop of the rectifier output voltage.

To investigate the steady state and transient performance of this generating system for given speed, a PSpice™ program has been written and run extensively. (see appendix D) Some representative results are presented in what follows.

Figure 3.32 shows the a.c. current waveforms (for all three generator phase) at 2100 rpm, 42 V d.c. output and 1.5 kW.

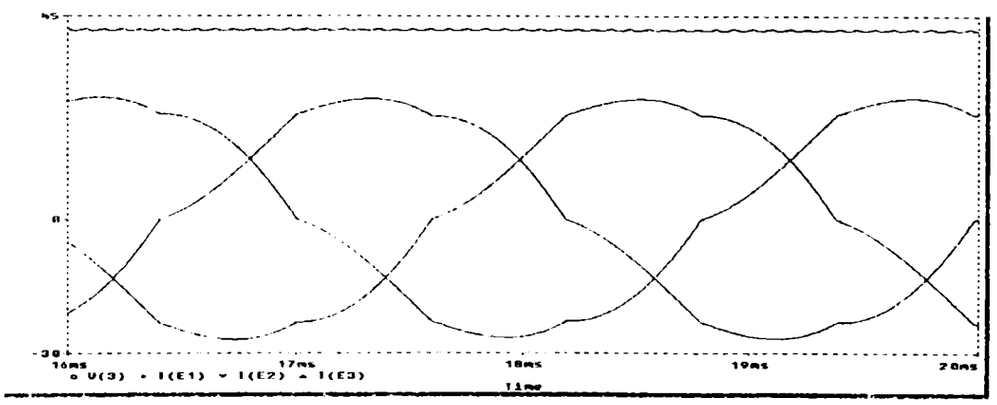

Figure 3.32. Phase currents at 2100 rpm, 42 V d.c., R_{load}=1.16Ω, 1.5kW.

Full power (3 kW) is delivered already at 4000 rpm and 42 V d.c. (figure 3.33).

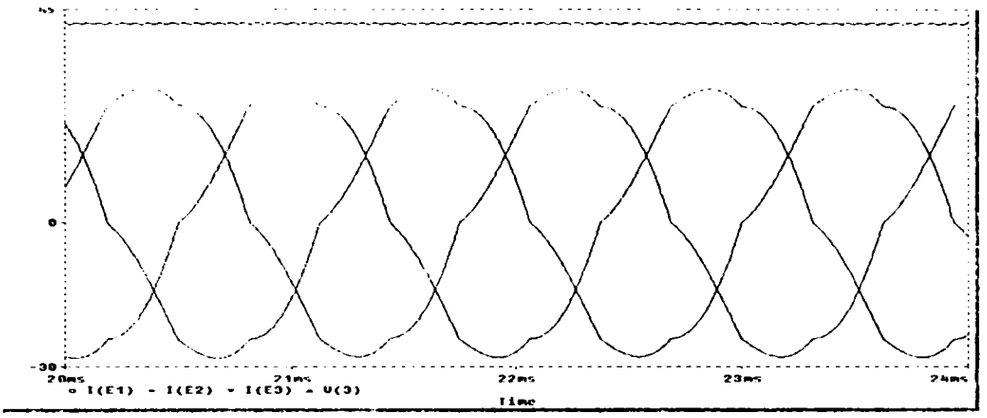

Figure 3.33. Phase currents and d.c. voltage (42 V d.c.) at 4000 rpm, power P=3 kW (R_{load}=0.58 Ω).

Finally, the performance at 42 V d.c., 18000 rpm, 3 kW with a sudden change (increase) in the load resistance from 0.58 Ω to 1.16 Ω, as shown on figure 3.34.

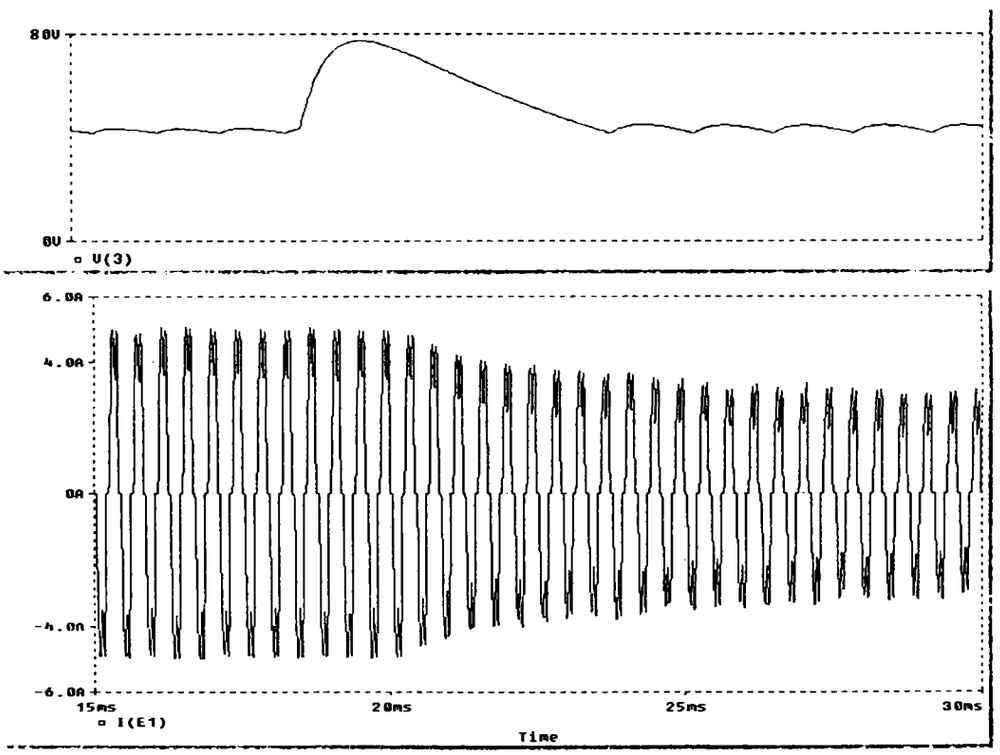

Figure 3.34. D.C. voltage and phase currents at 18000 rpm if R_{load} changes from 0.58 Ω to 1.16 Ω

The voltage recovery is very fast (about few milliseconds). A zoom of phase currents (figure 3.35) show their discontinuity.

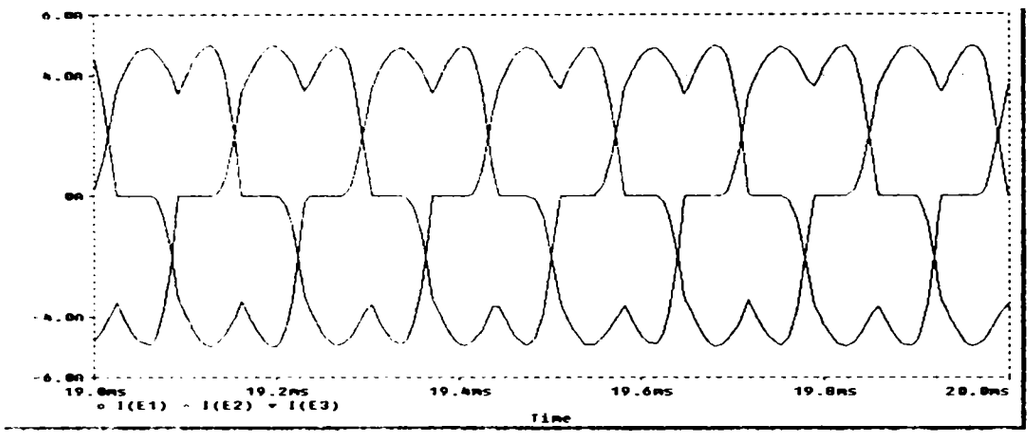

Figure 3.35. Zoom of generator currents at R_{load} = 0.58 W, d.c. voltage V = 42 V, at 18,000 rpm.

Also we should note that from 4000 rpm, the phase current amplitudes decrease steadily to 18000 rpm for constant power (3 kW). This shows that the copper losses decrease with speed. As the iron losses increase with speed (frequency), the efficiency remains almost constant over a wide speed range. In our case the efficiency remains above 70%.

The size of the filter capacitor depends on kVA rating of the rectifier; we can assume 30-40% of the rectifier power output as capacitor power. So, as indicated in the Pspice™ listing (from appendix) the capacitor value was obtained using the formula:

$$C_f = 0.33(P_b/\omega \cdot V^2) \tag{3.53}$$

Anyway, it seems that two-voltage system will be required by the load characteristics on the cars of the future. The rated current of both voltage channels (grids) is about the same.

For this reason, a generating system using power electronic converter (PEC) for producing a 42/14 V d.c. voltage output will be presented (figure 3.36).

The 14 V and 42V loads are series connected considering the car body as neutral point.

In this case, two additional IGBTs are used to cancel the neutral current when the load currents in the two power channels differ from each other.

Based on the power electronic converter configuration, a model of the generating system can be easily obtained.

A simplified model was choosing for the batteries, capacitors plus series connected resistances. PSpice™ model listing of the generating system can be found in appendix.

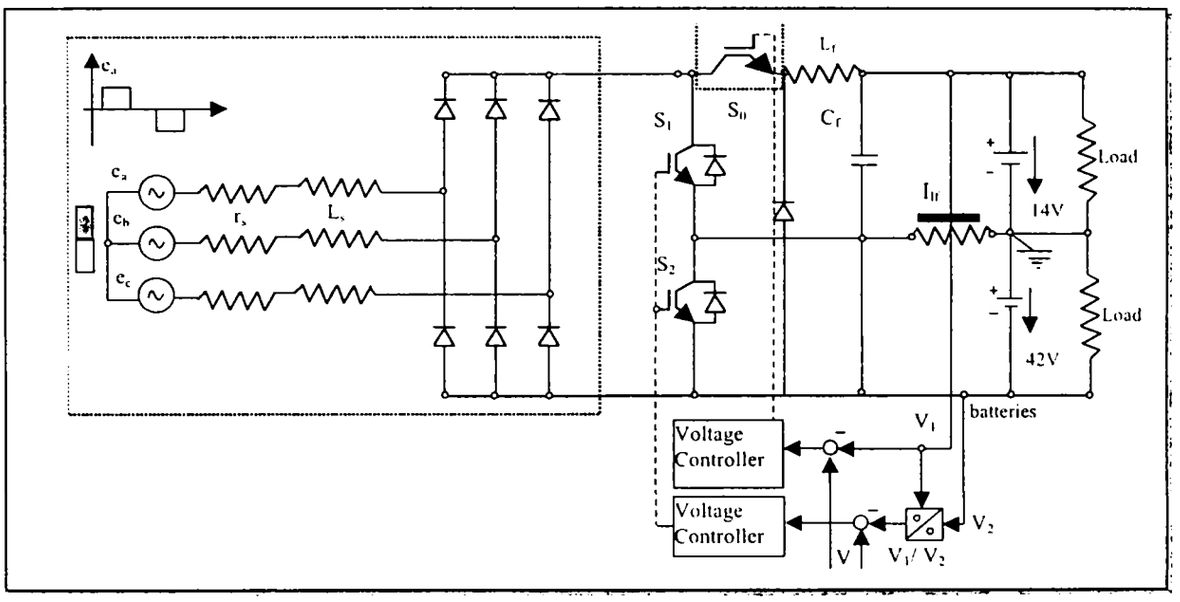

Figure 3.36. The dual 42 / 14 V d.c. generating system

The unidirectional switch S_0 (also, IGBT type), controls the sum of two voltages: $V = V_1 + V_2 = 56$ V d.c., so for the entire system. When a null current occurs, because the two loads are temporarily different from each, it has to be handled through the two switches S_1 and S_2. PI voltage controller with limitation and current regulators are used (figure 3.37).

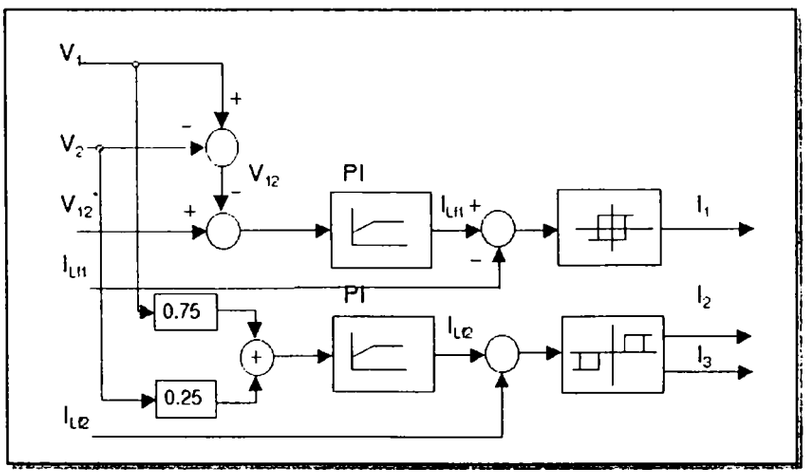

Figure 3.37. Details of the controller

Regulators structure respects power electronic converter structure and the regulation principle. First the total voltage is regulated and the output measure is the total prescribed current I^*_{lf1}.

Total prescribed current is done in a closed loop using a hysteresis regulator. The output is giving the signal to S_0 switch.

The role of the second PI regulator with limitation, is for keeping the ratio: $V_1/V_2 = 1/3$ constant, independently of the two loads charging status.

The output of this regulator is the unbalanced prescribed current for maintaining the two voltages ratio fixed. By fixing the output of the PI regulator at a maximum value of the admitted unbalanced prescribed current, maximum current through S_1 and S_2 switches is limited, so a soft over-current protection is achieved.

Also, the unbalanced current is measured (zero current I^*_{lf2}) and compared with the regulator output value. To control directly the S_1 and S_2 switches, two hysteresis regulators are used, one for each switch.

Digital simulation s have been run at constant speeds. Load sudden changes – balanced and unbalanced – have been investigated at different speeds.

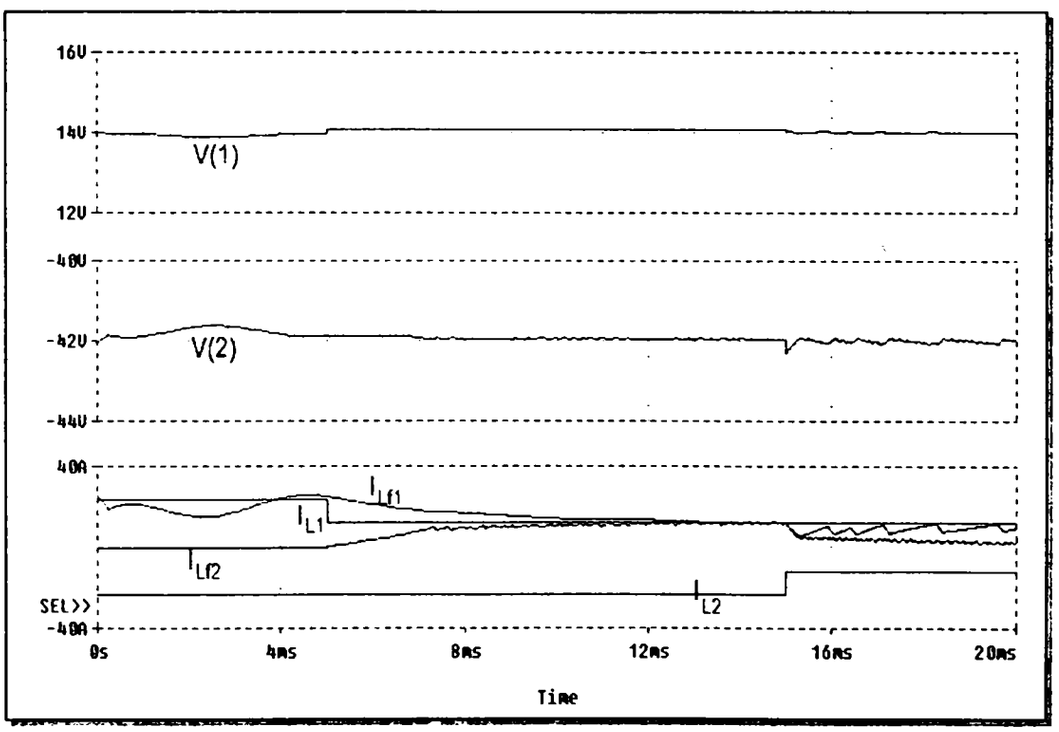

Figure 3.38. Digital simulation results for n_b = 1800 rpm

For the beginning, figure 3.38 shows us the voltages and currents for the two load channels at 1800 rpm speed.

At low speed, the generator has to support the maximum load, for this reason keeping the output voltage at constant values is done at the limit.

If a load step variation appears on one of the two networks and then on the other one too, we observe (as in figure 3.38) a small variation of the output voltages. In what follows, the result considering the same changes in load at 9000 rpm and 18000 rpm are presented.

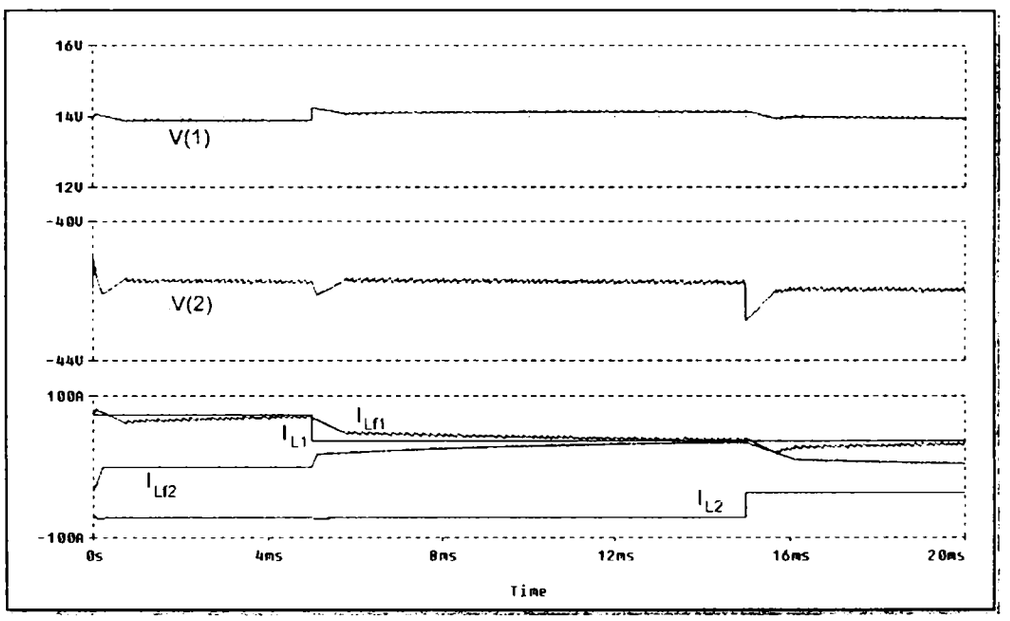

Figure 3.39. Digital simulation results for n = 9000 rpm

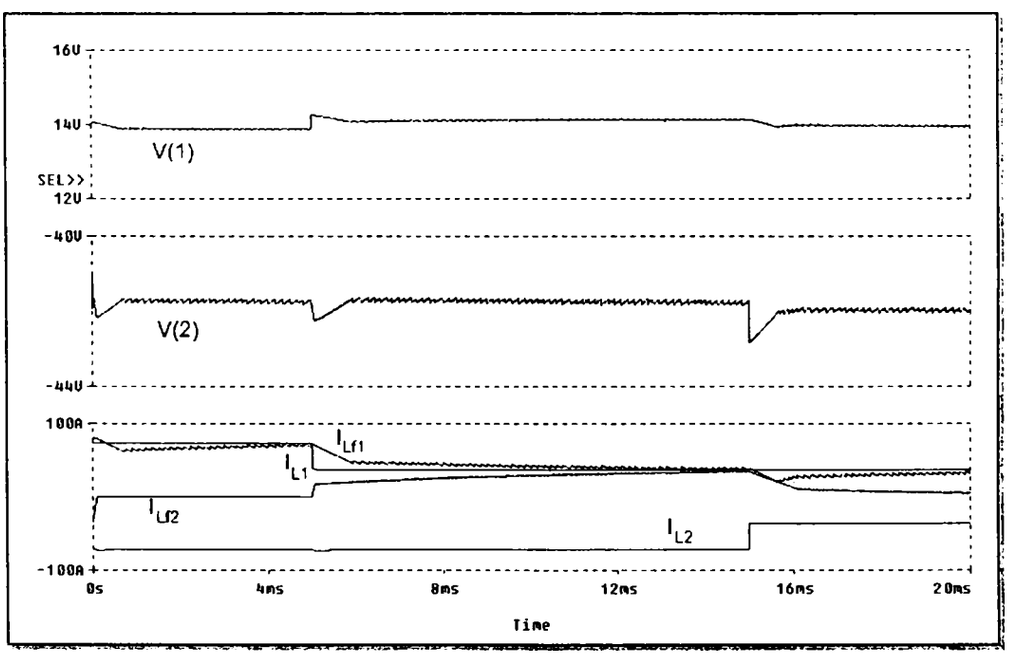

Figure 3.40. Digital simulation results for n = 18000 rpm

At high-speed generator operation, the converter output voltage is ten times higher than the nominal output voltage. We notice the output voltage ripples (figure 3.40), caused by the power converter which works with large differences between the input (from the generator) and output (to the loads and batteries) voltages.

These voltage ripples are acceptable from the consumer point of view. The batteries model was created using 300 mF, respectively 100 mF, in series with 0.01 Ω, respectively 0.03 Ω resistors. In reality, the battery equivalent capacity is much higher and so, the voltage ripples will be much smaller.

At current step variations, the output voltage is changing fast but it is faster recovered because of the PI regulators from the control system which includes two regulators, a fast acting one for current regulation and one more for voltage regulation, and this for each grid in part.

3.6. Conclusion

The FRG this new brush-less doubly salient permanent magnet generator is proposed with the same aim of combining the advantages of the SRM and BLDCM into one machine.

The most attractive features of the three-phase FRG are:

- The robust and easy to build rotor, without PM's or windings and with low inertia, important for high speed applications;
- The stator has PM's and windings, the demagnetization effect of PM's due to over-temperature is considerable reduced because of easy to cool feature given by their position (unlike BLDCM);
- The relative large air-gap, avoids the tight manufacturing tolerance that can adversely impact manufacturing cost;
- High performance PM's, with high coercive, linear magnetization characteristics and low temperature coefficient, help to produce higher output power for the same speed and active volume as Lundell generator or SRG;
- The elimination of the field coil, slip rings, brushes result in compact, maintenance free machine, suitable for working in a hostile environment;
- Low self inductance which is desired for high frequency operation;
- Low mutual inductance should be understood as a strong fault tolerant ability, important for critical application (aerospace and defense industries etc);
- The magnetic flux path per pole is completed within a radial plane, thus eliminating the need for axial flux carriers such as steel shaft and core in claw-pole generator;
- The cogging torque is always a major obstacle for doubly salient machines but as shown it can be drastically reduced.

Using the FEM analysis results from paragraph 3.2, we can draw a table in which, using a fringing factor, K_σ, we can establish the proper geometry topology of the machine:

$$1 + K_\sigma = \frac{ideal \ \max \ phase \ flux}{real \ \max \ phase \ flux} = \left(\frac{\lambda_{PMi}}{\lambda_{PM}} \right)_{\max} \tag{3.54}$$

The expression of $(\lambda_{PMi})_{max}$ is:

$$(\lambda_{PMi})_{max} = B_{PM} \tau_s L \tag{3.55}$$

$2\tau_s$ - stator pole span; L – stator stack length; B_{PM} – the PM radial flux density:

$$B_{PM} = B_r \cdot h_{PM} / (h_{PM} + g \cdot \mu_{rec} / \mu_0) \tag{3.56}$$

The fringing coefficient K_σ is related to geometrical parameters such as: g/h_{PM}, τ_s/h_{PM}, h_{pr}/h_{PM} with h_{pr} – the rotor pole height.

Such dependencies, FEM obtained, may then be used through adequate curve fitting to define K_σ (h_{PM}/g, h_{PM}/τ_s, h_{pr}/τ_s) functions.

The inductance L_s function is also calculated through FEM. It seems pretty obvious that we need to choose the variables h_{PM}/g, h_{PM}/τ_s, h_{pr}/τ_s such that K_σ were minimum.

In order to reduce the machine electrical time constant (inductance L_s) the PM radial height tends to be high. However above a certain value of h_{PM} the leakage inductance becomes predominant and thus any further PM height increase is not useful. Typical results obtained through 2D-FEA are shown in table 3.1.

Table 3.1. Fringing coefficient K_σ

Airgap	h_{PM}	h_{pr}/τ_s	h_{PM}/τ_s	$1 + K_\sigma$	K_σ	B_{in}
0.5	6	1	0.375	3.9193	2.91	1.12
0.5	2	1	0.125	1.9059	0.90	0.96
0.5	6	2/3	0.375	2.9555	1.95	1.12
0.5	2	2/3	0.125	1.9297	0.92	0.96
1.0	6	1	0.375	3.6159	2.61	1.03
1.0	2	1	0.125	1.9845	0.98	0.79
1.0	6	2/3	0.375	3.4652	2.46	1.03
1.0	2	2/3	0.125	2.1526	1.15	0.79

For the minimum K_σ case from table 1: $K_{\sigma min}$= 0.9; 1 / (1+ $K_{\sigma min}$)=0.526 for h_{pt}/τ_s=2/3 h_{PM} τ_s=0.125 for τ_s= 0.0138m, D_i= 0.07m.

Results such as those in table 3.1 show that there is no need to increase the PM height too much as both K_σ and L_s become only loosely dependent on it.

The final decision on PM height h_{PM} depends also on cost factors but the above inquiry should be essential in providing solid data for conceptual and optimal designs.

From the digital simulation runs we may draw remarks such as:

- the FRM seems capable to deliver constant rated power at constant voltage over a 4.4 to 1 speed range (from 4000 rpm to 18000 rpm) with half rated power down to 2100 rpm.

- the low inductance of FRM is at the origin of steady decreasing of stator phase currents with speed for constant power and voltage. Consequently the machine losses do not vary notably with speed and thus the efficiency remains high (above 70 % for the case in point).

- the voltage recovery under sudden load changes is very rapid (one millisecond in our case) in contrast to existing Lundell generators used for automobiles.

It follows that with a rugged simple topology, FRM could be a serious candidate for constant power and voltage for wide speed range applications.

A prototype, built and tested (as shown on the following figure) in U.S.A. [3.7]

Figure 3.41. Details from a 3 kW Flux Reversal Machine prototype

References:

[3.1] S. Andersen – *"Flux Reversal Machine"* – Master Thesis Project, September, 1996;

[3.2] R. Lagerquist, I. Boldea T.J.E. Miller– *"Sensorless Control of the Synchronous Reluctance Motor"* – Record of IEEE Transaction on Industry Applications, vol. 30, No. 3, 1994;

[3.3] Luo, D. Quin, T.A. Lipo – *"A Novel Two Phase Doubly Salient Permanent Magnet Motor"*- Record of IEEE – IAS, 1996;

[3.4] R. P. Deodhar, S. Andersen, I. Boldea, T.J.E. Miller – *"The Flux-Reversal Machine: a New Brushless Doubly-Salient Permanent Magnet Machine"* – Record of IEEE Transaction, 1997;

[3.5] E.C. Lovelance, T.M. Jahns, J.L. Kirtley Jr., J. H. Lang – *"An Interior PM Starter/Generator for Automotive Applications"* – Record of IEE 1998

[3.6] T.M. Zahias - *"Uncontrolled generator operation of interior PM synchronous machines following high speed inverter shut down"* - Record of IEEE - IAS 1998 - Annual Meeting;

[3.7] C. Wang, S.A. Nasar, I. Boldea – *"Three-phase flux reversal machine (FRM)"* – Record of IEE, 1999;

[3.8] I. Boldea - *"Automotive electric generator systems. A review"* - Record of IEEE, Patras, 1999;

[3.9] C. Wang, S.A. Nasar, I. Boldea – *"High Speed Control Scheme of Flux Reversal Machine"* – Record of IEEE 1999;

[3.10] I. Boldea, J. Zhang, S.A. Nasar – *"Characterization of Flux Reversal Machine in low speed (direct) servo drives – the pole – PM configuration"* – Record of IEMDC, 2001;

[3.11] I. Boldea, S. Scridon, L. Tutelea, C. Lascu, N. Muntean - *"The flux reversal machine (FRM) as an automotive alternator with 42/14 v d.c. dual output"* - "OPTIM 2000" International Conference, Brasov, Romania, May 2000;

[3.12] C.X. Wang, I. Boldea, S.A. Nasar – *"Characterization of Three Phase Flux Reversal Machine as an Automotive Generator"* – Record of IEEE, 2001;

[3.13] K. Yoshida, K. Kesamaru, Y. Hita – *"Eddy Currents Analysis of Surface-Mounted-PMSM by Finite Element Method"* – Record from IEE, 1998.

CHAPTER IV

BEGA - A NEW VARIABLE SPEED ELECTRICAL GENERATOR FOR AUTOMOBILE INDUSTRY

4.1. Introduction

In this chapter, a new type of electric machine will be introduced. Designed to operate as a variable speed generator, its main destination being the automobiles industry applications.

The topology, basis equations, a design procedure, some preliminary results through FEM analysis and practically, the virtual prototype will be presented. A new output voltage control method (because the generator is designed to operate at variable speed) will be introduced also. Many of the calculations are based on simplified models. The models have been estimated to be sufficient for a preliminary generator design.

As in previous chapters was presented, from reasons regarding especially: automobile fuel consumption reduction, increase of alternator efficiency, space compacting and weight reduction trends; new electric machines, with different topologies and configurations already have been designed (as already presented in previous chapters).

The variable reluctance synchronous machines with salient rotor, with or without PM's, were introduced recently for studies, gaining more field especially due to their robustness and efficiency. Their application on automobiles is delayed because of the control system high costs, which are few times larger than for the present car generating systems. [4.1]

This new generator - only system, with a biaxial excitation (Biaxial Excitation Generator for Automobiles - BEGA) is a hybrid synchronous machine. Some of its constructive particularities together with its simple low power control are the main advantages and from some point of view those are sufficient for using this electric machine in vehicle generating systems (comparing with [4.2], [4.4], [4.5]). Test results for a real prototype, included in chapter six, will confirm these affirmations.

4.2. Theory

4.2.1. Principle of Operation

In what follows, this new type of electric machine, designed for generative use will be introduced. This is designated mainly for electric energy supply of drive systems and electronic equipments from cars board systems and for batteries charging.

The biaxial excitation generator for automobiles is a hybrid synchronous machine whit a topology as follows:

- a three phase stator, like an asynchronous machine;
- a salient multi-pole rotor with multi-flux barriers;
- low cost permanent magnets (Ferrite) inserted inside the flux barriers;
- a rotor winding with field purpose. [4.8]

The operation principle of this generator is based on multiple flux barriers principle and on the permanent magnets inside those flux barriers and magnetized as shown in figure 4.1.

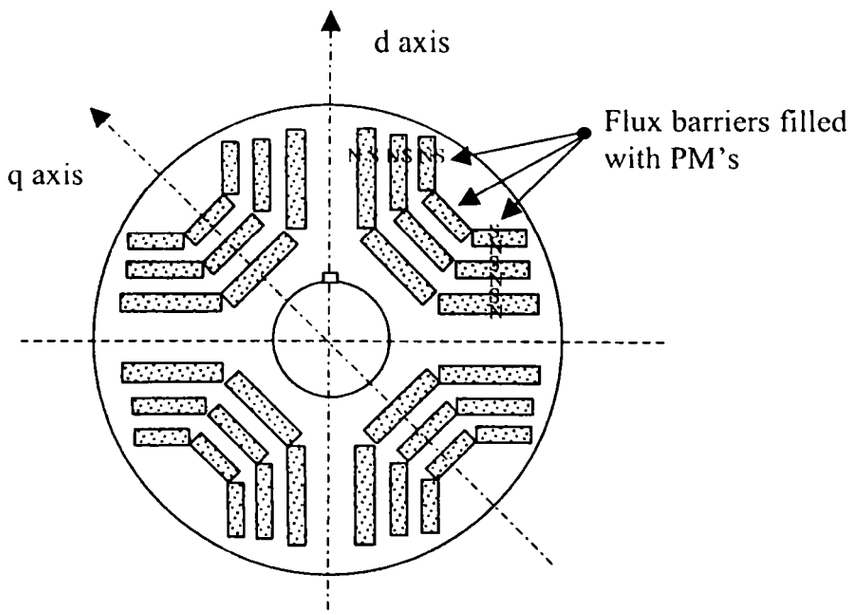

Figure 4.1. Four pole rotor with multiple flux barriers filled with PM's

(three layers)

In figure 4.1, only the permanent magnets magnetization is presented, without the field windings and rotor teeth saliency.

This electric machine is combining the advantages of a simple and effective electronic field control, practically the claw pole regulator can be maintained, with those given by a superior efficiency (up to 80%) and a good power/volume ratio.

Beside the higher manufacturing cost (but comparable with the modified Lundell generator), especially caused by the permanent magnets inserted in the rotor, the superior net efficiency and excellent power/volume ratio constitute the main advantages of this type of machine (comparing with [4.3]).

Operating at constant power (and voltage) a speed range up to 1/6 should be possible for this type of electric machine.

4.2.2. Configuration, The First Prototype

The initial proposed topology for a biaxial excitation generator with four rotor poles, which has been used as a prototype too, is shown in next figure:

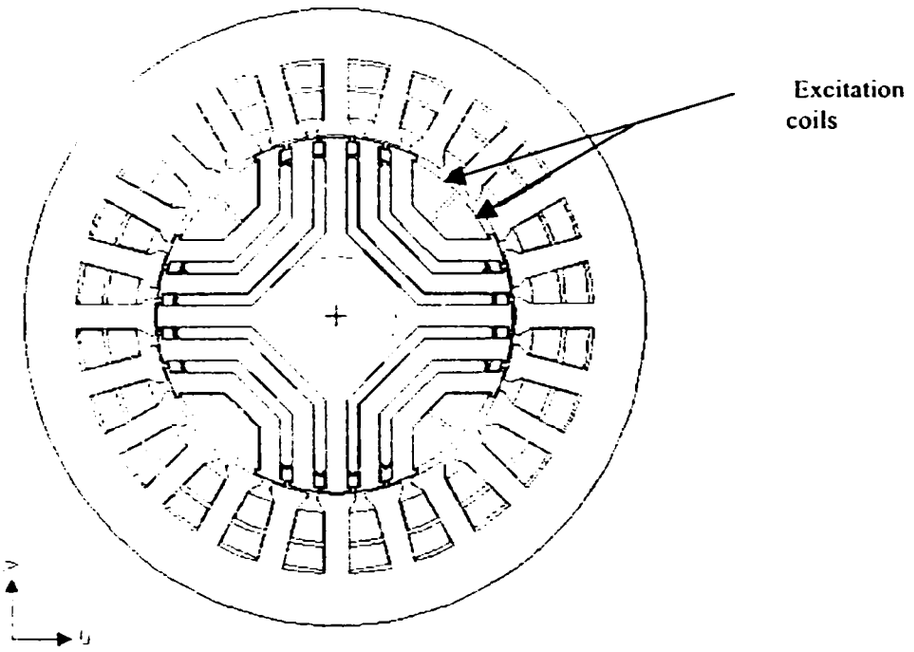

Figure 4.2. The four poles rotor topology of a first prototype of biaxial excitation generator

The rotor of this machine was already made for a reactance synchronous machine (just with flux barriers) so, the first choice was to fill the barriers of the existing rotor structure with low cost permanent magnets, respecting the magnetisation for those and by cutting some parts of the rotor sheets, the rotor field coils were inserted. The result of these delicate operations was the first prototype of BEGA.

Of course, FEM were done before making the prototype, and the preliminary results did encouraged us to build a full scale prototype in the sense of using this rotor geometry.

The permanent magnets inside flux barriers are magnetized in that way that the magnetic flux is on axis q (see figure 4.1 and figure 4.3), considering this, the generator will operate at unity power factor, recommended for diode rectifier operation.

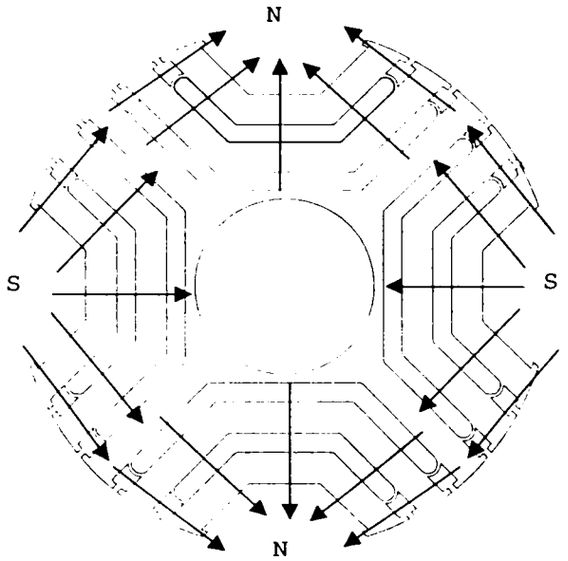

Figure 4.3. The PM magnetization and rotor saliency of the first BEGA prototype

The main equations of this machine are presented as follows, these are used for the designing process [4.10].

The voltage, for $\cos\varphi_1=1$ and zero magnetic flux in q axis ($i_d=0$, $\psi_q=0$):

$$V_1 = E_{01} - R_s I_{qrated} \;;\; I_{qr} = I_{rated}/2 \tag{4.1}$$

Where, the e.m.f. is:

$$E_{01} = 2\pi n P L_{mf} I_f \tag{4.2}$$

Considering that:

P – the number of pole pairs;

n – the speed, in rpm;

L_{mf} – the mutual inductance;

R_s – the stator phase resistance;

i_f – the field current.

The three phase stator coils are in a single layer, those can be made by Copper conductor, single or multi-layer (preferable from loses point of view).

For small loads (small I_q current):

$$\lambda_q = L_q I_q - \lambda_{PMq} < 0 \tag{4.3}$$

where: L_q – the q axis inductance;

λ_{PMq} – the PM magnetic flux across q axis.

Equation (4.1) can be modified for $\cos\varphi_1=1$ as follows:

$$V_1 = E_1 - R_s I_s \; ; \quad I_s < I_{rated} \tag{4.4}$$

$$I_s = I_d + j\, I_q \tag{4.5}$$

$$E_1 = 2\pi pn\, \lambda_s \; ; \quad \lambda_s = I\, \lambda_d + j\, \lambda_q\, I \; ; \tag{4.6}$$

$$\lambda_d = L_{mf}\, I_f + L_d I_d > 0 \; ; \; \lambda_q = L_q I_q - \lambda_{PMq} < 0 \tag{4.7}$$

with: $\lambda_q < 0$ and $\cos\varphi_1 = 1$, equations (4.4) – (4.7) show us a phasor diagram as indicated in next figure:

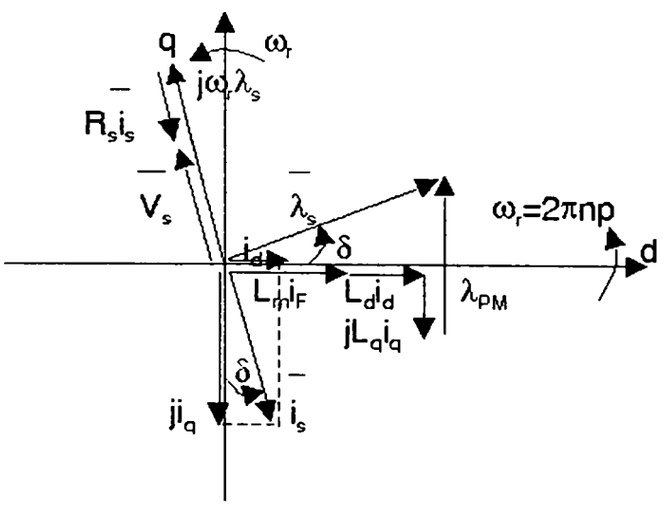

Figure 4.4. The phasor diagram for $\cos\varphi_1 = 1$

Similar for $i_q > I_{rated}/2$; $\lambda_q>0$.

To prevent PM demagnetization, in fact: $L_{qm} i_{rated} = \lambda_{PMq}$.

4.3. Conceptual Design

4.3.1. Basic design – by example

A conceptual design procedure which starts from next initial data will be presented in what follows, based on this design procedure, a prototype will be realised and tested.

The main generating system data are:

D.c. bus rated voltage: V_{dc}= 42 V

D.c. bus rated current: I_{dc}= 75 A (for more than 2xn_{min})

Automobile idle speed: n_{min}= 1500 rpm

Current at n_{min}: I_{dcm} = 75/2 A

Maximal generator speed: n_{max}= 9000 rpm

Additional data are required for a proper design. The following additional data will be considered:

- the air-gap magnetic flux density for no load operation: B_{g0}= 0.65 T

- the rated tangential force: f_r = 2.0 N/cm^2

- the stator rated current density: j_{cos}= 12 A/mm^2

- the field current density: j_{cof}= 9 A/mm^2

- the poles number: 2p = 4

- the stator length / bore diameter ratio: λ=L_s / ID = 0.6

With help of the above data, the bore diameter can be calculated and the electromagnetic torque, T_{ek} , assuming a given efficiency (η_{min}) for idle speed operation:

$$T_{ek} = \frac{V_{dc} I_{dcm}}{\eta_{nmin} 2\pi n_{min}} = \frac{42(75/2)}{0.8x2\pi 2(1500/60)} = 12.54 \text{ Nm} \qquad (4.8)$$

So, ID will be:

$$ID = \sqrt[3]{\frac{2T_{ek}}{f_v \pi \lambda}} = 0.09 \text{ m} \tag{4.9}$$

Stator stack length, L_s , is:

$$L_s = \lambda \times ID = 0.054 \text{ m} \tag{4.10}$$

Using a diode rectifier and having a d.c. load, we can assume that a unit power factor. The design of the rotor must be done using an iterative procedure and with help of FEM analysis fast results will be achieved [4.7], [4.9].

For the beginning, we can assume that permanent magnets of Ferrite, with $B_r = 0.39$ T, are used and that air barrier /core thickness ratio is 0.6 and an airgap of $g = 0.5$ mm, in which the flux density will be of $B_{PMg} = (¾)B_r = 0.3$ T.

We can now consider that a zero magnetic flux on q axis is obtained at rated current and $L_q i_{rated}/2 = \lambda_{PMq}$ ($L_{qm} \approx L_q/2$).

For idle speed, half of the rated current is provided, so $L_q i_{nmin} = \lambda_{PMq}$.

Consequently: $B_{PMg}/2 = 0.15$ T.

The airgap magnetic flux density provided by the field current (at no load operation) is about 0.65 T and the current contribution after d axis (unknown until now) should add something to the total amount (not so much).

The relation between the one phase r.m.s. current, I_1, and the output current, I_{dc}, is:

$$I_{dc} = \frac{3}{\pi}\sqrt{2}\cos\varphi_1 I_1 = K_i I_1 \tag{4.11}$$

$K_i = 1.347$

Also, the relation between the d.c. voltage and one phase r.m.s. voltage, is:

$$V_1 = \frac{V_{dc} I_{dc} + 3(V_D + R_D I_{dc}/K_i) I_{dc}/K_i}{3\left(\frac{I_{dc}}{K_i}\right)\cos\varphi_1} = \frac{V_{dc}}{K_V} \tag{4.12}$$

where V_D is the diode residual voltage and R_D the diode equivalent resistance.

Generally V_D= 0.6 - 0.8 V and $R_D I_{DC}/K_i < 1$ V.

To simplify the calculations, for V_{dc}= 42 V we can consider $V_D + R_D I_{dc}/K_i$ = 1.8 V (constant).

Consequently:

$$V_1 \approx \frac{V_{dc} I_{dc} + 3x1.8 I_{dc}/K_i}{3I_{dc}/K_i \cos\varphi_1} \tag{4.13}$$

For an assumed efficiency η_{nmin}, the voltage equation became (V_1=V_s):

$$3V_1(I_{rated}/2) = -(p_{copper}+p_{iron})_{nmin} + 3(2\pi n_{min}\lambda_s I_{rated}/2) \tag{4.14}$$

with $\eta_{nmin} = 0.8$

$$\frac{3V_1}{\eta_{nmin}} = 3x2\pi n_{min} P \lambda_s \tag{4.15}$$

For I_{dcmin} = 75/2 ; $I_{rated}/2$ = 75/2/1.347 = 27.84 A (4.16)

Also: $V_s = V_1$ = 20.658 V.

$$\lambda_s = \frac{V_1}{\eta_{nmin} 2\pi n_{min} P} \tag{4.17}$$

Now: $\lambda_s = B_{g1}(2/\pi)L_s \tau K_W W_1$ (4.18)

The coiling coefficient: K_{W1} (for q = 2, Y/Y = 6/6) is:

$$K_{W1} = \frac{\sin\frac{\pi}{6}}{q\sin\frac{\pi}{6q}} \tag{4.19}$$

The polar shoe τ is:

$$\tau = \frac{\pi ID}{2P} \tag{4.20}$$

To obtain a value of the magnetic flux density, we will first estimate it's value, from the field current, B_{gF1}:

$$B_{gF1} = B_{gF} \frac{4}{\pi} \sin \frac{\pi}{2} \frac{\tau_p}{\tau} \tag{4.21}$$

where τ_p polar shoe. For $\tau_p/\tau = 0.8$ will result:

$$B_{gF1} = 0.75T \tag{4.22}$$

The resulted air-gap magnetic flux density, at $I_{rated}/2$ (1500 rpm), can be assumed at the value of 0.05 T, with $B_{g1} = 0.8$ T.

The number of turns for one way (two ways in parallel are considered) is:

$$W_1 = \frac{\pi \lambda_s}{2 B_{g1} L_s \tau K_{W1}} \tag{4.23}$$

The number of turns in slot opening, W_c , is:

$$W_c = 2W_1/(Pq) \tag{4.24}$$

With $I_{rated} = 55.6$ A, $j_{cos} = 12$ A/mm^2, the copper diameter , d_{cos} , is:

$$d_{cos} = \sqrt{\frac{4}{\pi} x \frac{55.6}{2x12x10^6}} = 0.00171m \tag{4.25}$$

With a slot opening filling factor $K_{fill} = 0.45$, the slot opening useful area, A_{slot}, is:

$$A_{slot} = \frac{W_c (I_{rated}/2)}{K_{fill} j_{cos}} = 113{,}26mm^2 \tag{4.26}$$

The slot pitch, τ_s , is:

$$\tau_s = \tau / 3q \tag{4.27}$$

The stator base width is considered b_{s1} = 6 mm. Figure 4.3 show us the stator slot opening geometry.

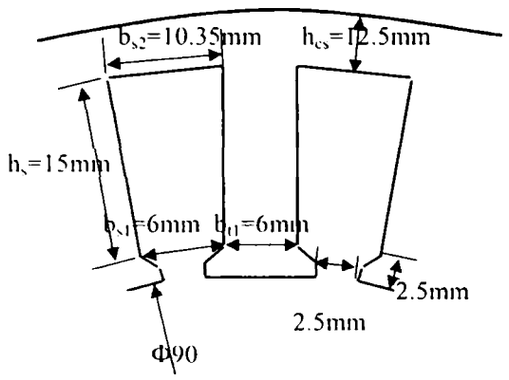

Figure 4.5. The resulted stator slot opening

Finally, with stator slot opening height h_{su} = 15 mm, b_{s2} = 10.35 mm, we will obtain a slot opening useful area closer to the imposed one (120 mm).

Stator yoke h_{cs} is:

$$h_{cs} = \frac{1}{\pi}\frac{B_{g1}\tau}{B_{cs}} \tag{4.28}$$

So, the outer diameter is:

$$OD = ID + 2x2{,}5x10^{-3} + 2h_s + 2h_{cs} = 0{,}15 \text{ m} \tag{4.29}$$

Now, we have al main data required for inductances and resistance calculation.

The field coils

With a known air-gap flux density, B_{gF}, and a saturation coefficient (which has to be verified) K_s:

$$W_F i_F = (B_{gF}/\mu_0) g K_c (1+K_S) \tag{4.30}$$

with $K_c = 1.15$ and $K_s = 0.40$, $g = 0.5x10^{-3}$ m

$$W_F i_F = \frac{0.65xx0.5x10^{-3}x1.15x1.4}{1.256x10^{-6}} = 416 Aturns \quad (4.31)$$

For a current density of: $j_{cof} = 9$ A/mm^2 and $K_f = 0.45$, half of the aria of the rotor slot opening A_W became:

$$A_W = \frac{W_F i_F}{K_{fill} j_{cof}} = \frac{416}{0.45x9.0} = 102.72 \text{ mm}^2 \quad (4.32)$$

The field coil length, l_{cF}, is:

$$l_{cF} = 2L_s + 1.5\tau + 4\pi W_{coil} / 2 = 2x0.054+1.5x0.07065+4\pi x0.001/2 = 0.276 \text{ m} \quad (4.33)$$

The voltage equation is:

$$V_{dc}K_D = \rho_{co}2PW_F l_{cF} j_{cof} = 42x0.92 = 2.3x10^{-8}x4xW_Fx0.276x9x10^{-6} \quad (4.34)$$

$$W_F = 169 \text{ turns/coil}; \quad i_F = W_F i_F / W_F = 416.6/169 = 2.465 \text{ A} \quad (4.35)$$

The coil dissipated power is p_{cof} :

$$p_{cof} = V_{cc} i_F = 42x2.465 = 103.5 \text{ W} \quad (4.36)$$

The $K_D = 0.92$ coefficient takes into account the d.c.-d.c. converter loses, a chopper is used for the field current control.

The conductor diameter, d_F, is:

$$d_F = \sqrt{\frac{4}{\pi}\frac{i_F}{j_{cof}}} = \sqrt{\frac{4}{\pi}x\frac{2.465}{9}} = 0.59mm \quad (4.37)$$

So, 169 turns are required, with a diameter of 0.59 mm (F insulation class).

Machine parameters

The stator phase resistance (two current ways in parallel) is:

$$R_S = \frac{1}{2}\left(\rho_{co} l_{cs} W_1 \frac{1}{\pi d_{cos}^2 / 4}\right) = \frac{1}{2} x \frac{2.25x10^{-3} x0.268x44}{\pi \frac{1.717^2}{4} 10^{-6}} = 0.057752\,\Omega \quad (4.38)$$

Where:

l_{cs} - the stator turn length:

$$l_{cs} = 2l_s + 0.02 + 2.5y = 2x0.054+0.02+2.5x0.07065 = 0.268 \text{ m} \quad (4.39)$$

and y- the coil opening

The coil rated loses, p_{cos} , will be:

$$p_{cos} = 3R_s i^2_{rated} = 3x0.0577x55.6^2 = 540 \text{ W} \quad (4.40)$$

The field coil resistance (4 coils in series connection) R_F is:

$$R_F = V_{dc}/i_F = 42/2.465 = 17.0385\ \Omega \quad (4.41)$$

The d axis magnetizing inductance, L_{dm}, is:

$$L_{dm} = K_{dm} L_m \quad (4.42)$$

where: $K_{dm} = 0.97$ ($\tau_p/\tau = 0.8$):

$$L_m = \frac{6x1.256x10^{-6} x(0.965x44)^2 x0.07065x0.054}{\pi^2 x2x1.15x0.5x10^{-3}(1+0.4)} = 3.265x10^{-3} H \quad (4.43)$$

The fringing inductance is considered 5% from L_m. So $L_{qm} = L_{dm}/10$ (which has to be demonstrated by FEM analysis).

So:

$$L_d = L_{sl} + L_{dm} \quad (4.44)$$

$$L_q = L_{sl} + L_{qm} \quad (4.45)$$

The q axis air-gap magnetic flux, at maximum current:

$$L_{qm} i_{srated} = 0.097x3.265x10^{-3}x55.6 = 1.7608x10^{-2} \text{ (Vs)} \quad (4.46)$$

The total q axis magnetic flux, at maximum current:

$$L_q i_{srated}=0.48x10^{-3}x55.6 = 2.6688x10^{-2}\ (Vs) \tag{4.47}$$

Now, PM sizing can be done for zero total q axis magnetic flux, at rated current or for zero air-gap magnetic flux on q axis.

For the first case, at high speed and power smaller than the rated one, it exists "to much" e.m.f. for q axis and so for small power the field current control, i_F (i_F=0), will be lost and so the power will be provided anyway.

Consequently, the second option will be picked up (zero flux on air-gap at rated current):

$$\lambda_{PM_q} = \frac{2}{\pi}\frac{B_{gPM}}{\sqrt{2}}\tau L_s K_{w1} W_1 = L_{qr} i_{qr} \tag{4.48}$$

From (4.48) $B_{gPM} \cong 0.22T$

It seems that using Ferrite permanent magnet (B_r = 0.39 T) is not imposed, flexible permanent magnets are good enough, B_r=0.25 - 0.30 T.

The mutual inductance L_{mF} is:

$$L_{mF}=\frac{\mu_0 W_F K_{F1}}{gK_c(1+K_s)}\frac{2}{\pi}\tau L_s K_{w1} W_1 = \frac{1.256x10^{-6}x169x1.15}{0.5x10^{-3}x1.15}x\frac{2}{\pi}x0.07065x0054x0.965x44 = 31.287x10^{-3}\ H$$

$$K_{F1} = \frac{4}{\pi}\sin\frac{\pi}{2}\frac{\tau_p}{\tau} = \frac{4}{\pi}\sin\frac{\pi}{2}x0.8 = 1.15 \tag{4.49}$$

Considering a 10% fringing inductance on field coil, the total inductance will be:

$$L_F = \frac{1.1x2p\mu_0 W_F^2 \tau_p L_s}{gK_c(1+K_s)} = \frac{1.1x4x1.256x10^{-6}x169^2x0.8x0.07065x0.054}{0.5x10^{-3}x1.15} = 0.598\ H \tag{4.50}$$

Calculating the efficiency at 1500 rpm.

For this, we have to consider a value for the iron loses. The frequency for this speed is 50Hz, so the iron loses will be small, generally smaller than:

$$p_{iron} < (p_{copper})_{1.5T;50Hz} W_{statoriron} \approx 6x\frac{1}{2}x\pi x\frac{(OD^2 - ID^2)L_s\gamma_{iron}}{4} = 6.4\ W \quad (4.51)$$

Even taking into account supplementary loses, the iron loses remain reduced. For a speed of 1500 rpm, a maximal value of 10 W is to be considered.

So, the total electrical efficiency, including diode loses at low speed, is:

$$\eta_{el} = \frac{P_{out}}{P_{out} + p_{cos} + p_{iron} + p_{diode} + p_{col}} = \frac{1575}{1575 + \frac{540}{4} + 3.18x22.8 + 103.5 + 10} \approx 0.80 \quad (4.52)$$

Initially, we supposed a value of 0,80 for the efficiency, so at maximum power this will be better. We have to consider the fact that diode loses are bigger than coil loses.

Anyway, besides a superior efficiency for this new type of generator (more than 80% for all speed range) the torque/weight ratio is better than claw pole generator.

Detailed test results for a prototype made using the above design results will be part of chapter six.

A computer program, BEGAProject.exe, developed using Visual C++ platform, has all the equation presented above integrated with other useful formulas and together with an optimisation method – which will be detailed presented in next part of this chapter – can be a good design tool that may be used for the design of a biaxial excitation machine.

A powerful help that guides the designer and familiarize him with the designing procedures and methods assists the program.

As an option, a geometrical file type ".dxf" can be created in order to help the designer to have the generator geometrical structure that might be analysed therefore using the finite element method of analysis.

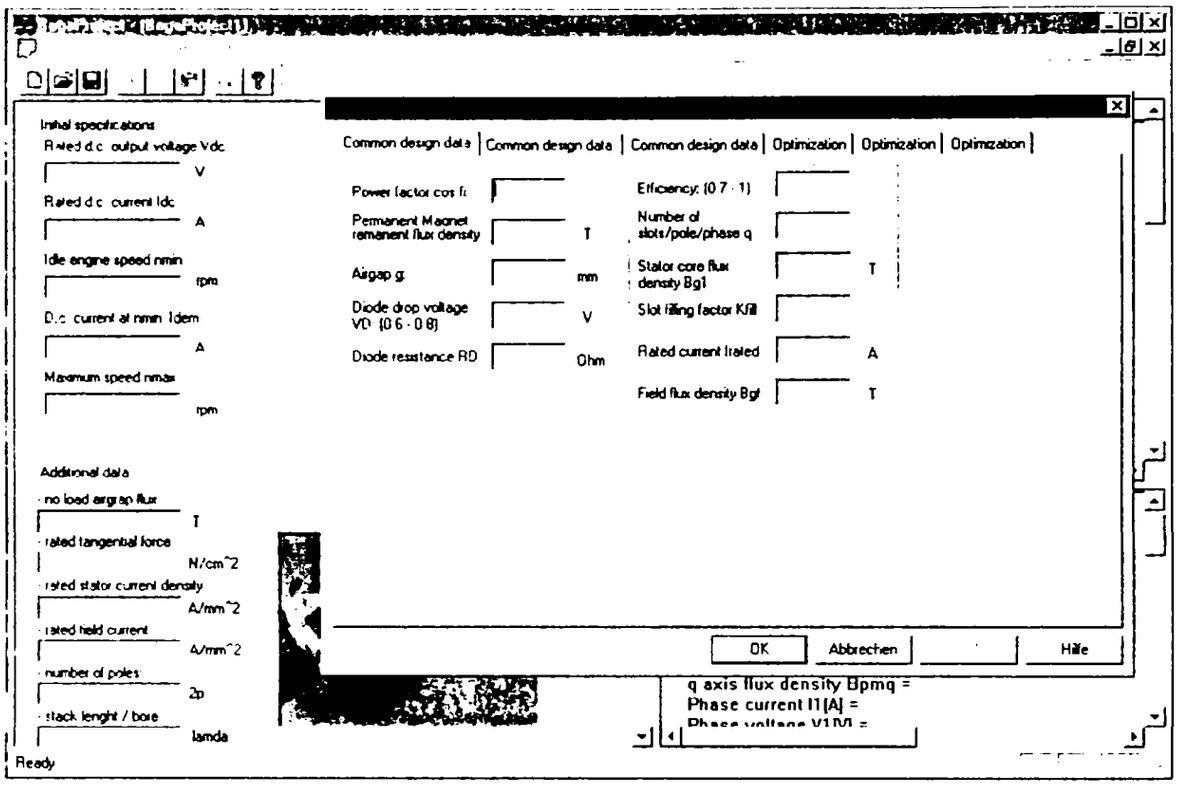

Figure 4.6. Details of the BEGAProject.exe – the design program developed for the biaxial excitation generator for automobiles

4.3.2. Geometrical Pre-optimisation Using FEM – Analysis for the First Prototype

Starting from the first prototype geometrical structure of the biaxial excitation generator for automobile, FEM analysis were done, some of the results will be included in this part of the chapter.

Traditional machine optimisation approach depends on an experienced designer to adjust machine parameters, using an analysis program to recalculate system performance at each step. For the beginning, the structure from fig. 4.7 has been analysed though FEM.

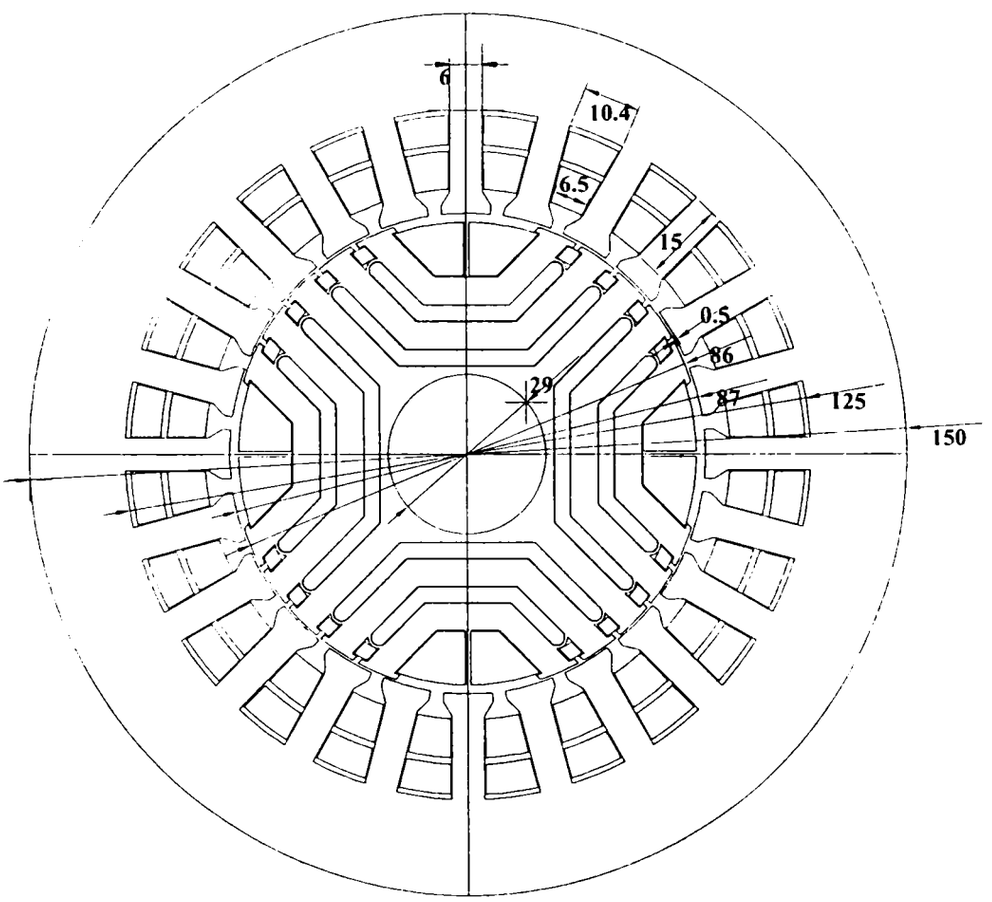

Figure 4.7. The first bi-dimensional geometric structure of the biaxial generator studied with help of finite element method of analysis (drawn with help of AutoCAD™)

Using the above dimensions, calculated with help of equations detailed in the previous part, according to the initial data for a 1,5kW generator (at idle speed: 1500rpm), respectively 3kW (for maximum speed: 9000rpm), the electromagnetic field produced by the presence of permanent magnets can be draw based on FEM analysis (fig. 4.8).

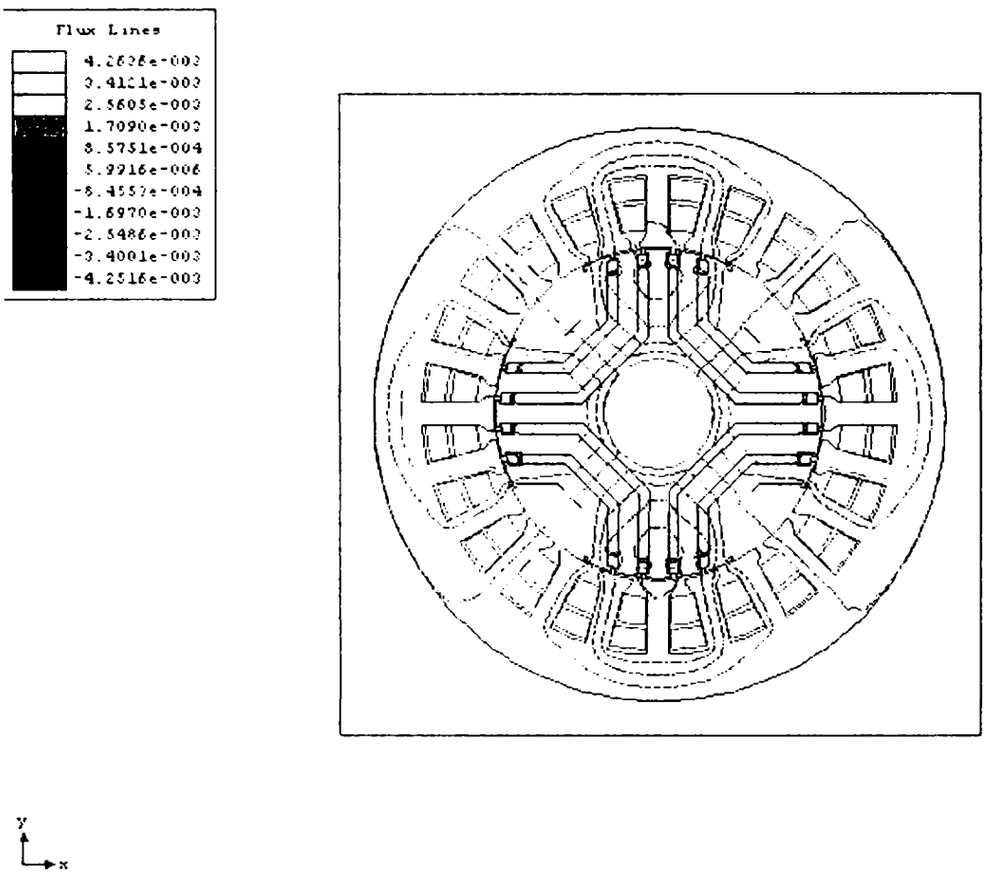

Figure 4.8. The electromagnetic field produced by the permanent magnets from the rotor barriers (drawn by FEM analysis using ANSOFT™)

As can be observed, the electromagnetic field lines from figure 4.8, are the result of permanent magnets inserted inside the flux barriers from the rotor, the PM magnetization is done so, to reduce (cancel) the q axis flux produced by the rotor field coil.

The PM's has to realize a q axis excitation for the generator and were choose with low energy density from both: manufacturing costs – expensive high energy PM's are not required - and small q axis cancelling flux – the rotor apparent topology indicates low energy PM's.

The following figure show us the air-gap magnetic flux variation because of PM presence.

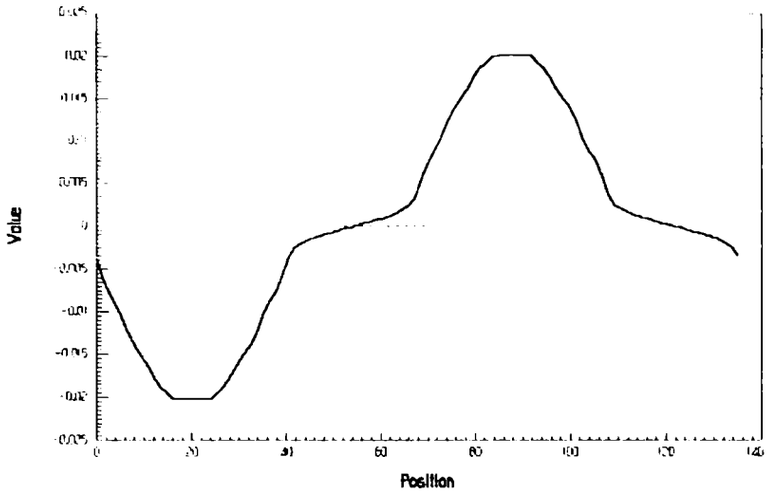

Figure 4.9. The radial air-gap magnetic flux because of PM's vs. position for u.l.

We can observe that the peak value of the flux is about 0,02Wb/u.l., a sufficiently large value (as will result in what follows) to cancel the q axis flux, from the stator .

The air-gap magnetic flux density will be presented in next figure:

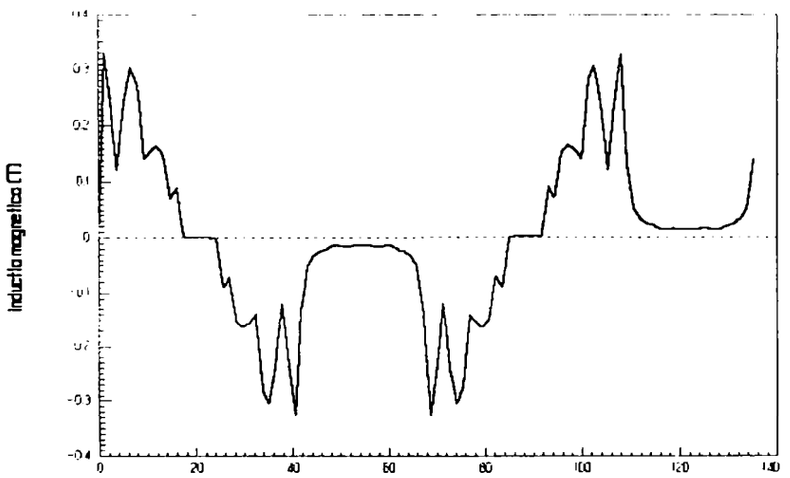

Figure 4.10. The air-gap magnetic flux density because of PM's vs. position

The presence of a high number of harmonics on air-gap magnetic flux density is a real impediment for a good evaluation of PM's influence, for this reason we will extract the fundamental (presented in fig. 4.11).

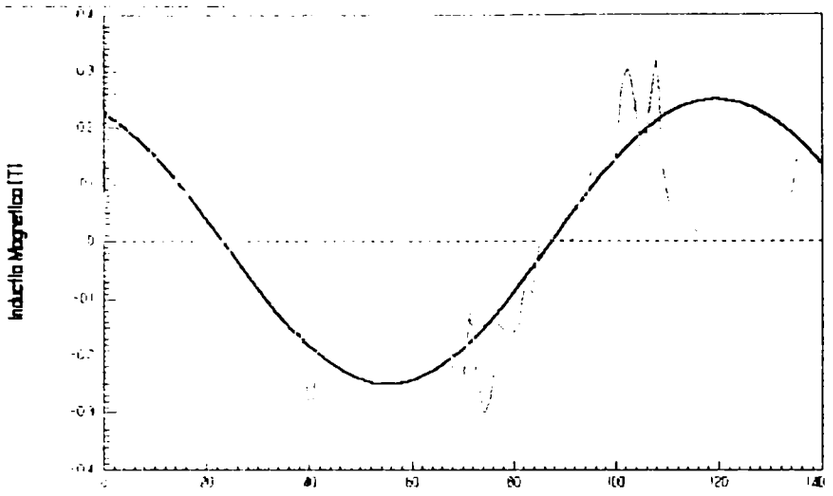

Figure 4.11. The air-gap magnetic flux density fundamental vs. position (from FEM analysis)

Because this new kind of electric machine has a topology which includes the presence of a number of PM's, the cogging torque variation will be useful.

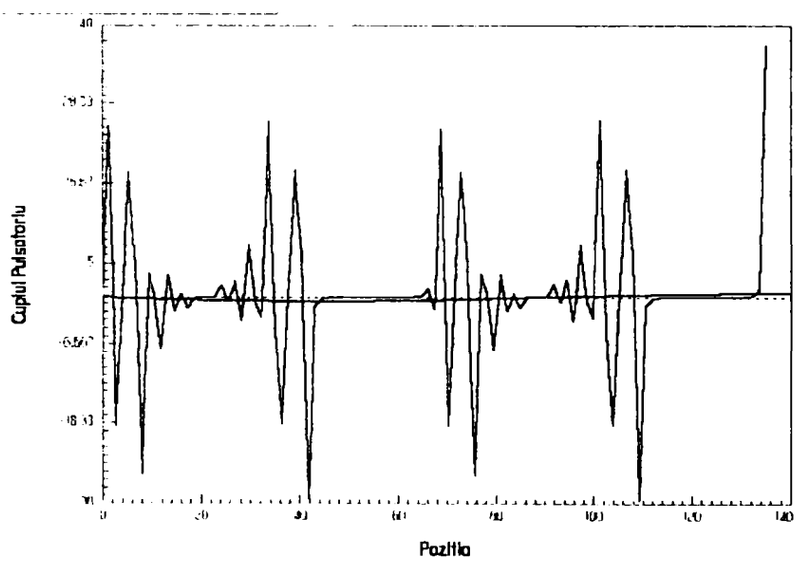

Figure 4.12. The cogging torque vs. position

As we can see from fig. 4.12, the cogging torque is present but it's influence is not a major problem for a good behaviour of the generator at high speeds (the fundamental is small).

For a value of the stator current equal to the rated one (on q axis), using the FEM analysis, the magnetic flux and flux density variations can be presented for both axis (d and q).

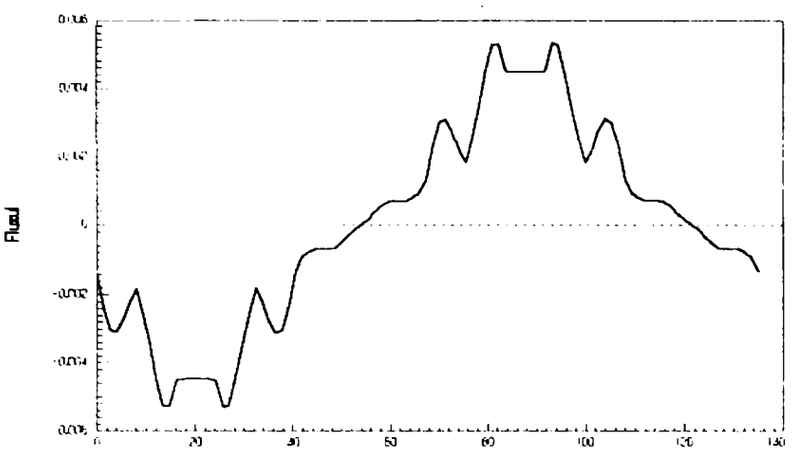

Figure 4.13. The resulted air-gap flux after q axis vs. position

From fig. 4.13 we can observe that the q axis flux has a small peak value, of only 0,005 Wb/u.l., this small value is due to PM's presence.

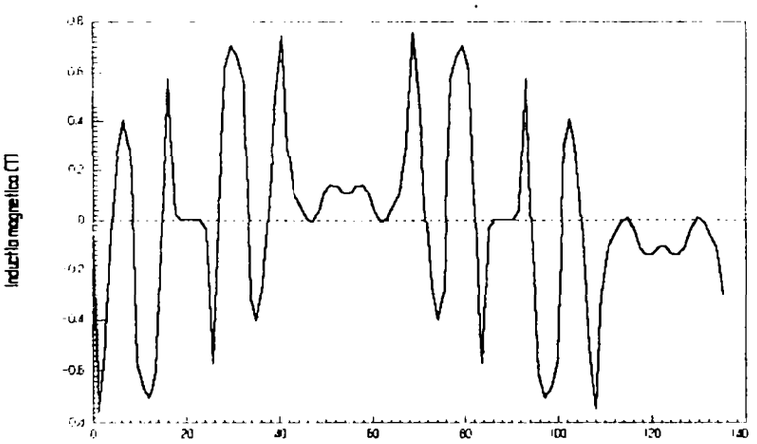

Figure 4.14. The q axis flux density vs. rotor position

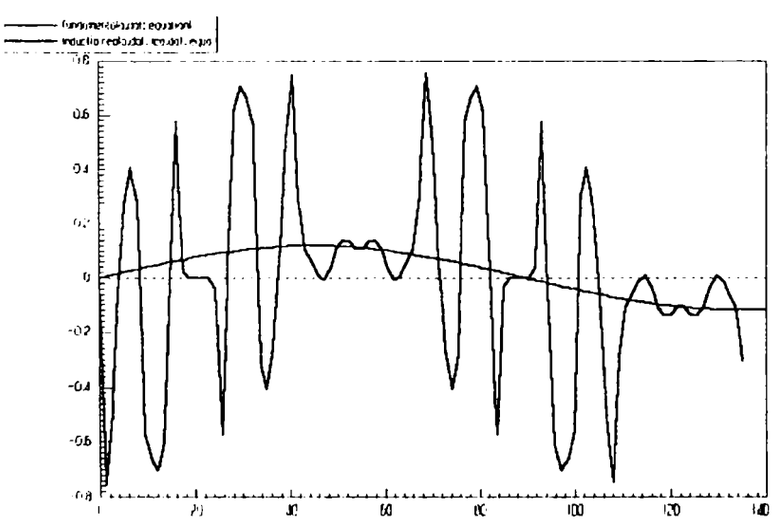

Figure 4.15. The q axis flux density fundamental vs. position (from FEM analysis)

From fig. 4.14 and 4.15 results a lower value of the q axis flux density (up to 0,1T), as it was expected.

To evaluate the PM influence on d axis (at rated current), the variations for the magnetic flux and flux density after this axis will be calculated by FEM analysis (figures 4.16, respectively 4.17), for N_{fi_f}=426Aturns.

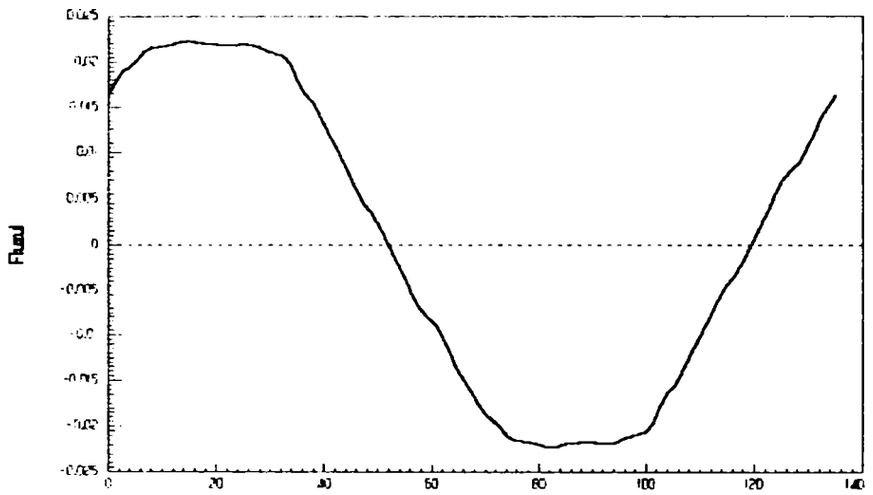

Figure 4.16. The d axis magnetic flux [Wb/u.l.] vs. rotor position

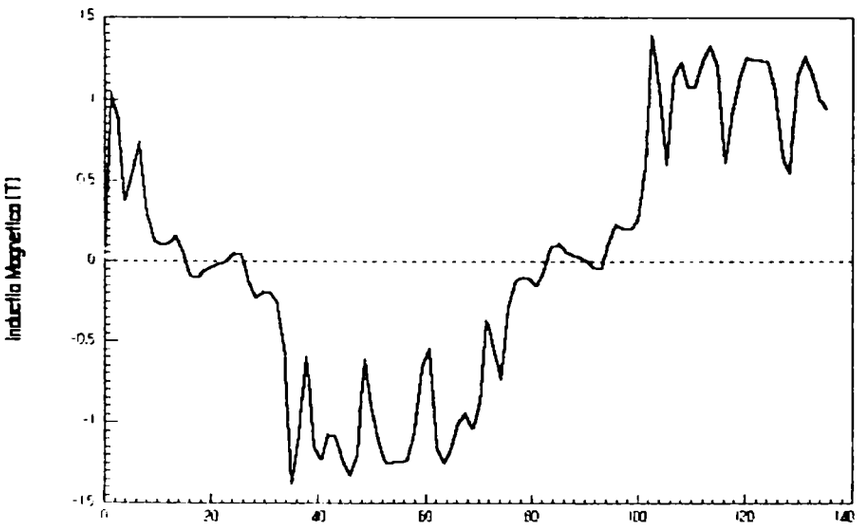

Figure 4.17. The d axis magnetic flux density [T] vs. rotor position

From figure 4.16 results that d axis flux has a value 4 times larger than the q axis flux (for stator rated current) with a peak value of 0.023 Wb/u.l..

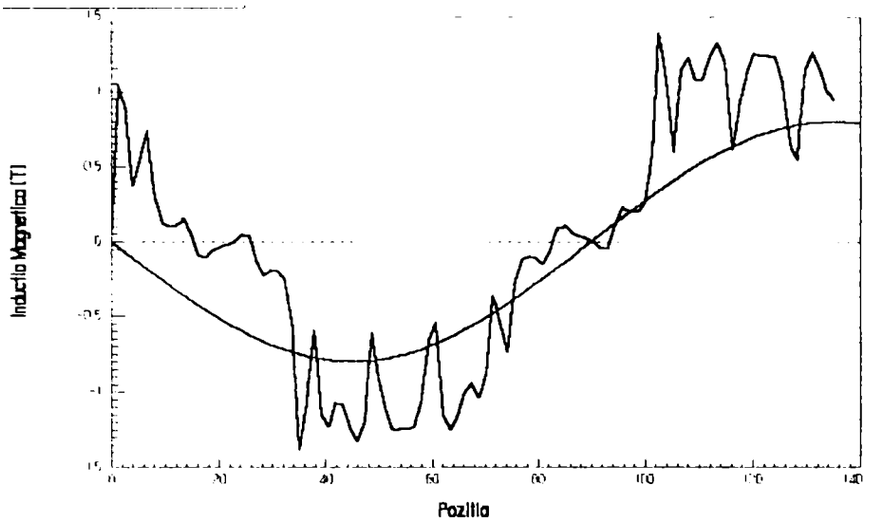

Figure 4.18. The d axis magnetic flux density fundamental (after FEM analysis)

The d axis flux density fundamental (fig. 4.18), has a peak value of 0.9T.

These preliminary results made using FEM analysis, confirms our initial suppositions regarding the generator behaviour, more exactly the influence of the PM's. It follows that with help of more analysis it's efficiency to be prove.

Direct axis reactance

The direct axis synchronous reactance is important in steady state performance of the machine. The currents are distributed sinusoidal in the stator winding such that the field produced peaks at the direct axis.

The current therefore peaks at the quadrature axis. The field winding is left un-energized or open circuit. The inductance of the direct axis winding in this case is the synchronous reactance X_d. Inductance is flux linkage per ampere of current, so:

$$L_d = \lambda_d / I_s \tag{4.53}$$

Since we are exciting the stator with equivalent Ampere-Turns we must take care to correctly include the proper number of turns. From the finite element vector potential solution we can easily find the flux passing through a coil. This is just the difference in the vector potential at the location of the two coil sides times the depth of the problem.

If we model one pole as described previously using anti-periodic boundary conditions, we have the inductance per phase per pole. We have to multiply this by the number of poles and divide it by the number of parallels to get the inductance per phase. To find the direct axis inductance we need another factor. Assume that the fictitious d axis winding has the same number of turns as the phase winding.

For an m phase machine, the d axis current would have to be m/2 times as great as the phase current to produce the same m.m.f. in the d axis as the m phase winding. So:

$$L_d = L_m / (m/2) \tag{4.54}$$

The per unit value of X_d is then:

$$X_d = L_d / Z_b \tag{4.55}$$

Transversal axis reactance

Similar to the direct axis reactance, we can found the transversal axis reactance. The transversal axis winding is the same as the direct axis winding but is displaced in space by 90^0 electrical. With no field current, we excite the transversal axis winding (current peaks on the direct axis) and set a homogenous Dirichlet boundary condition on the transversal axis. The ratio of transversal axis flux linkage to transversal axis current is the transversal axis synchronous inductance.

(Direct axis transient and sub transient reactance, X_d' and X_d''

The transient and sub transient reactance are used in many applications, from short circuit studies to transient and dynamic stability and sub-synchronous resonance, unbalanced operation, asynchronous operation etc. The definition of the transient reactance is based on the three phase sudden short circuit test. It is the equivalent reactance of the direct axis which applies after the first few cycles. To simulate this, the stator is excited with direct axis current as in previous case of synchronous reactance. The difference is that the current is now low frequency).

4.3.3. BEGA – Geometrical Pre-optimisation Through FEM – The Second Prototype

In order to optimise the air-gap flux and flux density, with direct effect on the output voltage waveform, other geometrical topologies were studied with help of FEM of analysis, some of those results will be included and explained in what follows.

So, after changing the rotor topology, in the way of cancelling the outer flux barriers from it and so, approaching the rotor structure as we intended on the theoretical proposal for this machine, we inserted in the same type of PM's inside the flux barriers watching the first results.

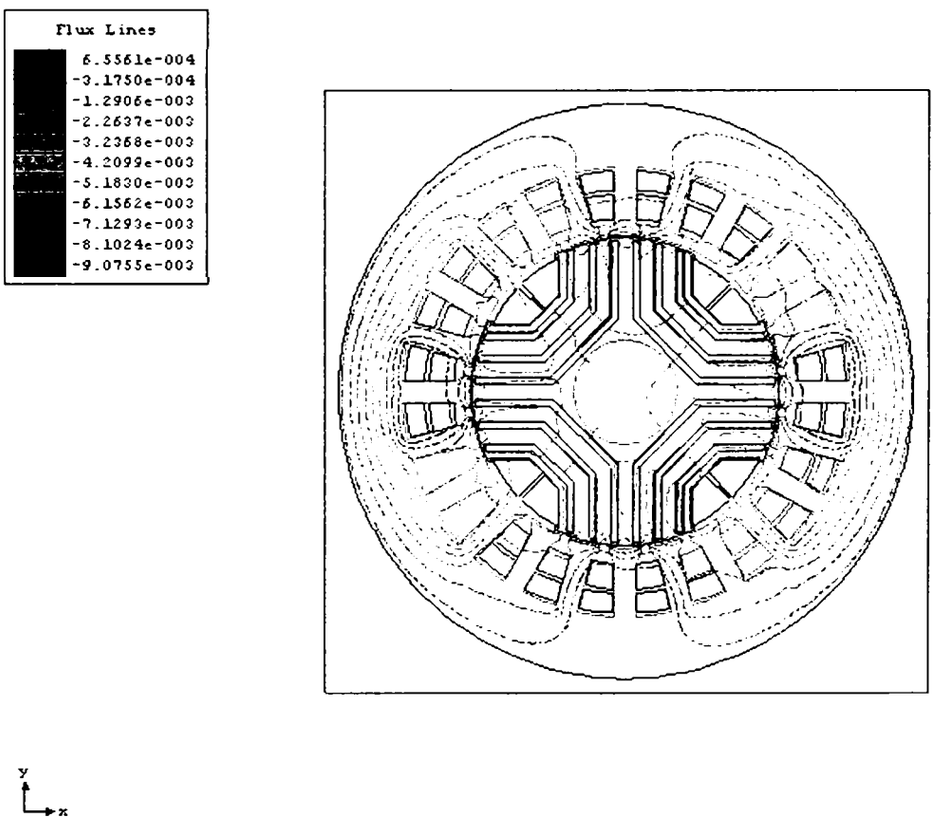

Figure 4.19. The electromagnetic field distribution on a d axis magnetisation (after 2D-FEM analysis)

Eliminating the extreme flux barriers from the rotor structure we hoped that the flux wave shape would be improved. The results after these first changes are presented in next figures.

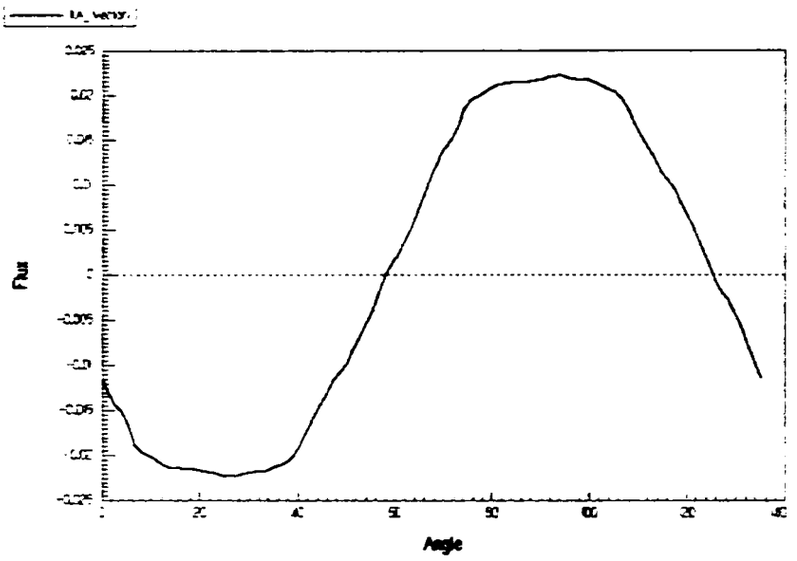

Figure 4.20. The d axis magnetic flux [Wb/u.l.] vs. rotor position (after 2D-FEM analysis)

It can be observed that, comparing to figure 4.16, the shape of the magnetic flux is more linear, even if it's maximum value did not changes much.

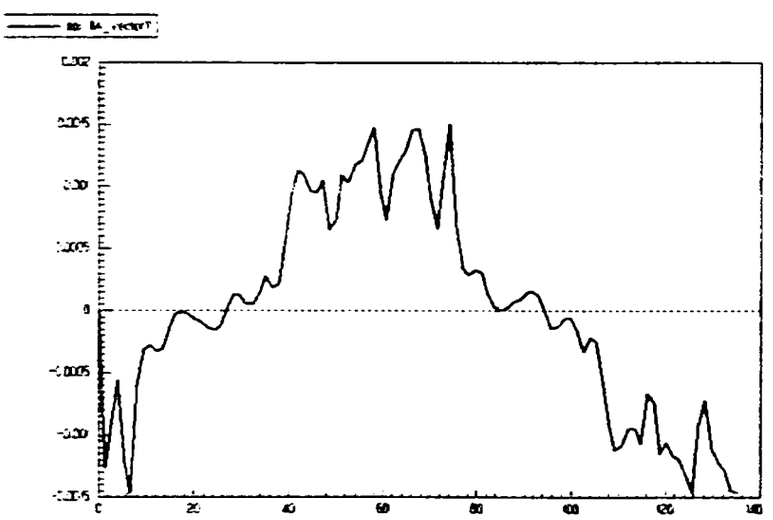

Figure 4.21. The d axis magnetic flux density [T] vs. rotor position (after 2D-FEM analysis)

Again, the flux density shows us that more improvements on the geometrical structure of the rotor may be done.

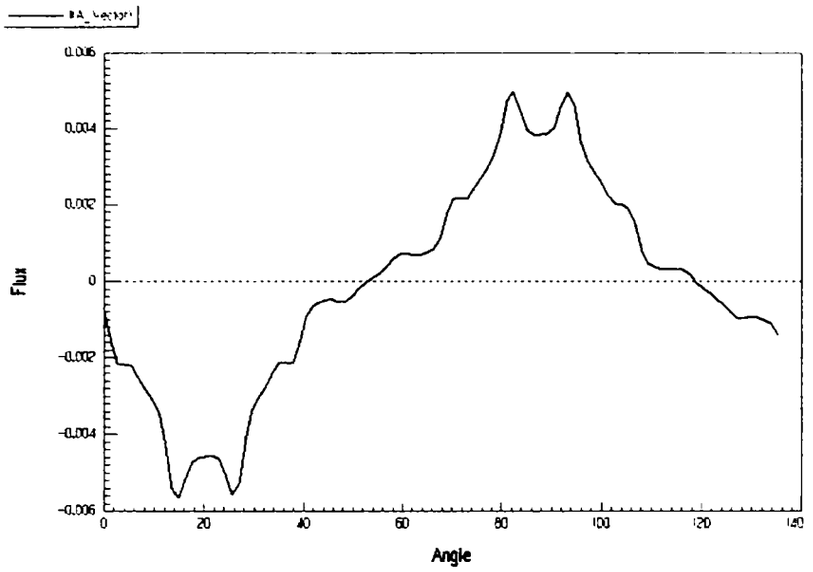

Figure 4.22. The q-axis magnetic flux [Wb/u.l.] vs. rotor position (after 2D-FEM analysis)

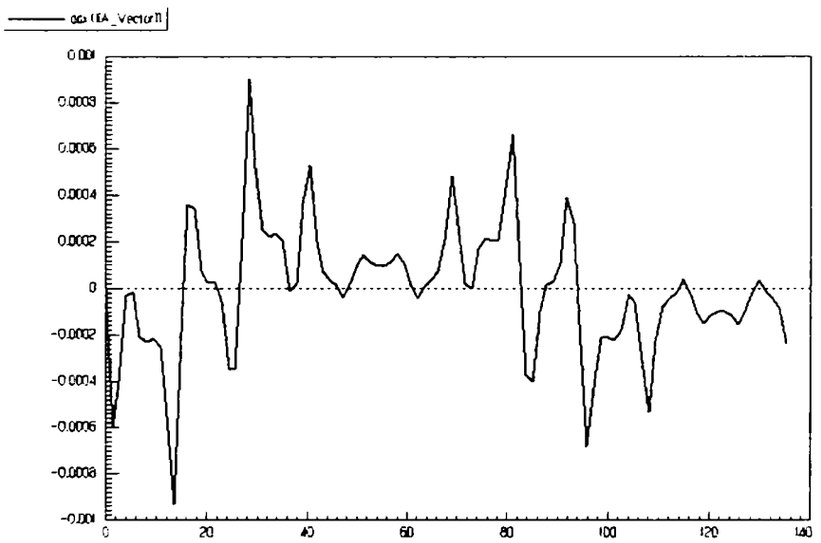

Figure 4.23. The q-axis magnetic flux density [T] vs. rotor position (after 2D-FEM analysis)

As can be observed, for this new geometrical structure, simple and easy to implement with help of a FEA, some improvement are obtained.

Even if we know that using PM's with high magnetic properties are not required for this type of electrical machine, we tested this alternative too. In this way we substituted the

previous Ferrite PM's with new ones having B_r = 0.39 T, the results after this change are presented in next figures.

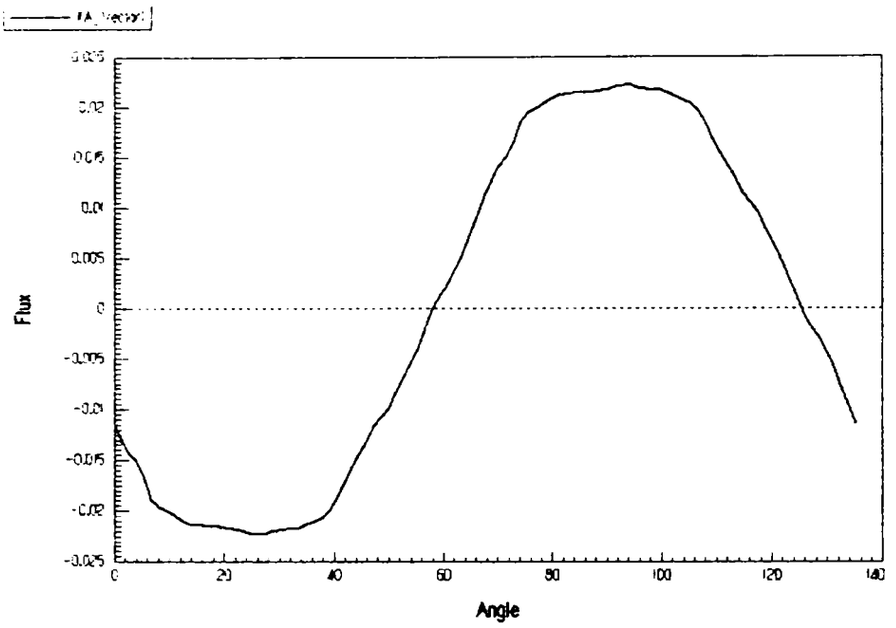

Figure 4.24. The d-axis magnetic flux [Wb/u.l.] vs. rotor position (after 2D-FEM analysis)

A new strategy for the rotor configuration of this machine will be introduced in what follows, in this new approach; the permanent magnets are inserted only on the side flux barriers of the rotor poles. The flux barriers situated between the rotor pole will be not filled with PM's.

The main scope for choosing this configuration is to reduce the use of the permanent magnets - with direct effect on manufacturing cost - and to obtain at least the same behaviour from electromagnetic point of view of the machine.

The magnets inserted in the rotor are, as before were, of ferrite with low power density, B_r= 0.25 T

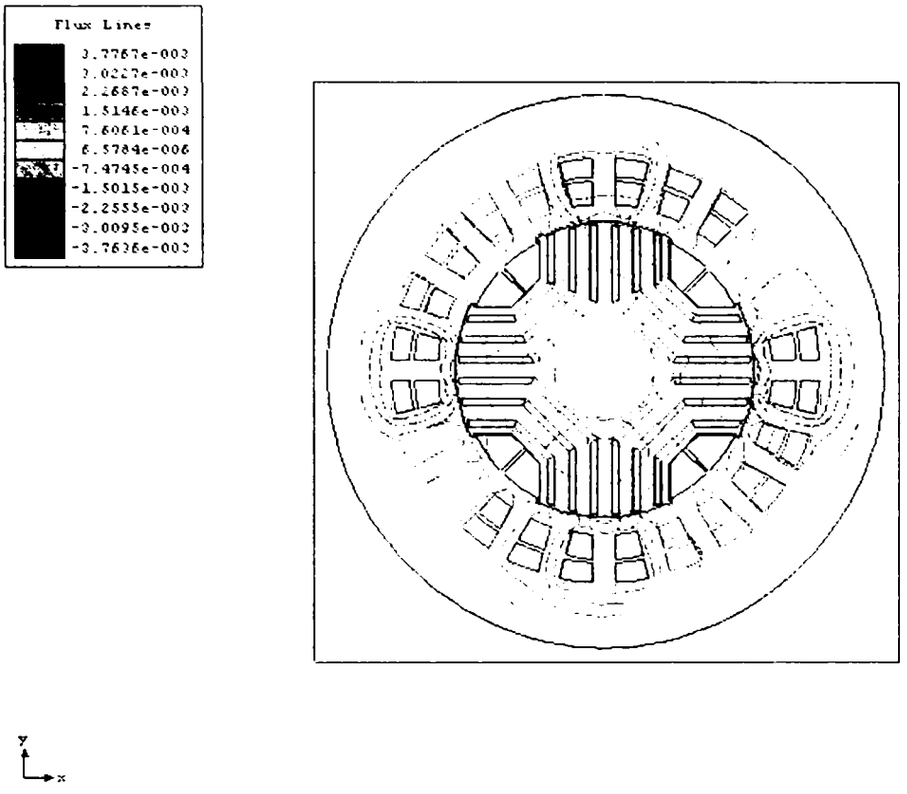

Figure 4.25. The electromagnetic field through a new geometrical topology of BEGA (after 2D- FEM analysis)

For this configuration, the magnetic flux and flux density were calculated through FEA, the results are shown in figures 4.26 – 4.28

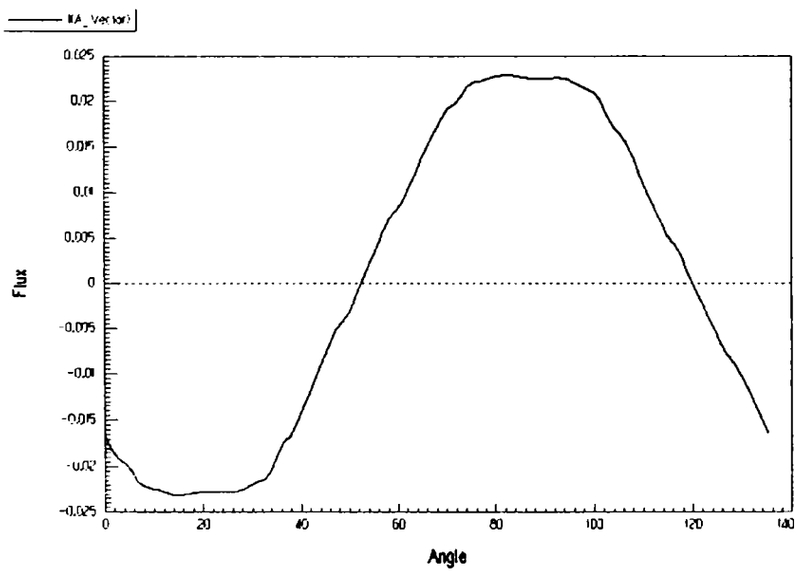

Figure 4.26. The d-axis magnetic flux [Wb/u.l.] vs. rotor position (after FEM analysis)

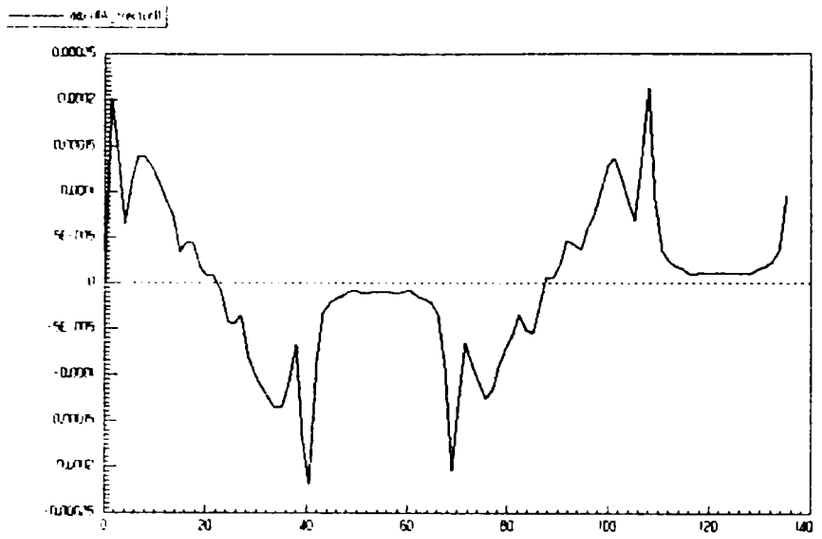

Figure 4.27. The q-axis magnetic flux density [T] vs. rotor position (after 2D-FEM analysis)

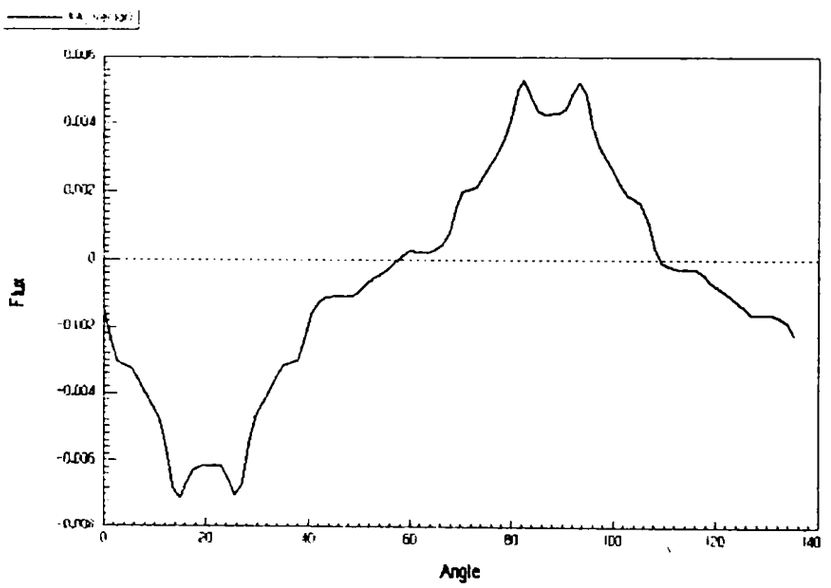

Figure 4.28. The q-axis magnetic flux [Wb/u.l.] vs. rotor position (after 2D-FEM analysis)

The first result was an increase of the radial magnetic flux on d axis by keeping the q axis flux approximately at the same value and shape.

Going forward, we tried to see the result of increasing of the flux barriers number from the electromagnetic point of view.

New flux barriers were inserted in the rotor of the BEGA, the results are shown in what follows.

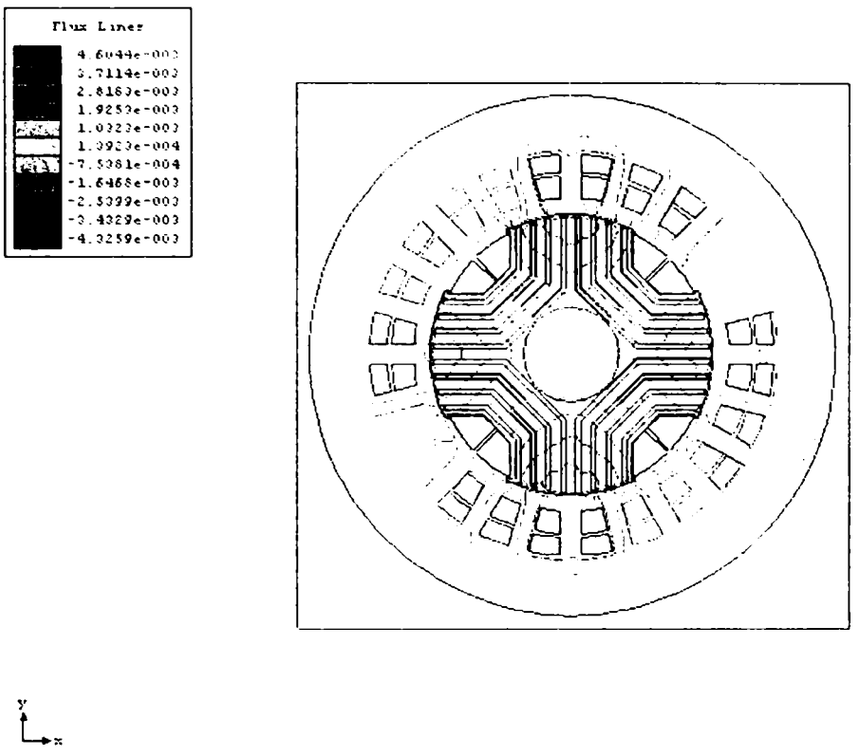

Figure 4.29. The electromagnetic field for the new configuration of BEGA rotor (after 2D-FEM analysis)

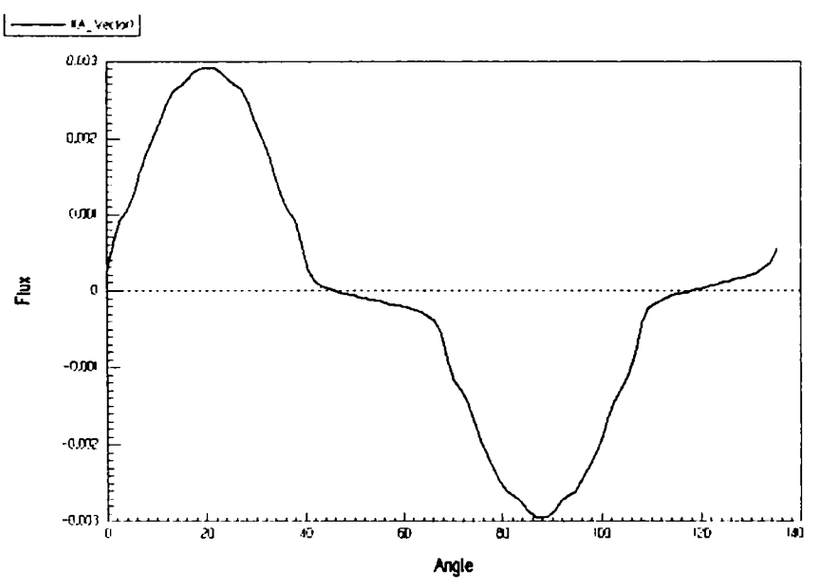

Figure 4.30. The d-axis magnetic flux [Wb/u.l.] vs. rotor position (after 2D-FEM analysis)

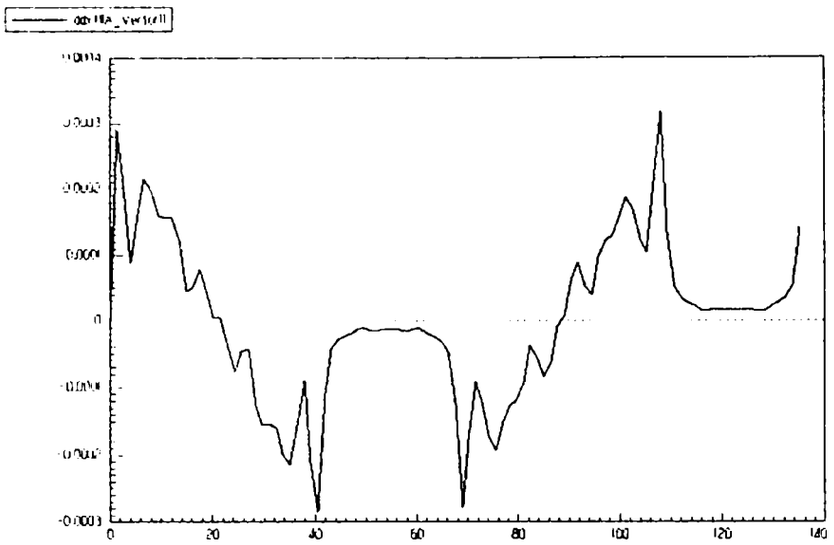

Figure 4.31. The q-axis magnetic flux density [T] vs. rotor position (after 2D-FEM analysis)

The direct effect of increasing the number of flux barriers in the rotor was positive but from mechanical and economical point of views the effect was opposite, this is way we didn't took into consideration this last alternative for the rotor geometry.

Anyway, some other improvements were done for the rotor geometry, some of those were already presented and some of them will make the core of the next part of this chapter.

After many changes in the rotor shape of this new electrical machine, we considered that we have to ensure for the field coils a proper slot opening, to fix the wedges for those without having any consequences when the generator is running at high-speed values.

More precisely, for running in better condition to a maximum rotational speed of 9000rpm, as we designed it, the generator must have a robust rotor – from mechanical point of view.

In this way, adding the need of low slot opening harmonics, we decided to adopt the next geometrical structure for the BEGA rotor (see figure 4.32).

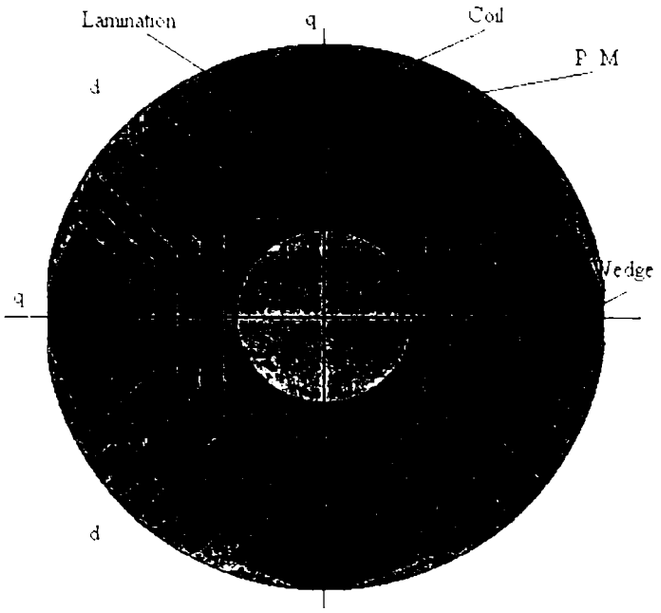

Figure 4.32. The rotor of the second prototype of BEGA

So, having this new rotor topology, new FEA were done, the results after these changes will be included in what follows.

The electromagnetic field for the BEGA, the magnetic flux and the flux density in the air-gap are next figures.

Figure 4.33 show us the flux lines through the machine when the stator windings are covered by the rated current, the rotor being in the d-axis, for this position the electromagnetic torque in the rotor has a maximum value of 45Nm.

The Permanent Magnets from the rotor are from Ferrite, as will be detailed in the chapter six.

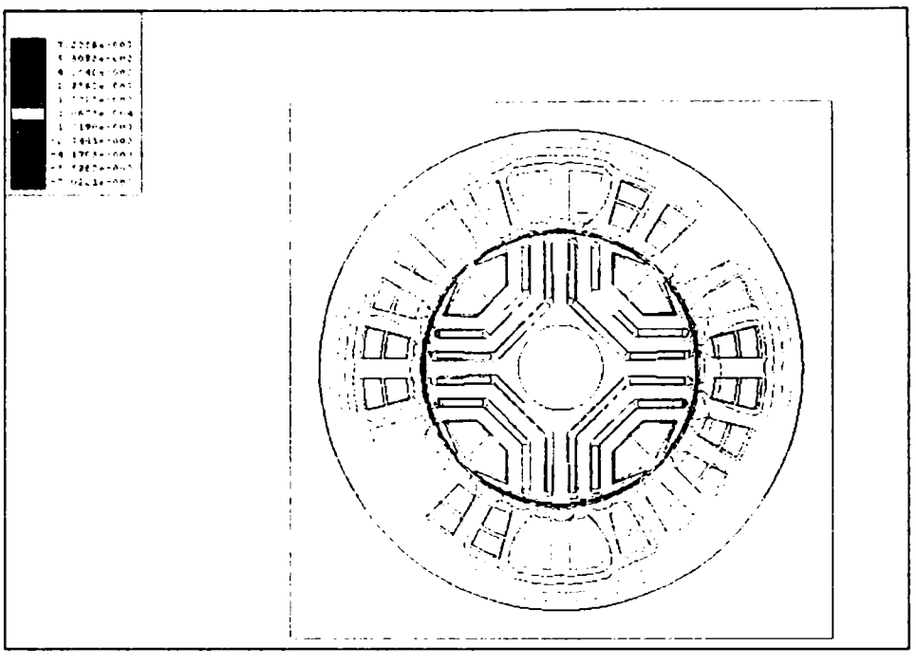

Figure 4.33. The electromagnetic field for the second prototype of BEGA (after 2D-FEM analysis)

The influence of this new shape of the rotor will be observed in the air-gap flux and flux density waveforms.

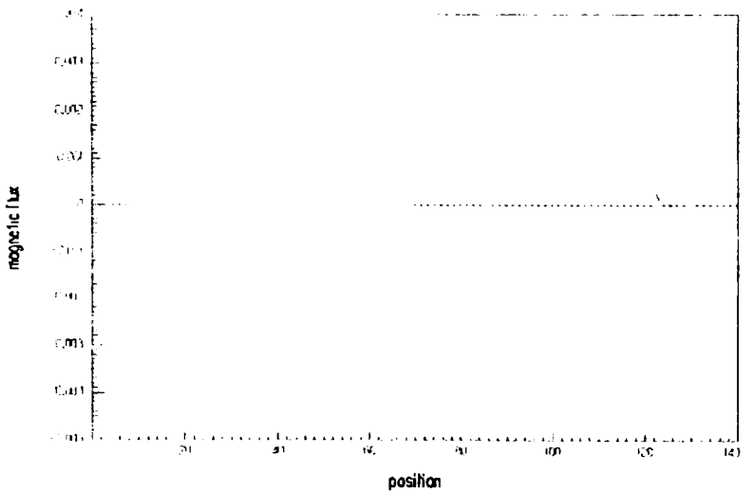

Figure 4.34. The air-gap PM magnetic flux [Wb/u.l.] vs. rotor position (FEM analysis)

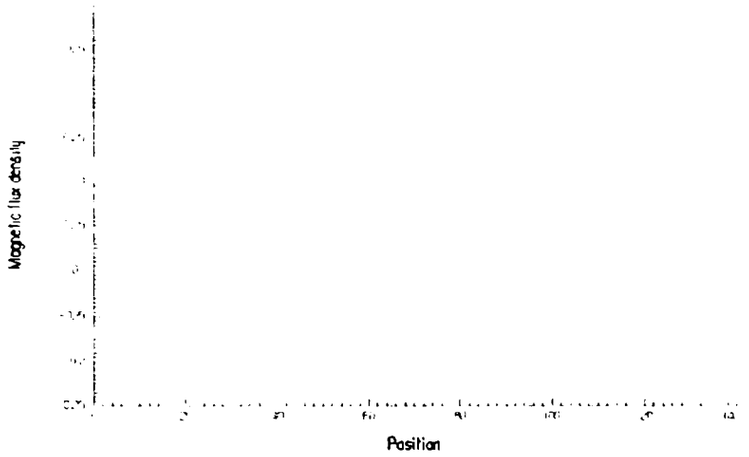

Figure 4.35. The air-gap PM magnetic flux density [T] vs. rotor position (FEM analysis)

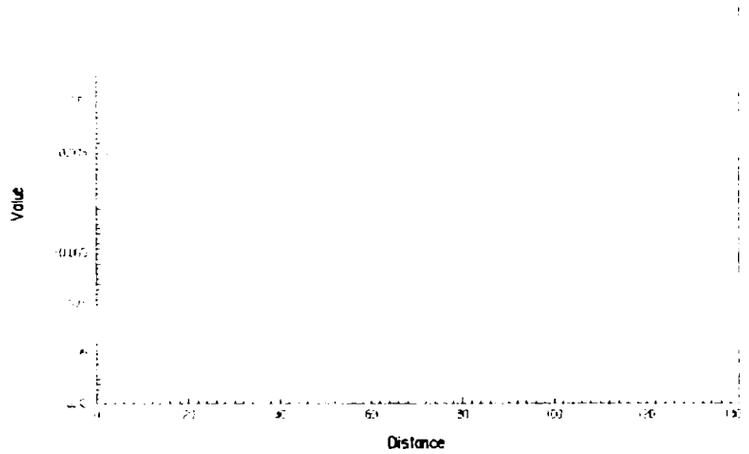

Figure 4.36. The air-gap d-axis magnetic flux [Wb/u.l.] vs. rotor position (FEM analysis)

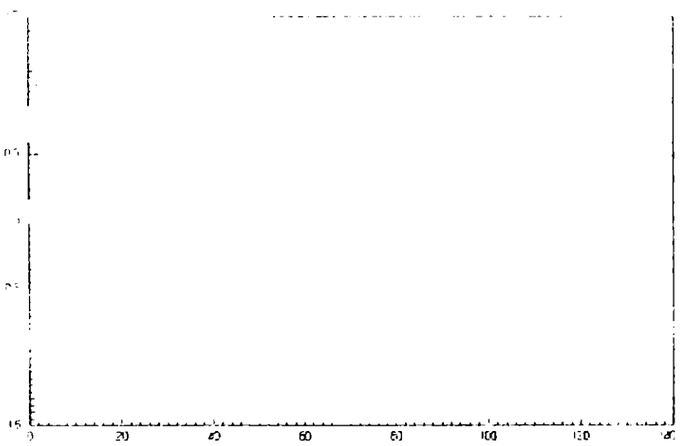

Figure 4.37. The air-gap d-axis magnetic flux density [T] vs. rotor position (FEM analysis)

So, beside the mechanical role, of keeping the wedges closely inside the rotor during high speed running, the new rotor structure has a good influence in the sense of improving the waveform of the air-gap flux. This remark will be maintained further after following the next figures.

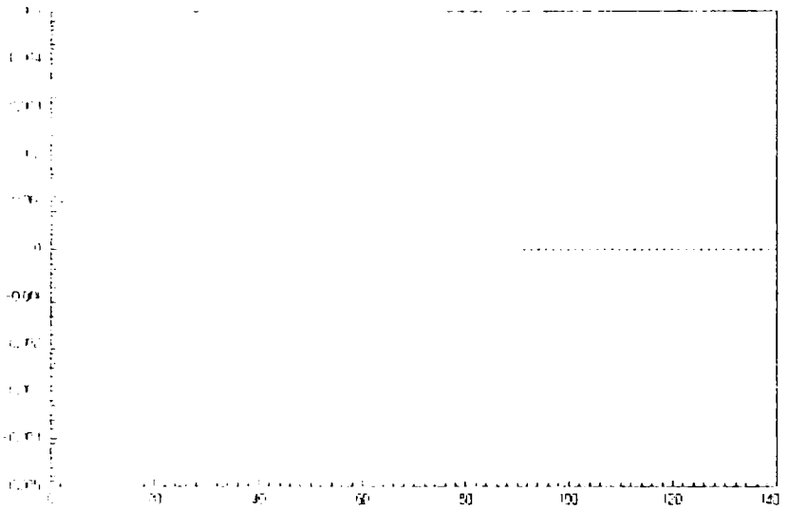

Figure 4.38. The air-gap q-axis magnetic flux [Wb/u.l.] vs. rotor position (FEM analysis)

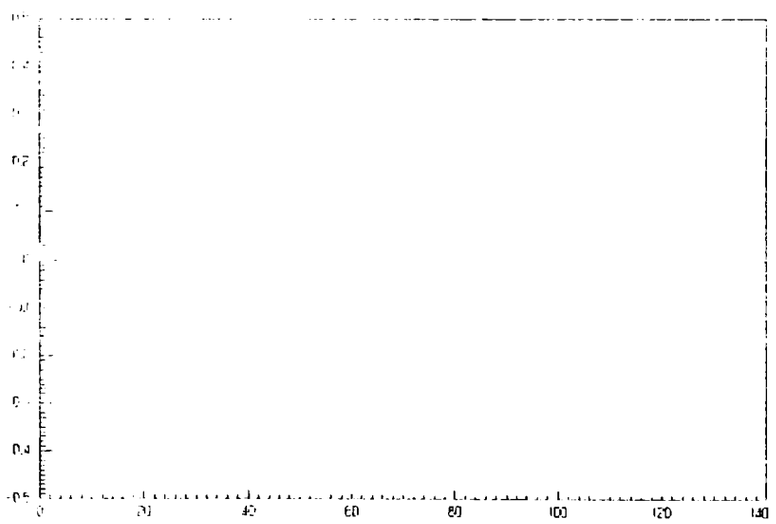

Figure 4.39. The air-gap q-axis magnetic flux density [T] vs. rotor position (FEM analysis)

During the FEA made for this machine, a question has been following us, this was regarding the influence between the PM magnetization and the field winding current polarity, does the current polarity through the field windings change the output power of the machine? The answer to this question is obtained through experiments in chapter six.

Moreover, when the direction of I_q is changed, so that it magnetizes the PM's, the distribution of the flux and flux density in axis q changes accordingly as shown in the figures bellow.

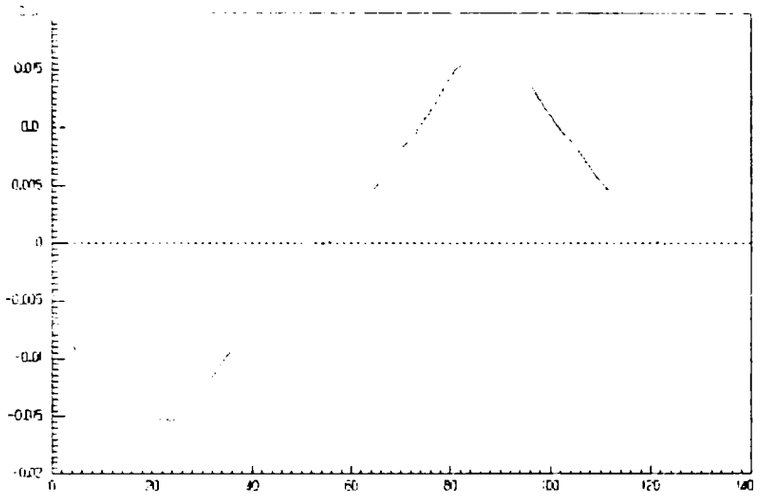

Figure 4.40. The air-gap q-axis magnetic flux [Wb/u.l.] vs. rotor position (FEM analysis)

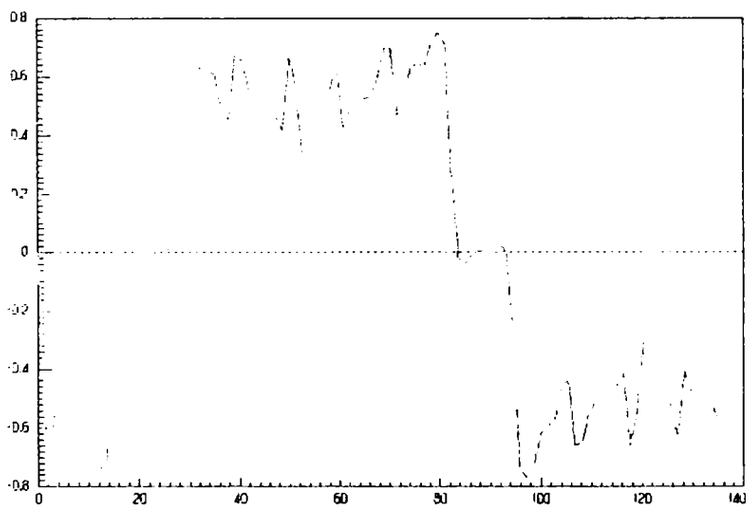

Figure 4.41. The air-gap q-axis magnetic flux density [T] vs. rotor position (FEM analysis)

It is evident that the sense of the current through the windings influences the air-gap flux and flux density.

A better comparison is obtained when looking the flux lines on both situations, see next figure. The drawings for the final prototype are included in appendix C.

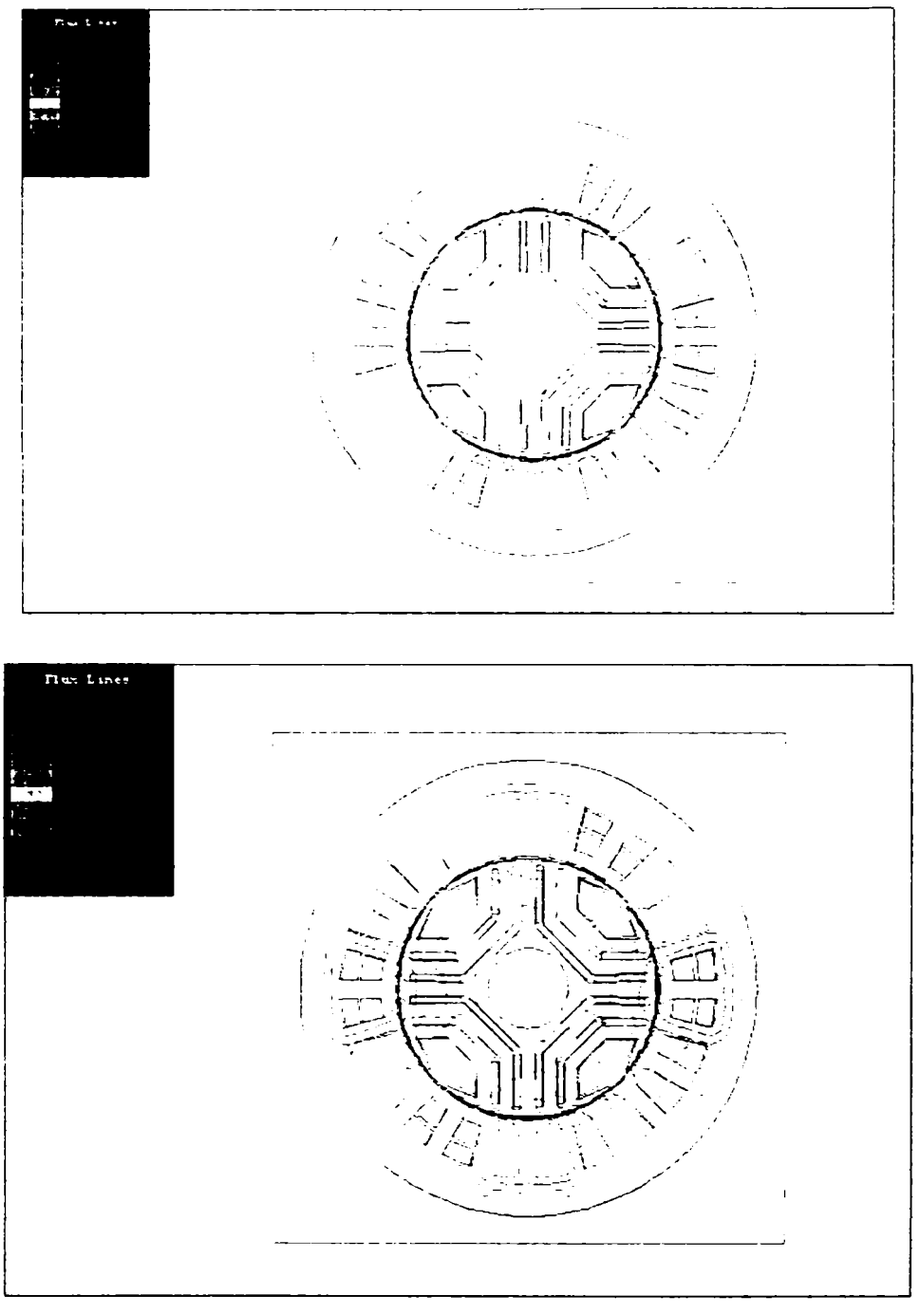

Figure 4.42. The electromagnetic field for q-axis situation on two situations: for one sense of the windings current and then for the opposite sense of the current while keeping the same values (FEM analysis)

4.4. Optimal Design - The Method

4.4.1. Mathematical Formulation of the Optimisation Problem

The biaxial excitation generator for automobile design can be described as a function of the geometrical dimensions and electromagnetic parameters and has to meet some specifications as well. The task of machine design optimisation can usually be formulated as a general non-linear programming problem, as follows:

Find $X = (X_1, X_2, X_3, \ldots X_N)$, X 0,

such that F(K,X) is an optimum,

subject to: G_i (K, X) 0, I=1, 2, ... M,

where F is known as the objective function, G_i is called the constraint function, X is a vector of N real variables (primary parameters), K is a set of constraints (secondary parameters).

The objective function may be the cost, weight and efficiency. The criterion for choosing the objective function depends on the design parameters. While the manufacturer may be interested in the minimization of the production cost, the consumer may wish to maximize the efficiency of the machine. The constraint functions may be the performance requirements of the generator or some other parameters related to the generator. These constraints limit the variation of the motor dimensions to a feasible region where the generator's desired performance requirements and additional limitations are satisfied. In generator design optimisation, both the objective function and the constraints are non-linear and multivariable functions.

The number of design parameters of the biaxial excitation generator is large. Therefore we choose to optimise certain parameters (primary parameters) while keeping the others (secondary parameters) as constants.

For the study, a direct search method, Hooke-Jeeves modified method, is used. The pattern search is a comparative method that relies on evaluating the objective function at a

sequence points (within the feasible region) and comparing its values I order to reach the optimal value.

A point in a pattern search is accepted as a new point if the objective function is found to have a better value at this point than its value at the previous point. The details of the modified Hooke - Jeeves method are as follows:

$X^{(K-1)}$ previous base point;

$X^{(K)}$ current base point;

$X^{(K+1)}$ pattern point, the point obtained after the pattern move.

4.4.2. Exploratory Moves

Given a specified step size, which may be different for each coordinate direction and may change during the search, the exploration proceeds from an initial point, $X^{(K-1)}$, using the specified step size in each coordinate direction. In the exploration move, both directions (positive and negative) of each coordinate are investigated. The best current base point, $X^{(K)}$, is chosen from these three points (the two exploratory points and the previous base point $X^{(K-1)}$). When all N (N= for the present study) coordinates have been investigated, the exploratory move is completed.

The resulting point is termed a "current base point", $X^{(K)}$.

4.4.3. Pattern Moves

A pattern move consists of a move along the direction from the previous to the current base point. Thus, a new pattern point is calculated as:

$$X^{(K-1)} = X^{(K)} + a(X^{(K)} - X^{(K-1)})$$

where a is an accelerating factor.

After arriving at the point $X^{(K+1)}$, the unmodified Hooke - Jeeves initiates a new exploratory move. In the modified Hooke - Jeeves approach, adopted for the design optimisation of the biaxial excitation generator, a new pattern move is initiated without any exploration and a new pattern point, $X^{(K+2)}$, is obtained:

$$X^{(K+2)} = X^{(K+1)} + a(X^{(K+1)} - X^{(K)})$$

This is done to reduce the computation time. However, the success of this pattern point is checked. If the result of this pattern move is a better point than the current base point $X^{(K+1)}$, then this pattern move point is accepted as the current base point. If the pattern move does not produce improvement, then the pattern move is discharged and the search returns to the current base point $X^{(K+1)}$ instead of returning to the previous base $X^{(K)}$ as in the original Hooke - Jeeves method.

Note that $X^{(K+1)}$ is not worse than $X^{(K)}$ in the Hooke - Jeeves method. At the current base point $X^{(K+1)}$, another exploratory move with a smaller step size is undertaken to find a new pattern point. The search is finished when the step size becomes sufficiently small.

The procedure used for the biaxial excitation generator design optimisation is presented in what follows, see appendix B, too.

4.4.4. Variables, Constraints and the Objective Function

From the large number of design variables that might affect the performance of the generator, some of them have only small influence but a few of the variables can either be treated as fixed or expressed in terms of the others. Therefore, it is important to select the independent variables (primary parameters) in the design optimisation carefully.

The following parameters were chosen as the primary parameters for the optimised design:

j_{cob} – the current density in the stator windings;

L/D_r – the stack length per rotor diameter ratio;

f_x – the tangential specific force on the rotor surface;

B_s – the stator back iron flux density;

hfbt – the ratio between the flux barrier thickness and the air-gap;

The constraints set considered for the optimised design are:

- The power factor at rated load;
- Minimum allowed efficiency for minimum weight;
- Maximum allowed weight for maximum efficiency;
- Temperature rising of the windings from the stator;
- Generator total costs (as an alternative – it is not included on the final configuration of the program because the manufacturing costs were not considered, so, a correct price of the generator can not be obtained).

The objective functions are:

- the minimum weight, or
- the maximum efficiency.

The computer program, BEGAProject.exe, developed for the design procedure can select the optimisation criterion, optimisation following cost minimisation or following the efficiency of the generator. Figure 4.32 presents this feature of the computer program.

The initial file of the program contains many other entries (variables) as well, interrelated as in the conceptual design, at lowest speed and power, to obtain the total weight and efficiency.

In essence, when a constraint condition is violated, the modified objective function is heavily penalized through the value of penalty factors and so on, until the final number of optimisation step has been reached.

The use of the Hooke–Jeeves modified method for machine design optimisation was chose to prevent the traditional machine optimisation approach that mostly depends on an experienced designer, who can manually adjust the machine parameters and so to influence the results with designer's experience who can only identify a local optimum, not always the best one.

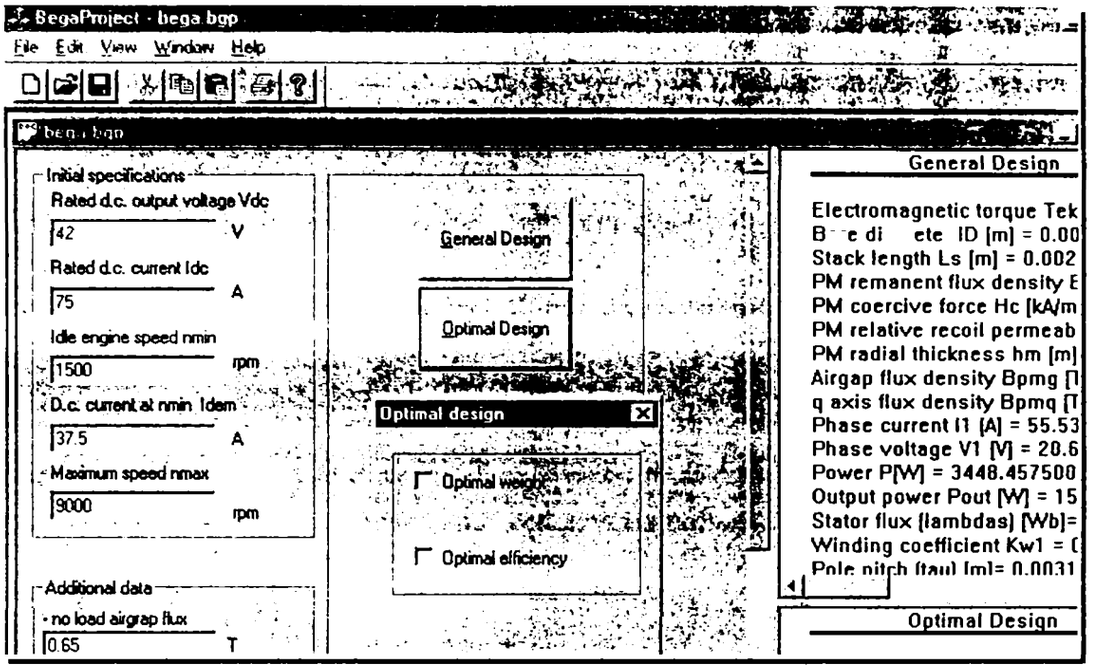

Figure 4.43. The criterions for the optimal design of the biaxial excitation generator, using the BEGAProject.exe computer program

The program has another feature of generating output data during the optimisation process that can help the designer to follow the evolution of the desired variable (output value).

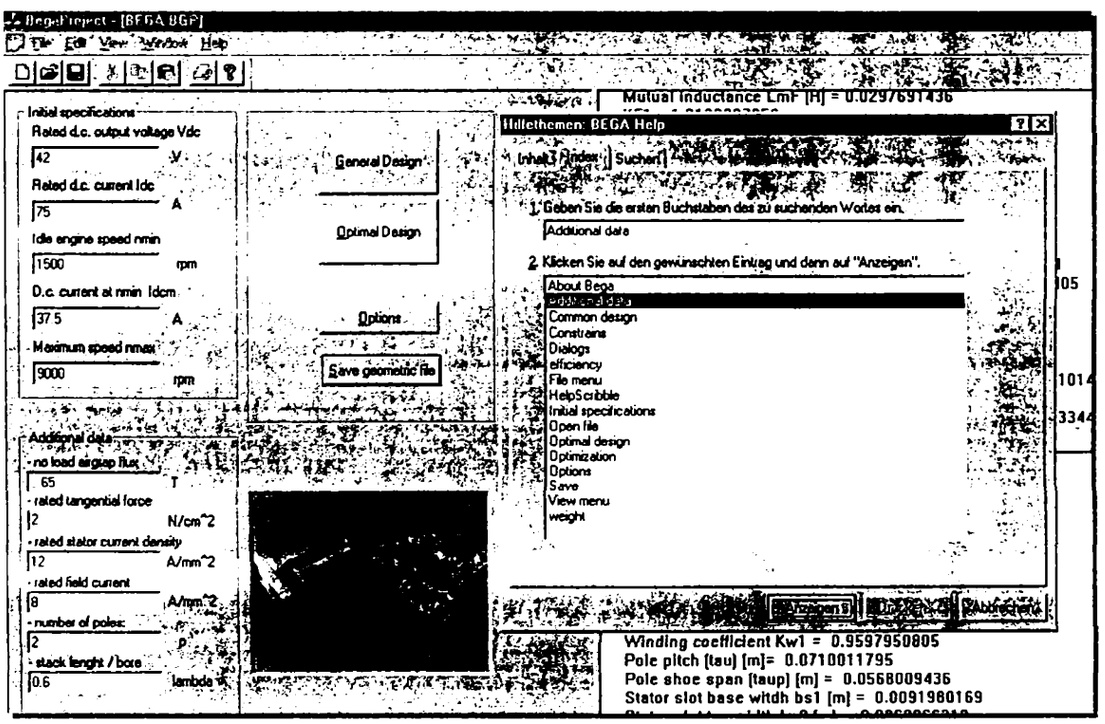

Figure 4.44. The help menu for the BEGAProject.exe computer program to design the biaxial excitation generator

The designing program has an useful help menu (see figure 4.42) that can help the user to easily understand the menus from the software program and the designing procedure, constraints, limits, penalties etc.

To proof the correctness of the designing procedure and to see the advantages offered by the modified Hooke–Jeeves method, as an optimisation way, the BEGAProject.exe software program has been tested.

For the beginning, using the main data from the analytical design example included in this chapter, a general design followed by an optimisation using both, the maximal efficiency and the optimal weight, as optimisation criteria, has been done.

The results of the general design and of the optimisation designs are presented in annex E, as there are resulting from the BEGAProject.exe software program ("result.dat" – for the basic design, respectively "optimal.dat" – for the results after the optimisation).

It can firmly said that the results are as we expected, the general design results are very close to the results calculated in the example as for the optimisation results, the method used for this procedure offered us the final result in short time:

- 12 sec. for the optimisation of the machine using the maximum efficiency as main criterion;
- 8 sec. for the optimisation of the machine using the minimum weight as main criterion.

The length of time was recorded while the software program was running on a PC having the following features: Processor Architecture: Intel Processor Type: x586 - Pentium with MMX Support; Operating System: WINDOWS 98 4.10; Memory: 191 MB Free Hard Disk Space: 541088 KB Free on the drive where the program was installed and the tests were performed.

It has to be mentioned that the step values for the parameters used for the optimisation process are:

- jcobstep = 0.01 [A/mm^2] – for the current density;
- Bcsstep = 0.01 [T] –for the stator core flux density;

- fxstep = 0.01 [N/cm^2] – for the tangential force;

- lamstep = 0.1 – for the stack length per bore diameter ratio;

To make the tests more valid, some characteristics regarding the evolution of the main parameters of the machine during the optimisations processes, too.

First, choosing to make the optimisation design, having the maximum efficiency as declared target, the final results, shown in appendix E, were obtained after 65 steps.

Second, the minimum weight has been choose as declared target for the optimisation design, the final results, shown in appendix E, too, were obtained also after 65 steps.

The results for the main parameters are presented in what follows (figure 4.45 and figure 4.35) and are obtained from the ".dat" – files created to follow the evolution of these parameters (for the efficiency, the total weight and for the total cost of the materials).

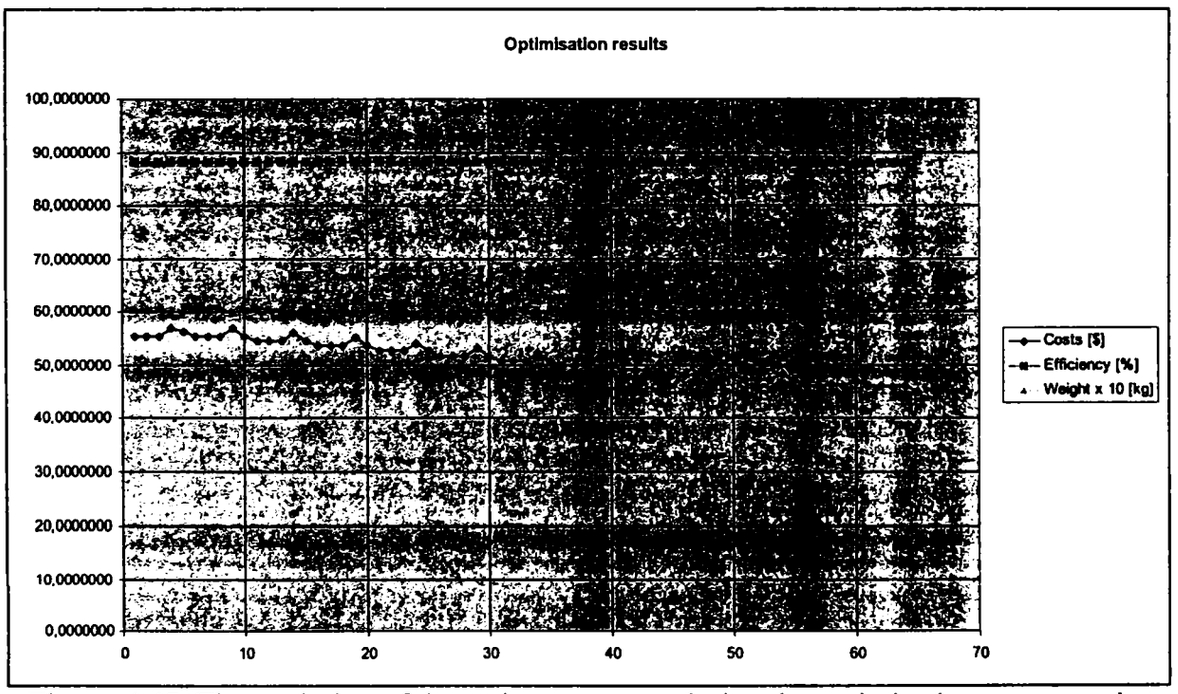

Figure 4.45. The evolution of the main parameters during the optimisation process using the BEGAProject.exe computer program (following the maximum efficiency)

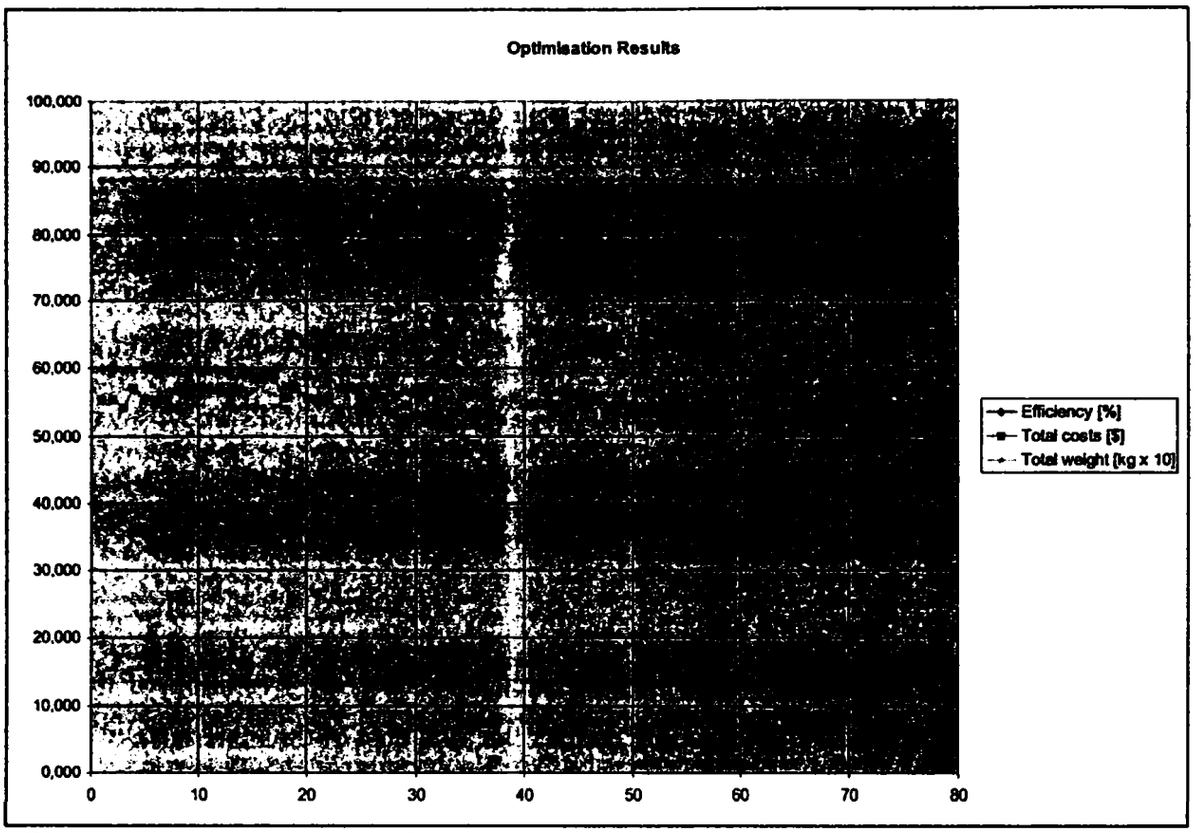

Figure 4.46. The evolution of the main parameters during the optimisation process using the BEGAProject.exe computer program (following the minimum weight)

4.5. Conclusion

In this chapter, a simple analytical design procedure for the new type of generator for automobile industry together with optimisation preliminary results, using the FEM analysis and an optimisation using the modified Hooke-Jeeves method, are presented.

Geometrical topologies analysis, using the FEM, and optimisation using the same method are included successfully on this chapter and will be proved by the real tests that will be done on the two prototypes.

Again, the FEM of analysis has been successfully used for simple and fast optimisations on the geometrical configuration but also on the material selection, used for building virtually a prototype for the machine under research.

Two prototypes were built and studied for two of those geometrical structures, the results of the tests will be part of next chapters of the dissertation.

Designing the new generator based on a simplified example method and the optimisation procedure are detailed presented and explained, offering to the readers an alternative regarding the design approach for an electrical machine.

Some of the main features of the design program are presented in this chapter, so, offering to the readers the possibility to familiarize with it.

Designed to replace the actual claw pole generators which prove their limited power according to the growing electric energy demand from new automobiles electric systems and working at high speeds – where iron loses in claw pole massive poles are unacceptable – the here proposed new generator – the biaxial excitation generator for automobiles – assure a low voltage regulation due to the flux barriers PM combination, a low power control and full power diode rectifier in the stator, good power/volume ratio and superior efficiency with cost comparable to those of existing Lundell generator systems.

The advantage beside other PM generators, part of them presented in 1st chapter of this dissertation are related to the no load voltage, for high speed, and to the low cost for the permanent magnets and for the power control system (a simple low power chopper placed in the field circuit).

Preliminary results together with manufacturing costs evaluation for this new type of electric machine constitute sufficient reasons for considering its operation as an automobile alternator.

The generating system digital simulations, performances and test results from next two chapters will establish the BEGA system.

References

[4.1] E. C. Lovelace, T. M. Jahns, J. L. Kirtley Jr., J. H. Lang - *"An interior PM Starter/Generator for Automotive Applications"* - Record from IEE 1998;

[4.2] I. G. Kassakian, H. C. Wolf, I. H. Miller, C. H. I. Murton - *"Automotive electrical system circa 2005 "* - IEEE Spectrum, August, 1996, pp. 22 – 27;

[4.3] S. Kuppers - "Numerische Verfahren zur Berechnung und Auslesung von Drehstrom Klauenpolgeneratoren" - Shaker Verlag, Aaachen 1996;

[4.4] M. Vaida, M. Boules, R. Henry - *"A high efficiency, high power generation system for automobiles "* - Record of IEEE - IAS 1995 - Annual Meeting, pp. 709 – 716;

[4.5] H. I. Gut, I. Müller - *"New aspects for analyzing and optimizing modern motorcar generators"* - Record of IEEE - IAS 1994 - Annual Meeting, vol.1, pp.3–8;

[4.6] T. M. Zahias - *"Uncontrolled generator operation of interior PM synchronous machines following high speed inverter shut down"* - Record of IEEE - IAS 1998 - Annual Meeting, vol.1;

[4.7] I. Boldea - *"Automotive electric generator systems. A review"* - Record of IEEE, Patras – Greece, 1999;

[4.8] I. Boldea - *"Parametrii maşinilor electrice"* – Romanian Academy Publishing House - Bucharest 1991;

[4.9] I. Boldea - *"Reluctance Synchronous Machines and Drives"* - Clarendon Press, Oxford, 1996;

[4.10] I. Boldea, S. Scridon, L. Tutelea - *"BEGA - A Biaxial Excitation Generator for Automobiles"* - "OPTIM 2000" International Conference, Brasov, Romania;

[4.11] I. Boldea, Ew. Ritchie, Fr. Blaabjerg, S. Scridon, L. Tutelea - *"Characterization of the Biaxial Excitation Generator for Automobiles"* - "OPTIM 2002" International Conference, Brasov, Romania;

[4.12] E. Schmidt, W. Brandl – *"Comparative Finite Element Analysis of Synchrnonous Reluctance Machine with Internal Rotor Flux Barriers"* – Record of IEEE, 2001;

[4.13] J. Kaukonen, J. Pyrhönen, J. Nerg, J. Luuko, M. Niemelä, O. Pyrhönen – *"Salient Pole Synchronous Motor Saturation in a Direct Torque Controlled Drive"* – Record of IEEE, pp.1397-1401;

[4.14] E. C. Lovelace, T. M. Jahns, J. L. Kirtley Jr., J. H. Lang - *"A Saturating Lumped Parameter Model for an Interior PM Synchronous Machine"* - Record from IEEE 1999, pp.553-555;

[4.15] N. Bianchi, S. Bolognani – *"Magnetic Models of Saturated Interior Permanent Magnet Motor based on Finite Element Analysis"* – Record of IEEE, 2000;

[4.16] A. Vagati, A. Canova, M. Chiampi, M. Pastorelli, M. Repetto – *"Improvement of Synchronous Reluctance Motor Design through Finite Element Analysis"* – Record of IEEE, 1999;

[4.17] K. Folsach, J.H. Davies, T.J.E. Miller, M.I. McGilp, M. Olaru – *"Analytical and Numerical Computation of Air-Gap Magnetic Fields in Brushless Motors with Surface Permanent Magnets"* – Record of IEEE, 2000;

[4.18] B.S.P. Pereira, M.F. Islam – *"Interior Permanent Magnet Motor Having Several Improved Features"* – Record of Electric Machines and Power Systems, vol.25, pp. 1135-1144, 1997;

[4.19] E. C. Lovelace, T. M. Jahns, T. A. Keim, J. H. Lang – *"Mechanical Design Considerations for Conventionally-Laminated, High-Speed, Interior PM Synchronous Machine Rotors"* – Record of IEEE, 2001;

[4.20] J.H. Lee, J.C. Kim, D.S.Hyun – *"Effect Analysis of Magnet on Ld and Lq Inductance of Permanent Magnet Assisted Synchronous Motor Using Finite Element Method"* – Record of IEEE, 1999;

[4.21] W.L. Soong, N. Ertugrul, E.C. Lovelace, T.M. Jahns – *"Investigation of Interior Permanent Magnet Offset – Coupled Automotive Integrated Starter/Alternator"*- Record of IEEE, 2001.

CHAPTER V

BEGA CAR GENERATING SYSTEM SIMULATION

5.1. Introduction

This chapter includes the digital simulations for an automobile generating system that includes as power generator a bi-axial excitation generator (BEGA), designed according to the data and formulas from chapter four and built through a real prototype as will be presented in chapter six.

For the BEGA generator having the final structure as proposed in the previous chapter, we can indicate the main features of it that constitutes the choice for use as an automobile alternator:

- The stator has a simple structure, like a regular three phase winding induction machine;
- The rotor has both PM's and fielding windings;
- It is robust and relative easy to build (except PM's insertions);
- The manufacture costs are not so large, it doesn't needs any special technology;
- High performance given by high power density and high efficiency possibility;
- Easy to maintain, especially considering the required power electronics;
- Wide speed range even if it has slip rings and brushes;

Simulation for a three-phase equivalent circuit model will be obtained using Matlab™ simulations.

The rotor design and construction of the BEGA is a challenging task due to the conflicting characteristics of improved performance and rotor complexity. The BEGA machine can be

modelled with wide, and theoretically infinite, speed ranges for constant power operation. In order to get a constant and stabilized voltage output of the generating system, a controller has to be used. [5.1] to [5.5]

Combining the d.c. bus circuit model with the proposed field current control circuit, detailed PSpice™ simulations will be carried out.

5.2. Model Construction

The models of the generator and of the entire generating system are done using two different simulation ways (and using different software): one for finding the generator parameters and steady-state characteristics (using the Matlab™ software) and the second one for obtaining the transient results for the entire generating system (using the PSpice™ software).

So, first, for the generator, simple and effective Matlab™ simulations will be carried out. The results will be useful and will be compared with the results from the design program (chapter four) and those from the real tests, especially regarding the electromagnetic torque of the machine for the considered rated speed of 3000 rpm.

For the steady-state simulation model of the generator, all the main parameters of the machine are according to the design result from the "BEGAProject.exe" dedicated design program (see chapter four). The model is detailed presented in Appendix D. No additional losses were not considered in the simulation models.

The model of the generating system is based on real components, which are normally on the power generating systems on automobiles and these components will be used for the real tests of the system, tests that will confirm and validate the theory regarding the bi-axial generator behavior and the system effectiveness.

Having the design parameters of the BEGA and the power electronics structure of the generating system, the model of the system may be conceived.

As explained already, the biaxial excitation generator for automobiles is a hybrid synchronous machine whit a topology as follows:

- a three phase stator, like an asynchronous machine;
- a salient multi-pole rotor with multi-flux barriers;
- low cost permanent magnets (Ferrite) inserted inside the flux barriers;
- a rotor winding with field purpose.

For the model construction of this machine, a d-q axes modelling, followed by transformation in three phase model through Park equations seems to be the proper solution in this way. [5.7]

5.3. Model Implementation

All types of electrical alternators proposed have the output voltage control stage made with high costs. [5.6]

This impediment is slightly reduced for this new type of electric machine, which constitutes the core for the previous and the next chapters, too.

The field control, as an additional control for the constant power range, through a simple four-quadrant chopper, suffices for this machine in generating mode (fig. 5.1).

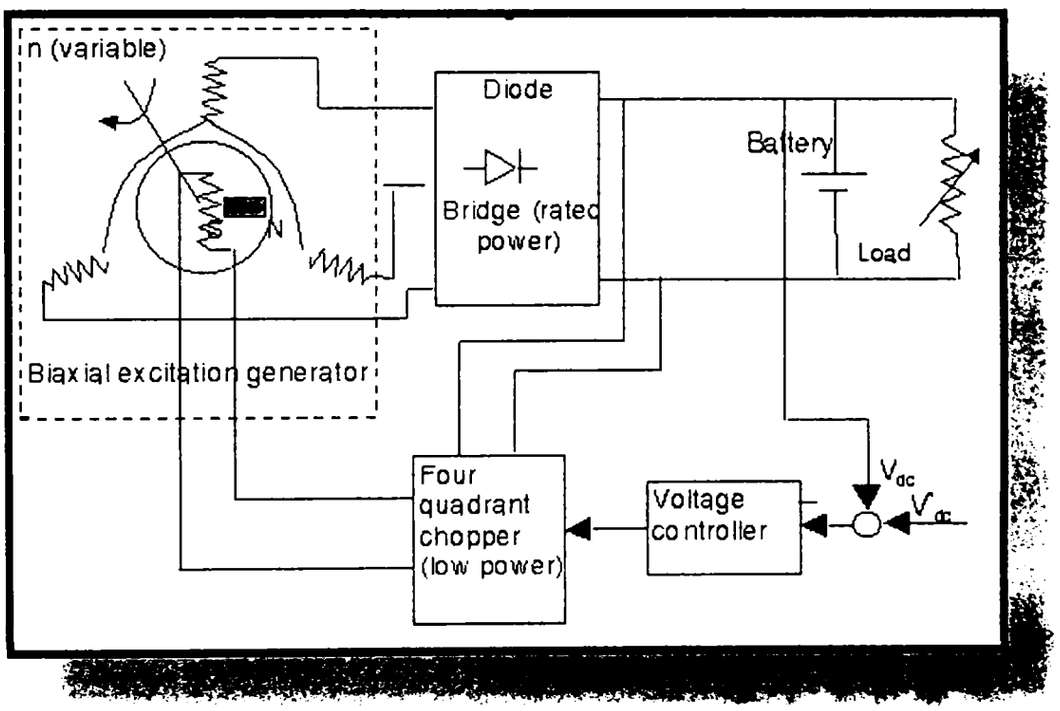

Figure 5.1. The low cost regulation of the biaxial excitation generator for automobiles

As mentioned, this control is done using a 4-quadrant chopper - of low power, so, built at lower costs than all systems previously presented (see chapters one to three).

The complete generating system for a 42 V d.c. bus line output voltage is an integrant part of this dissertation and it will be treated theoretically – by simulations - in this chapter.

5.4. Simulation Results

5.4.1. BEGA Generator - Digital Simulation Results

First, some of the main parameters of the BEGA are presented for different speeds, as indicated in figure 5.2.

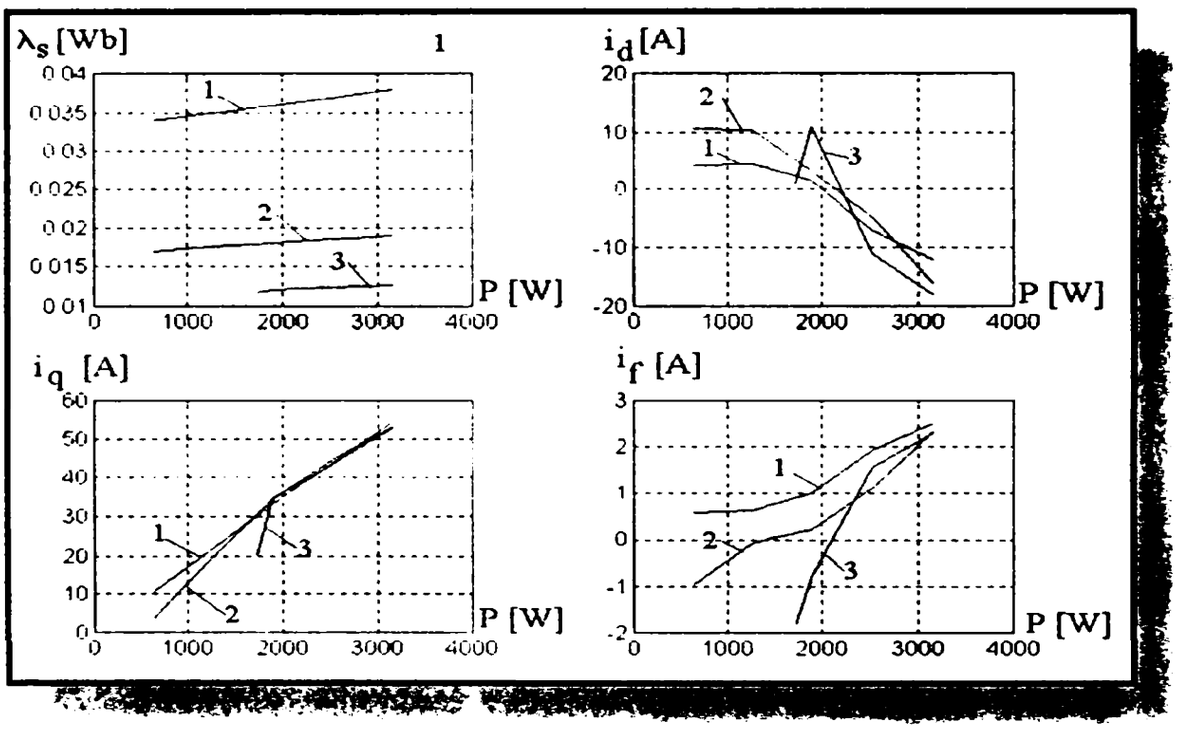

Figure 5.2. Simulation results for: Stator flux (λ_s) vs. power; d axis current (i_d) vs. power; q axis current (i_q) vs. power; Excitation current (i_F) vs. power (where: 1-50Hz; 2-100Hz; 3-300Hz)

The flux is the "heart" of the design and simulation result, as shown in the above figure, the shapes of the stator flux for the entire power range and different speeds are concludent. Of course, the shapes for the currents (for d and q axes and the field current) are presenting us the particularities of the BEGA generator.

For the same frequencies, using a simple no-load model, the results are as shown in figure 5.3.

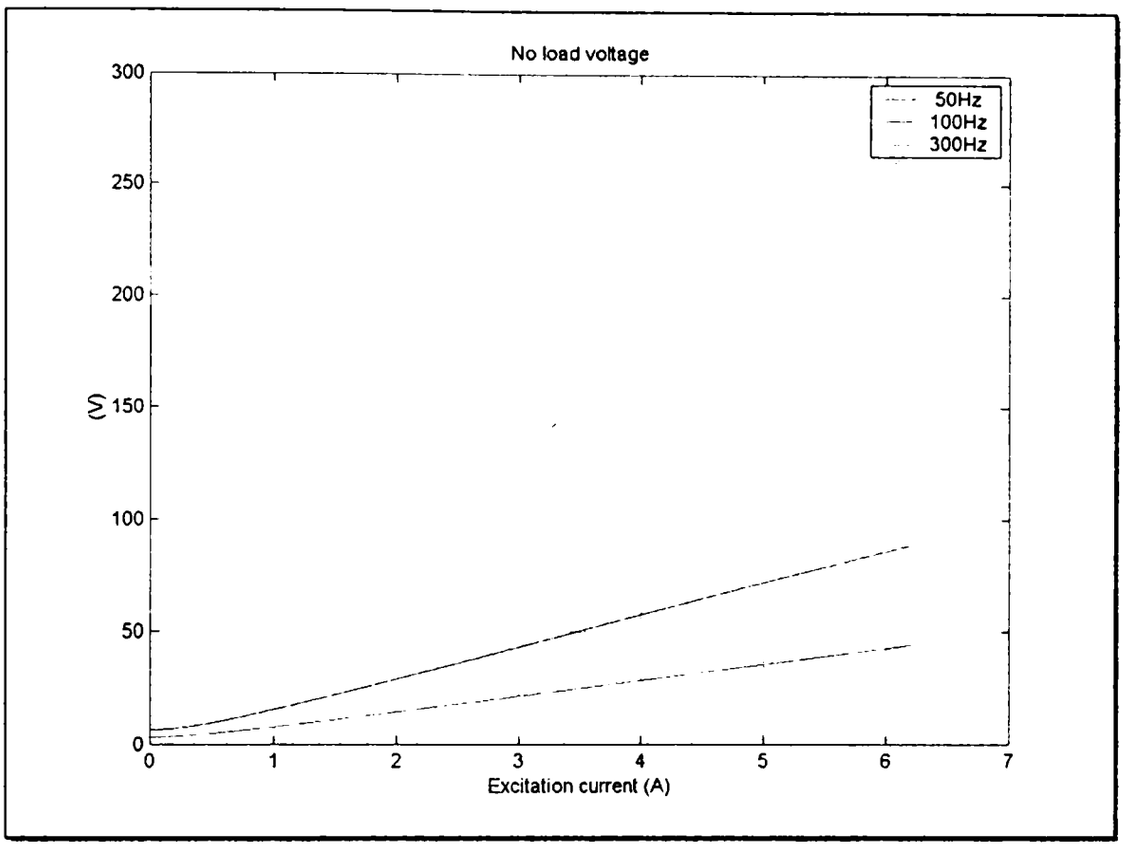

Figure 5.3. The no-load digital simulation results for the BEGA generator

As will be obtained later by tests, the resulted no-load voltage shapes will look as there are presented in figure 5.3, so, the model for the no-load simulation is correct even if no additional losses were considered.

More, the short-circuit characteristics of the BEGA machine were calculated and the results are presented in figure 5.4. To offer a better image of the short-circuit characteristics, the field current range was enlarged.

For an infinite value of the frequency, the curve is also represented in figure 5.4 (the lowest shape from the figure), to see the limit of the short-circuit characteristics.

As can be observed, the short-circuit current reaches a high value (of about 100A) for the rated value of the field current (I_f =3A).

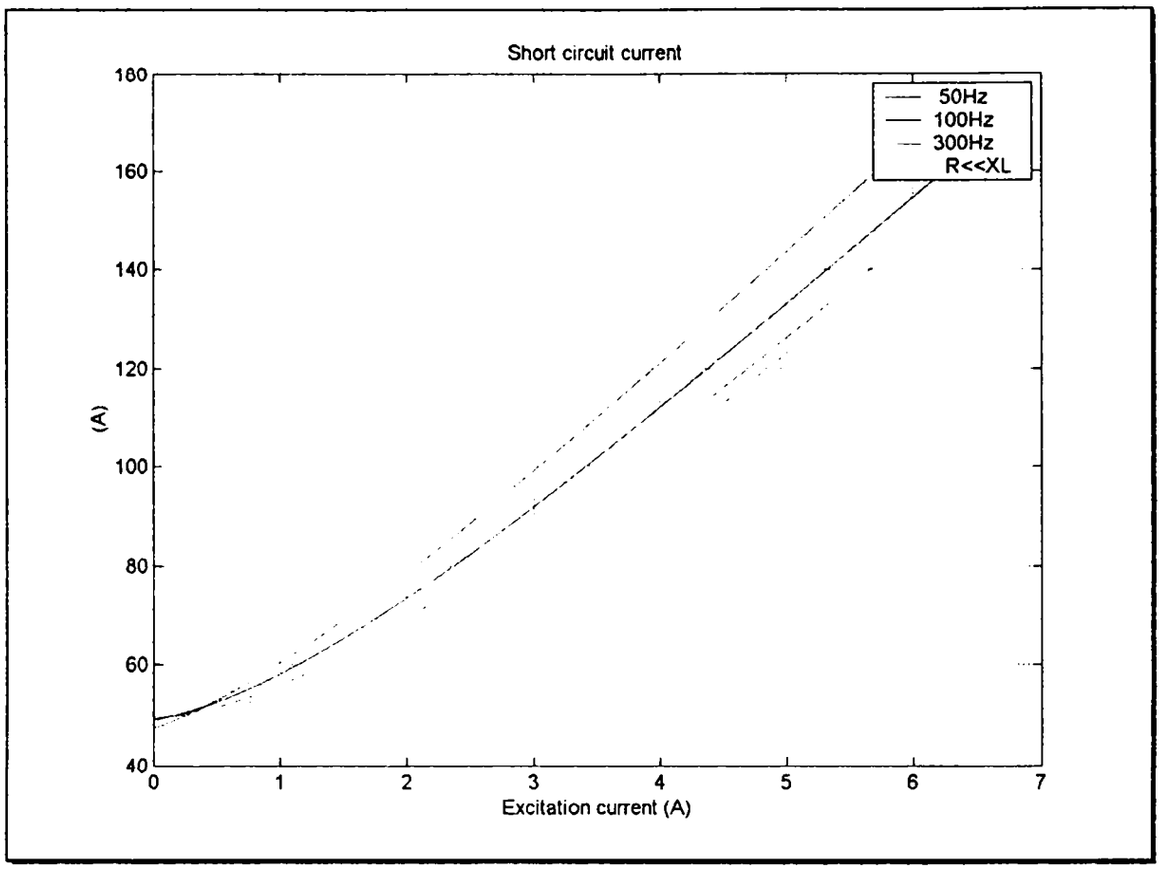

Figure 5.4. The short-circuit digital simulation results for the BEGA generator

In what follows, the external characteristics of the BEGA machine are shown. The parameters used for the model were the same as the calculated ones.

The phase voltage vs. phase current shapes are drawn for zero field current (the shapes from the left-down side of the figure) and for the rated value of the field current (the shapes from the right side of the figure). Again, the curves were done for the important frequencies, of 50Hz, 100Hz and 300Hz.

It can be observed that at the beginning, the phase voltage increases with the load, that is because of the flux from the PM's, but after that it decreases.

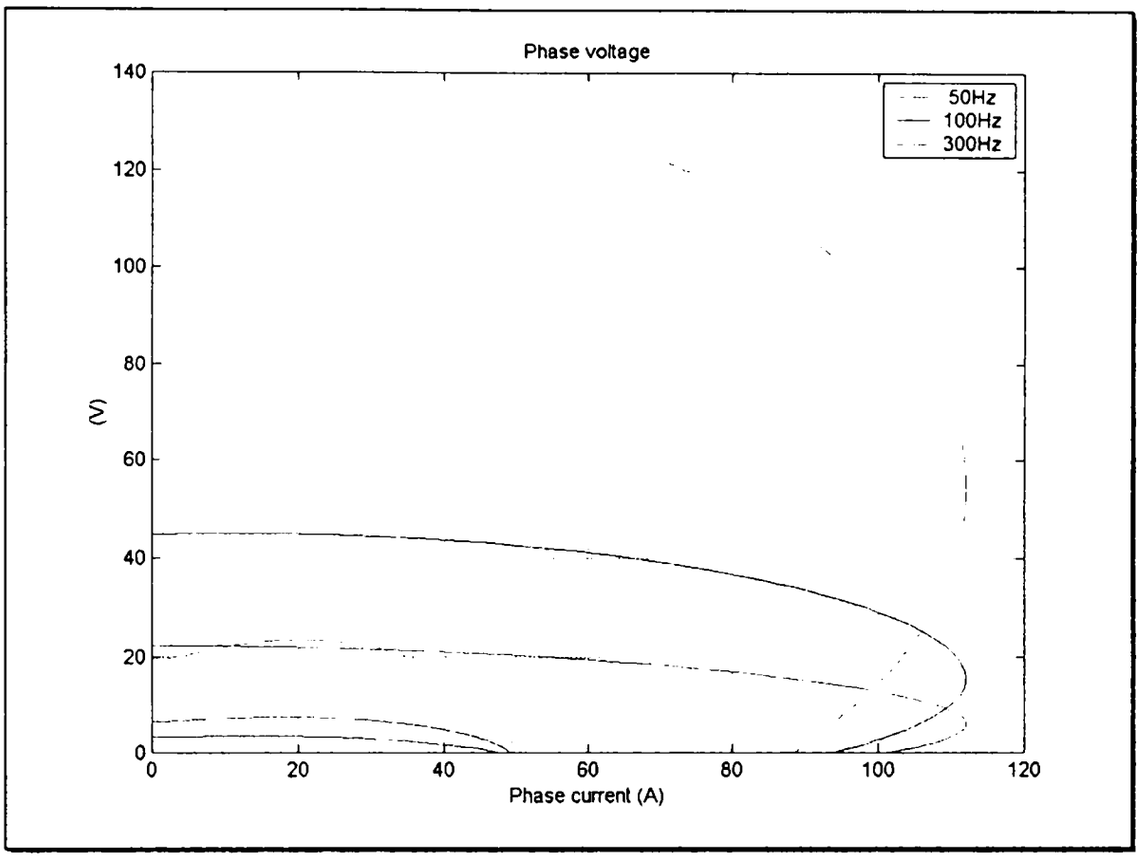

Figure 5.5. The external characteristics, digital simulation results for the BEGA generator

The electromagnetic torque of the machine is one of the most important parameters. To compare the calculated value of the electromagnetic torque (through design program) with the value obtained by digital simulation (using the FEA or other digital simulation software) and then through real tests, is an important task.

As will be observed from figure 5.6, the rated value of the electromagnetic torque resulted from the digital simulation has the same value as was calculated from the design program (see Appendix E) of $\mathbf{T_n = 24Nm}$.

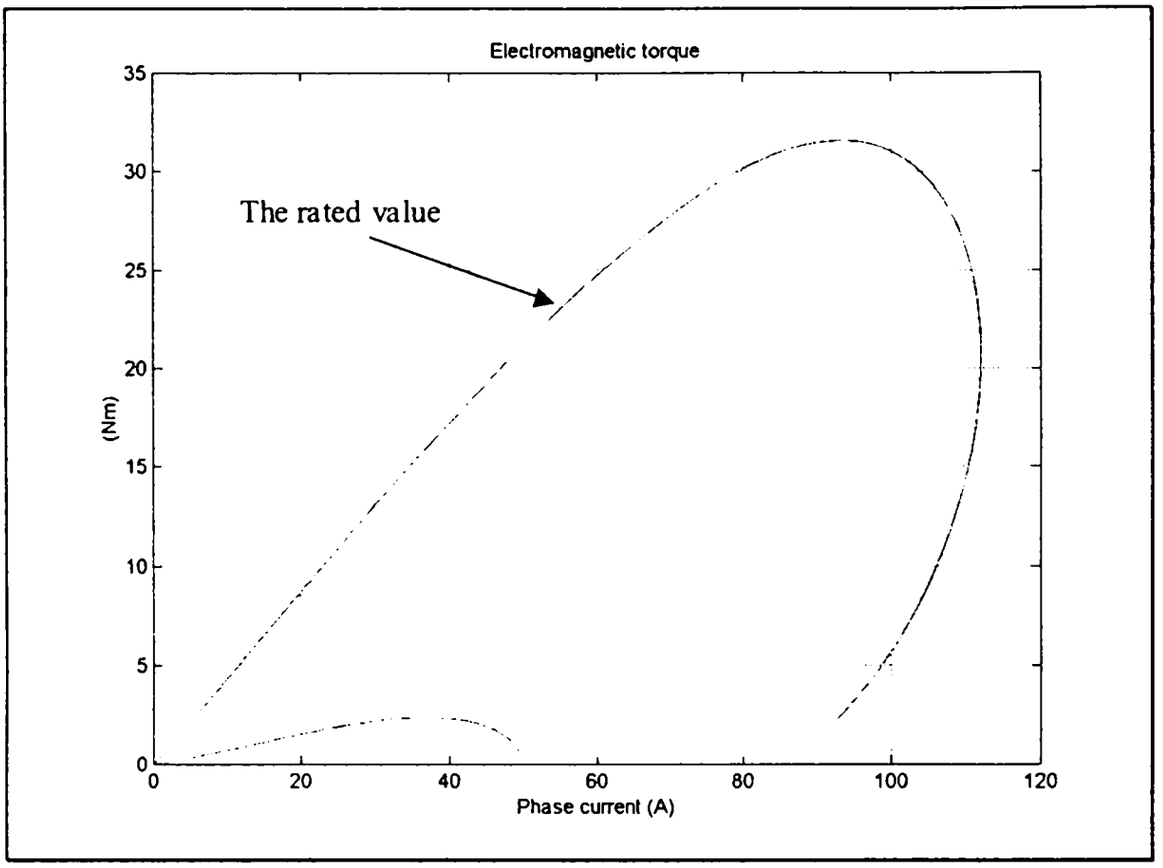

Figure 5.6. The electromagnetic torque vs. stator phase current, digital simulation results for the BEGA generator

The electromagnetic power vs. phase current characteristics, for different frequencies, are shown in figure 5.7. The iron losses were not considered.

The influence of the field current can be easily identified, the shapes were represented for zero and the rated value of the field current.

The shapes are approximately linear up to the rated current.

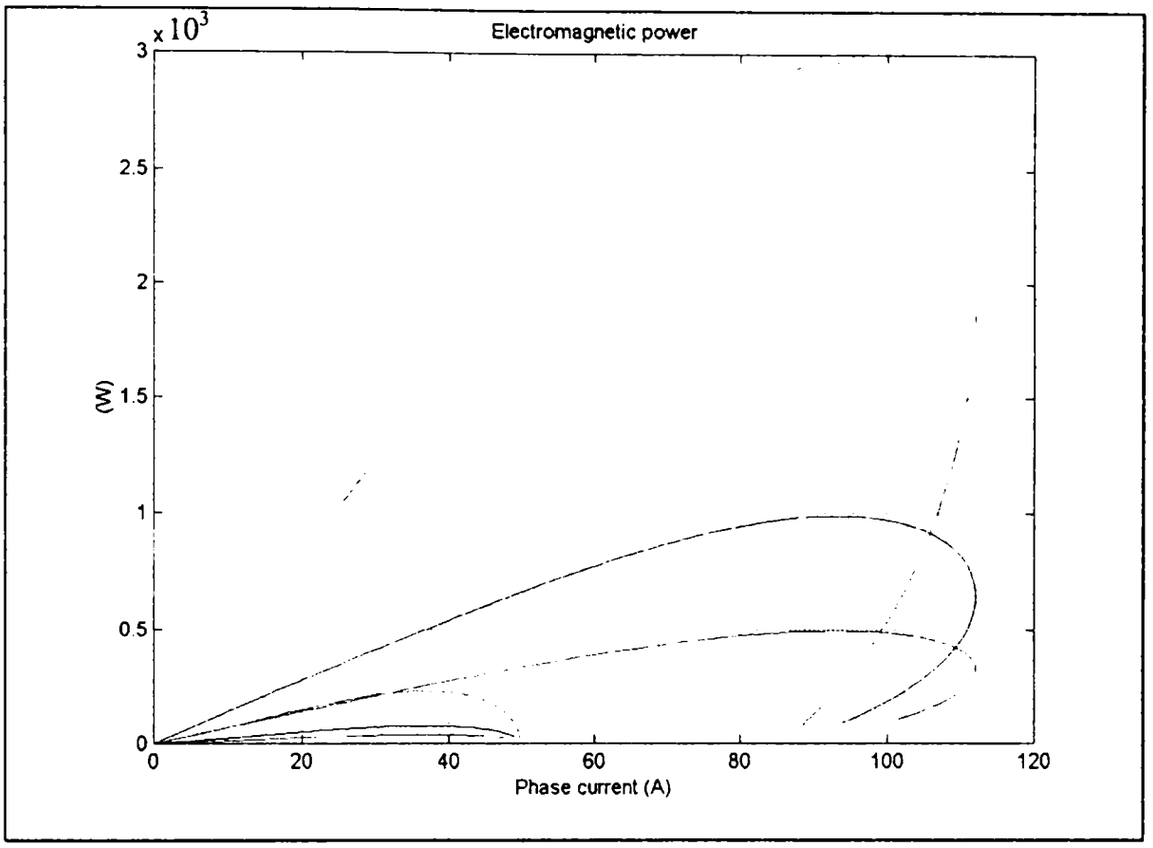

Figure 5.7. The output power vs. phase current, digital simulation results for the BEGA generator

Having the main parameters and steady-state characteristics of the BEGA generator, we can go forward and find some results from the digital simulations for the transients of the proposed generating system, using the BEGA as a electrical generator.

5.4.2. BEGA Generating System - Transients Digital Simulation Results

The results of the PSpice™ digital simulations for the generating system presented before, will be shown in what follows. Notice that the simulation starts considering the system operating at the desired speed instantly.

Pspice™ complete simulations not shown here from lack of space show that while for 1500rpm 1.5 kW at 42V d.c. is available, from 1650 rpm forward (already) full power (3kW, at 42Vd.c.) is available which is much better than in claw pole generators.

Notice the negative field current values at high speeds and lower loads.

Load simulation results for three batteries and load resistor in parallel are presented in what follows.

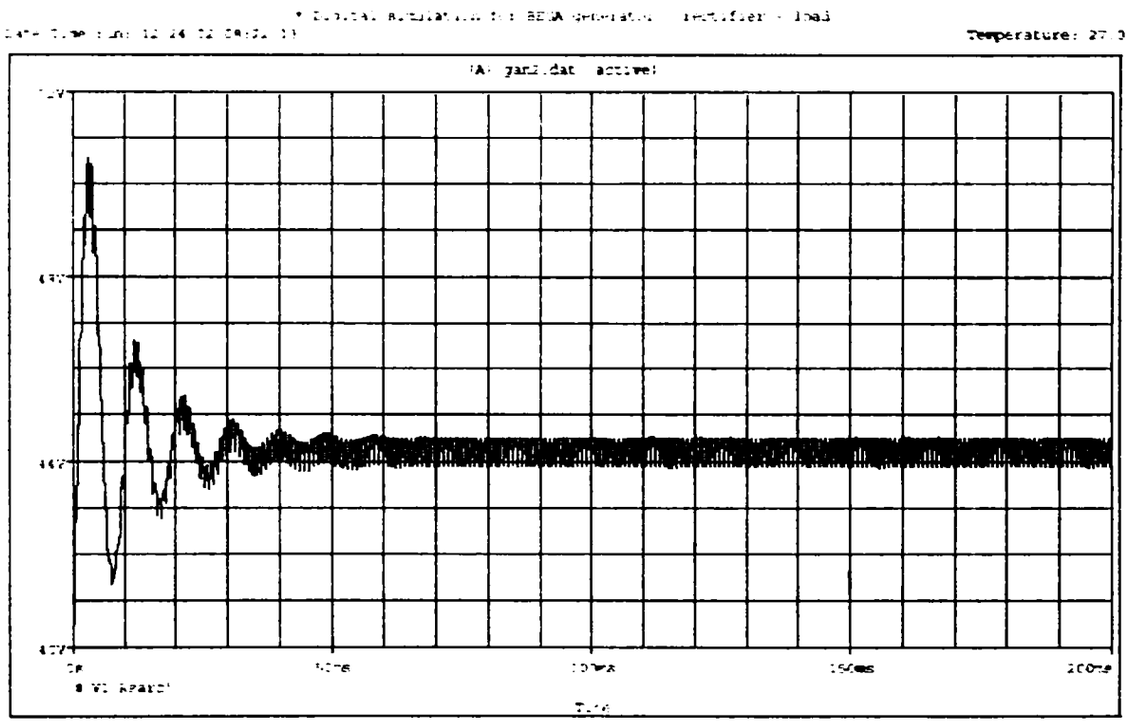

Figure 5.8. Batteries and resistor load voltage at 9000 rpm, 42 V d.c., R_{load}=1Ω

Both, the load voltage and current are shown in figures 5.8 and 5.9.

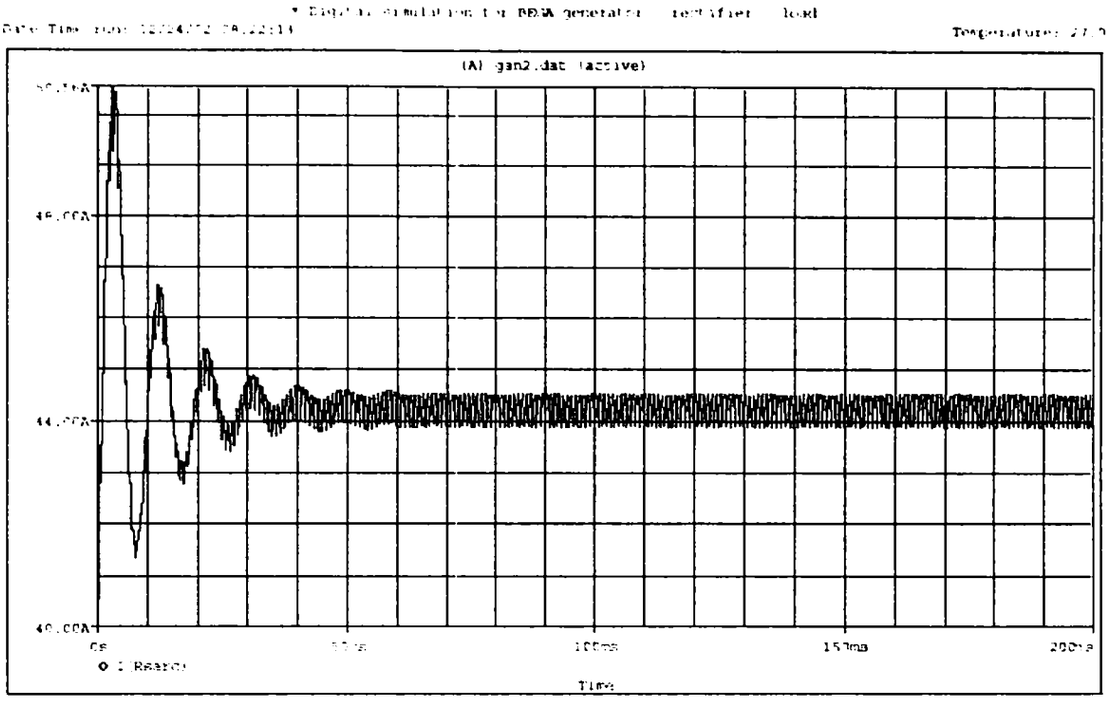

Figure 5.9. Batteries and resistor load current at 9000 rpm, 42 V d.c., $R_{load}=1\Omega$

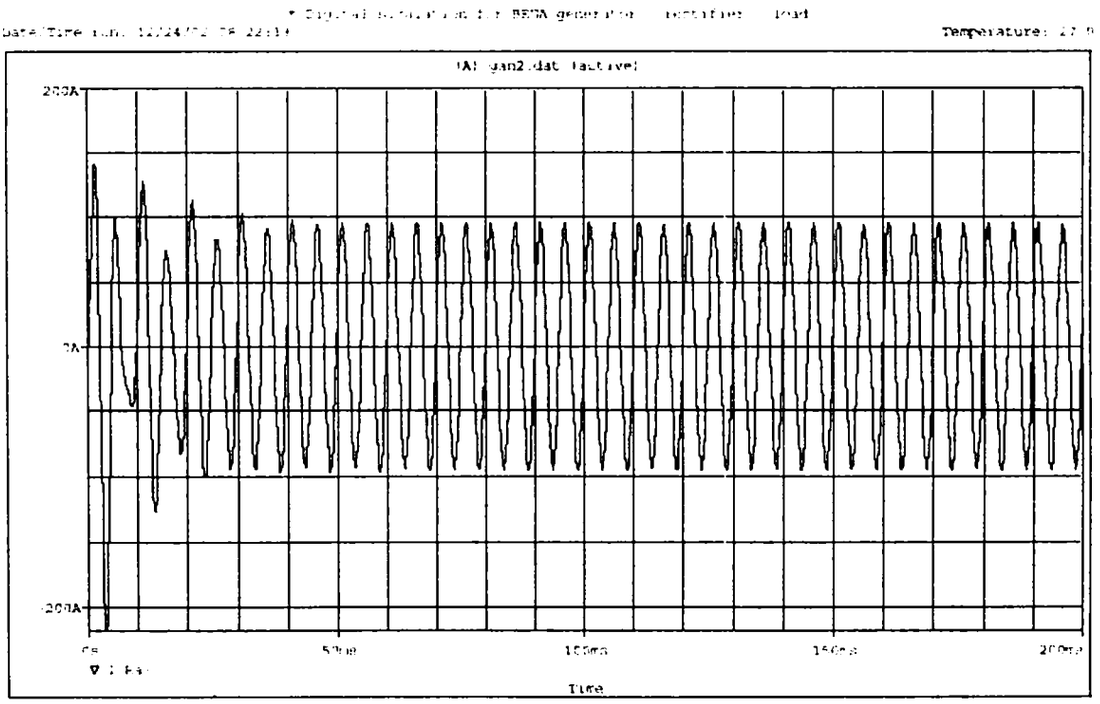

Figure 5.10. Phase current at 9000 rpm, 42 V d.c., $R_{load}=1\Omega$

The system response is quite fast, less than 10 ms are required to stabilize the phase current during the starting procedure.

Now, for a certain period of time of 100ms, the load resistor is connected in parallel with the three batteries system. The load resistance value is changed to $R_{load}=0.7\Omega$.

The effect of adding the load resistor is strong, the current through the batteries drops significantly when the load resistor is connected (see figure 5.11).

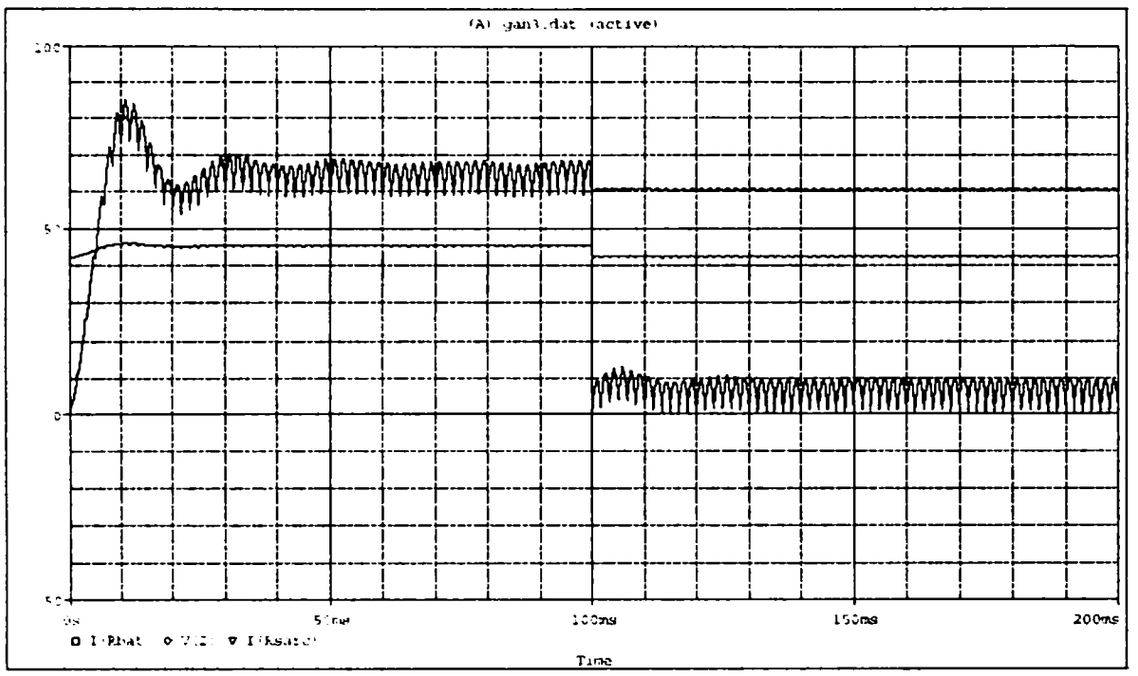

Figure 5.11. Transients when adding the load resistor at 3000 rpm, 42 V d.c., R_{load}=0.7Ω, field current I_f = 1.5A

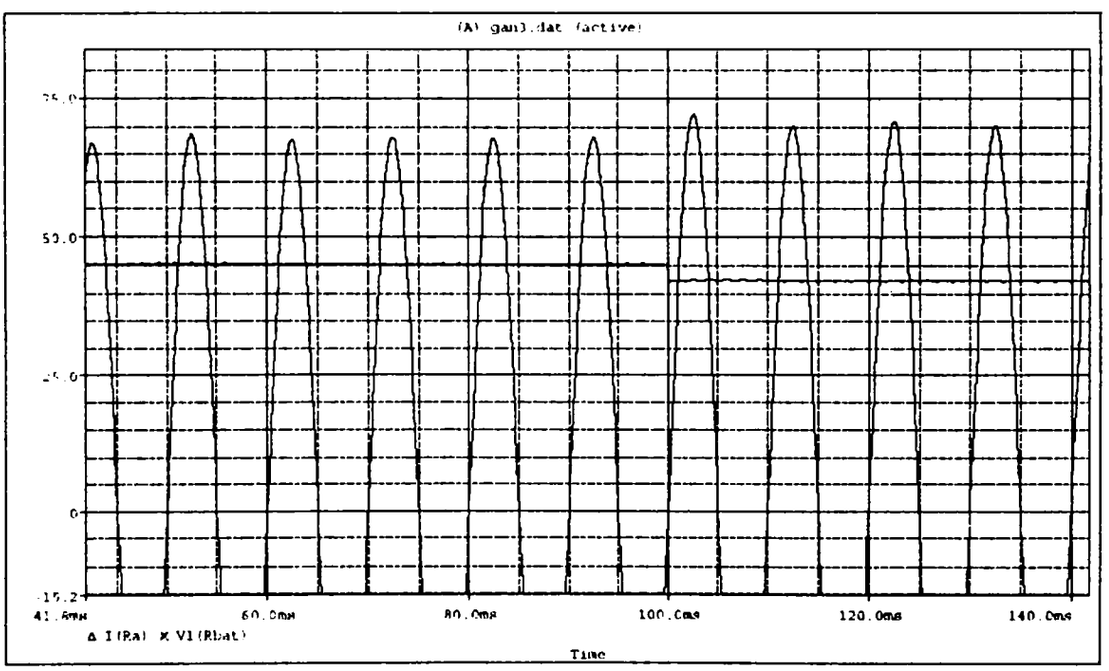

Figure 5.12. Details of the transients during the add of the load resistor at 3000 rpm, 42V d.c., R_{load}=0.7Ω

As shown in figure 5.12, the generating system has no problem during the load connection. Both, the load voltage and current are going to the new values during a very short time.

If the field current has a larger value, the drop of the batteries current will be smaller than before, as figure 5.13 correctly presents.

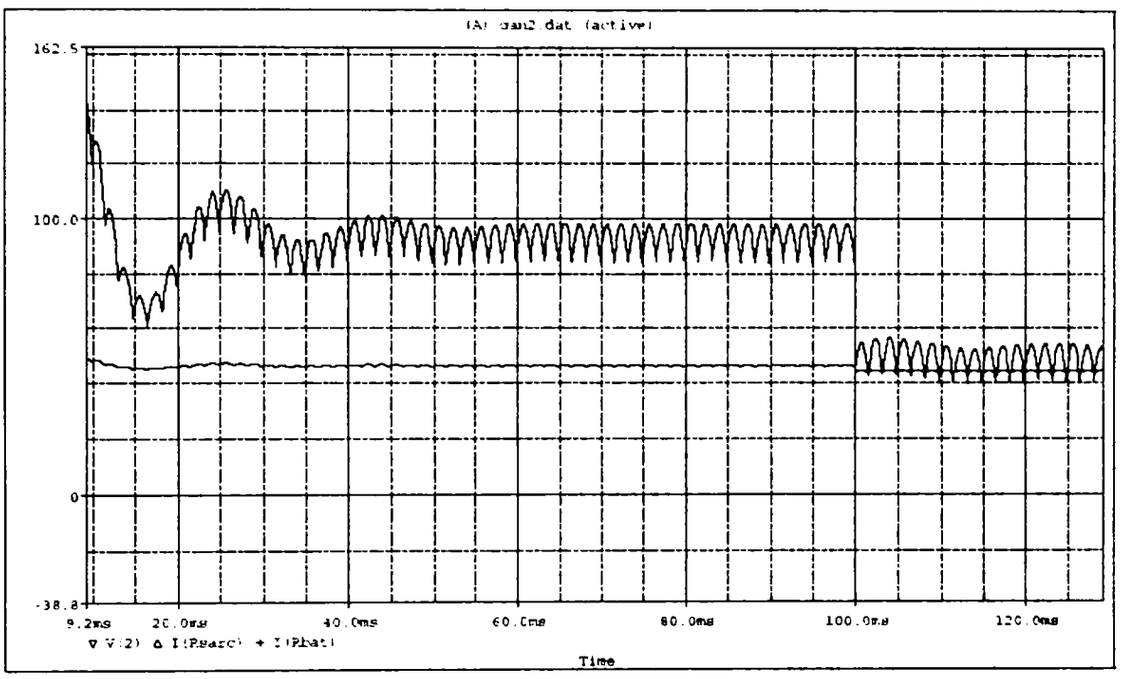

Figure 5.13. Transients when adding the load resistor at 3000 rpm, 42 V d.c., R_{load}=0.7Ω, the field current is I_f= 3A

As will be shown in chapter six, the same phenomena will appear in reality, too.

Now, in figure 5.14 we will have the transient results for the maximum operating speed of the BEGA generator, considered in the design program, too.

Again, the response of the system is coming very fast, the current through the batteries is dropping significantly when the load resistor is connected.

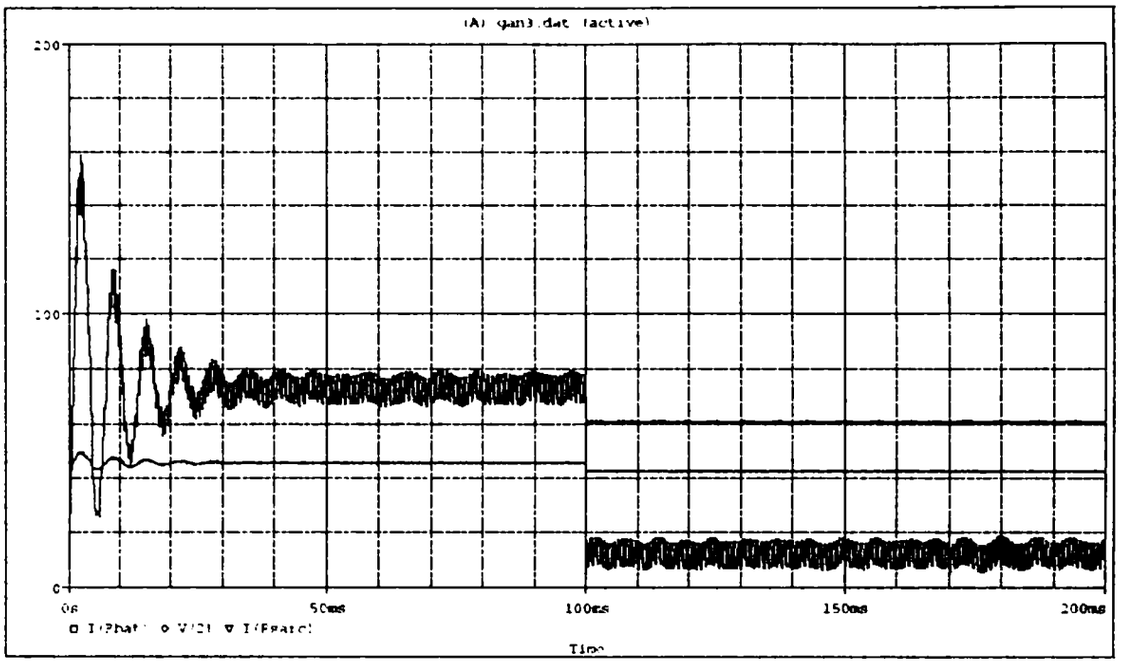

Figure 5.14. Transients for adding the load resistor at 9000 rpm, 42 V d.c., R_{load}=0.7Ω, the field current is I_f= 1.5A

Of course, more digital simulations may be done, including the field current regulation, through a low power/low cost chopper. These digital simulation can be considered subject for future works in this research field.

5.5. Conclusion

Extended digital simulations and their results was the core of this chapter. Here were investigated the steady-state characteristics of the BEGA generator and the transient results from the digital simulation models.

Two models, created using different dedicated software, and their results, were presented and detailed discussed.

Even if no field current regulation was considered, the generating system proves its good behaviour during sudden changes of loads.

For a large load range, the voltage varies very tiny and that is because of the presence of the q-axis PM's.

As the digital simulation results show us, theoretically, the BEGA generator might be successfully used as an automobile generator.

In what follows, the real tests, on a scale prototype, will concluded all digital simulation results from this chapter.

References:

[5.1] E. C. Lovelance, T. M. Jahns, J. L. Kirtley Jr., J. H. Lang - *"An interior PM Starter/Generator for Automotive Applications"* - Record from IEE 1998

[5.2] I. G. Kassakian, H. C. Wolf, I. H. Miller, C. H. I. Murton: *"Automotive electrical system circa 2005 "* - IEEE Spectrum, August, 1996, pp. 22 – 27

[5.3] M. Vaida, M. Boules, R. Henry - *"A high efficiency, high power generation system for automobiles"* - Record of IEEE - IAS 1995 - Annual Meeting, pp. 709 – 716;

[5.4] H. I. Gut, I. Müller - *"New aspects for analyzing and optimizing modern motorcar generators"* - Record of IEEE - IAS 1994 - Annual Meeting, vol.1, pp. 3 – 8;

[5.5] T. M. Zahias - *"Uncontrolled generator operation of interior PM synchronous machines following high speed inverter shut down"* - Record of IEEE - IAS 1998 - Annual Meeting, vol.1;

[5.6] I. Boldea - *"Automotive electric generator systems. A review"* - Record of IEEE, Patras, 1999;

[5.7] I. Boldea - *"Reluctance Synchronous Machines and Drives"* - Clarendon Press, Oxford, 1996;

[5.8] I. Boldea, S. Scridon, L. Tutelea - *"BEGA - A Biaxial Excitation Generator for Automobiles"* - "OPTIM 2000" International Conference, Brasov, Romania;

CHAPTER VI

BEGA – THE PROTOTYPES AND TEST RESULTS

6.1. Introduction

This chapter of the dissertation includes test results for the two existing prototypes of BEGA and is structured in two main parts, the first one – that follows – includes some results from the tests done for the first prototype and the second parts presents extended results given by tests done for the final prototype of BEGA.

As mentioned, the BEGA generator uses a laminated salient pole rotor with hetero-polar electromagnetic excitation (2p = 4, 6, 8 poles) to eliminate the large addition losses in the existing claw-pole solid-iron rotor.

Through a reduction in the number of poles from 12 (14) for claw-pole rotor generators (CPRG) with ring-shape single coil excitation to 4 (6, 8) poles, BEGA suggests increased excitation copper losses and larger yokes. The frequency (for given or higher speeds) is however smaller. The stator core losses plus the rotor excitation power losses are to be smaller than in CPRG. [6.1-6.6]

Another feature of BEGA rotor is the presence on the rotor of multiple flux barriers filled with low cost (ferrite) PM's designed to fully compensate (destroy) the q axis stator produced flux linkage ($(\lambda_q)_{Irated}/2=0$).

Now as the diode rectifier produces unity power factor, for, say, half rated load , $\lambda_q = 0$. It follows that $I_d = 0$. Thus the d axis armature reaction is forced to zero.

6.2. Summary of the Results for the First Prototype

For the beginning, results from different measurements done for the first prototype are included. These results can be considered sufficient to create an overview for the first prototype behaviour.

As mentioned before (in chapter four), the first prototype was built using the lowest budget possible in order just to establish if the theoretical proposal was feasible or not.

The stator and the rotor of the first prototype, together with details of the rotor sheet and permanent magnets are the core of the next figure.

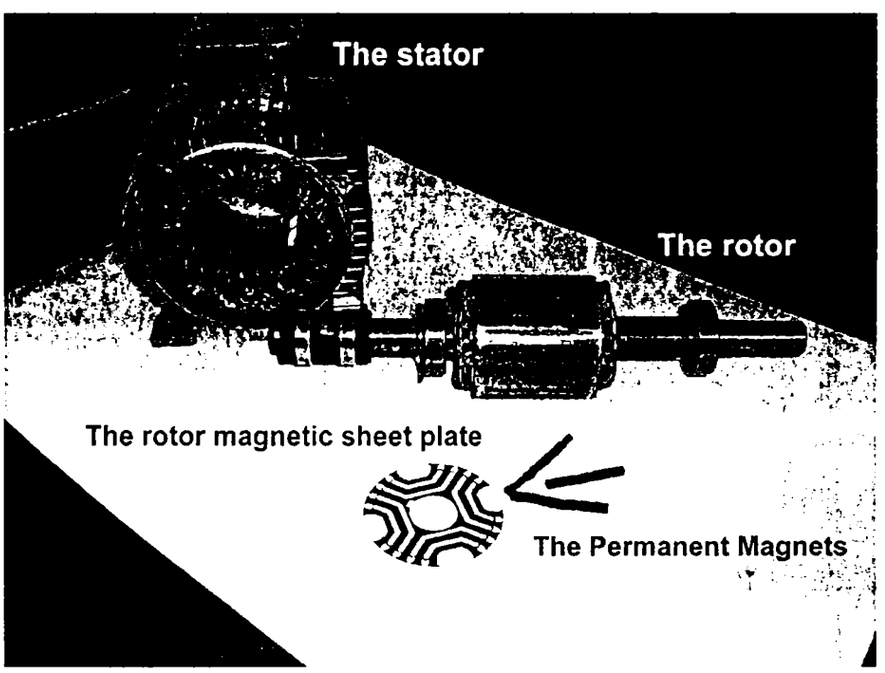

Figure 6.1. Details of the first prototype of BEGA

The first prototype of BEGA was made using the main data, resulted from the example of the basic design presented in chapter four, the main drawback was that for the rotor windings, the number of total wires couldn't be as calculated on the basic design, this from mechanical reasons, the wedges needs to keep the windings inside rotor diameter when the machine is rotated at speeds that can reach 9000 rpm's. So, the maximum field current couldn't have values above 2.5 A.

No load test results

The generator was driven by a 7.5 kW – 2 poles – induction motor, using a Hitachi (U/f control type) frequency converter to feed the motor and change the speed.

For different values of excitation current, the induced voltage given by the generator was measured using a regular multi-meter (figure 6.2).

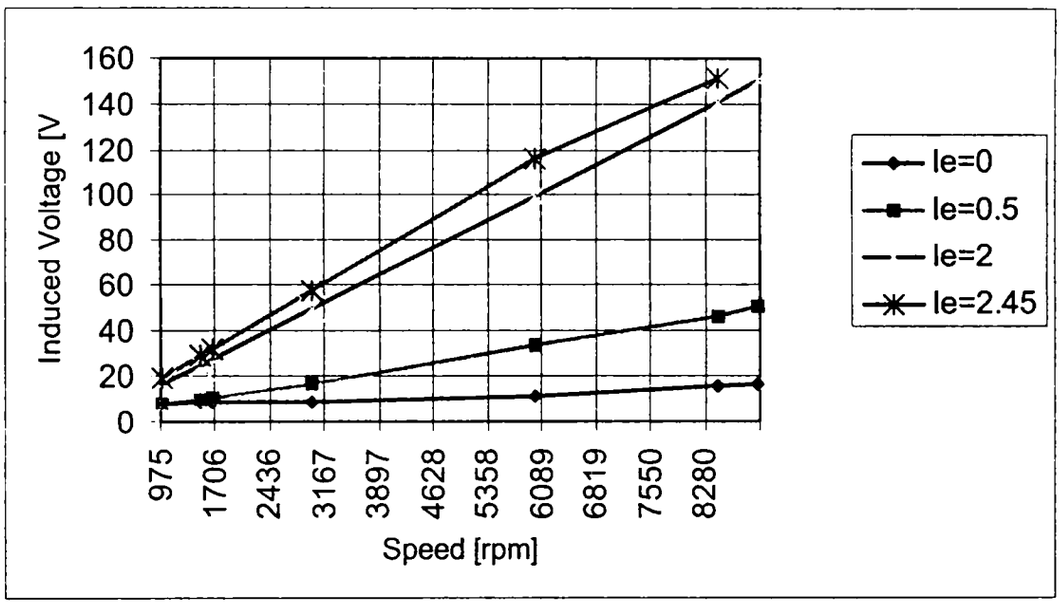

Fig. 6.2. The induced voltage vs. speed for different excitation currents

As can be seen from the above no load characteristics, the rated value of the line induced voltage of the generator is strongly influenced by the field current. If no current goes through the field coils, the induced voltage did not change much it's value, from 15 V to 18 V.

The situation is not the same if the field current has a larger value, the rated value of the line voltage changes its value from 20 V (at 1000rpm – the idle speed) up to 150 V (at maximum speed – 9000 rpm), so, the influence of the field on generator response.

Inductances

The rotor of the generator is locked with the d axis (respectively with the q axis) positioned in the direction of the magnetic axis of the stator winding a. The stator windings are connected to a a.c. voltage supply. The setup for making such tests it will be enclose in the second part of this chapter.

The *d* axis and *q* axis inductances have been measured in a.c. standstill tests (figure 6.3).

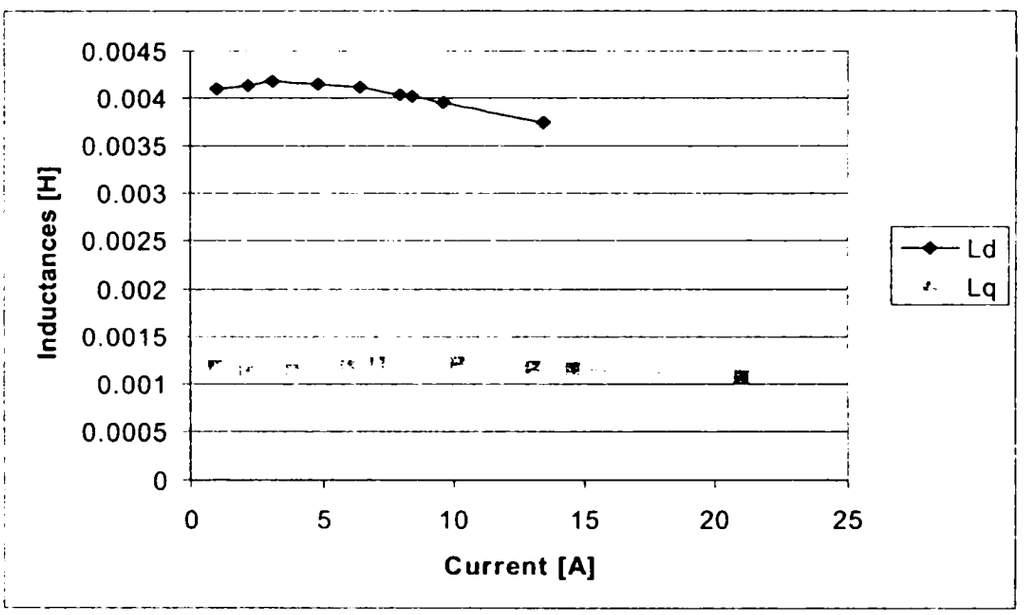

Fig. 6.3. The *d* axis and *q* axis inductances vs. current

The results from figure 6.3 lead us to emphasize the conclusion that ratio between the direct inductance and the quadrature inductance: $L_d/L_q=2.66$ is not as we expected from the calculations from the basic design.

Short-circuit test

The short-circuit test has been performed only for this prototype and just for two cases: without excitation current and for an excitation current of I_e=1.9A (figure 6.4).

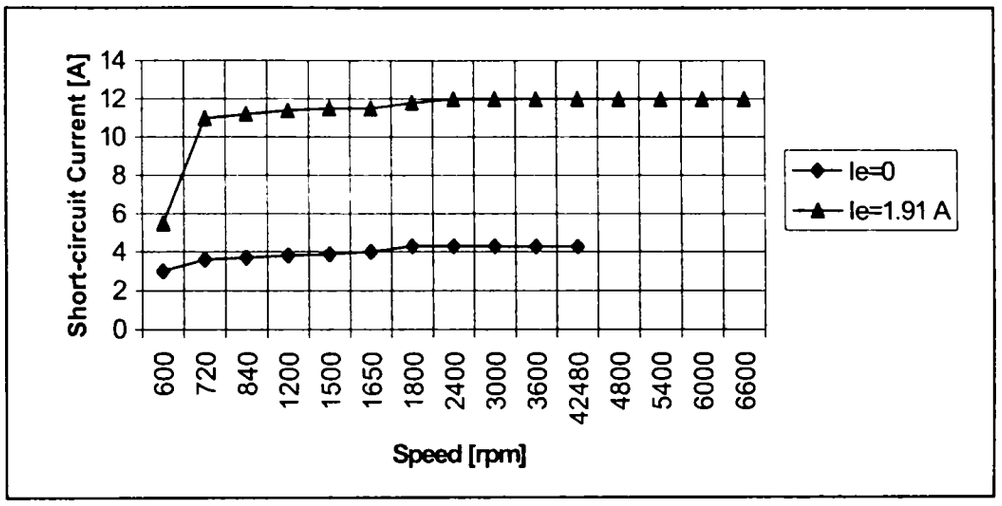

Fig. 6.4. The short-circuit current vs. speed for 0A and 1.9A excitation currents

As shown in figure 6.4, the short-circuit current strongly depends on the field current, the influence of the permanent magnets looks to be minor. Anyway, the short-circuit current reaches not high values, so the influence of the PM's is reduce and the losses seems to be large.

6.3. Results for the Final Prototype

The final prototype, built according to the design program presented in chapter four, has been tested, in detail, to find out it's parameters and follow the set rules in a real generating system, conceived to meet the real situation on a generating system with 42 V d.c. bus voltage.

This prototype, see figure 6.5 was made, with the financial and logistic support of the Institute of Energy Technology, from Aalborg University.

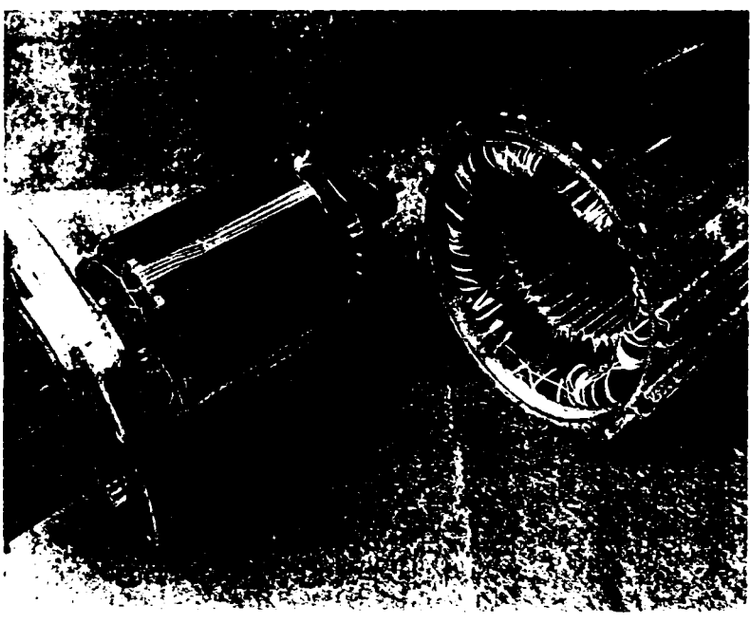

Figure 6.5. Details of the final prototype of BEGA

The main scope of the following tests is to determine the machine parameters, characteristics and performances.

We can use test results to:

- find machine's model for different operating modes;
- outline the practical limits for the operating domain of the electric machine, from excitation, load, environmental condition points of view;
- compare with the results obtained during the design process, in order to improve both, the design strategy and manufacturing technology;

- find out time constants and machine parameters useful for control strategy and machine integration in drive system.

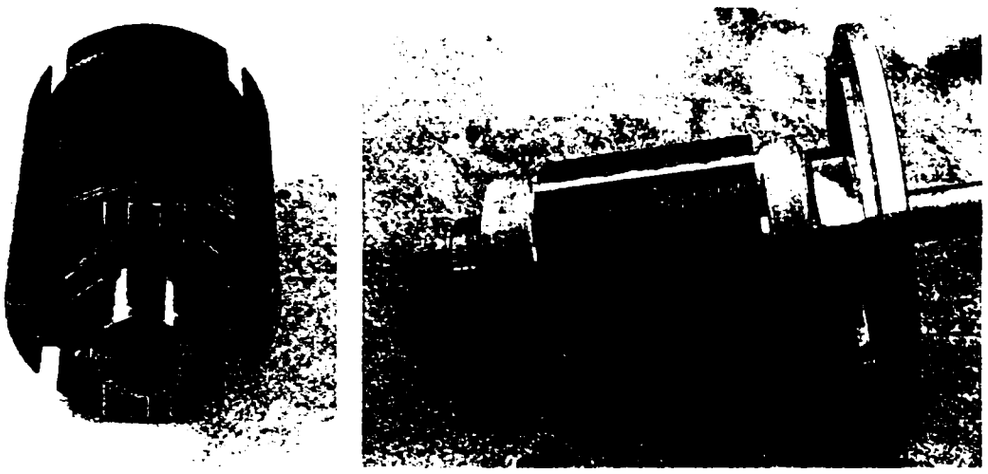

Figure 6.6. Other details of the rotor of BEGA final prototype

(with PM's only - left image and together with field coils – right image)

All static and no load experimental tests were done in the Laboratories from the Institute of Energy Technology, from Aalborg University, in Denmark.

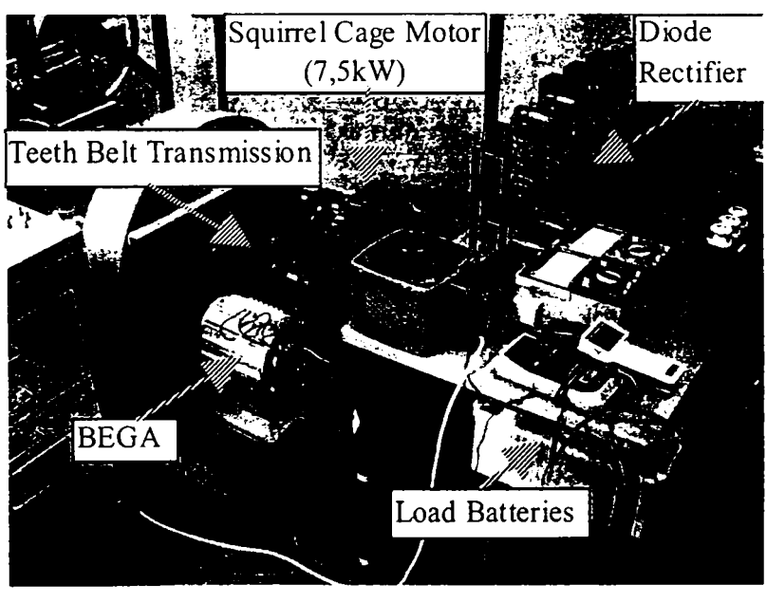

Figure 6.7. Details of the main setup for testing of the generating system

The rest of the experimental tests were done in the Electrical Machines Laboratories from Electrical Engineering Faculty, at the University "Politehnica" of Timisoara and on Bee Speed Automatizari SRL tests stand.

6.3.1. The Static Tests

The generator prototype was tested regarding the following:

- the resistances

- the fill factors

- the inductances

6.3.1.1 Resistances

The stator phase resistance and the field resistance were measured using a digital multi-meter.

The values obtained are: $R_s = 0,17\ \Omega$ for the stator phase and $R_f = 6,5\ \Omega$ for the field coil (four coils in series connection). Those are almost as were predicted on the design program.

6.3.1.2 Fill Factors

The cross-sectional area of the windings was estimated by the design program to fit in a slot area of 113,26 mm^2 for the stator windings and a rotor slot area of 102,72 mm^2 for the field windings.

Those corresponds to a fill factor of:

$K_{fill1} = 0,45$ for stator winding, consequently:

$K_{fill2} = 0,45$ for the field winding.

By measuring the field and stator windings diameters, the corresponding areas were calculated and those are very close to the assumed values, even better than the assumed ones. We obtained after measuring the real winding sizes: $K_{fill1} \approx 0{,}48 \approx K_{fill2}$

6.3.1.3 Inductance & Resistance Measurements

The direct axis inductance and resistance together with the quadrature axis inductance and resistance were measured using a LCR-meter. The rotor of the machine was locked consequently on both positions.

Figure 6.8. Details of the LCR meter during tests

The values measured using LCR meter are presented in next figures and are showing us the variation of the d-axis and q-axis inductances and resistances.

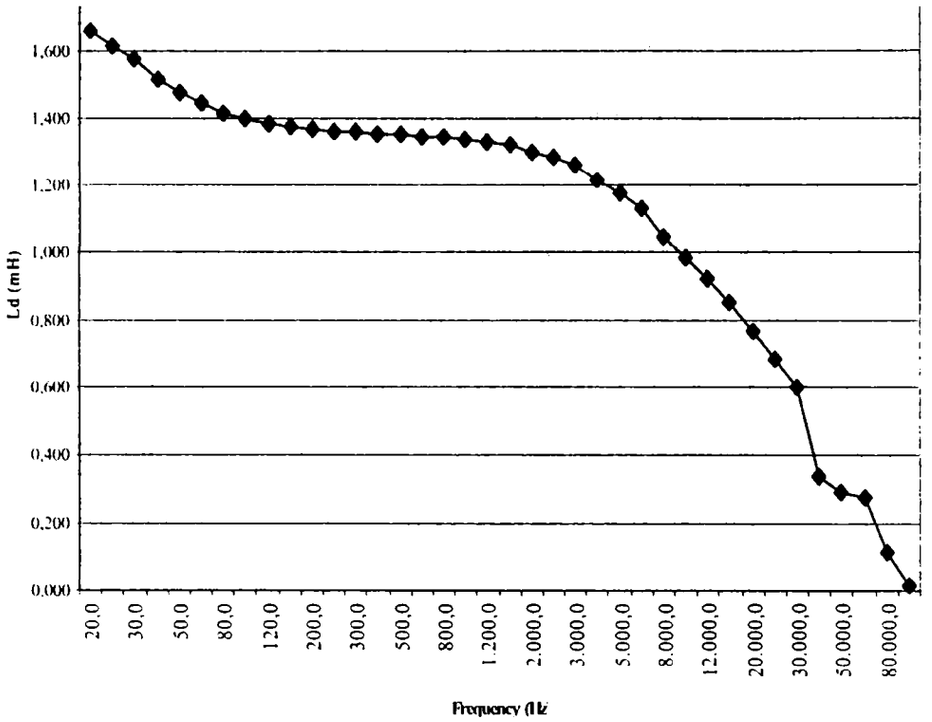

Figure 6.9. The direct axis inductance versus frequency

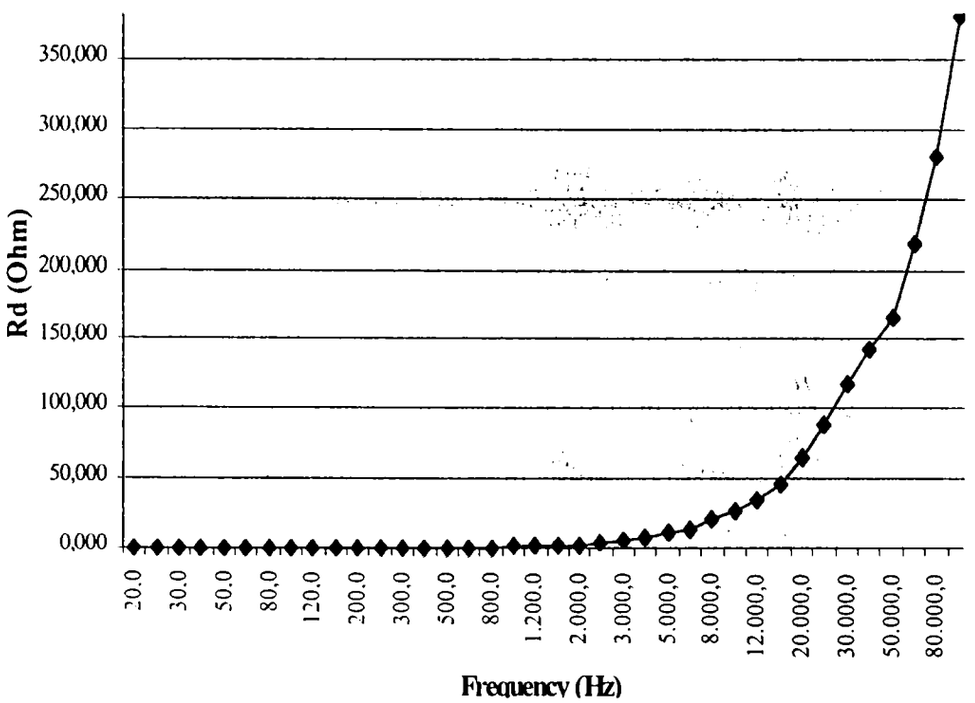

Figure 6.10. Direct axis resistance versus frequency

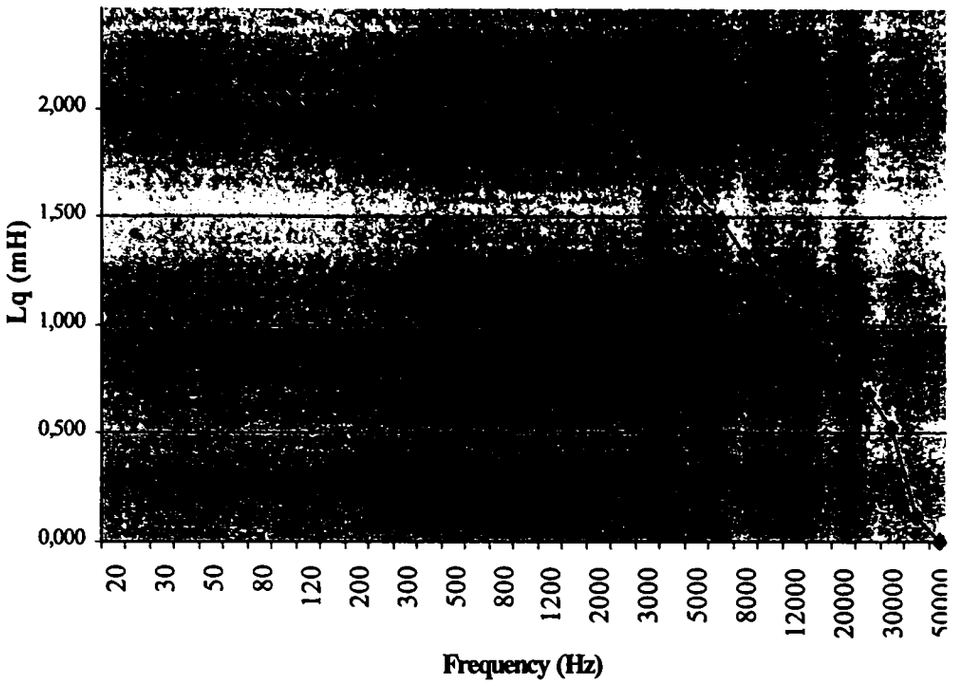

Figure 6.11. The quadrature axis inductance versus frequency

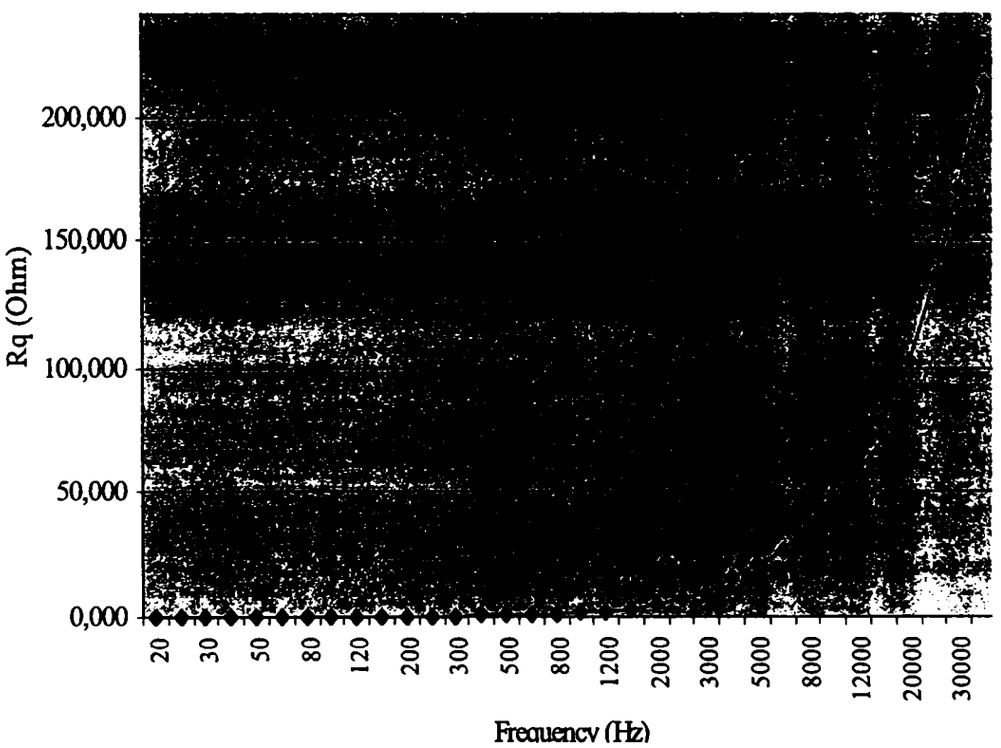

Figure 6.12. Quadrature axis resistance versus frequency

6.3.1.4. Standstill d-axis Tests

To find the direct axis reactance, the measurement setup from figure 6.13 is used. The rotor is locked with the d axis positioned in the direction of the magnetic axis of the stator winding a. The stator windings are connected to a d.c. voltage supply through a resistor, used to set up the initial value of the current through the stator windings prior to short-circuiting. [6.9]

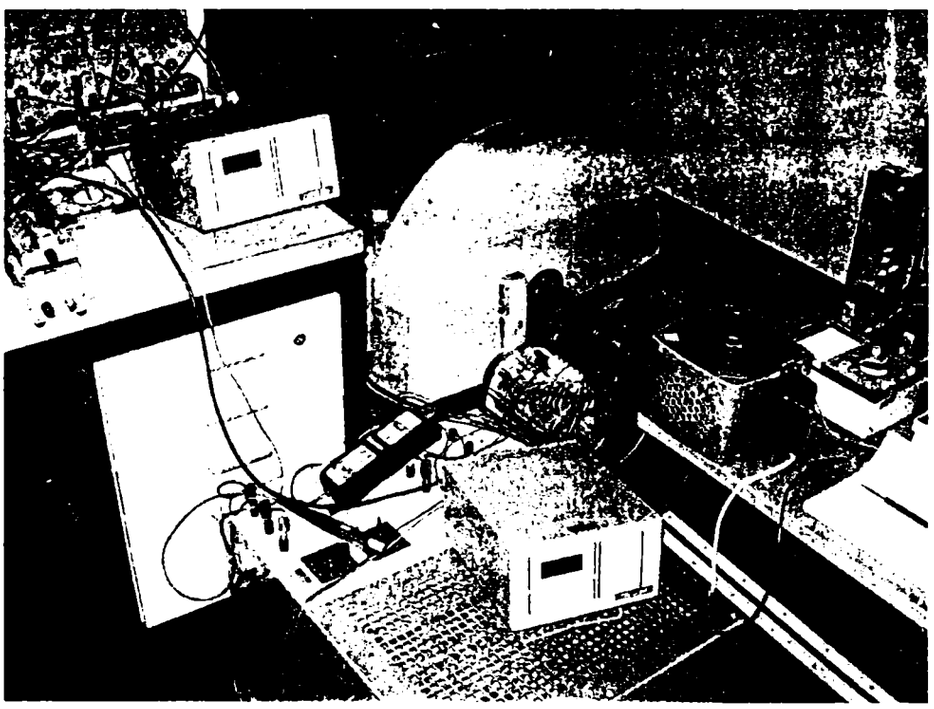

Figure 6.13. Details of the setup during d.c. decay tests

The transient current $i_d(t)$ is acquired using an oscilloscope together with a current insulated transducer. The stator voltage is set to 12 V d.c. and the transient current to an approximate value of 3.3 A.

From static transient tests, the direct axis reactance was calculated.

The most used method to determine the direct axis reactance is using the results from the ideal no load and symmetrical three phase short circuit permanent operations.

From the first one, the e.m.f., V_s, is measured and from the second, the short circuit current, I_{sc}, both measurements are made at the same excitation level resulting the direct axis synchronous reactance as follow:

$$X_d = V_s / I_{sc} \tag{6.1}$$

This relative simple method requires two separate tests and implies mechanical coupling between the machine under tests and a driving motor.

Another method is the standstill frequency method that requires a complex test stand with a variable frequency power generator.

A more simple method is the d.c. decay (transient) method [6.12] which is a standstill method and consist of applying a step voltage into the stator winding of the machine by closing the breaker K and recording the corresponding current waveforms.

In this case the direct axis reactance is:

$$X_d = \frac{R_s \omega_n}{I_{d0}} \int_0^\infty i_d(t) dt \tag{6.2}$$

The phase resistance, R_s, measured value is 0.17Ω. With the rotor locked in d axis position, and than in q axis position (rotating with 90^0 electrical degrees), the operational reactance were measured using an oscilloscope to monitor the direct currents waveforms. The R_f resistance is of 5 Ω.

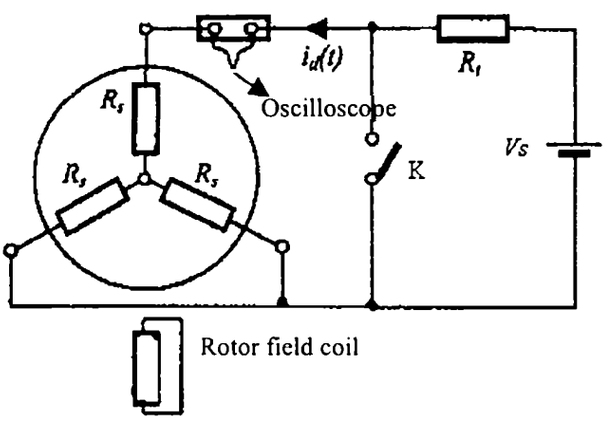

Figure 6.14. The scheme of the setup for the d axis d.c. decay tests

The R_f resistance is for protection of the d.c. source when K is closed.

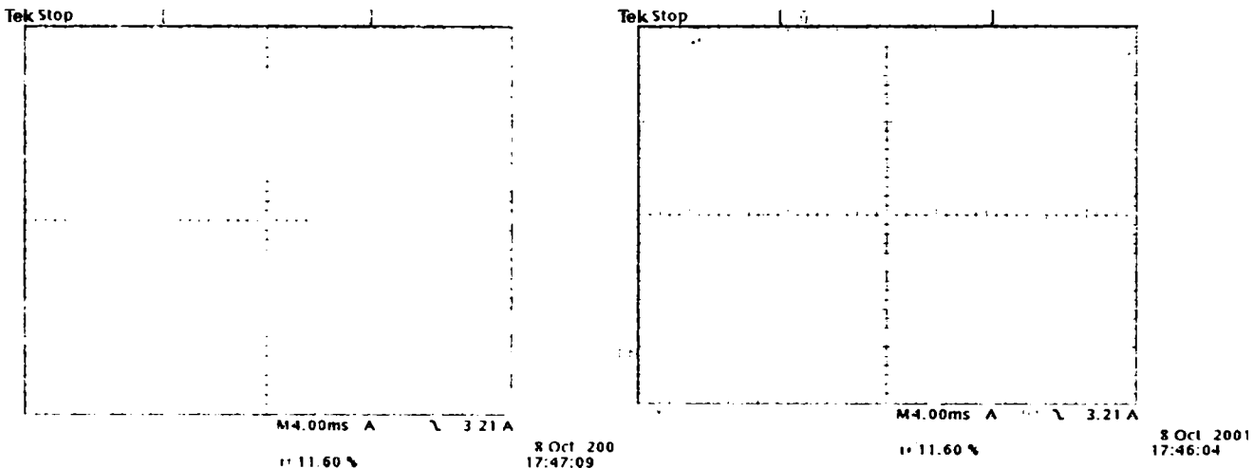

Figure 6.15. The measured current (left side) and the offset (right side) for the d-aligned position

The current that will cross the windings is set to 3.30 A, as indicated in the left side of figure 6.15. To assure a correct measure of the current through the d.c. decay tests, the offset that might affect the measurements – see the right image from figure 6.15 – is canceled by mathematical ways.

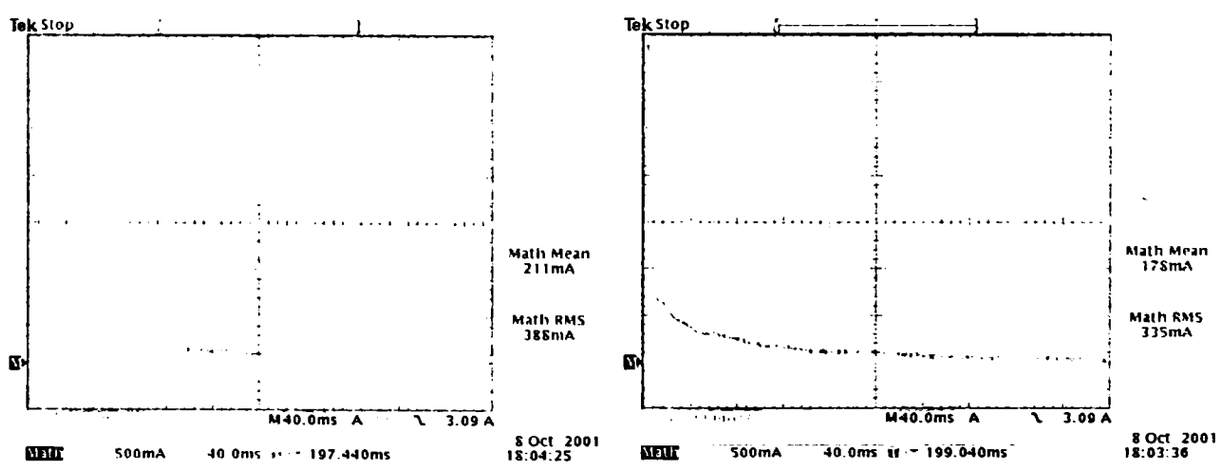

Figure 6.16. The measured current (yellow) and the calculated one (red) for different times of the tests

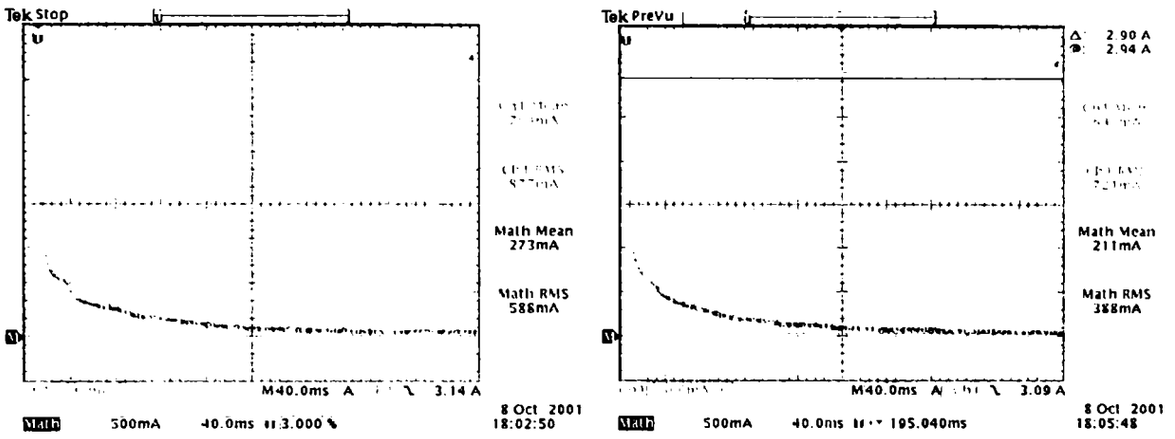

Figure 6.17. The final two d-aligned d.c. decay test with the measured current (yellow/light color) and the calculated one (red/dark color), the current initial value: 2.9A

Keeping the rotor of the machine along the d axis, we injected a d.c. current of ±1.3A in the field coils. Transient results for this situation are shown in what follows.

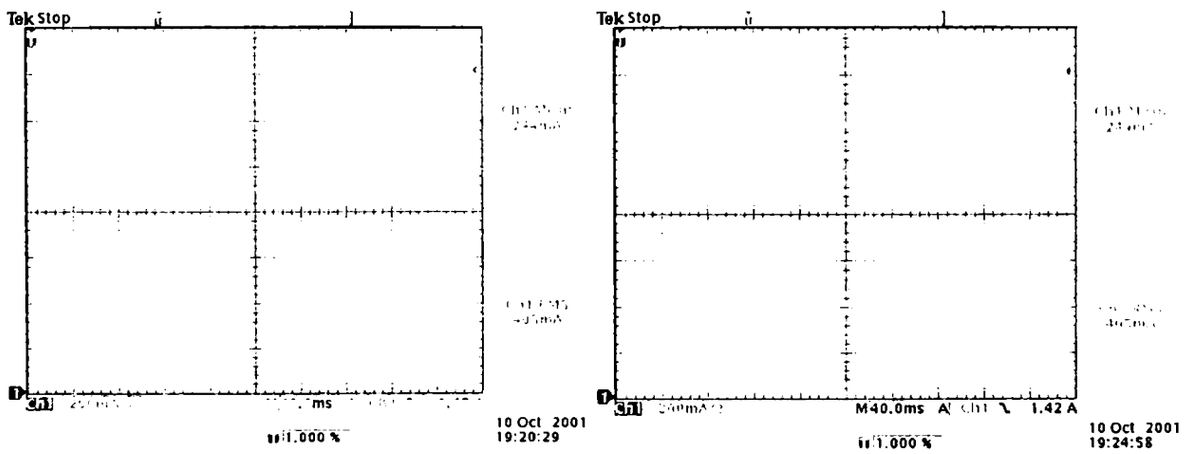

Figure 6.18. The d.c. decay test with the measured current, the field current has a value of 1.3A, the stator windings are opened

From these figures we can determine that the influence of the rotor cannot be determined when the stator is opened.

So, we closed the stator circuit and measured the transient current from d.c. decay test from the rotor

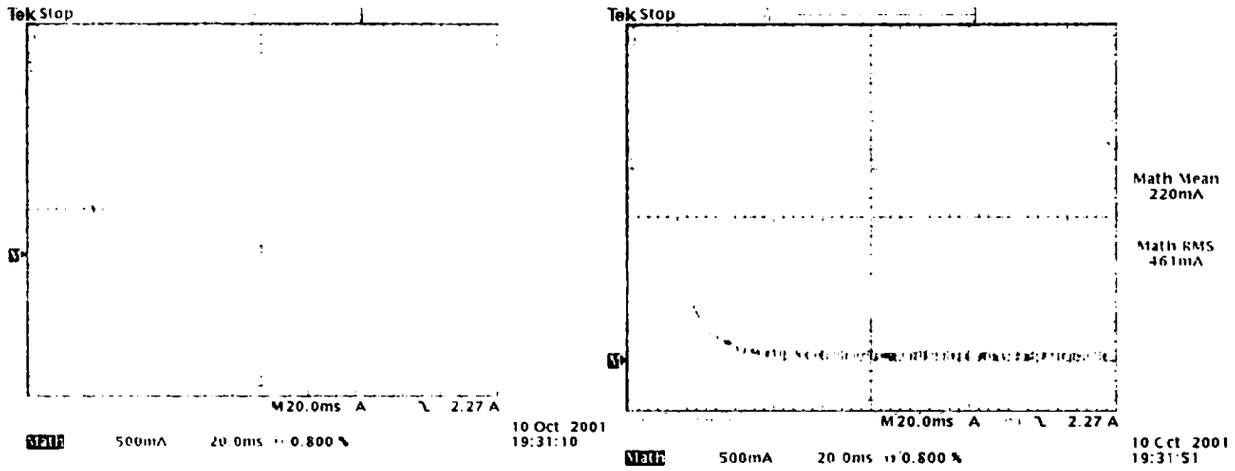

Figure 6.19. The d-aligned d.c. decay test with the measured current (yellow/light color) and the calculated one (red/dark color), the field current has a value of (-1.3)A

We can observe that making the d.c. decay test from the rotor point of view, so by introducing a current through the field windings while the stator windings are short-circuited, the current waveform are slightly different during the d.c. decay phenomena, without any relevance.

The d-axis inductance, obtained from the d.c. decay tests is $\mathbf{L_d = 4.1mH.}$

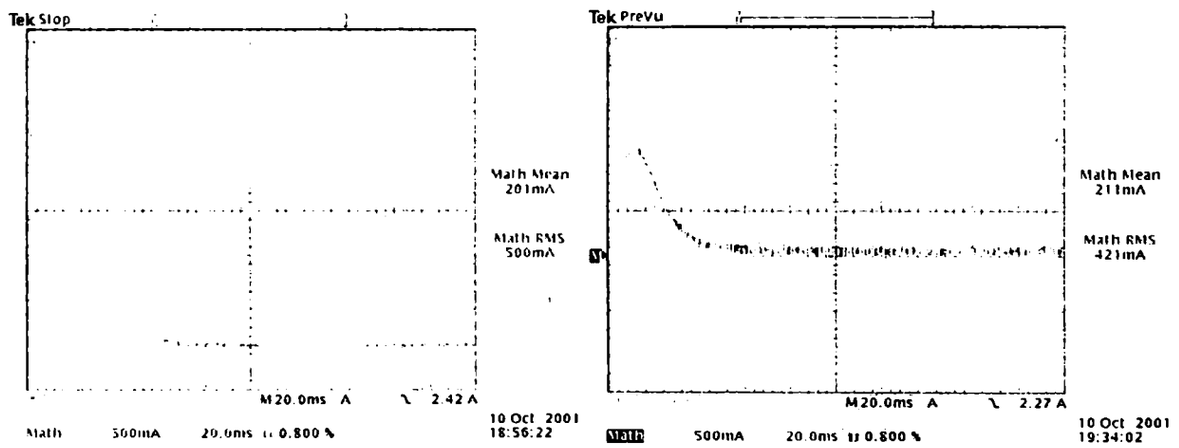

Figure 6.20. The d-aligned d.c. decay test with the measured current (yellow/light color) and the calculated one (red/dark color), the field current has a value of (+1.3)A

To find the direct axis inductance, the ".dat" files from the decay tests were read and by eliminating the noise and the offset, the value of the integral is calculated. The method

used for the calculations is the trapeze method, made with help of Matlab™ and presented in Appendix D.

6.3.1.5. Standstill d-axis and q-axis a.c. Tests

First, by keeping the machine on q axis, the stator is supply in a.c. (at 50Hz)and the field in d.c. - in two different ways: once having a polarity and then having the other one.

So, the stator and field current waveforms are monitored and where the field current reaches the minimum value, the terminals of the field winding are marked indicating the correct current polarity for the excitation current. During this test, the stator voltage is set to 75 V a.c. and the current to 3 A, the field voltage is 12 V d.c. and the current is 1.5A.

Studying carefully the BEGA topology, we observed that the field current i_q is important because it has to be opposite to the i_{PMq} induced current, produced by the permanent magnet placed in the rotor flux barriers.

For this, we can consider that if the i_q and i_{PMq} have the same direction, a small saturation effect appears. So, we have to make additional static tests to provide the right supply for the field winding. For the q-axis situation, the result from figure 6.24, are showing us the influence of the PM's along the q-axis.

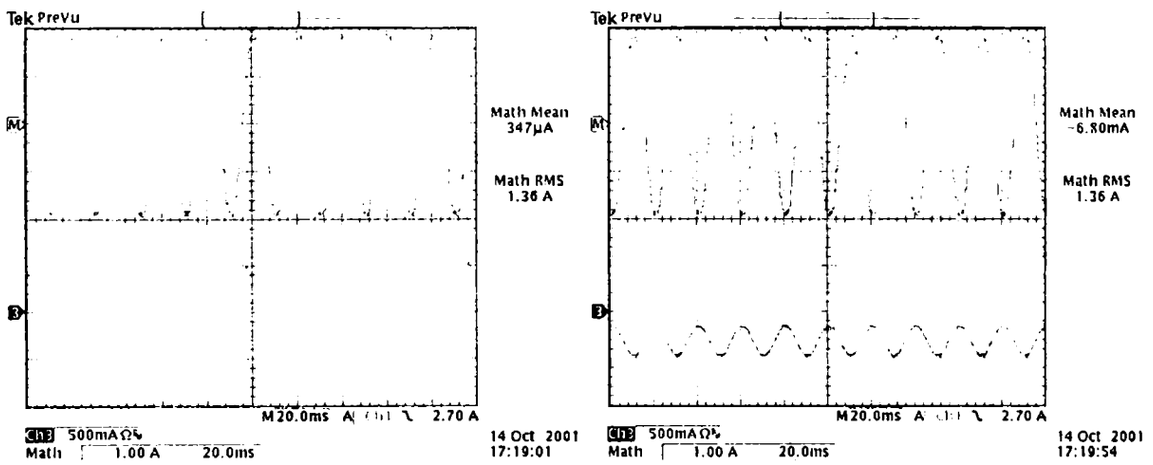

Figure 6.21. The q-aligned a.c. test with the i_q measured current waveform (M) and the field current waveform (3)

The occurrence of a.c. current in the field winding for q axis stator a.c. current, at standstill, with d.c. field current present, is due, most probably, to cross coupling saturation effect.

As expected, the field current differs from one case to the other one, the waveform (3) acquired using a performing digital oscilloscope, pointed out the influence of the PM's along q-axis.

Taking into account the supposition that if both i_q and i_{PMq} are having the same direction, a saturation effect will appear, for the same voltage, V_{-q}, on the stator, we measure the current, i_{-q}. As the a.c. inductance is bigger when $L_q i_q < 0$, $\lambda_{PMq} > 0$ it follows that i_{-q} will be smaller for the case of correct field coil supplying.

The results for the d-axis situation are detailed in the following figure.

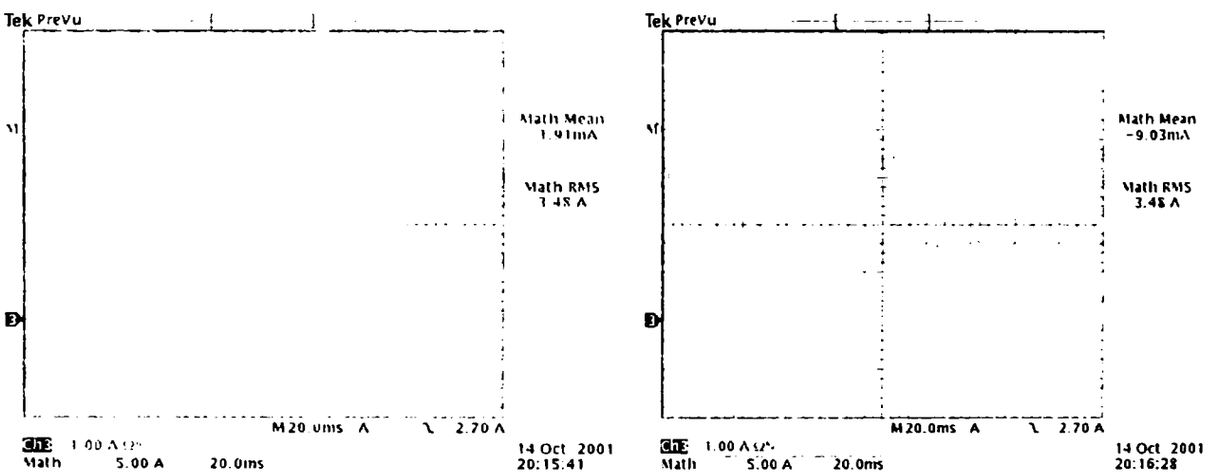

Figure 6.22. The results for the d-axis a.c. test, the stator (M) and the field current (3) waveforms

It can be seen that for the d-axis situation, the difference between the field current waveforms for both cases, doesn't exist, that means that the rotor is well locked in the d-axis, there is no influence from the PM's in this axis.

Having already the sign of the field voltage from the previous test, let us find the correct rotation direction of the rotor, to provide the predicted results.

For this we supply the field coil with a small d.c. current, normally we don't have to supply it for this test but for a better result, considering that the PM's are not high density PM's,

we will supply it, but as mentioned, with small current. In the same time, the stator phases are supplied in order to respect the phase notations, so the machine operates now as motor.

The motor will start moving in one specific direction, this means that in generator operating mode it has to be drive in the opposite rotational direction.

Next, using a power supply source as shown in figure 6.26, the prototype has been tested in the way of monitoring the field voltage while the d-axis/q-axis voltage is kept at constant value. These tests are done as a back-up for the d and q axes inductances and resistances calculation, made as presented in 6.3.1.3. adding supplementary results regarding the parameters and characteristics of BEGA. The supply voltage in the stator is about 0.6x(machine's rated voltage).

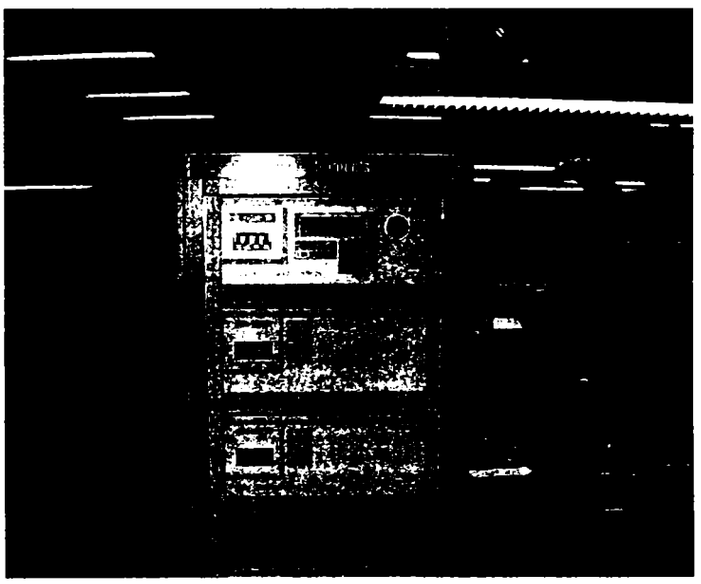

Figure 6.23. Details from the setup used for standstill a.c. tests using the California Instruments a.c. power source of 5kVA

Keeping the field winding opened or short-circuited, the voltage THD or the current THD were measured with the help of a power analyzer. The frequency range, during these tests, is from 20Hz to 500Hz (maximum available from the power source).

The results for the measurements using the California Instruments a.c. power source are presented in appendix F.

Having those static tests made, we can go to the next step, the dynamic tests.

6.3.2. Dynamic Tests

The setup for the running tests is presented in next figure, where the BEGA generator and the driving motor are shown.

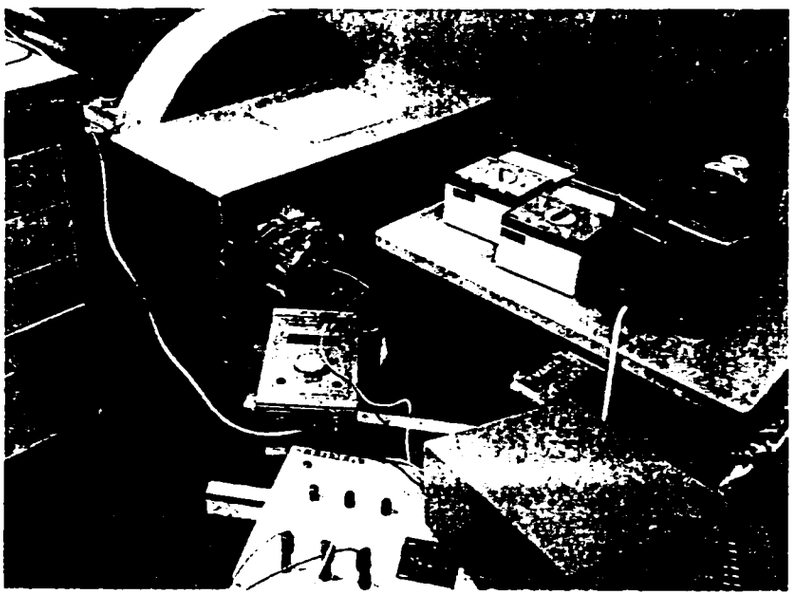

Figure 6.24. Details from the running tests for the final prototype of BEGA

The generator was tested in order regarding its behavior and to find the:

- Current
- Voltage
- Output power
- Efficiency
- Temperature rise

The dynamic tests were made running the generator from 1000 to 9000 rpm.

To run the generator, the setup from the Aalborg University laboratory included two rigid 1 to 2 transmissions by teeth belts were used, drive by an ASEA 7.5 kW induction motor, with 2 poles and the main data as follows:

MOTOR TYPE	MBT 132 SB, IEC 34-1, 3~50HZ SQUIRREL CAGE ASYNCHRONOUS MOTOR
Protection degree	IP 54
Rated power	7.5 kW
Rated speed	2890 rpm
Star connection	660 V / 8.4 A
Delta connection	380 V / 14.6 A
Insulation class	F
cos φ	0.91
Weight	42 kg
Cat. Number	ML1422003 - AB

The induction motor was driven by a VLT 5000 series, Danfoss frequency converter, with the following main data:

CONVERTER TYPE	VLT 5006
IN	3~380-500 V, 50/60 Hz, 9.1 A / 8.3 A
OUT	3x0 - U_N – 0 - 1000 Hz, 10.0 A / 8.2 A, 7.6 kVA
Protection degree	IP20
Ambient operating temperature	Max 45^0C / 113^0F

The stand contains also:

- a three phase diode rectifier with Semikron diodes, type SK
- 3 car batteries, Bosch Silver type (12 V d.c., 55Ah, 420A).
- different devices and apparatus were used for protection against short-circuit and overloads.

6.3.2.1 Setup and No-Load Tests

For the no load test, the setup was as shown in next figure, the frequency converter and the d.c. supply sources are pointed out.

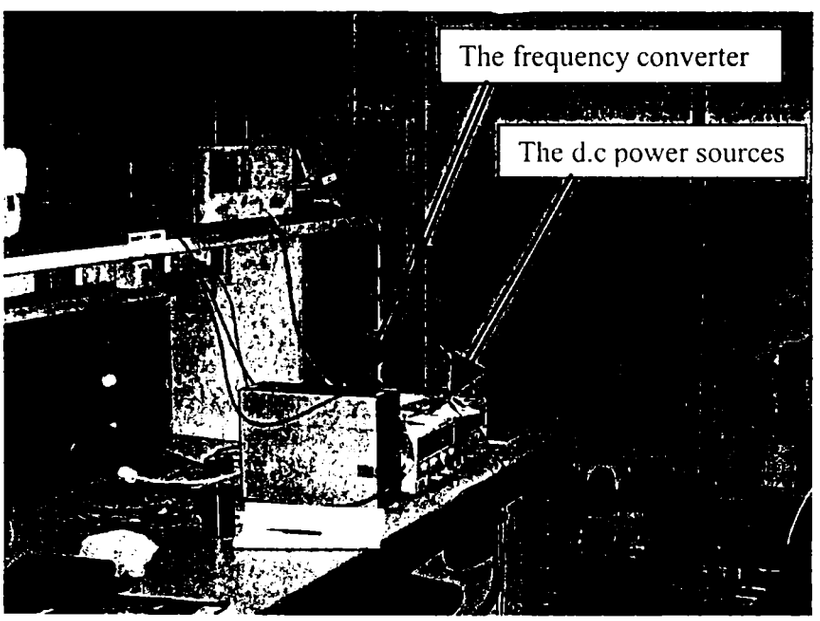

Figure 6.25. Details from the setup used for running tests

6.3.2.1.1. Determination of THF

From the no load tests we can evaluate the THF (telephonic harmonic factor) and so the output voltage distortion. The THF factor is important because all electrical consumers like on-board electronic diagnosis systems, board computer and air conditioning electric and

electronic circuits, are placed near the generator, so, both the harmonic amplitudes and order are important.

We can determine this factor using the formula:

$$THF=\frac{100}{V}\sqrt{V_1^2\lambda_1^2+V_2^2\lambda_2^2+...+V_n^2\lambda_n^2} \tag{6.5}$$

where: V – the measured output voltage of the generator;

V_n – the value of the n - order harmonic;

λ_n – the share factor for the frequency corresponding to the n - order harmonic.

The experimental setup used for the no load test is presented in figure 6.26.

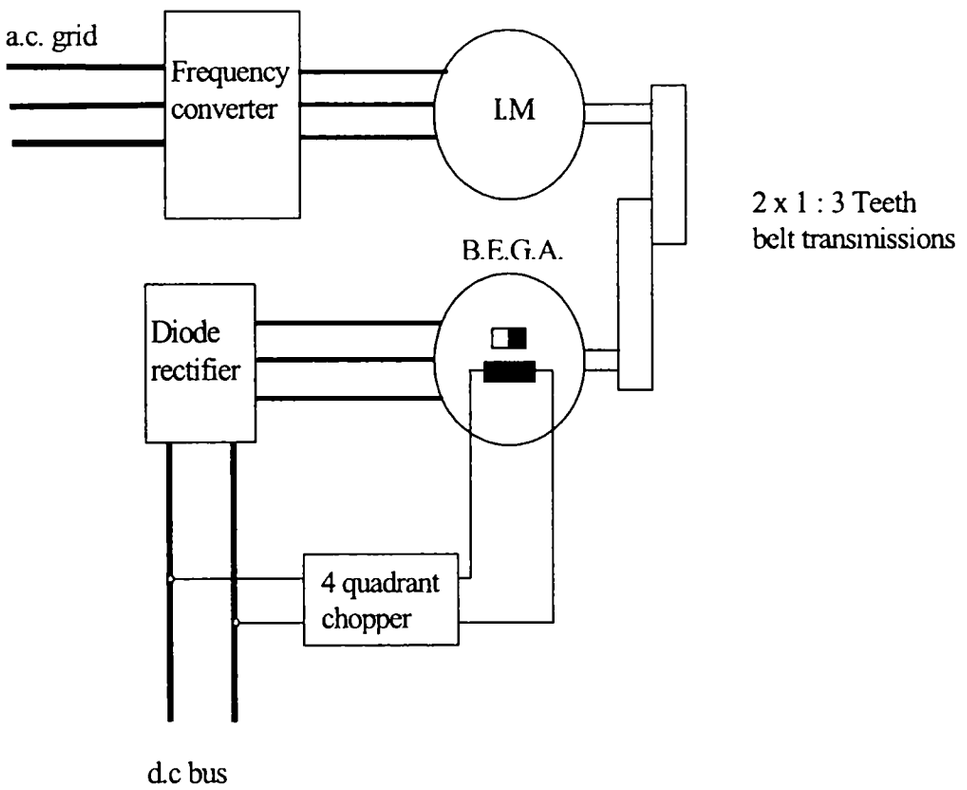

Figure 6.26. The scheme of the setup used for dynamic tests

6.3.2.1.2 No-Load Test With and Without Excitation Current

The e.m.f. voltage wave forms are indicated in the next figures

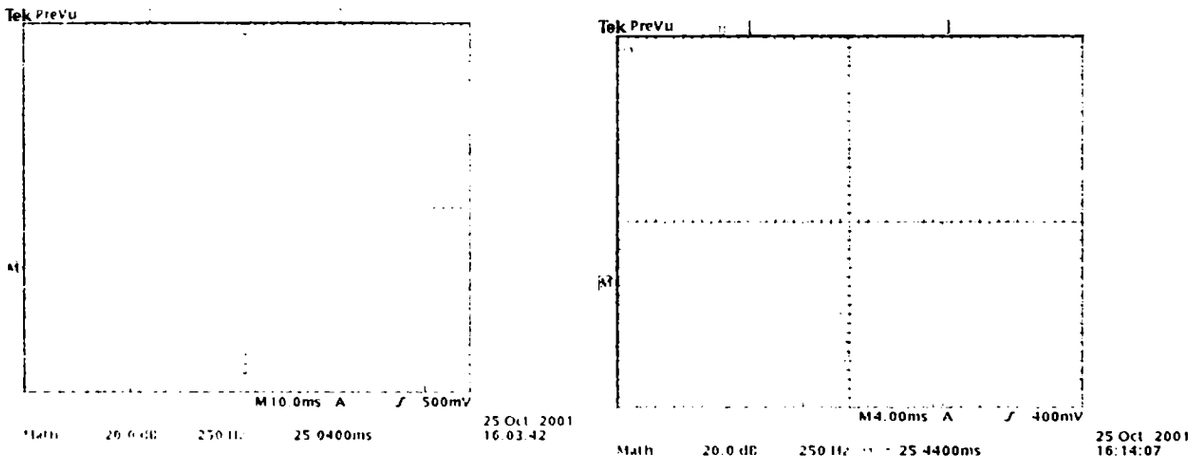

Figure 6.27. The e.m.f. and the FFT for 1000rpm and 4000rpm wit zero excitation current

The output voltage waveform is recorded and with help of a power analyzer and using the FFT (Fast Fourier Transformed) for the voltage waveform, the content of harmonics and the values were determined.

The value obtained for *THF* was *THF* = 5.3%.

In parallel with the power analyzer, an oscilloscope was used to visualize the output voltage waveform and the FFT of the back e.m.f.

To complete the no-load tests, the output voltage was measured for the entire range of the field current (-3A to +3A). The results are presented in figure 6.28.

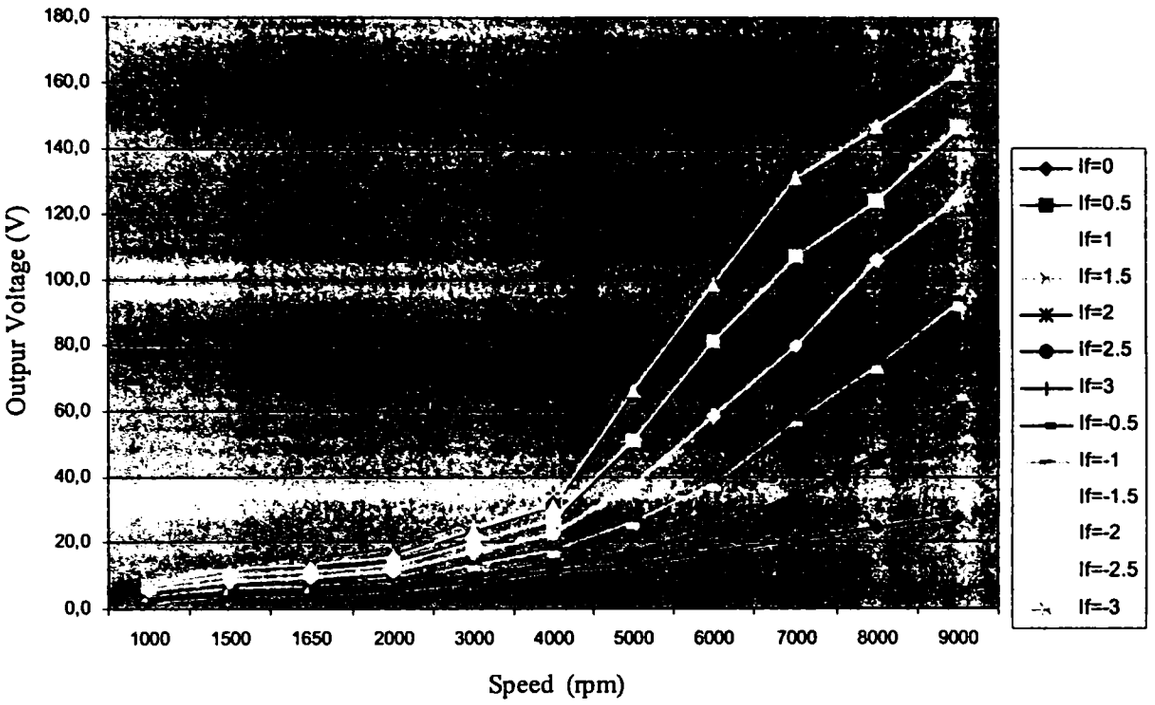

Figure 6.28. The e.m.f. vs. speed for different field currents

From the above figure we can draw the conclusion that for field currents having the same absolute value but different signs, the e.m.f. are approximately the same, so, the influence of the sign of the field current did not affect much the output of the generator, more details regarding this influence will be presented further in this chapter.

Anyway, comparing these results with the results for the first prototype, slightly differences may be observed. The BEGA prototype was tested with and without excitation on both rotational directions.

6.3.3 Setup and The Load Tests

For the load tests were used three automobile batteries and a load resistor to simulate different loads coming from the d.c. bus. These tests were done in the electric machines laboratory from University "Politehnica" of Timisoara, using the same structure of the setup. The difference consists in the use only of a 1:2 rigid belt transmission instead of two 1:3 and the driving frequency converter which now is a Hitachi J300 series.

6.3.3.1 Load Tests With Load Resistor (With and Without Excitation)

For the beginning, the load tests were done on a resistor load of 0,7 Ω. To measure the load voltage and current a Tektronics, TDS 224 type, oscilloscope was used.

The results will be presented in what follows:

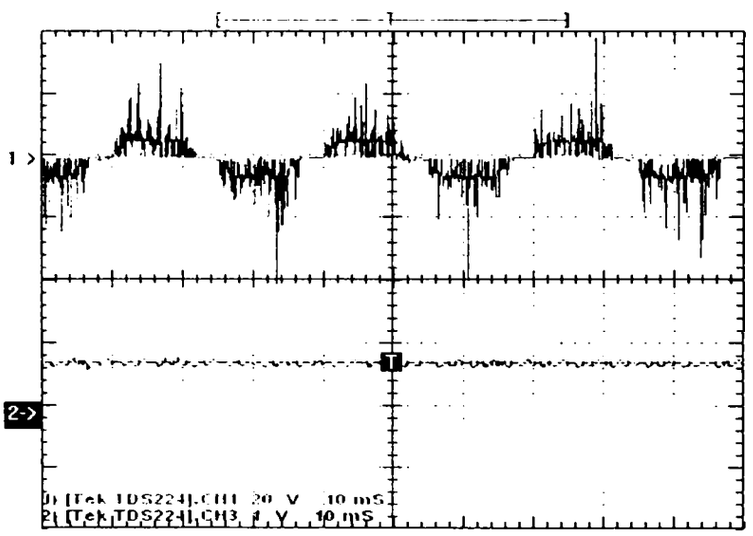

Figure 6.29. The load current (2) and line voltage (1) for 1000 rpm, no excitation current

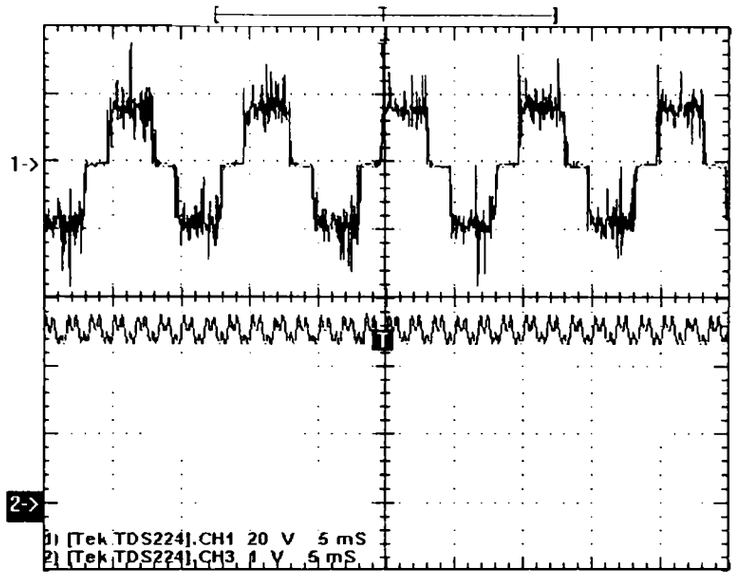

Figure 6.30. The load current (2) and line voltage (1) for 3000 rpm, no excitation current

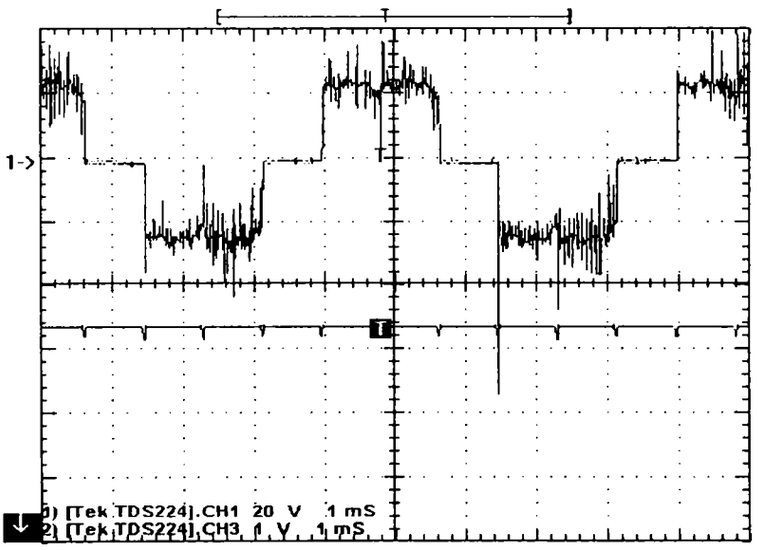

Figure 6.31. The load current (2) and line voltage (1) for 6000 rpm, no excitation current

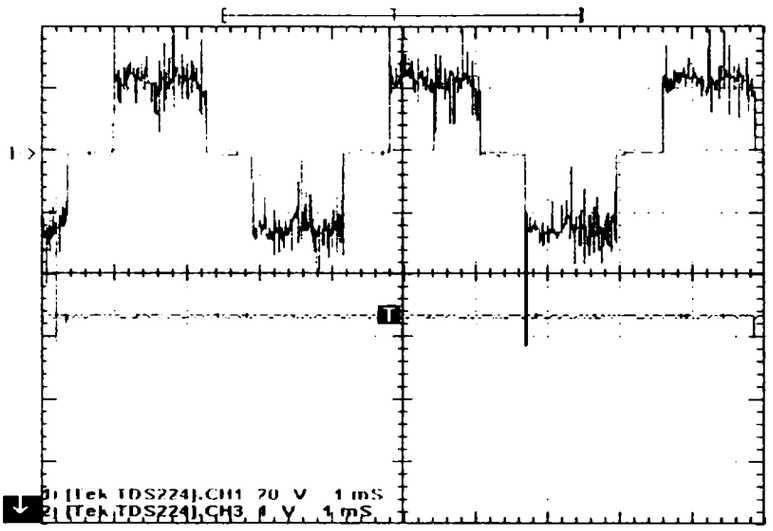

Figure 6.32. The load current (2) and line voltage (1) for 8000 rpm, no excitation current

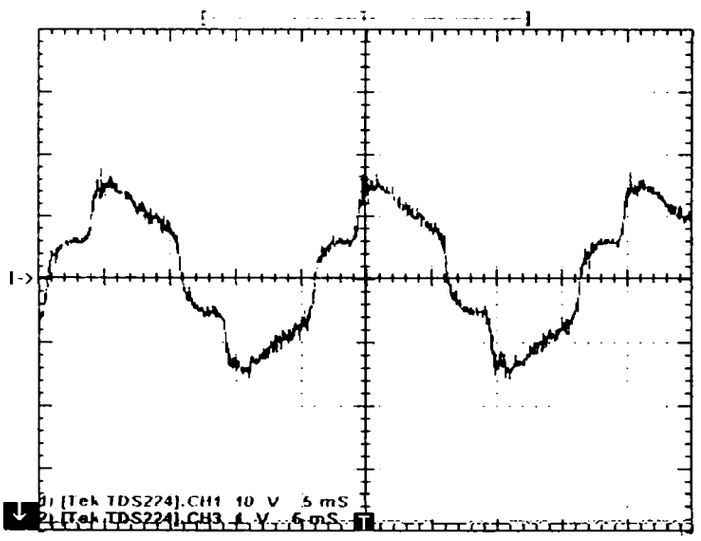

Figure 6.33. The load current (2) and line voltage (1) for 1500 rpm, 1,5A the field current

To complete this test, the results will be presented for the entire range of the driving speed and field current (see figure 6.37)

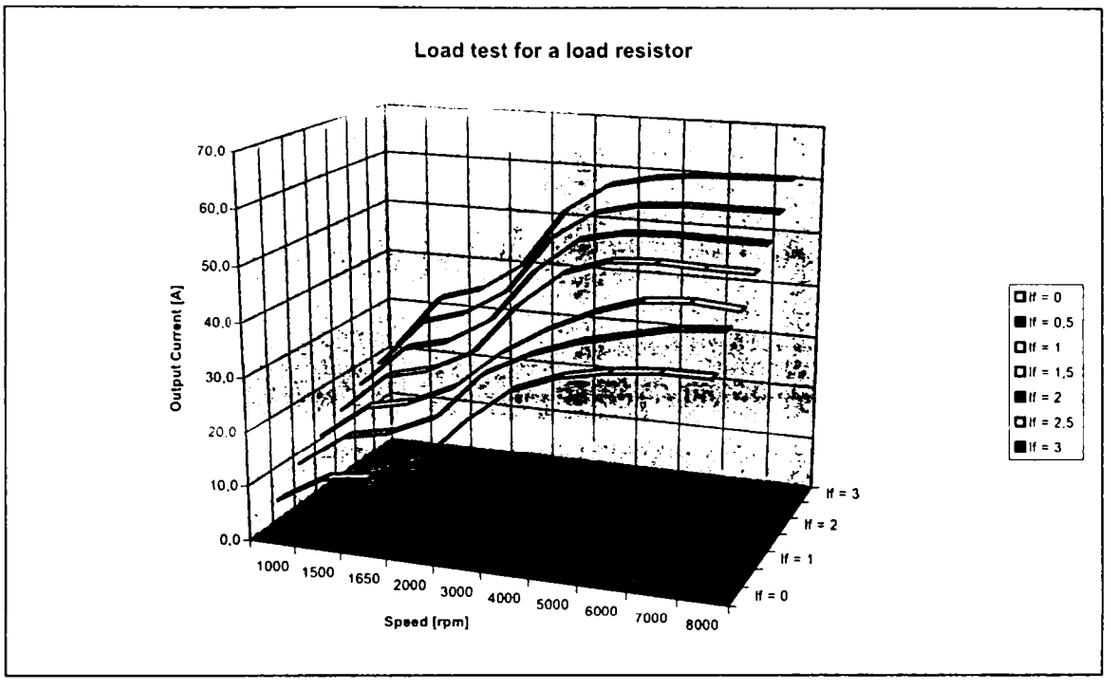

Figure 6.34. The load current vs. speed for different values of the field current, for rectifier plus resistive load (0.7Ω)

Other important characteristic of the prototype is shown in figure 6.38, where the load voltage vs. load current dependence, for different field currents, is presented.

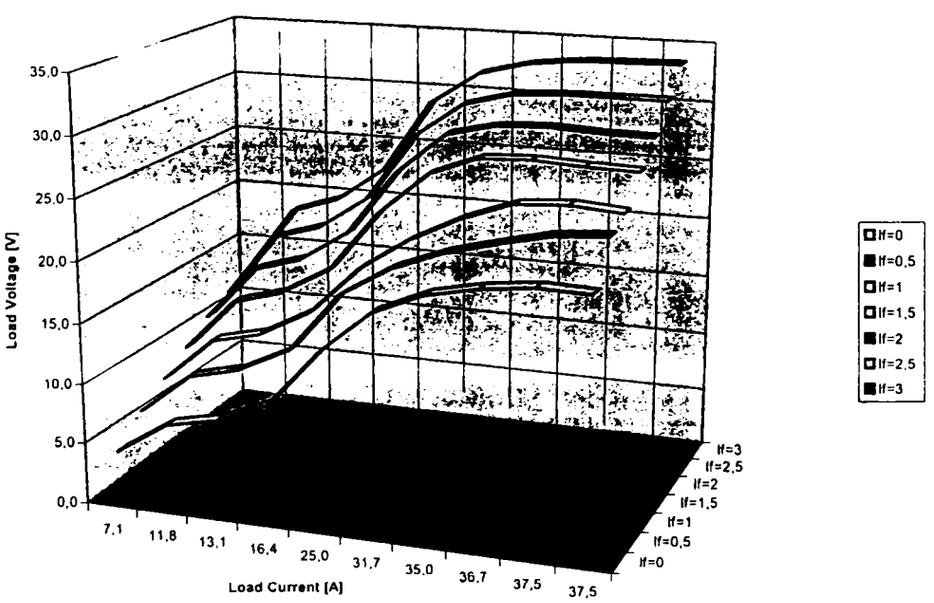

Figure 6.35. The load voltage vs. load current, for different values of the field current

A very interesting result is obtained when the load resistance changes its value; the table with the results is included in appendix F.

6.3.3.2 Load Test With 3 Batteries (With and Without Excitation)

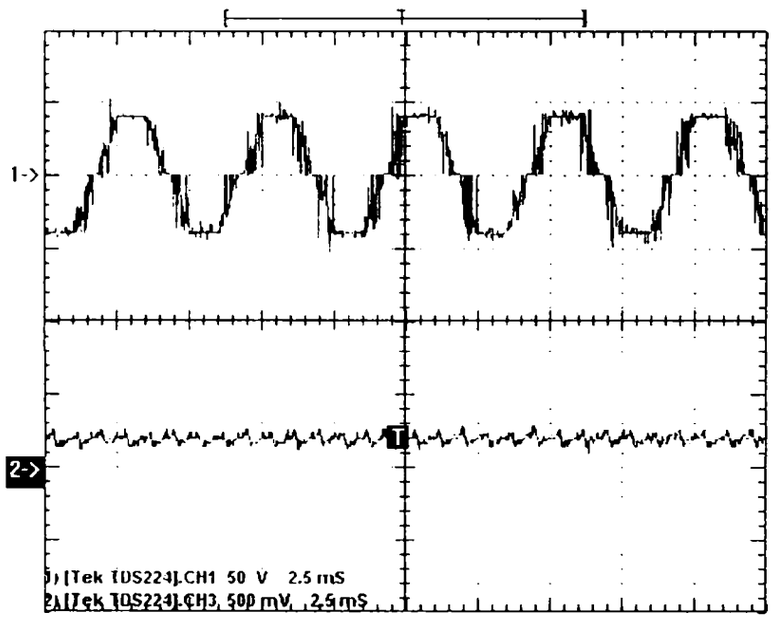

Figure 6.36. The load current (2) and line voltage (1) for 6000 rpm, no field current

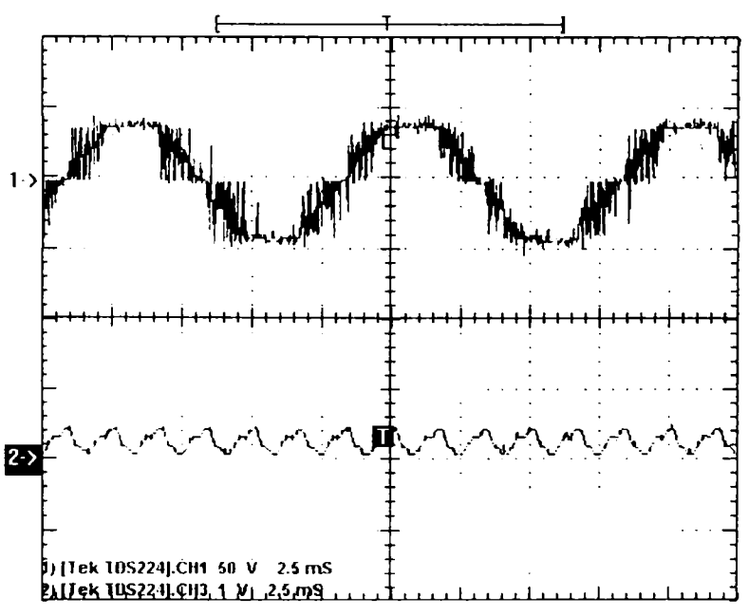

Figure 6.37. The load current (2) and line voltage (1) for 3000 rpm, 1,5A the field current

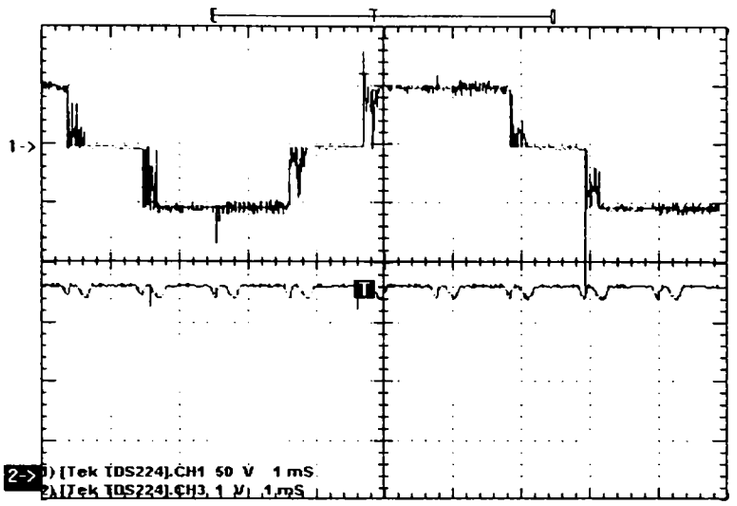

Figure 6.38. The load current (2) and line voltage (1) for 39 rpm, 2A the field current

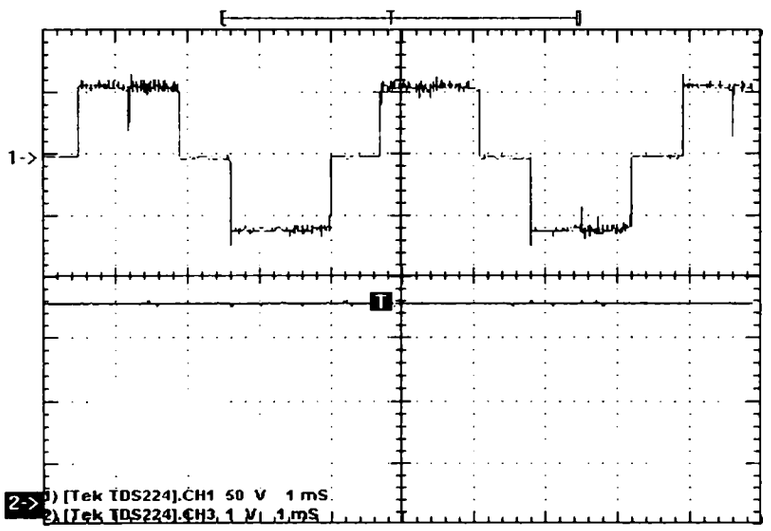

Figure 6.39. The load current (2) and line voltage (1) for 7000 rpm, 2,5A the field current

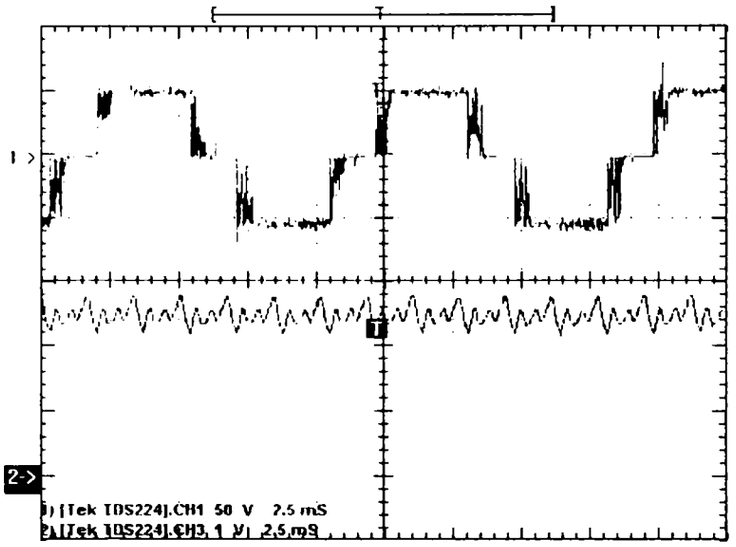

Figure 6.40. The load current (2) and line voltage (1) for 3000 rpm, 3A the field current

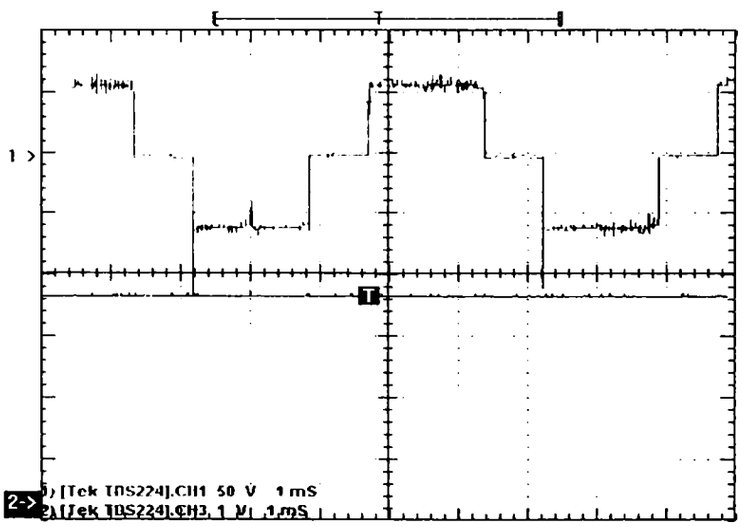

Figure 6.41. The load current (2) and line voltage (1) for 6000 rpm, 3A the field current

The complete characteristic for this case is presented in next figures.

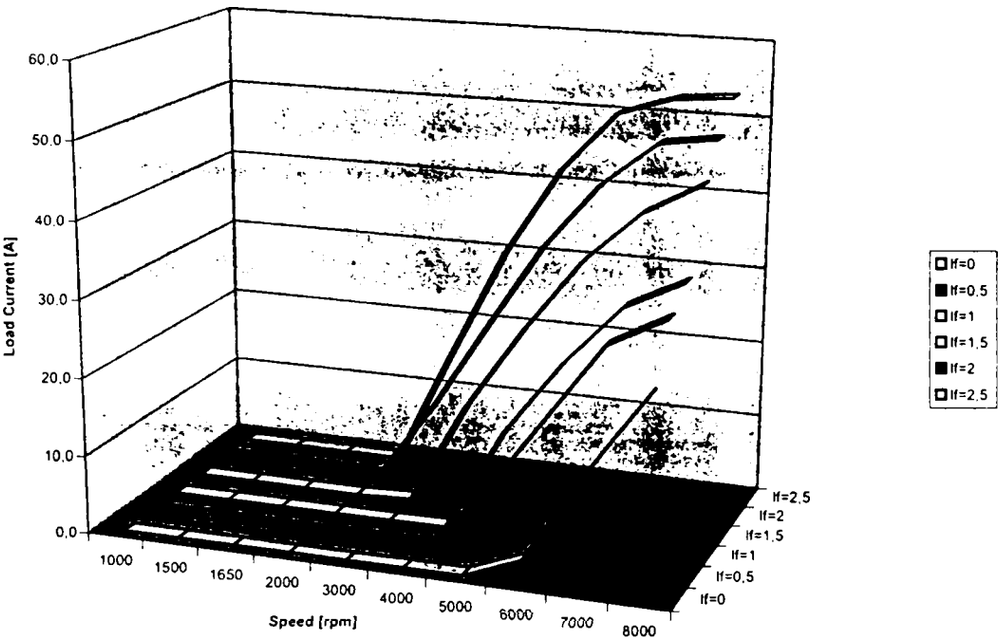

Figure 6.42. The load current vs. speed for different field current values

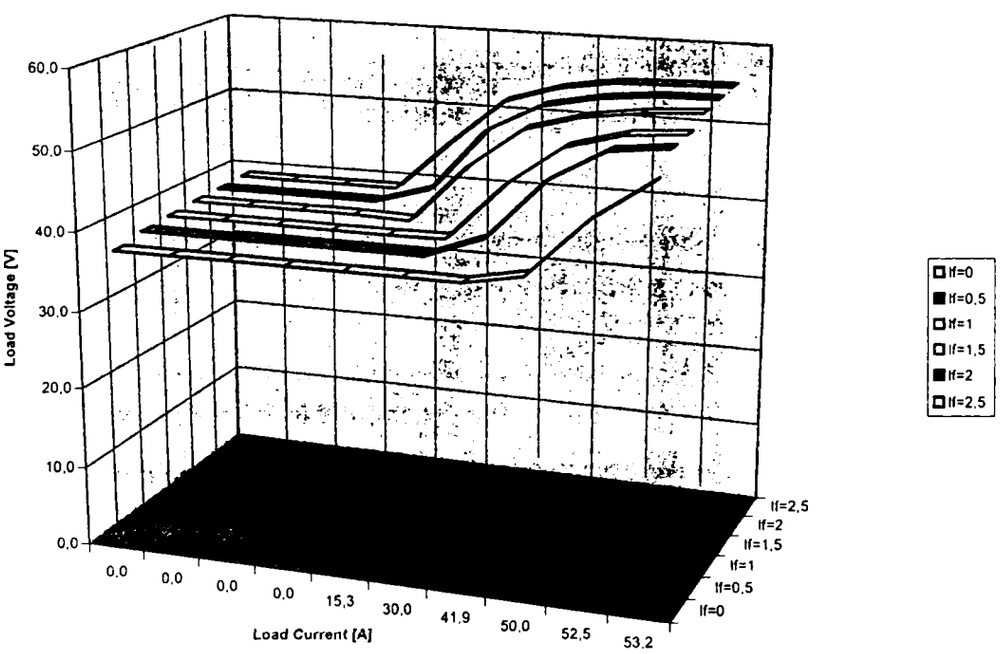

Figure 6.43. The load (battery) voltage vs. load current for different field current values

Of course, the load voltage has a minimum value of about 40 V, because of the batteries.

6.3.3.3 The Load Test Having 3 Batteries and a Load Resistor (With and Without Excitation)

The load test in this case is done to see the generator behavior when a sudden supplementary load appears. The load resistor has a value of 0.7Ω.

As shown in next figure, when the load resistor is connected to the power generating system, the generator field current.

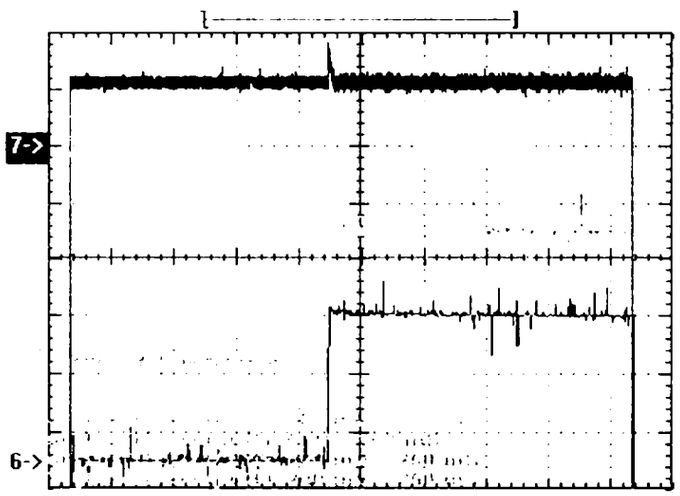

Figure 6.44. The load current (4) load voltage (5) and the current through the load resistor (6) for 6000 rpm generator speed, 2A - the field current (7)

A small reaction from the excitation side of the generator can be observed, when the load resistor is connected, but the spike has not a large value and the duration it is very small.

6.3.4. Generating System Tests

In this parts, some significant results that can help us to see the prototype behaviour in a real 42 V d.c. generating system will be presented. The system structure is the same as indicated in figure 6.45.

For the beginning, we have monitored the load current and voltage to see the influence of the three batteries on generator output when those are connected or disconnected from the system.

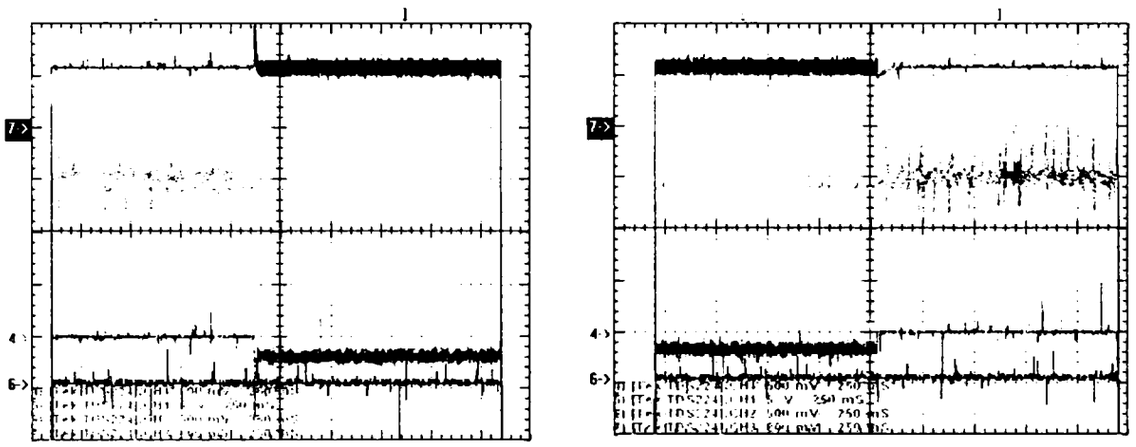

Figure 6.45. Starting the charging process of the three batteries at 3000 rpm, excitation current 2,5A (left image) and sudden disconnection of the batteries (right image): batteries load current (4 - green) and voltage (5 - turquoise), field current (7 - red)

As can bee seen, the voltage (in turquoise color) is strongly filtered because of the batteries impedance.

Not the same situation is for the field current (in red color) and for the load (batteries) current (in green color). As will be presented further, as we expected, the speed has an influence too on currents waveforms. A spike on the field current waveform may be observed, so the generator reaction exists.

The blue color waveform is the current through the load resistor, in parallel with the batteries that is not connected for the moment.

Further, keeping the same speed and field current for the generator, we introduced a load resistance of 0,7Ω in the main circuit.

The results are shown in next figure.

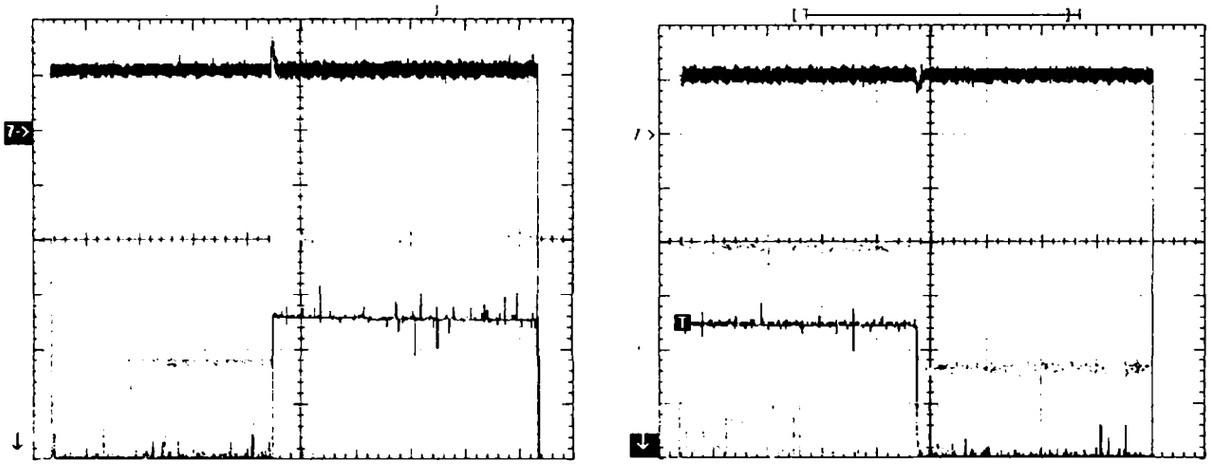

Figure 6.46. Introducing the load resistance (of 0,7Ω) during the charging process of the three batteries, at 3000 rpm, excitation current 2,5A (left image) and sudden disconnection of the resistance (right image): batteries load current (4 - green) and voltage (5 - turquoise), field current (7 - red), resistance current(6 - blue)

A small drop on the batteries voltage can be seen following the turquoise waveform (5), during the transient process.

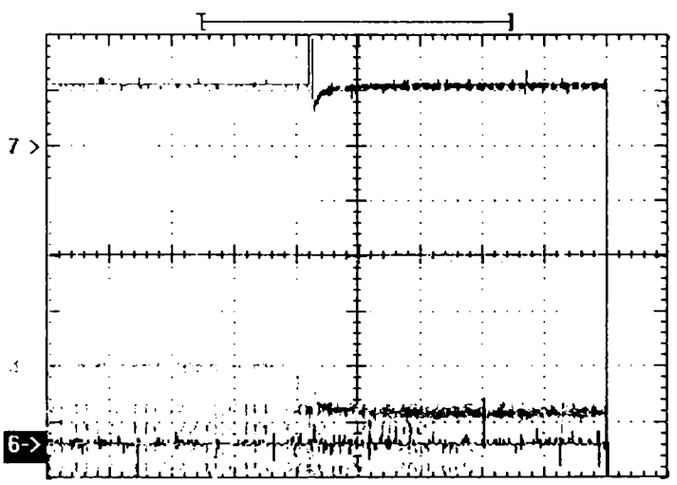

Figure 6.47. Charging start of the three batteries at 6000 rpm, excitation current 2,5A: batteries load current (4 - green) and voltage (5 - purple), field current (7 - red)

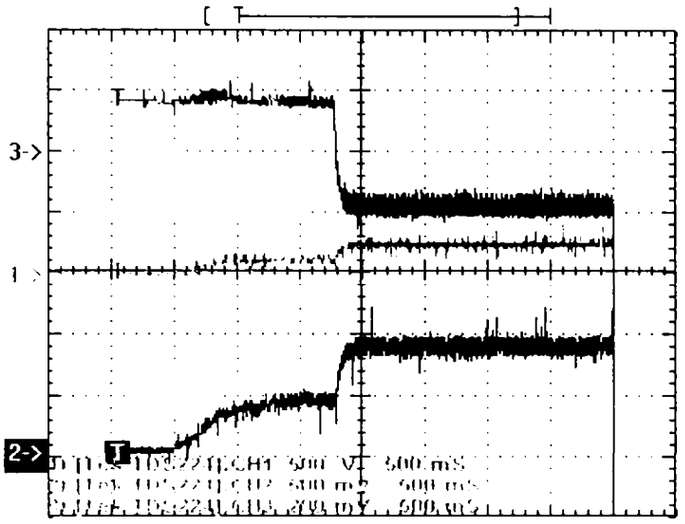

Figure 6.48. Charging of the three batteries at 3000 rpm, excitation current 1,7A and sudden change of the field current sign: batteries load current (2 - blue) and voltage (1 - green), field current (3 - red)

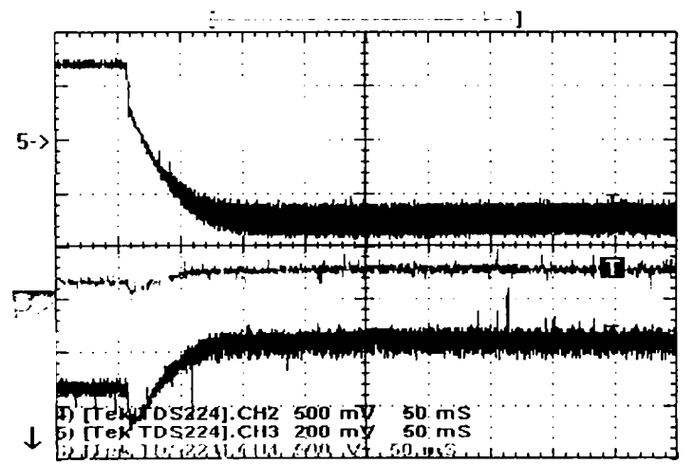

Figure 6.49. Charging of the three batteries at 3000 rpm, excitation current 3A and sudden change of the field current sign: batteries load current (4 - blue) and voltage (6 – green), field current (5 - red)

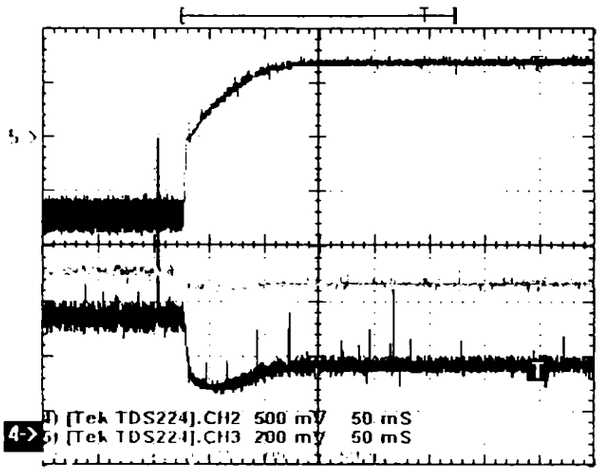

Figure 6.50. Charging of the three batteries at 3000 rpm, excitation current -3A and sudden change of the field current sign: batteries load current (4 - blue) and voltage (6 – cyan), field current (5 - red)

6.3.5. Temperature Measurements

The prototype was designed with a temperature sensor to measure the temperature in the stator coil. During all tests, the temperature was measured to provide that all tests were made respecting the temperature condition in other words to assure a correct behavior of the generator without any influence from the temperature rising.

The generator inner temperature was not larger than 40^0C in term of a long duty cycle, the maximum values were obtained during the load tests, with load resistor beside the three batteries.

6.4. Final FEM Improvements

As the results of the tests shown, the prototype of the BEGA generator need to be improved, especially from the voltage and current harmonics points of view.

In this way, but taking into consideration the costs of the materials, a simple change on the generator structure may improve both: the harmonics and the total costs of the generator.

So, inserting the PM's only on the base of the flux barriers, the weight of the machine and the total costs are drastically reduced, more, the influence of this new arrangement will be on the generator behavior.

Figure 6.51 shows the electromagnetic field on the BEGA, through 2D-FEA.

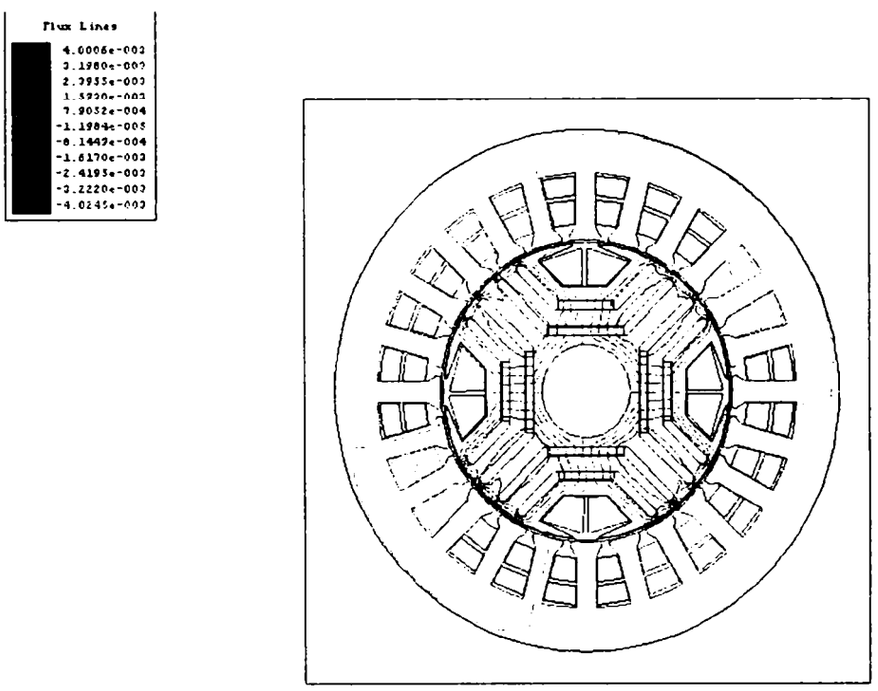

Figure 6.51. The electromagnetic field for the new configuration of the BEGA

To see the changes that are expected from this new configuration more 2D-FEA were done, the results are shown in what follows.

For the beginning, the d-axis main measures are calculated, the magnetic flux, flux density and the electromagnetic torque. The peak value of the flux density is about 1 T, for the rated current in the stator windings (same used in the analysis from chapter 4).

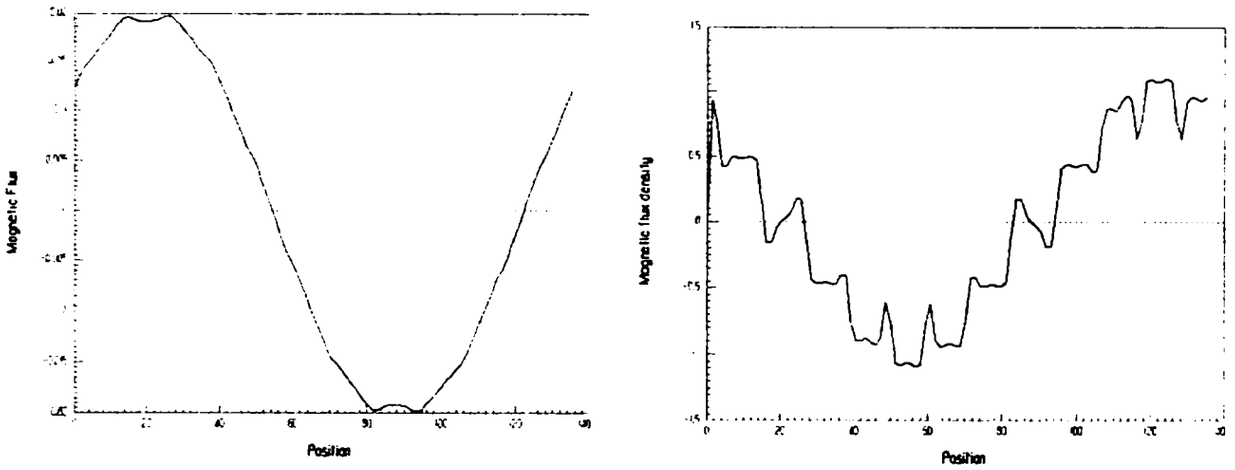

Figure 6.52. The magnetic flux (left) and flux density (right) waveforms for the new configuration of the BEGA on d-axis

The calculated electromagnetic torque has a value of: 6.631 Nm, represents the PM/I_d interaction torque (I_q=0). Now, for the q-axis, the main measures are calculated for having the corresponding stator current through the windings (figure 6.53).

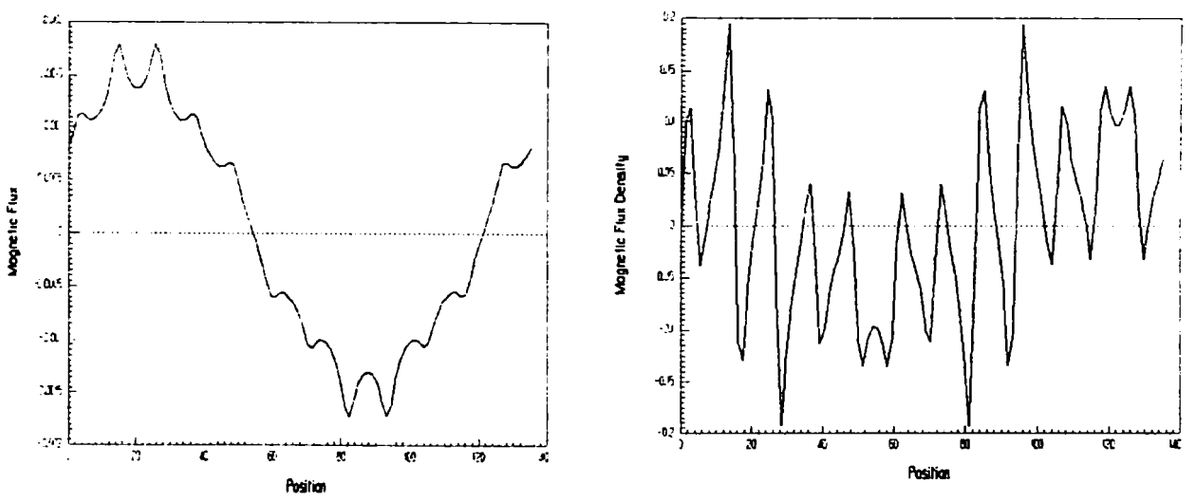

Figure 6.53. The q-axis magnetic flux (left) and flux density (right) waveforms for I_q>0 and I_d=0

It is clear that the changes mentioned above are improving the BEGA behavior, as we expected but, of course, some other changes can be done, in order to improve the BEGA behavior, like smoothing the flux barriers and the rotor poles - to reduce the total harmonics and so, the THF, those changes can be considered as a subject for further study in this way.

6.5. Conclusion

As was predicted by analytical design equations, the direct axis synchronous inductance has a larger value than the quadrature axis synchronous inductance. The difference between the direct axis synchronous inductance and the quadrature axis synchronous inductance it is not very big and this because the machine rotor saliency is not very high and of the influence of permanent magnets, upper lamination bridges.

In both, design and optimization using the finite element analysis procedures, the content of harmonics for the output voltage has been carefully treated.

The d.c transient tests gives us information regarding the transient inductance on both direct and quadrature axis.

From no-load tests, the calculated *THF* has a large value but the influence is reduced because this type of electrical generator is designed to work on automobiles so on isolated equipments, where the influence of high order harmonics is small.

Anyway, considering the presence of many electronic devices on automobile board, the generator geometry has to be optimized using the finite element method, in order to reduce the slots influence.

It should be noted that :

- Full power range controll is available up to 6000 rpm and higher, but at 9000 rpm even with negative field current (figure 7) not less than 54% rated power can be delivered.
- The excitation current should be controlled for positive and negative values through a 4 quadrant chopper.
- The values of i_q remain positive but i_d could be either positive or negative depending on speed and load.
- Half rated power is delivered at 1500 rpm but full power is already available from 1650rpm.

References

[6.1] I.G. Kassakian, H.C. Wolf, I.H.Miller, C.H.I. Hurton - *"Automotive electrical system circa 2005"* - IEEE Spectrum, August 1996, p. 22-27.

[6.2] M. Naidu, M. Boules, R. Henry - *"A high efficiency, high power generation system for automobiles"* - Proceedings of IEEE- IAS 1995 -Annual Meeting, pp. 709- 716;

[6.3] H.I.Gutt, I. Mueller - *"New aspects for analyzing and optimizing modern motorcar generators"* - Proceedings of IEEE-IAS 1994 - Annual Meeting, vol.1, pp. 3-8;

[6.4] C.D. Syverson et all - *"Hybrid alternator with voltage regulator"* - U.S. Patent 5502368, March 26, 1996;

[6.5] Mizuno, Takyuki, C/O Kabushiki, Kaisha Meidensha - *"Hybrid excitation type permanent magnet synchronous motor"* - European Patent Application 941056335, 12.04.1994;

[6.6] Mutter Albert - *"Elektrische maschine und deren anwendung zum fahrzeugbetrieb"* - Patentschrift DE 413943C2, 03.12.1991;

[6.7] T.M. Jahns - *"Uncontrolled generator operation of interior PM synchronnes machines following high speed inventer shut down"* - Proceedings of IEEE-IAS 1998 - Annual Meeting, vol.1;

[6.8] I.Boldea, S. Scridon, L. Tutelea: *"BEGA – a biaxial excitation generator for automobiles"* - Proceedings of the 7th International Conference OPTIM 2000, Brasov, May 10-11 2000, pp.345-352;

[6.9] V. Z. Groza, M. Biriescu – *"Measurement of Reactance of Synchronous Machine at Standstill"* – Record from IEEE, 1999;

[6.10] F. Caricchi, F. Crescimbini, F. Giulivi Capponi, L. Solero – *"Permanent-Magnet, Direct-Drive, Starter /Alternator Machine with Weakened Flux Linkage for*

Constant Power Operation Over Extremely Wide Speed Range" – Record from IEEE, 2001;

[6.11] W.L. Soong, N. Ertugrul, E.C. Lovelace, T.M. Jahns – *"Investigation of Interior Permanent Magnet Offset-Coupled Automotive Integrated Starter/Alternator"* – Record of IEEE, 2001;

[6.12] A. Kilthau, J.M. Pacas – *"Measurement of the Parameters of the Synchronous Reluctance Machine including Cross Saturation"* – Record of EPE 2001, Graz;

CHAPTER VII

CONTRIBUTION & CONCLUSION

7.1. Finite Element Method of Analysis

The finite element method is a numerical method of solving linear and non-linear partial differential equations. It offers an accurate and powerful design tool, allowing material properties, non-linearity and structural details to be taken into account.

Compared to the equivalent magnetic circuit analysis, FEM-analysis tends to be more time consuming but it can produce much more accurate and reliable results.

Any time a technical problem leads to a differential equation that cannot be solved through a finite form, we have to use one of the approximate methods (based on series development or numerical methods), by evaluation of the unknown integral in specified points inside the definition interval through simple mathematical methods.

The finite element method is a general numerical analysis technique which belongs to the direct methods and which assure an approximate solution for the field problem.

Because it can be easy model complicated geometries and non-linear magnetic materials, the finite element is a powerful tool for electromagnetic fields studies.

One finite element can be described as a closed region, with a family of functions depicted in its interval. This family is a linear combination of the prescribed values of the field in discrete points (source nodes) and inside the element.

The field form is presented by a finite number of triangles. Inside each triangle, the field is specified as a function of nodes values.

Generally, there are known three calculation methods for the field solution of the electric machine, through the finite element method, through the electromagnetic torque and through the enhanced force and these are:

- the Lorentz force method;

- the Maxwell method;

- the Coulomb method.

The experience demonstrates that obtaining with accuracy the force and the torque from filed solution through the finite element method may be difficult.

Choosing a certain method instead of another one, we might have different solutions in calculating the force and the torque. The influence is because of the finite element network, of the integration method and of the frontier conditions.

Theoretically, all three force and electromagnetic torque calculation methods should lead to the same correct result, this is why knowing all of them is essential.

The calculation method based on Lorentz force:

$$\vec{F} = i(\vec{l} \times \vec{B}) ; \tag{7.1}$$

this method can generate errors because of the inaccuracy in calculating the magnetic flux density (B) from the potential vector, and of machine geometry.

Avoiding the errors is possible through the increase of the finite elements, which will affect the duration of the calculation.

The Maxwell calculation method uses for the force determination, the following formula:

$$f_n = \frac{1}{2\mu_0}(B_n^2 - B_t^2) ; \tag{7.2}$$

so, the negative effect of the errors, cause by the magnetic flux density calculation, is doubling because it is squared multiplied, for both, the normal component (B_n) and the tangential component (B_t).

The doubling error effect is more effective for the areas where the flux density reaches high values. Choosing the integration way for the electromagnetic torque calculation, that has to be the optimal one, through the center of the neighboring finite elements and perpendicular to each frontier element.

The Coulomb method for torque and force calculation, the so called "the virtual work method", is based on energy considerations:

$$F=\frac{\partial W}{\partial p}; \tag{7.3}$$

so, it implies the energy / co-energy calculation from the field solution.

The easiest way to determine the differential is using the finite differences approximations. It seems that using two field solutions for calculating the force is the main drawback for this method

To solve this disadvantage, a virtual displacement of the object under study is proposed, by giving virtual displacement factors (v) for the finite elements network nodes, indicating the relative virtual displacement to each node from the network: all the nodes with interest having v=1, all nodes from the surrounding space having v – under-unit, the rest of the nodes having v=0.

The analysis using FEM are performed in this dissertation, using the commercial software package "Ansoft™ Maxwell 2D Field Simulator". This package can provide an easy-to-use solution for various problems including electromagnetic field calculation, electrostatic and magneto-static calculation.

Besides the FEM analysis calculation, the software package also includes a post processor which can perform such tasks as BH plotting and data manipulating. All results given by 2D FEM analysis is for unit length machine, so the conversion to the real stack length needs to be made.

The method basically involves the split of the machine cross section into smaller finite elements. The partial variation of magnetic potential throughout the machine is described by non-linear partial differential equation derived from Maxwell equation.

The finite element method (FEM) can be used to change the structure of the machine, the material properties and the excitation, in the rotor and/or the stator of machine. The solution of a continuum problem by FEM process always follows an orderly step-by-step process.

The first step is to divide the continuum or solution region into elements. A variety of elements shapes may be employed in the same solution region. The finite element model contains information about the device to be analyzed such as geometry (subdivided into finite elements), materials, excitations and constraints.

The material properties, excitations and constraints can often be expressed quickly and easily but geometry is usually difficult to describe. The finite elements can be very small where small geometric details exist, such as airgaps and can be much larger elsewhere.

Before the system equations are ready for solution, they must be modified to account for the boundary conditions of the problem. Each degree of freedom at a grid point may be unconstrained (unknown) or constrained.

The assembly process gives a set of simultaneous equations that we solve to obtain the unknown nodal values of the problem. If the problem describes steady or equilibrium behavior then we must solve a set of nonlinear algebraic equations. If the problem is unsteady, the nodal unknowns are a function of time and a set of linear or nonlinear ordinary differential equations must be solved.

The solution of the system equations can be used to calculate other important parameters. For example, in electromagnetic problems, the nodal unknowns are the components of magnetic flux density. From these components the inductance, the torque and other electromagnetic parameters can be calculated.

7.2. Summary

The thesis is structured in seven main chapters, each of them having a final part containing chapter's conclusion from where one is pure theoretical – of general conclusion – in which, the FEM is shortly introduced for the analysis of the electromagnetic field and parameters of the electric machined, together with some proposals regarding the possibility of continuing the research activity in this subject of variable speed electrical generators.

Chapter I – structured in three parts – includes a synthetically analysis from constructive, efficiency and costs points of view, for the most known types of electrical generators existing or proposed to be used for the automobile industry.

The first part introduces the new electrical generators types, already in use for the automobile industry, as the claw-pole generator and proposes a simple calculus method to determine the approximate costs for a generator, taking into account the geometrical size and the component materials. The second part contains the analysis by the finite element method for a part of the known electrical generators with the declared scope of pointing out some of them characteristics or parameters, comparing these new topologies with the advantages and drawbacks for both the electric machine but also for the required power electronics and their controls. Today, before using a machine in a operational system, researches and analysis, especially using the FEM, are expected and easy to implement. The third part, as for the next five chapters, is dedicated to discussions and conclusion.

Chapter II – transposes the switched reluctance machine in a simple variant, proposed to be applied as an electrical generator for the automobile industry, where it is already used for some hybrid car configurations.

Considering both, the advantages and the disadvantages of this type of electric machine, the demanding use of it on a larger scale, including for the existing hybrid automobiles on the market, made the decision of studying it in this thesis easier.

Chapter III – is entirely dedicated for the study of the new electric machine, recently presented and which confirms to be a solid candidate for electrical generators with direct appliance in the electrical energy generating systems from the automobiles board. Starting from the conceptual design of this electric machine, continuing with analysis using the FEM and finishing with digital simulations for the generating system, including the power

electronics and the control, the third chapter practically opens the going on mode of the next three chapters from this PhD. thesis, anticipating the steps that will be followed in this way.

Chapter IV – introduces in premiere, a new type of synchronous electric machine, with a bi-axial excitation (from both, the internal Permanent Magnets and the field windings), conceived and designed to successfully substitute the actual alternators. One analytically design model, together with many studies, made using the FEM, and an optimal design procedure – with direct results regarding the built of a real prototype of 3 kW, are the core for this new type of electrical generator.

Chapter V – shows extended digital simulations for the proposed generating – distribution system on 42 V d.c. bus, which has in it's structure a BEGA type of electrical generator.

Chapter VI – includes the results of a series of measurements and tests made to accomplish the efficiency in using the BEGA generator in automobile industry specific applications. There are presented both test results for the machine and for the entirely generating system for the proposed 42 V d.c bus.

Chapter VII – is a theoretical chapter, this presents, shortly, the using of the FEM for calculating of some electromagnetic parameters, with direct appliance in electric machine researches. It also includes the personal contributions of the author, beside some perspectives and proposals regarding future approaches that will continue the studies for this vast research field.

7.3. Personal Contributions

All chapters include personal and original materials of the author of the thesis. Some of these original materials are already published in specialized scientific papers and other have to appear.

The main author's contributions are:

© the use of the bi-dimensional analysis, through the FEM, for making simple but efficient comparisons, with direct effects, for different types of electric machines;

© the proposal of applying of new simple and easy to use formulas for cost estimations;

© showing a two-phase, with low costs, of a switching reluctance machine, starting from the induction machine with modified windings in the stator and new structure of the rotor;

© using the FEM analysis to draw some conclusion regarding the optimal geometry of the switched reluctance machine, which is proposed for study;

© designing, starting from simplified equations, of a switched reluctance machine that is proposed than to operate as a generator;

© introducing two new types of electrical generators with reduced costs, from which one in world premiere, the first one – the flux reversal generator – being presented only theoretically, and the second one – the bi-axial excitation generator – being presented by two real prototypes;

© using a series of base formulas, the permanent magnets electric machines characteristics, designing a virtual prototype for the flux reversal machine;

© proposing and simulating through specific digital simulation tools, two structures of generating systems that may be used in the automobile industry, a dual one – with two different voltages, 14 V d.c. bus and 42 V d.c. bus – and one for a 42 V d.c. bus;

© making simple analysis using the FEM to improve the cogging torque, typical for electric machines with permanent magnets;

© presenting the design of the bi-axial excitation generator for automobiles (BEGA) and proposing an optimization method for the designing process;

© making digital simulations for a generating system that includes the BEGA generator and showing of the simulation results;

© building of two prototypes and putting them under experimental evaluations;

© publishing of three papers to diverse International Conferences, as co-autor:

- I. Boldea, S. Scridon, L. Tutelea: *"BEGA – a biaxial excitation generator for automobiles"* – "OPTIM 2000" International Conference, Brasov, Romania, May 2000;
- I. Boldea, S. Scridon, L. Tutelea, C. Lascu, N. Muntean - *"The flux reversal machine (FRM) as an automotive alternator with 42/14 v d.c. dual output"* - "OPTIM 2000" International Conference, Brasov, Romania, May 2000;
- I. Boldea, E. Ritchie, F. Blaabjerg, S. Scridon, L. Tutelea – *"Characterization Of Biaxial Excitation Generator For Automobile"*- "OPTIM 2002" International Conference, Brasov, Romania, May 2002.

7.4. Future Work

First thing that has to be done is to study, using the FEM of analysis, the BEGA generator, to find out more optimisations that will reduce the total harmonics factor, which now has a large value.

Than, testing the final prototype of the BEGA generator, as it is now - integrated in the simple 42 V d.c. generating system or changing the configuration to a 14/42 V d.c. generating system - using simple but robust control strategies shall be done. Even if dynamic tests were done, more solutions and configuration has to be done to obtain all that this machine can offer.

Third, creating a setup facility, with alternative generators and control boards, by using and improving the existing prototypes and perhaps building other, detailed generating systems, with plenty of configuration possibilities.

Even though the biaxial excitation generator for automobiles (BEGA) shows great perspectives, it has some drawbacks that can give the impression of a non-competitive machine, like: the use of both, the Permanent Magnets and field windings for excitation and the presence of sleep rings which may limit the maximum operation speed of the machine together with the relative predicted high manufacturing costs, especially for inserting and cluing the PM's inside the flux barriers. All these drawbacks can be removed after a complete evaluation of the BEGA, and could be done in cooperation with specialized manufacturing companies.

Finally, a large volume of research work has to be carried out, especially to find and investigate all possible applications for the biaxial excitation generator, this issue being possible only through a huge effort. The first step in this direction is shown here and with a strong research team, more results will follow.

THESIS LIST OF REFERENCES

[1.] P. P. Acarnley, R.J. Hill, C.W. Hooper -*"Detection of Rotor Position in Stepping and Switched Motors by Monitoring of Current Waveforms"*- IEEE Transactions on Electronics, Vol.IE-32, No.3, August, 1985;

[2.] P. P. Acarnley, P.G. McLaren - *"Optimum Magnetic Circuit Configurations For Permanent Magnet Aerospace Generators"*- IEEE Transactions on Aerospace and Electronic Systems, vol. AES 21, no. 2, March 1985;

[3.] S. Andersen – *"Flux Reversal Machine"* – Master Thesis Project Sept. 1996;

[4.] G.Barakat, A.Foggia, M.Ivanes, A.Masson, R.Periot -*"Three Dimensional Computation of a Claw-Pole Synchronous Machine Performance"* Laboratoire d'Electrotechnique de Grenoble, France;

[5.] R.C. Becerra, M. Ehsani, T.J.E. Miller -*"Commutation of SR Motors"*- IEEE Transactions on Power Electronics, Vol.8, No.3, July 1993;

[6.] N. Bianchi, S. Bolognani – *"Magnetic Models of Saturated Interior Permanent Magnet Motor based on Finite Element Analysis"* – Record of IEEE, 2000;

[7.] M. Biriescu – *"Masini electrice rotative – parametri, caracteristici, incercari"* – Editura de Vest, Timisoara, 1997;

[8.] Boldea I.- *"Automotive electric generator systems. A review"* - Record of IEEE, Patras, 1999;

[9.] Boldea I.- *"Parametrii maşinilor electrice"* – Romanian Academy Publishing House - Bucharest 1991;

[10.] Boldea I.- *"Reluctance Synchronous Machines and Drives"* - Clarendon Press, Oxford, 1996;

[11.] Boldea I.-*"Transformatoare si masini electrice"*- Ed.D.P.Bucureşti 1994;

[12.] Boldea I., S.A. Nasar, L.E. Unnewehr -*"Permanent Magnet Reluctance and Self Synchronous Motors"*- CRC Press Boca Raton Ann Arbor London Tokyo;

[13.] Boldea I., Ew. Ritchie, Fr. Blaabjerg, S. Scridon, L. Tutelea - *"Characterization of the Biaxial Excitation Generator for Automobiles"* - "OPTIM 2002" International Conference, Brasov, Romania;

[14.] Boldea I., S. Scridon, L. Tutelea - *"BEGA - A Biaxial Excitation Generator for Automobiles"* - "OPTIM 2000" International Conference, Brasov, Romania;

[15.] Boldea I., S. Scridon, L. Tutelea, C. Lascu, N. Muntean - *"The flux reversal machine (FRM) as an automotive alternator with 42/14 v d.c. dual output"* - "OPTIM 2000" International Conference, Brasov, Romania, May 2000;

[16.] Boldea I., E. Serban, R. Babau -*"Flux Reversal Stator PM Single Phase Generator With Controlled D.C. Output"*- OPTIM '96;

[17.] Boldea I., J. Zhang, S.A. Nasar – *"Characterization of Flux Reversal Machine in low speed (direct) servo drives – the pole – PM configuration"* – Record of IEMDC, 2001;

[18.] Klaus Bolenz – *"Design Modifications of the Electrical System to use Intermittent Engine Operation"*- Record of IEE, 1996;

[19.] W.J. Bonwick -*"Voltage waveform distorsion in synchronous generators with rectifier loading"*- IEEE Proceedings, Vol.127, No.8, January 1980;

[20.] B.K. Bose, T.J.E. Miller, P.M. Szczesny -*"Microcomputer Control of Switched Reluctance Motor"*- General Electric Company, Corporate Research And Development, Schenectady, New York;

[21.] D. E. Cameron, J. H.Lang -*"The Control of High-Speed Variable Reluctance Generators In Electric Power Systems"*- IEEE Transactions on Industry Aplications, Vlo.29, No.6, Nov.-Dec.1993;

[22.] F. Caricchi, F. Crescimbini, F. Giulii Capponi, L. Solero – *"Permanent-Magnet, Direct Drive, Starter/Alternator Machine with Weakened Flux for Constant-Power Operation Over Extremely Wide Speed Range"* – Record of IEEE, 2001;

[23.] F. Caricchi, F. Crescimbini, E. Santini, L. Solero – *"High-Efficiency Low-Volume Starter/Alternator for Automotive Applications"* – Record of IEEE, 2000;

[24.] Chai J., Yao R., Chen P. -*"Principles for Switched Reluctance Motors Design"*- Proceedings, Part 2, International Conference on the Evolution and Modern Aspects of Synchronous Machines; 27 - 29 August 1991, Zürich, Switzerland, pp.445 – 448;

[25.] Chan S., Bolton H.R., -*"Development of sub-KW single phase switched reluctance motor drives";*

[26.] K. T. Chau, M. Cheng, C.C. Chan – *"Performance Analysis of 8/6-Pole Doubly Salient Permanent Magnet Motor"* – Record of IEEE, 1996;

[27.] G. Cimuca, M.M. Radulescu, B. Robyns, S. Brisset – *"Back-EMF Approach for Sensorless Operation of Small Electronically-Commutated Permanent-Magnet Motors"* – Record of OPTIM-2002, International Conference, Brsov, Romania;

[28.] M.J. DeBortoli, S.J. Salon -*"Computation of Forces and Torque in Electromagnetic Devices Using the Finite Element Method"*- Department of Electric Power Engineering Rensselaer Polytechnic Institute Troy, N.Y., USA;

[29.] N. A. Demerdash, R. Wang, R. Secunde – *"Three Dimensional Magnetic Fields in Extra High Speed Modified Lundell Alternators Computed by a Combined Vector-Scalar Magnetic Potential Finite Element Method"* – Record of IEEE, 1992;

[30.] R. P. Deodhar -*"The flux-MMF Diagram Technique and Its Applications in Analysis and Comparative Evaluation of Electrical Machines"*- University of Glasgow, October 1996;

[31.] R. P. Deodhar, I. Boldea, T. J. Miller – *"The Flux-Reversal Machine: a New Brushless Doubly-Salient Permanent Magnet Machine"* – Record of IEEE Transaction;

[32.] T. Dordea – *"Masini Electrice"* – Editura Didactica si Pedagogica, Bucuresti, 1977;

[33.] Faiz J. -*"Prediction of Static Magnetization Characteristics of Switched Reluctance Motors for General Rotor Positions"*- EPE - Firenze, vol.1, 1991, pp.355 – 359;

[34.] C.A. Ferreira, Eike Richter -*"Detailed Design of a 250kW Switched Reluctance Starter/Generator for an Aircraft Engine"*- SAE Technical Paper Series, April, 1993;

[35.] K. Folsach, J.H. Davies, T.J.E. Miller, M.I. McGilp, M. Olaru – *"Analytical and Numerical Computation of Air-Gap Magnetic Fields in Brushless Motors with Surface Permanent Magnets"* – Record of IEEE, 2000;

[36.] N.N. Fulton, P.J. Lawrenson -*"Switched Reluctance Drives for Electric Vehicles"*- Intelligent Motion, June 1993, Proceedings;

[37.] Fulton N.N., Stephenson J.M. -*"A Review of Switched Reluctance Machine Design"*- Proceedings ICEM '88, Sept. 12-14, Pisa, Italy, pp.423 – 428;

[38.] V. Z. Groza, M. Biriescu – *"Measurement of Reactance of Synchronous Machine at Standstill"* – Record from IEEE, 1999;

[39.] H. J. Gutt, J. Mueller – *"New Aspects for Developing and Optimizing Modern Motorcar Generators"* – Record of IEEE 1994;

[40.] Harris M.R., Finch J.W., Mallick J.A., Miller T.J.E. -*"A Review of the Integral - Horsepower Switched Reluctance Drive"*- IEEE Transactions on Industry Applications, vol. IA-22, No.4, July - August 1986, pp. 716 – 721;

[41.] Hava A.M., Blasko V., Lipo T.A. -*"A modified C-dump Converter for Variable Reluctance Machines"*- IEEE Transactions on Industry Aplications, vol.28, nr.5, Sept./Oct. 1992;

[42.] M. Hecquet, P.Brochet -*"Validation of Coupled Electric Permeance Net-work Model on a Claw-Pole Alternator"*- Ecole Centrale de Lille, France;

[43.] Gerhard Henneberger -*"Elektrische Motorausrüstung"*- Bosch GmbH;

[44.] G. Henneberger -*"Improvement of the output performance of claw pole alternators by additional permanent magnets"*- D10 Special machines and actuators;

[45.] G. Henneberger, S. Küppers –*"Field Calculation and Dynamic Simulation of a Claw Pole Alternator"*- Electrical Machines and Drives 11-13 Sept. 1995 Conference Publication No.412, IEE, 1995;

[46.] G. Henneberg, S. Küppers, I. Ramesohl -*"Numerical Calculation, Simulation and Design Optimization of Claw-Pole Alternators for Automotive Application"*- Institute for Electrical Machines, University of Technology Aachen;

[47.] G. Henneberger, S. Küppers, I. Ramesohl -*"The Influence of the Number of Poles on the Output Performance of a Claw-Pole Alternator"*- Institute for Electrical Machines, University of Technology Aachen;

[48.] G. E. Horst – *"Auxiliary starting switched reluctance motor"* – European Patent Application, EP 0695020A2;

[49.] Iqbal Husain, M. Ehsani -*"Rotor Position Sensing in Switched Reluctance Motors Drives by Measuring Muttualy Induced Voltages"*- IEEE Transactions on Industry Applications, Vol.30, No.3, May-June 1994;

[50.] G. A. Jack, J.W. Finch, J.P. Wright -*"Adaptive Mesh Generation Applied to Switched Reluctance Motor Design"*- IEEE Transactions on Industry Applications, Vol.28, No.2, March-April 1992;

[51.] T.M. Jahns - *"Uncontrolled generator operation of interior PM synchronnes machines following high speed inventer shut down"* - Proceedings of IEEE-IAS 1998 - Annual Meeting, vol.1;

[52.] T. M. Jahns, Wen L. Soong – *Pulsating Torque Minimization Techniques for Permanent Magnet AC Motor Drives – A Review"* - Record of IEEE, 1996;

[53.] Jufer M., Crivii M., Hatefi K., Poffet P., Osseni, R., -*"Synchronous electronically comutated motors - design and comparison"*- Proceedings ICEM '90;

[54.] Jufer M., Crivii M., Poffet P. -*"Conception du moteur reluctant à comutation electronique"*- Proceedings MOP – 1990;

[55.] G. I. Kassakian, H. C. Wolf, I. H. Miller, C. H. I. Murton - *"Automotive electrical system circa 2005 "* - IEEE Spectrum, August, 1996, pp. 22 – 27;

[56.] J. Kaukonen, J. Pyrhönen, J. Nerg, J. Luuko, M. Niemelä, O. Pyrhönen – *"Salient Pole Synchronous Motor Saturation in a Direct Torque Controlled Drive"* – Record of IEEE, pp.1397-1401;

[57.] Kilthau A., J.M. Pacas – *"Measurement of the Parameters of the Synchronous Reluctance Machine including Cross Saturation"* – Record of EPE 2001, Graz

[58.] P. C. Kjaer, G. Gallegos-Lopez -*"Single Sensor Regulation in Switched Reluctance Motor Drives"*- University of Glasgow, SPEED Laboratory, Scotland, U.K.;

[59.] P.C. Kjaer, G. Gallegos-Lopez, T.J.E. Miller -*"Active Clamp Resonant DC Link Inverter for Current Controlled Switched Reluctance Motors"*- SPEED Laboratory, University of Glasgow, Scotland, U.K.;

[60.] P.C. Kjaer, T.J.E. Miller, J.J. Gribble -*"Dynamic Testing of Switched Reluctance Motors for High-Bandwidth Actuator Applications"*- University of Glasgow, SPEED Laboratory, Scotland, U.K.;

[61.] P. C. Kjaer, T.J.E. Miller, J.J. Gribble -*"High-Grade of Switched Reluctance Machines"*- University of Glasgow, SPEED Laboratory, Scotland, U.K.;

[62.] E. Kokornaczyk, M. Stiebler -*"Substitution of Measuring Hardware in Sensorless SR-Motors by Software"*- Intelligent Motion, June 1997 Proceedings;

[63.] S. Kuppers "Numerische Verfahren zur Berechnung und Auslesung von Drehstrom Klauenpolgeneratoren" - Shaker Verlag, Aaachen 1996;

[64.] Kwon Y.A., Reichert K. -"*Chopping-less Operation of a Nonlinear Switched Reluctance Motor*"- Proceedings, Part 2, International Conference on the Evolution and Modern Aspects of Synchronous Machines; 27 - 29 August 1991, Zürich, Switzerland, pp.465 – 468;

[65.] R. Lagerquist, I. Boldea T. J. E. Miller– *"Sensorless Control of the Synchronous Reluctance Motor"* – Record of IEEE Transaction on Industry Applications, vol. 30, No. 3, 1994;

[66.] P. Laurent, B. Multon -"*Sensorless Position Measurement Based on PWM Eddy Current Variation for SRM*"- EPE '95 Sevilla;

[67.] Lawrenson P.J. -"*A brief status review of Switched Reluctance Drives*"- EPE, vol.2, nr.3, October 1992;

[68.] J.H. Lee, J.C. Kim, D.S.Hyun – *"Effect Analysis of Magnet on Ld and Lq Inductance of Permanent Magnet Assisted Synchronous Motor Using Finite Element Method"* – Record of IEEE, 1999;

[69.] Jung-Chien Li -*"A Saturation Model for the Switched Reluctance Motor to Maximize the Torque with Minimum Ripple"*- Department of Electrical Engineering, National Taiwan Ocean University, Keelung, Taiwan;

[70.] F. Liang, J. Miller, X. Xu – *"A Vehicle Electric Power Generation System with Improved Output Power and Efficiency"* – Record of ELECTROMOTION International Conference, 1998;

[71.] Y. Liao, Th. A. Lipo – *"A New Doubly Salient Permanent Magnet Motor for Adjustable Speed Drives"* – Record of IEEE, 1992;

[72.] E. C. Lovelace, T. M. Jahns, T. A. Keim, J. H. Lang – *"Mechanical Design Considerations for Conventionally-Laminated, High-Speed, Interior PM Synchronous Machine Rotors"* – Record of IEEE, 2001;

[73.] E. C. Lovelace, T. M. Jahns, J. L. Kirtley Jr., J. H. Lang – *"An Interior PM Starter/Generator for Automotive Applications"* – Record of IEE 1998;

[74.] E. C. Lovelace, T. M. Jahns, J. L. Kirtley Jr., J. H. Lang - *"A Saturating Lumped Parameter Model for an Interior PM Synchronous Machine"* - Record from IEEE 1999, pp.553-555;

[75.] E. C. Lovelace, T.M. Jahns, J.H. Lang – *"Impact of Saturation and Inverter Cost on Interior PM Synchronous Machine Drive Optimization"* – Record of IEEE, 1999

[76.] Lumsdaine A., J.H. Lang -*"State Observers for Variable-Reluctance Motors"*- IEEE Transactions on Industrial Electronics, Vol.37, No.2, April, 1990;

[77.] J. Luo, S. Huang, S. Chen, T.A. Lipo – *"Design and Experiments of a novel Axial Flux Circumpherential Current Permanent Magnet (AFCC) Machine with Radial Airgap"* – Record of IEEE, 2001;

[78.] X. Luo, D. Qin, Th. A. Lipo – *"A Novel Two Phase Doubly Salient Permanent Magnet Motor"* – Record of IEEE, 1996;

[79.] Manzone A., A. Pincetti, D. de Costantini – *"Fault Tolerant Automotive Systems: an Overview"* – Record of IEEE, 2001;

[80.] C. Martis, M.M. Radulescu, K. Biro – *"Dynamic Analysis of a Switched Variable Reluctance Permanent Magnet Small Motor"* – Record of ELECTROMOTION, 1999;

[81.] P. Materu, R. Krishan -*"Estimation of Switched Reluctance Motor Losses"*- IEEE Transactions, Reprinted, 1988;

[82.] P. J. McCleer, J.M. Miller, A.R. Gale, M.W. Degner, F. Leonardi – *" Nonlinear Model and Momentary Performance Capability of a Cage Rotor Induction Machine Used as an Automotive Combined Starter-Alternator"* – Record of IEEE, 2001;

[83.] S. R. McMinn, W.J. Rzesos, P.M. Szczesny, T.M. Jahns -*"Application of Sensor Integration Technique to Switched Reluctance Motor Drives"*- IEEE Transactions on Industry Applications, Vol.28, No.6, Nov.-Dec. 1992;

[84.] K. K. Meidensha – *"Hybrid excitation type permanent synchronous motor"* – European Patent Application, 0620634A1;

[85.] T.J.E. Miller -*"Faults and Unbalance Forces in the Switched Reluctance Machine"*- IEEE Transactions on Industry Applications, Vol.31, No.2, March-April 1995;

[86.] Miller T.J.E. -*"Switched Reluctance Motors and Their Comtrol"*- Magna Physics Publishing and Clarendon Press, Oxford 1993;

[87.] Mizuno, Takyuki, C/O Kabushiki, Kaisha Meidensha - *"Hybrid excitation type permanent magnet synchronous motor"* - European Patent Application 941056335, 12.04.1994;

[88.] M. Moallem, Chee-Mun Ong, L.E. Unnewehr - *"Effect of Rotor Profiles on the Torque of a Switched Reluctance Motor"*- IEEE Transactions on Industry Applications, vol.28, No.2, March-April 1992;

[89.] Mutter A. – *"Elektrische Antriebe mit kombinierter elektrischer und Dauermagneterregung"* – Deutsches Patent und Markenamt, Patentschrift DE 4139843C2;

[90.] Mutter Albert - *"Elektrische maschine und deren anwendung zum fahrzeugbetrieb"* - Patentschrift DE 413943C2, 03.12.1991;

[91.] M. Naidu, M. Boules, R. Henry - *"A high efficiency, high power generation system for automobiles"* - Proceedings of IEEE- IAS 1995 -Annual Meeting, pp. 709- 716;

[92.] M. Naidu, J. Walters – *"A 4 kW, 42 V induction machine based automotive power generation system with a diode bridge rectifier and a PWM inverter"* – Record of IEEE, 2001;

[93.] P. Pedersen, L. Christensen, F. Blaabjerg, L. Oestergaard – *"A New Dynamic Model for a Doubly Salient Permanent Magnet Motor"* – Record of IEEE, 1996;

[94.] B.S.P. Pereira, M.F. Islam – *"Interior Permanent Magnet Motor Having Several Improved Features"* – Record of Electric Machines and Power Systems, vol.25, pp. 1135-1144, 1997;

[95.] M.M. Radulescu, Z. Biro, C.M. Pop – *"Two-Phase Electronically-Comutated Permanent-Magnet Small Motor without Position Sensor"* - Record of ELECTROMOTION, 1999;

[96.] Radun A. - *"Design Considerations for the Switched Reluctance Motor"*- University of Kentucky, USA;

[97.] Radun I.-*"Generating With the Switched Reluctance Motor"*- University of Kentucky, USA;

[98.] W. F. Ray, M.T. Ebrahim -*"A Novel High Speed Switched Reluctance Generator"*- EPE'95 Seville;

[99.] Ray W.F., Lawrenson P.J., Davis R.M., Stephenson J.M., Fulton N.N., Blake R.J. - *"High Performance Switched Reluctance Brushless Drives"* - IEEE

Transactions on Industry Applications, Vol IA-22, No.4, July - August 1986, pp.722 – 729;

[100.] S. J. Salon – *"Finite Element Analysis of Electrical Machines"* – Kluwer Academic Publishers 1995;

[101.] Sabonnadiere J.C., Konrad A. -*"Computing EM Fields"*- IEEE Spectrum, November 1992, pp. 52 – 56;

[102.] E. Schmidt, W. Brandl – *"Comparative Finite Element Analysis of Synchronous Reluctance Machine with Internal Rotor Flux Barriers"* – Record of IEEE. 2001;

[103.] R. D. Schultz – *"Performance Model of an Automotive Starter-Generator"*- Record of IEEE, 2000;

[104.] Z. John Shen, S.P. Robb, F.Y. Robb, M. Fuchs, D. Berels, K. Hampton – *"Load Dump Protection in 42V Automotive Electrical Distribution Systems"* – Record of IEEE, 2001;

[105.] W.L. Soong, N. Ertugrul, E.C. Lovelace, T.M. Jahns – *"Investigation of Interior Permanent Magnet Offset – Coupled Automotive Integrated Starter/Alternator"*- Record of IEEE, 2001.

[106.] Stille E.– *"Exciting arrangement for homopolar machine"* – UK Patent Application, GB2247362A;

[107.] Syverson et all – *"Hybrid Alternator with Voltage Regulator"* – United States Patent, 5502368;

[108.] H. Thiemer – *"Influence of Automotive 42V Power-net on Small PM DC Motors"* – Record of IEEE, 2001;

[109.] Kimmo Tolsa, Pertti Silventoinen, Jussi Salo, Juha Pyrhönen -*"Torque Control of the Switched Reluctance Motor Minimizing Copper Losses"*- Department of Energy Technology, Lappeenranta University of Technology, Finland;

[110.] Vagati I., A. Canova, M. Chiampi, M. Pastorelli, M. Repetto – *"Improvement of Synchronous Reluctance Motor Design through Finite Element Analysis"* – Record of IEEE, 1999;

[111.] M. Vaida, M. Boules, R. Henry - *"A high efficiency, high power generation system for automobiles "* - Record of IEEE - IAS 1995 - Annual Meeting, pp. 709 – 716;

[112.] Verma S.P. -*"Design and Performance of Special Reluctance Motors with Regard to Torques, Vibration and Noise"*- Proceedings, Part 2, International Conference on the Evolution and Modern Aspects of Synchronous Machines; 27 - 29 August 1991, Zürich, Switzerland, pp. 494 – 499;

[113.] Wang A., I. Boldea, S.A. Nasar – *"Characterization of Three Phase Flux Reversal Machine as an Automotive Generator"* – Record of IEEE, 2001;

[114.] Wang A., S.A. Nasar, I. Boldea – *"High Speed Control Scheme of Flux Reversal Machine"* – Record of IEEE 1999;

[115.] C. Wang, S.A. Nasar, I. Boldea – *"Three-phase flux reversal machine (FRM)"* – Record of IEE, 1999;

[116.] R. Wang, N.A. Demerdash – *"Extra High Speed Modified Lundell Alternator Parameters and Open/Short –Circuit Characteristics from Global 3D-FE Magnetic Field Solutions"* – Record of IEEE, 1992;

[117.] Longya Xu, Th.A. Lipo -*"Analysis of a New Variable Motor Utilizing Only Two Transistor Switches"*- IEEE Transactions on Industry Applications, Vol.26, No.2, March-April 1990;

[118.] Yanhong Xue, Shaotang Chen – *"Instability Issues for Control System in Induction Generator"* – Record of IEEE, 2001;

[119.] K. Yoshida, K. Kesamaru, Y. Hita – *"Eddy Currents Analysis of Surface Mounted PMSM by Finite Element Method"* – Record of IEE, 1999;

[120.] T.M. Zahias - *"Uncontrolled generator operation of interior PM synchronous machines following high speed inverter shut down"* - Record of IEEE - IAS 1998 - Annual Meeting;

[121.] Zaim M.E., Tahi S., Laporte B. -*"Calculation and Performances of Smooth Stator Reluctance Machines"*- Proceedings, Part 2, International Conference on the Evolution and Modern Aspects of Synchronous Machines; 27 - 29 August 1991, Zürich, Switzerland, pp.500 – 505;

APPENDIX A

THE FLUX REVERSAL MACHINE (FRM) AS AN AUTOMOTIVE ALTERNATOR WITH 42/14 V D.C. DUAL OUTPUT

Ion BOLDEA Sever SCRIDON Lucian TUTELEA Cristian LASCU Nicolae MUNTEAN
Department of Electrical Engineering, University Politehnica of Timisoara, V. Parvan 2 Blvd., 1900-Timisoara, Romania
Phone/Fax: +40 56 204402; E-mail: boldea@lselinux.utt.ro

Abstract: *The paper introduces a stator-PM, doubly salient, three-phase alternator with flux linkage reversal (FRM) in the stator phases concentrated coils. A diode rectifier and a single IGBT chopper are sized to form a 56V d.c. output. The 14V and 42V loads are series connected with the car body as neutral point.*
Two additional IGBTs are used to cancel the neutral current when the load currents in the two power channels differ from each other. Configuration details, FEM field analysis results within a conceptual and then an optimization design and balanced and unbalanced load transients simulations for constant voltage control constitute the core of the paper. They suggest good power density, efficiency, load rejection capacity for speeds from 1800 rpm to 18 krpm, and from 1. 5 kW to 3 kW power levels.

Keywords: *Automotive electrical Equipment; High Speed Reluctance generator; Special design and calculation of electrical machine, Finite Element Method, magnetic field in electrical machine; Pspice simulations.*

1. Introduction

Claw-pole alternators with diode rectifier and rotor field coil current control [1] are still used exclusively as automotive generators.
While rugged and having good power density, their efficiency tends to be low (below 50% at full load and maximum speed) due to large copper losses and large claw pole eddy current losses mainly. The growing demand for more power on modern cars has prompted efforts to increase the claw-pole generator output through additional PMs situated on the pole faces or between them [2], double claw-pole rotors (back to back) or two rotor parts, one excited and one with PMs [3,4]. Improvements by such methods range from a few percent of output increase at idle engine speed (with PM on claw pole faces) or at high speeds (PMs between rotor poles) [2] up to even doubling the output with double claw pole rotors [3], [4] and rather long stacks.
Also 40% more output at engine idle engine speed has been claimed with MOSFET controlled rectifier triggered at optimum power angle [5]. Still the situation remains unchanged at higher speeds. Increasing the number of poles, for given external stator diameter increases the output [2] but the efficiency is getting even worse.
For higher powers and same volume higher speeds are required. For speeds above 6000 rpm the eddy current loss in the claw poles due to airgap flux harmonics (caused by slot openings and m.m.f. harmonics) become prohibitive.
For higher speeds PM alternators with full power electronic control have been proposed [1,5,7]. Mechanical and thermal difficulties with PMs on the rotor, at high speeds, seem to be the main liability of such configurations, besides added costs.
Brushless alternators with dual (a.c. – a.c.) stator windings and salient pole rotors with short-circuited coils in an adequate pole number combination are documented in [8]. However the voltage recovery under sudden load variation tends to be slow while wide speed range 5 to 1 or more) constant voltage has not been demonstrated yet. Also the efficiency tends to be modest.
A dual winding (d.c. & a.c.) with $2p_1$ and $2p_2$ number of poles and a $p_1 + p_2$ salient pole windingless rotor may also in principle be used for the scope [9]. However the power density is rather low and the voltage recovery for load sudden variation tends to be slow.
The reluctance synchronous alternator (without or with PM in axis q on the rotor) with PWM inverter connected to the battery ([9] - chapter 8) may also be a candidate. Still a full power 6 SCR PWM converter is required.
Switched reluctance generators (SRG) with full power electronics connected to the battery may also be a solution. The wide speed constant power and voltage stable operation as well as the fast voltage

recovery under sudden load variation are still to be demonstrated.

Double saliency (SRG-like) generators with stator PM's and pulsating (homopolar) flux linkage have been proposed long ago [10]. Still the rather large electrical time constant leads to slow load rejection while homopolar flux variation in the coils makes only partial use of stator coils.

To reduce the electrical time constant and to make better use of stator copper (for higher efficiency) the flux reversal PM machine (FRM) was introduced [11]. It is a double saliency (SRG – like) machine with a pair of PMs with alternate polarity placed on each stator pole. It may be single or three phase.

In a single-phase configuration, the FRM has been proved, only through digital simulations, capable to produce constant voltage for wide speed range (10 to 1) and fast load rejection [12].

In this paper a 3 phase FRM with a special converter for 42/14V d.c. output for high speeds and powers (3kW or more at 18krpm and more) is introduced. Configuration details, FEM analysis results, conceptual & optimal design, unbalanced load transient studies – through digital simulations – constitute the main paragraphs of the present paper.

2. The FRM as an Automotive Generator

A typical 6/8 pole FRM –with stator PMs is shown in figure 1.

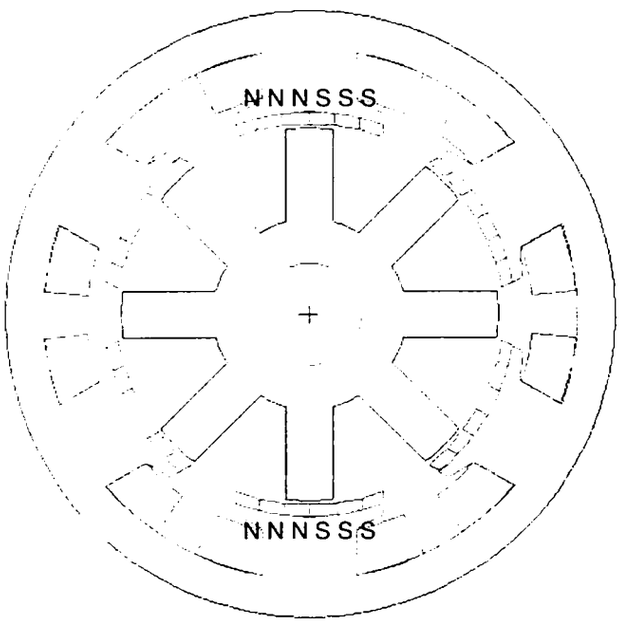

Fig. 1. Three phase FRM

Each phase contains two coils in series. Stator pole angles are in general $2\pi/N_r$ radians and their interpoles: $2\pi/3N_r$. Rotor poles span between π/N_r and $2\pi/3N_r$ radians. The number of stator poles N_s is a multiple of 6 with the rotor poles number N_r as multiple of 8.

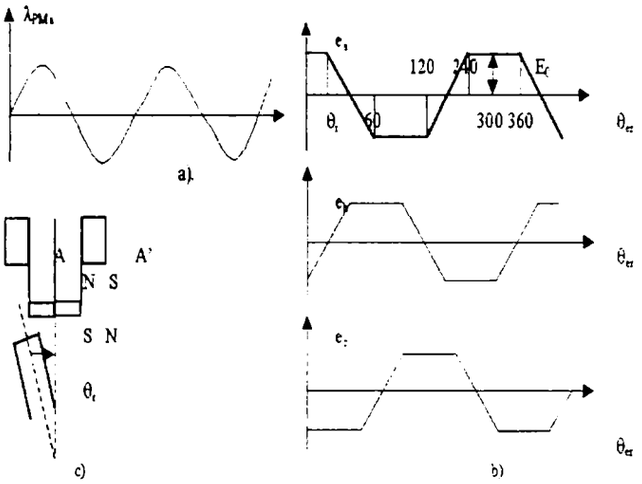

Fig. 2. Stator flux a), e.m.f. b), and pole angle θ_r c)

It follows clearly from figure 2 that the FRM works in a way similar to the d.c. brushless motor. The main differences are that the PMs are placed on the stator and the stator phase coils are placed on salient poles. Notice also that, despite the double saliency, the phase inductance does not depend essentially on the rotor position [13].

The power electronic converter (PEC) for producing a 42/14Vd.c. voltage output is presented on figure 3.

The two-voltage system is required by the load characteristics on the cars of the future. The rated current of both voltage channels is about the same.

The unidirectional switch S_0 (IGBT) controls the 56V system. When a null current occurs, because the two loads are temporarily different from each stator, it has to be handled through the two SCRs S_1 and S_2.

The control quantities are chosen as V_1 (total, 56V) and the voltage ratio V_1/V_2.

PI controllers were used.

There are in conduction, in general, three switches in series (D_1, D_6, S_0 or D_1, D_6, and S_1 or S_2). This is an indication of a fairly high efficiency of the balancing converter, which handles only the load unbalances.

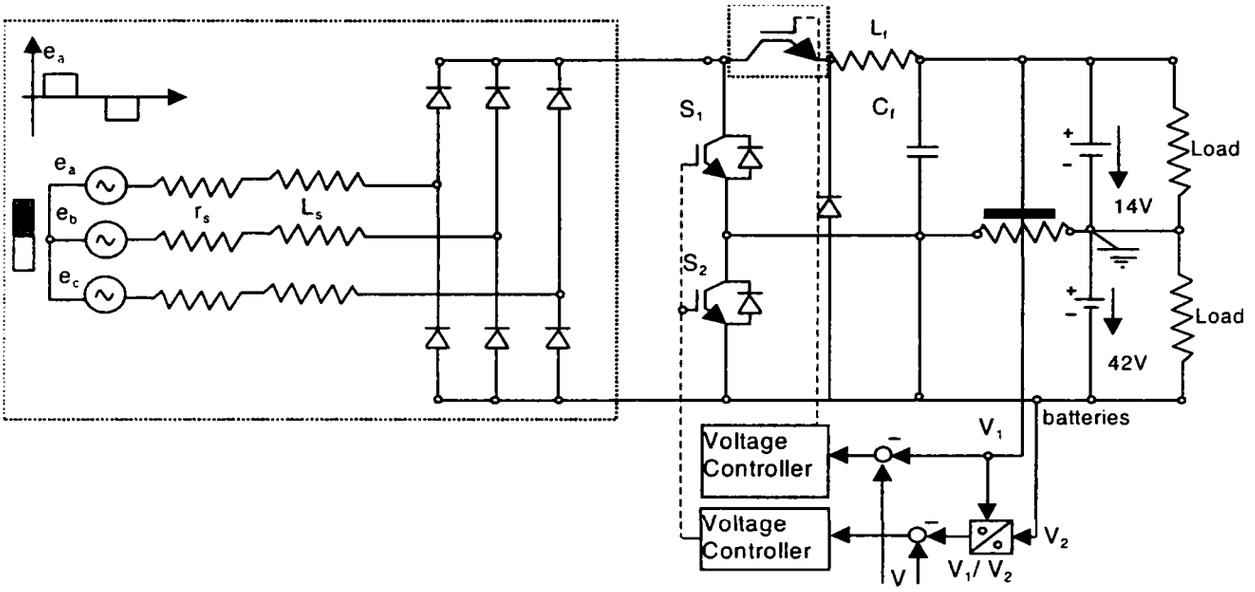

Fig. 3. The proposed 42/14V generator system

The full power electronic control in a low inductance generator (such as FRM) also suggests fast voltage recovery after load variation, in presence of the batteries, which behave like "huge" capacitors.

3. FEM Analysis Results

Though it was easy to depict the ideal phase e.m.fs. their real waveform and level computation requires either very elaborate analytical of FEM field analyses. Two-dimensional FEM suffices unless the stack length is unusually short. FEM is also used to calculate the phase inductance while the end-connection leakage inductance component is to be added, however based on analytical expressions.

Typical FEM flux plots for zero and maximum flux PM flux-linkage in phase A, are shown on figure 4. (the flux linkage versus rotor position is given in figure 2a).

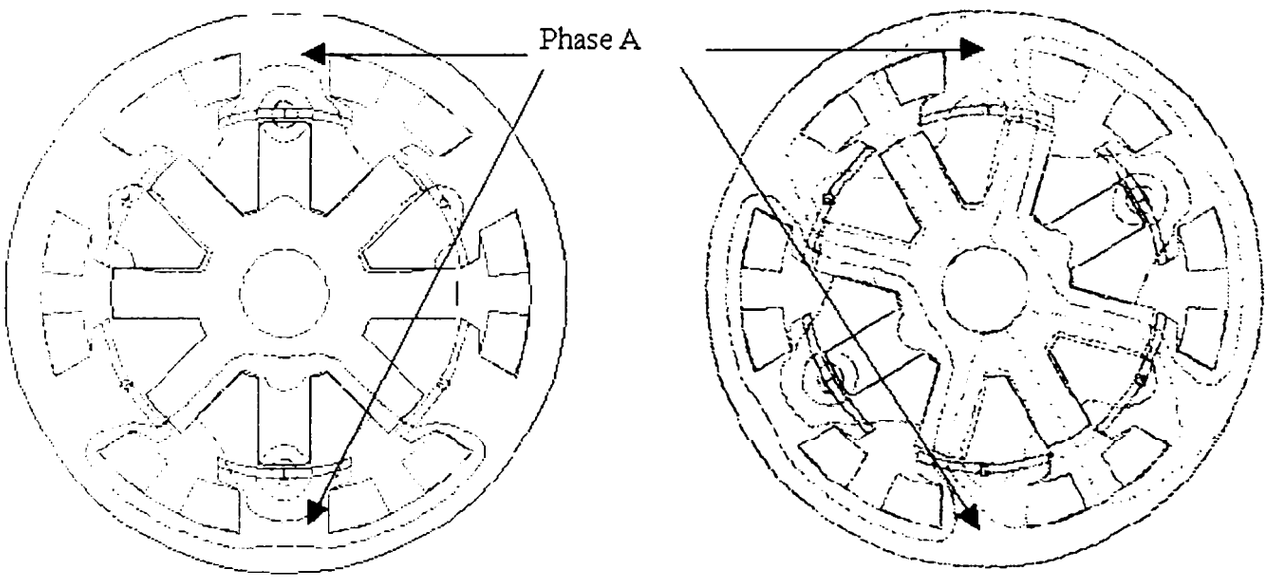

Fig. 4. PM flux plots through FEM
a). zero PM flux in phase A;
b). maximum PM flux in phase A

It is important to calculate a kind of fringing coefficient K_σ :

$$1 + K_\sigma = \frac{ideal \ \max . phase \ flux}{real \ \max . phase \ flux} = \left(\frac{\Lambda_{PMi}}{\Lambda_{PM}}\right)_{\max} \quad (1)$$

The expression of $(\Lambda_{PMi})_{max}$ is:

$$(\Lambda_{PMi})_{max} = B_m \tau_s L \quad (2)$$

$2\tau_s$ – stator pole span; L – stator length; B_m – the PM radial flux density:

$$B_m = B_r h_{PM} / (h_{PM} + g \mu_{rec} / \mu_0) \quad (3)$$

With: h_{PM}– the PM radial height; g – the airgap; B_r – remanent flux density.

The fringing coefficient K_σ is related to geometrical parameters such as: g/h_{PM}, τ_s/h_{PM}, h_{pr}/h_{PM} with h_{pr} – the rotor pole height.

Such dependencies, FEM obtained, may then be used through adequate curve fitting to define K_σ (h_{PM}/g, h_{PM}/τ_s, h_{pr}/τ_s) functions.

The inductance L_s function is also calculated through FEM. It seems pretty obvious that we need to choose the variables h_{PM}/g, h_{PM}/τ_s, h_{pr}/τ_s such that K_σ were minimum. Quite a few FEM runs are required for the scope even if the starting values are realistic.

In order to reduce the machine electrical time constant (inductance L_s) the PM radial height tends to be high. However above a certain value of h_{PM} the leakage inductance becomes predominant and thus any further PM height increase is not useful. Typical results obtained through 2D FEM are shown in table 1.

Table 1. Fringing coefficient K_σ

Airgap	h_{PM}	h_{pr}/τ_s	h_{PM}/τ_s	$1 + K_\sigma$	K_σ	B_m
0.5	6	1	0.375	3.9193	2.91	1.12
0.5	2	1	0.125	1.9059	0.90	0.96
0.5	6	2/3	0.375	2.9555	1.95	1.12
0.5	2	2/3	0.125	1.9297	0.92	0.96
1.0	6	1	0.375	3.6159	2.61	1.03
1.0	2	1	0.125	1.9845	0.98	0.79
1.0	6	2/3	0.375	3.4652	2.46	1.03
1.0	2	2/3	0.125	2.1526	1.15	0.79

For the minimum K_σ case from table 1: $K_{\sigma min}$= 0.9 ; $1/(1+ + K_{\sigma min})$=0.526 for h_{pr}/τ_s=2/3 h_{PM}/τ_s=0.125 for τ_s= 0.0138m, D_r= 0.07m.

Results such as those in table 1 show that there is no need to increase the PM height too much as both K_σ and L_s become only loosely dependent on it.

The final decision on PM height h_{PM} depends also on cost factors but the above inquiry should be essential in providing solid data for conceptual and optimal designs.

Flux / current/ position curve families obtained through actual FEM may be used to determine the e.m.f. waveforms and interaction and cogging torque.

These waveforms may be curve fitted and later on used in digital simulations of system's transients.

The e.m.f. waveform may be decomposed into harmonics:

$$e_{ai}(\theta_r) = \sum_{\nu=1,3,5} E_\nu \cos \nu(N_r \theta_r - (i-1)2\pi/3); \quad i=1,2,3 \quad (4)$$

As in figure 2, the e.m.f. of phase a, is maximum for θ_r=0.

The actual e.m.f. E_0 is calculated through it's ideal value E_{0I} (rectangular) whose constant value spans approximately over a geometrical angle of $2\pi/N_r$ and is calculated using equation (1):

$$E_0 = K_{skew} E_{0i} / (1 + K_\sigma) \quad (5)$$

The coefficients K_σ (for fringing) and K_{skew} (for rotor skewing) provide for realistic results.

With: $$E_{0i} = \frac{d\Lambda_{PMi}(x)}{dx} 2 \cdot n_c \frac{dx}{dt} \quad (6)$$

n_c – turns / coil.

$$\Lambda_{PMi}(x) = (\Lambda_{PMi})_{\max} \frac{2x}{\tau_s}; \quad -\tau_s/2 \le x \le \tau_s/2 \quad (7)$$

L – stack length

Finally (with (2) –(3)):

$$E_{0i} = B_{gPMi} \frac{h_{PM}}{h_{PM} + g\frac{\mu_{rec}}{\mu_0}} 8 n_s L \tau_s N_r n \qquad (8)$$

The skewing coefficient $K_{skew} \approx 0.9$ for 120^0 electrical degrees (15^0 mechanical) skewing of rotor.

4. Generator Conceptual Design

By conceptual design we understand sizing the machine (for given specifications) through making use of analytical electromagnetic and thermal models.

4.1. Design specifications:

d.c. output voltage: V_0= 56V (14V + 42V)
output power at n_b=30rps: P_b= 1.5kW
output power from 150rps to 300rps: 3kW
efficiency: above 75%.

The ratio of powers for the two voltage loads is proportional to the respective voltages and thus the rated current is the same for both d.c. networks.

As expected, the highest torque occurs at 30rps for 1.5kW so the machine has to be sized for this situation. Verifications are to be made to check the performance for higher speeds.

Giving the efficiency $\eta_{bt} \approx 0.85$ for 30rps and 1.5kW, the rotor aspect ratio $\lambda = L/D_r = 1.2$ and the peak tangential force f_x= 1.6 10^4N/m^2, we may determine the rotor diameter D_r:

$$D_r = \sqrt[3]{\frac{2P_b}{\eta_b f_x \pi \lambda 2\pi n_b}} = 0.06769\,m \approx 0.07m \qquad (9)$$

The stack length $L = \lambda \cdot D_r = 0.0812$m (10)

Giving the number of stator poles N_s= 6 and rotor poles N_r= 8 we may find τ_s:

$$\tau_s = \pi D_r / 2N_r = 0.01374\text{m} \qquad (11)$$

For trapezoidal current control, in general, two phases are on and thus the electromagnetic power P_{eb} is:

$$P_{eb} = P_b/\eta_{bt} = 2E_0 I_c = 2E_0 K_{skew} I_c / (1 + K_\sigma) \qquad (12)$$

Choosing the airgap g=0,5 mm, PM height h_{PM}= 6 mm, we may obtain first the ideal average airgap flux density [3].

$$B_{gPMi} = B_m \approx \frac{h_{PM} B_r}{h_{PM} + g\frac{\mu_{rec}}{\mu_0}} = 1.079\ T \qquad (13)$$

For MQ3 – F38H PM material, at 75^{0}C, B_r =1.213T and H_c = 0.652MA/m, recoil permeability μ_{rec} is:

$$\mu_{rec} = B_r / H_c = 1.4812 \cdot \mu_0 \qquad (14)$$

Based on the above data we may choose an initial value for the fringing coefficient $1/(1+K_\sigma) \cong 0.6$ and calculate the actual average flux density (per half stator pole)

$$B_{gPM} = B_{gPMi} \cdot 0.6 = 0.645\text{T} \qquad (15)$$

Based on the above value of B_{gPM}, a preliminary design of the whole magnetic circuit (stator and rotor) is to be done. Further on through FEM a more precise value of K_σ is obtained. With this new value of K_σ the magnetic circuit sizing is adjusted.

Going back to (13) with E_{0i} from (9) we may calculate the pole m.m.f. N_cI_c:

$(I_cN_c)_b \cong P_b/(20.85 B_{gPM} 8 L \tau_r N_r N_c) = 638$ Aturns/pole (16)

Assuming a design current density (highest in fact) for minimum speed n_b and P_b , j_{cob}= 12x10^6 A/m^2, the slot area for the coil is obtained.

The stator magnetic circuit may be adjusted to make sufficient room for coils.

Further on the electrical parameters R_s and L_s are calculated as in standard electric machines . A core loss model is developed and applied for stator and rotor core loss calculation.

With winding, core and mechanical losses known, a unidimensional thermal model is applied to calculate the overtemperatures to make sure that the PMs are not in danger of demagnetization.

The number of turns per coil N_c is essential in securing enough voltage and power at lowest speed n_b.

Taking into consideration the diode rectifier only (the chopper is idle in this situation), the voltage equation writes:

$$2E_0 - 2R_s I_c - 3\omega_b L_s I_c/\pi = V_0 \qquad (17)$$

With $R_s = 1.7\text{x}10^{-4} N_c^2$ (Ω); $L_s \cong 0.8\text{x}10^{-5} N_c^2$ (H); $E_0 \cong 4.5\text{x}10^{-2} N_c n$ (V); (from (5) &(8)); V_0 = 56V and $n = n_b$ = 30rps, we find N_c from (17) ($N_c \cong$ 32turns/coil $E_0 = 1.4N_c$).

From (16), the phase trapezoidal current:

$I_c = N_c i_c / N_c = 750/32 = 23.43$A.

So the average electromagnetic power at minimum speed N_c =30 rps is, according to (12):

$$P_{cb} = 2E_{lb}I_c = 2099\text{W} \qquad (18)$$

After the total efficiency is calculated sizing reruns are done to reduce the size accordingly.

Now that the machine conceptual design methodology has been put forward, we may proceed to extended digital simulations to explore the steady state and transient performance up to maximum speed in presence of the power electronics converter and voltage and current controllers (figure 3).

5. System's digital simulations

For the system's digital simulations we do require the mathematical model of the generator, power electronics converter (PEC) and for the voltage controllers.

The generator model for constant speed reduces itself to the phase voltage equations:

$$L\frac{d}{dt}\begin{vmatrix} i_a \\ i_b \\ i_c \end{vmatrix} = \begin{vmatrix} V_a \\ V_b \\ V_c \end{vmatrix} - R_s \begin{vmatrix} i_a \\ i_b \\ i_c \end{vmatrix} + \begin{vmatrix} e_a(\theta_r) \\ e_b(\theta_r) \\ e_c(\theta_r) \end{vmatrix} \qquad (19)$$

$$\theta_r = 2\pi \int n dt + \theta_0 , \qquad (20)$$

with $e_a(\theta_r)$, $e_b(\theta_r)$ and $e_c(\theta_r)$, as in [4]

We have to add to this model the PEC equations. Based on the PEC configuration (figure 3) its model is easy to obtain in Pspice.

Finally, the voltage controllers of PI type are adopted. Current controllers are added (figure 5).

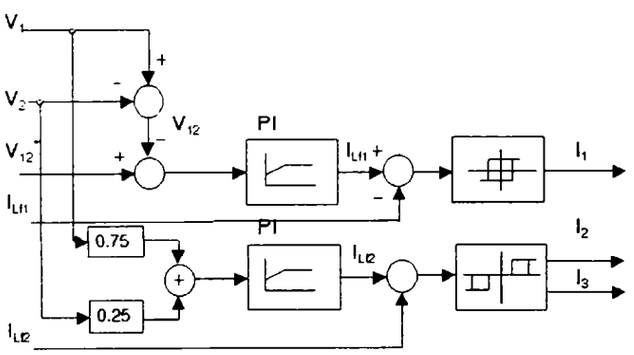

Fig. 5. Details of the controller

A simplified battery model (capacitors plus series connected resistances) is used.

Digital simulations have been run at constant speeds. Load sudden changes - balanced and nonbalanced - have been investigated at n_b= 30 rps, n_m =150 rps and n_{max} = 300 rps (fig. 6, 7, 8).

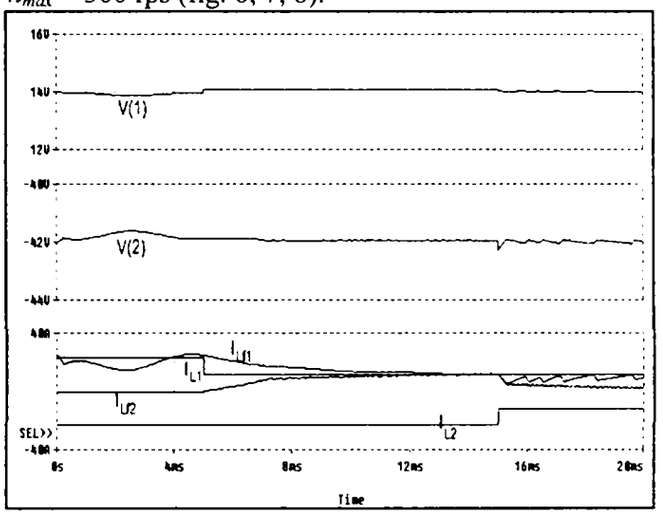

Fig. 6. Digital simulations results for n_b= 30 rps

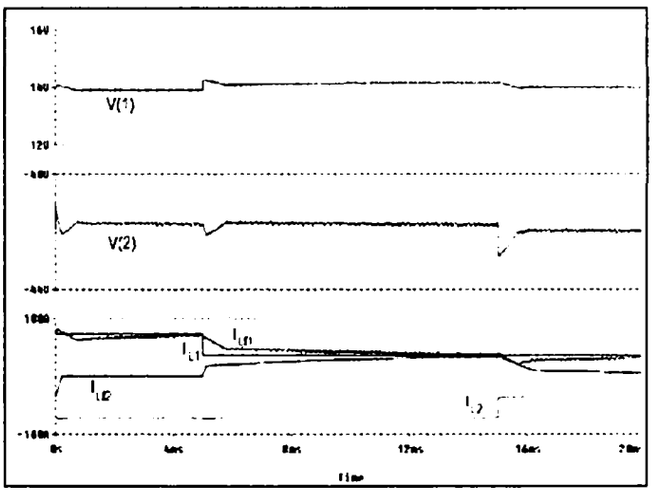

Fig. 7. Digital simulations results for n_b= 150 rps

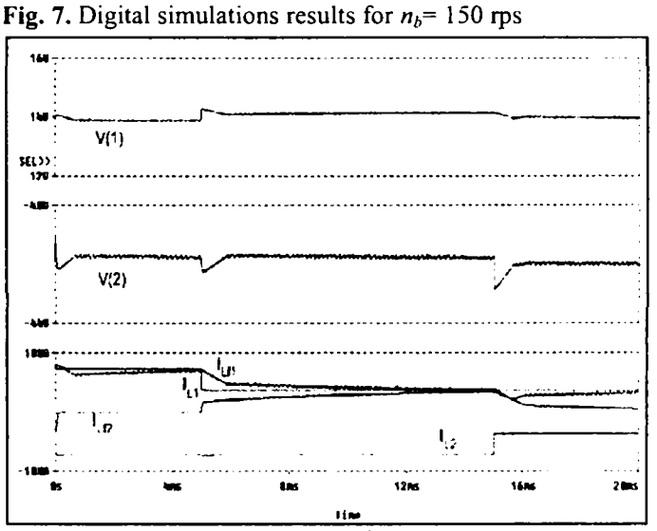

Fig. 8. Digital simulations results for n_b= 300 rps

Discussion:
At low speed, the generator have to support the maximum load, for this reason keeping the output voltage at constant values is done at the limit.
If a load step variation appears on one of the two networks and then on the other one too, we observe (as in figure 6) a small variation of the output voltages.
When the generator is working at the highest speed, the output voltage is ten times higher than the nominal output voltage. We notice the output voltage ripples (figure 8), caused by the power converter which works with large differences between the input (from the generator) and output (to the loads and batteries) voltages. Those ripples are acceptable from the user point of view because in reality the battery's equivalent capacitance is bigger than in digital simulations and so the voltage ripple will be much smaller.

6. The Optimization Design

6.1. The method

We selected the direct search modified Hooke – Jevees method for the optimization design due to its rather low computation time.
Two distinct objective functions *F(x)* are considered:
- minimum weight or
- maximum efficiency

A dedicated C++ software code called FRM-97 has been written for the scope.
The variables in the FRM-97 are:
j_{cob}(A/m^2) - current density at lowest speed n_b and power P_b.
$\lambda = L / D_r$ - stack length / rotor diameter
f_x (N/m^2) - tangential specific force
B_{cs} (T) - stator back iron flux density.
The initial data file contains many other entries (variables) as well.
These variables are interrelated as in the conceptual design, at lowest speed n_b and power P_b, to produce the total weight and efficiency.
We set j_{cob}, λ, f_x and B_{cs} to initial values and define a serial of exploratory and pattern moves and accuracy checks of step size.
According to the modified Hooke – Jevees method a certain number of moves with smaller and smaller steps lead to the minimum of weight or of the reciprocal of efficiency.
The optimization design means certain machine geometry for a particular combination of variable values.

6.2. The constraints

First of all the stator core (pole) temperature is imposed to have a certain value acceptable to the PMs (T_{core} = 75 – 100^{0}C). Then the variables are limited to some values, our case $j_{cob} < 16 \cdot 10^6$ (A/m^2); $f_x < 7 \text{x} 10^4$ N/m^2; $B_{cs} < 1.5$T.
Minimum allowed efficiency for minimum weight search and respectively maximum allowed weight for maximum efficiency searches are set.
To render the problem as an unconstraint one we make use of sequential unconstraint minimization technique (SUMT). The modified objective function is:

$$F(x,r) = F(x) + \sum_{j=1}^{m} r_j^2 \left[\max\left(0, g_j(x)\right)\right]^2 \qquad (21)$$

where r_j is a penalty factor and $g_j(x)$ is the constraint condition and:

$$\begin{aligned} \max(0, g_j(x)) &= 0 \text{ when } g_j(x) \le 0 \\ &= g_j(x) \text{ when } g_j(x) > 0 \end{aligned} \qquad (22)$$

The functions $g_j(x)$ are, for example:

$$\begin{aligned} g_1(x) &= j_{cob} - j_{cobmax};\ j_{cobmax} = 16 \cdot 10^6 \text{ (A/m}^2\text{)} \\ g_2(x) &= B_{cs} - B_{csmax};\ B_{csmax} = 1.5\text{T} \end{aligned} \qquad (23)$$

In essence when a constraint condition is violated, the modified objective function is heavily penalized through the value of the penalty factor r_j.

6.3. Optimization design results

Sample results for the specifications in paragraph 4 are presented in tables 2 & 3.

Table 2. Minimum weight optimization (FRM-97)

Lambda (initial)	**1.2**	**1.0**	**0.8**	**0.5**
G total (weight) kg	4.1114	4.114	4.116	4.116
Eta (efficiency)	0.811	0.81	0.8117	0.8114
K_s (saturation coefficient)	0.014	0.0143	0.15	0.015

Table 3. Maximum efficiency optimization

Lambda (initial)	1.2	1.0	0.8	0.5
G total (weight) kg	6.983	6.998	6.999	7.0
Eta (efficiency)	0.936	0.937	0.937	0.937
K_s (saturation coefficient)	0.0075	0.00777	0.00812	0.0093

An optimal minimum weight design printout is shown in table 4.

Table 4.

```
/*////////////////////////////////////////////////////*/
/* FLUX REVERSAL MACHINE - OPTIMAL DESIGN/*/
/*      Design results - International units      /*/
/*////////////////////////////////////////////////////*/
```

Optimization data		
Machine type (1-motor, 0-generator)		0.000000e+00
Optimization (1-efficiency, 0-weight)		0.000000e+00
Li/Dr	lambda	1.000000e+00
Stator core flux density	Bcs	1.200000e+00
Fx	fx	2.160000e+04
Jcob	jcob	1.300000e+07
Core design		
Electromagnetic power	Peb	1.848825e+03
Voltage	Vdc	5.600000e+01
Rotor external diameter	Dr	6.280942e-02
Ideal stack length	L	6.280942e-02
Stack length	Ls	6.611518e-02
Electromagnetic torque	Teb	8.407135e+00
PM remanent flux density	Br	1.184275e+00
PM coercive forc	Hc	5.120500e+05
PM radial thickness	hm	4.000000e-03
Stator core radial depth	bcs	2.248857e-03
Rotor core radial depth	bcr	2.248857e-03
External stator core diameter	Dse	1.052662e-01
Weights		
Copper weight	Gcopp	1.116053e+00
Stator poles weight	Gps	3.669505e-01
Stator core weight	Gcs	3.474244e-01
Rotor poles weight	Gpr	5.164271e-01
Rotor core weight	Gcr	1.087588e-01
Aluminum frame weight	GAl	1.658160e+00
Total weight	Gtotal	4.113774e+00
Loses		
Copper loss at base speed	Pcopp	3.151701e+02
Core loss at base speed	Pcore	3.655382e+00
Calculated saturation factor	Ks	1.403546e-02
Calculated efficiency	etab	8.113259e-01

We should mention that the optimization process converges in general after up to about 100 iterations. Also as shown on tables 2 and 3, starting from very different initial values of variables, the same optimization design results are obtained. This is to say that a global optimization solution is obtained.

7. Conclusion

The paper presents a new automobile generator with stator PMs. Extensive digital simulations and design optimisation show promise of good performance for larger powers.

8. References:

1. G. Henneberger *"Automotive Electric Equipments"* (in german) F. Vieweg & Sohn Verlag Gmbh, Braunschweig, 1990
2. G. Henneberger, S. Kueppers, I. Ramesohl *"Numerical Calculations, Simulation and Design Optimization of Claw Pole Alternators for Automotive Application"* In: Proceedings of IEEE – International Conference Of Electric Machines & Drives, 1996, p.311 – 315
3. T. Radomski *"Alternating Current Generators"* US Patent 4,882,515, 1989
4. Ch. D. Syverson, N. Mankato *"Hybrid Alternator"* US Patent 5,97,975, 1995
5. F. Liang, J. Miller, S. Zarei *"A Control Scheme to maximize Output Power of a Synchronous Alternator in a Vehicle Electrical Power Generator System"* In: Proceedings of IEEE – IAS – 1996 Annual Meeting, 1 vol.2, p.830-835
6. G. Amaratunga, P. Acarnley, P. McLaren *"Optimum Magnetic Circuit Configurations for Permanent Magnet Aerospace Generators"* In: IEEE Transactions, vol. AES –21 no. 2, 1985, p.230-254
7. H. J. Gutt, J. Mueller *"New Aspects for Developing and Optimizing Modern Motorcar Generator"* In: Proceedings of IEEE IAS 1994 Annual Meeting
8. S. Nonaka, K. Kesawara *"Analysis of New Brushless Self-Excited Single Phase Synchronous Generator by Finite Element Method"* In: Proceedings of IEEE IAS, 1994 Annual Meeting, vol. 1 p. 198-203
9. I. Boldea *"Reluctance Synchronous Machine and Drives"* In: OUP 1996, p. 97-106
10. B. Sarliogly, Y. Zhao, T. A. Lipo *"A Novel Doubly Salient Single Phase PM Generator"* In Proceedings of IEEE-IAS 1994, Annual Meeting, part one p. 9-15
11. R. Deodhar, S. Anderson, I. Boldea, T. J. E. Miller *"The Flux Reversal Machine – a New Brushless doubly Salient, PM Machine"* In: Proceedings of IEEE-IAS , 1996, Annual Meeting, vol. 2, p. 786-793
12. I. Boldea, E. Serban, R. Babau, *"Flux Reversal Stator-PM Single Phase Generator With Controlled d.c. Output"* In: Proceedings of OPTIM 1996 International Conference, Brasov Romania, p.1123-1131

BEGA - A BIAXIAL EXCITATION GENERATOR FOR AUTOMOBILES

Ion BOLDEA- IEEE Fellow **Sever SCRIDON** **Lucian TUTELEA**
Department of Electrical Engineering, University Politehnica of Timisoara, V. Parvan 2 Blvd., 1900-Timisoara, Romania
Phone/Fax: +40 56 204402, E-mail: boldea@lselinux.utt.ro

Abstract: *This paper proposes a novel, biaxial excitation, generator for automobiles (BEGA) which has a three phase stator and a salient pole excited heteropolar rotor with multiple flux-barriers filled with low cost permanent magnets. Low voltage regulation is obtained due to the flux-barrier PM combination and, with field (excitation) low power control and a full power diode rectifier in the stator, good power/volume and superior efficiency (80% or more) are obtained at costs comparable to those of existing Lundell generator systems.*
The novel system configuration, principle, performance, equations, conceptual design, finite element field analysis, performance caracteristics and preliminar tests results for a 3kW, 9000rpm, 42 V d.c. case study make the core of the paper.

Keywords: *Automotive Electrical Equipment; High speed permanent magnet synchronous generator; Pspice simulations; Magnetic field in electrical machine; Finite Element Method*

1. Introduction

Claw-pole generators (fig. 1.a) with a diode rectifier in the stator and d.c. output voltage control through a low power d.c.-d.c. converter acting on the field winding voltage (fig. 1.b) are standard devices on practically all contemporary on road vehicles (automobiles).
They are rather robust have low cost and good power/volume at the expense of rather low over all efficiency (below 50 –55 % at full load and speed).
As more and more electric power is required on the cars of the future [1] and the speed and efficiency of claw-pole rotor generators are low (limited), new configurations are explored, besides assisting claw-pole rotors with PMs [2].
PM rotor generators with radial [3] or axial [4] airgap have been recently proposed but the costs of the strong PMs (NeFeB) and of the rated power static converter (controlled rectifier or diode rectifier plus d.c.-d.c. converter) still seem prohibitely high even for 42 V d.c. levels.

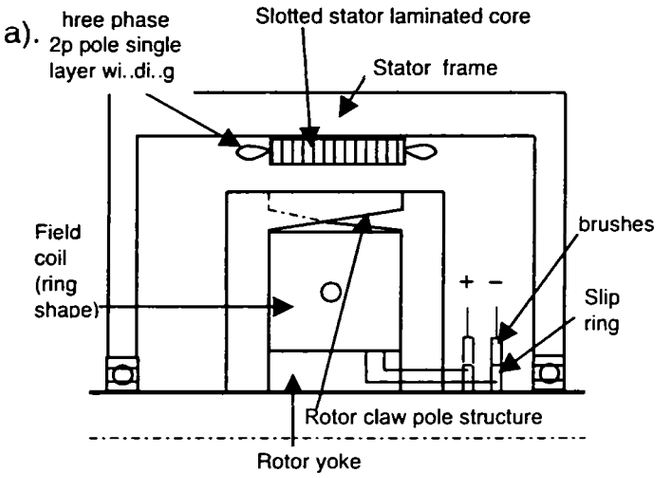

Fig. 1. Claw-pole rotor generator

Though other configurations such as switched reluctance, reluctance or doubly salient stator PM have been suggested to be considered for automotive applications [5], no full scale competitive prototypes have been demonstrated to the best of our knowledge. This is why we do not refer to them here.
In an effort to increase power and efficiency without raising costs notably or further more sacrifying power, a generator which blends the advantages of field current (low power) electronic control with unity power factor, zero (and negative) q axis flux linkage operation of a multiple flux barrier salient pole rotor with low cost (ferrite) PMs in axis q is hereby proposed.
Thus, basically the field current (low power) control as used in claw-pole generators may be maintained. Also the large claw-pole eddy current losses are eliminated.
In what follows, we start with the presentation of a biaxial excitation generator for automobiles (BEGA) topology and operation principles and continue with the mathematical model (core loss included), a conceptual design methodology by example (3 kW at 42/14 V), performance assessment at various speeds

and loads, and preliminary experimental results to validate the calculated performance.

Note: Ref [6]-[7] also introduce some hybrid excitation (coil heteropolar in axis *d* plus some PMs) but the PMs are of high energy (and costs) and are placed in axis *d* in two separate sections [6] or the excitation coil on stator produces homopolar excitation [7] or the rotor configuration is combersome and PM fringing flux is large [8].

In all these cases, the rotor and stator length (and volume), losses and rotor weight are higher than for BEGA and no use of high saliency on the rotor is made.

2. The biaxial excitation generator for automobiles (BEGA)

The claw-pole rotor generator [2] has two main drawbacks:

- the large (and increasing with speed) solid-iron claw-pole eddy current losses; low efficiency is a consequence.
- The large voltage regulation (due to large inductances) with large e.m.f., and thus full field current even at high speeds. Large voltage and flux harmonics at high speeds, cause additional core losses.

As only a full power diode rectifier is used to obtain d.c. output, with field current (low power) control, the claw-pole rotor generator controller (and system) is manufactured at total low costs.

Maintaining the same power electronics controller in a new solution is considered here the key to a moderate costs and better performance new configuration.

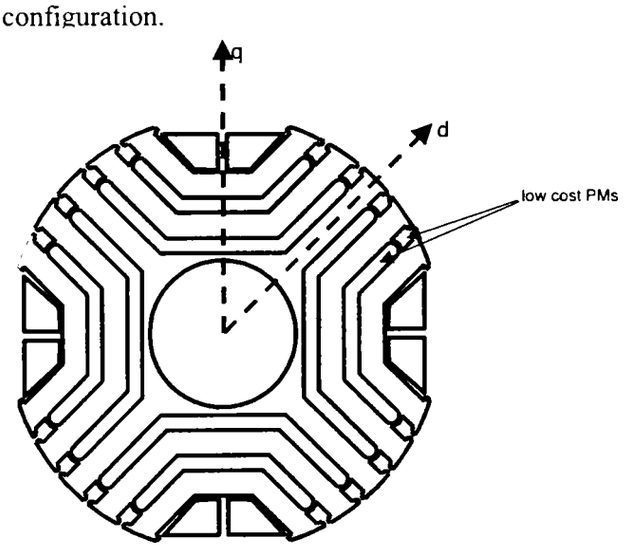

Fig. 2. The 4 pole rotor of BEGA.

The BEGA (figure 2) uses a laminated salient pole rotor with heteropolar electromagnetic excitation (2p = 4, 6, 8 poles) to eliminate the large addition losses in the existing claw-pole solid-iron rotor.

Through a reduction in the number of poles from 12 (14) for claw-pole rotor generators (CPRG) with ring-shape single coil excitation to 4 (6, 8) poles BEGA suggests increased excitation copper losses and larger yokes. The frequency (for given or higher speeds) is however smaller. The stator core losses plus the rotor excitation power losses are to be smaller than in CPRG.

Another feature of BEGA rotor is the presence on the rotor of multiple flux barriers filled with low cost (ferrite) PMs designed to fully compensate (destroy) the *q* axis stator produced flux linkage ($(\lambda_q)_{Irated}/2=0$).

Now as the diode rectifier produces unity power factor, for, say, half rated load , $\lambda_q = 0$. It follows that $I_d = 0$. Thus the *d* axis armature reaction is forced to zero.

Consequently, at half full load, the total e.m.f. E_{tl} is equal to no load (excitation) e.m.f. E_{0l} and thus the voltage equation (per phase) becomes similar to the case of a d.c. generator:

$$V_l = E_{0l} - R_s I_{qr} \;;\; I_{qr} = I_{rated}/2 \qquad (1)$$

With: $$E_{0l} = 2\pi n P L_{mf} I_f \qquad (2)$$

P – pole pairs; n – speed in rps; L_{mf} – mutual inductance; R_s – stator phase resistence; i_f - field current.

As expected the stator winding should be of single layer three phase type to simplify its manufacturing.

For lower loads (lower I_q) $\lambda_q = L_q I_q - \lambda_{PMq} < 0$ (3)

With: L_q – q axis inductance ; λ_{PMq} – q axis PM flux linkage.

Still the power factor remains unity. Equation (1) is now to be stightly modified to:

$$V_l = E_l - R_s I_s \;;\; I_s < I_{rated} \qquad (4)$$

$$I_s = I_d + \mathrm{j}\, I_q \qquad (5)$$

$$E_l = 2\pi p n\, \lambda_s \;;\; \lambda_s = I\, \lambda_d + \mathrm{j}\, \lambda_q\, I \;; \qquad (6)$$

$$\lambda_d = L_{mf} I_f + L_d I_d > 0;\; \lambda_q = L_q I_q - \lambda_{PMq} < 0 \qquad (7)$$

with $\lambda_q < 0$ and $\cos\varphi_1 = 1$, equations (4) – (7) lead to the vector diagram of figure 3.

Similary for $i_q > I_{rated}/2$; $\lambda_q > 0$.

To avoid PM demagnetization in fact $L_{qm} i_{rated} = \lambda_{PMq}$.

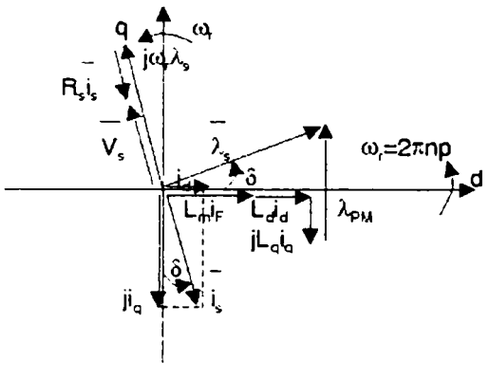

Fig. 3. The vector diagram for low load and unity power factor

So at half load $\lambda_q = 0$ and thus $I_d = 0$ ($\delta = 0$) but at lower loads as $\lambda_q < 0$, $I_d > 0$, that is magnetising.

At high loads $\lambda_q > 0$, but even for maximum load $\lambda_{qm} < 0$ to avoid PM demagnetization.

Notice that in claw-pole rotor generators $I_d < 0$ which explains the strong distortion of flux distribution at high speeds.

In our case I_d is small in general and, when the load decreases, the value of field current has to be reduced to zero, or even to negative values for high speeds.

The large voltage regulation is thus reduced notably with BEGA by adequate design.

3. Finite element analysis (FEA)

The FEA is aimed at demonstrating the possibility of full compensation (canceling) of q - axis airgap flux linkage at rated load with over compensation at lower loads by ferrite PMs in the hybrid rotor as on figure 2.

The study is done on a given geometry (figure 4).

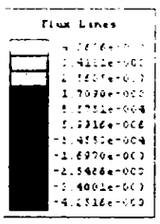

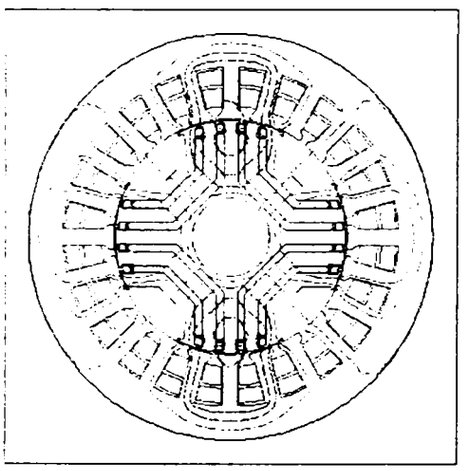

Fig. 4. Investigated cross section

Giving the geometry on figure 4, with $n_s = 22$ turns per slot and ferrite PMs with $B_r = 0.39$ T and $H_c = 225$ kA/m we are to find the I_{qr} current for which the total q axis airgap flux linkage in axis q is zero.

Notice that the end leakage inductance is not accounted for, so in fact for a higher $I'_{qr} < I_{qr}$ the zero q axis airgap flux condition is obtained.

The variation of q axis flux linkage / unit machine length:

$$\lambda_q / L_s = 2 / \pi \cdot B_{ql} \cdot \tau \cdot k_{wl} \cdot w_l \text{ ; Wb/m} \quad (8)$$

$$w_l = p\, q\, n_s;\ p = 2;\ q = 2 \quad (9)$$

τ - pole pitch $\tau = \pi\, ID / 2p = \pi\, 85 / 4$ mm (10)

$k_{wl} = 0.965$ (for $q = 2$, $Y / \tau = 1$ (full pitch winding)).

To account for the slot leakage flux the value of B_{ql} is calculated at the root of stator slots.

The q axis airgap flux density is shown on figure 5.

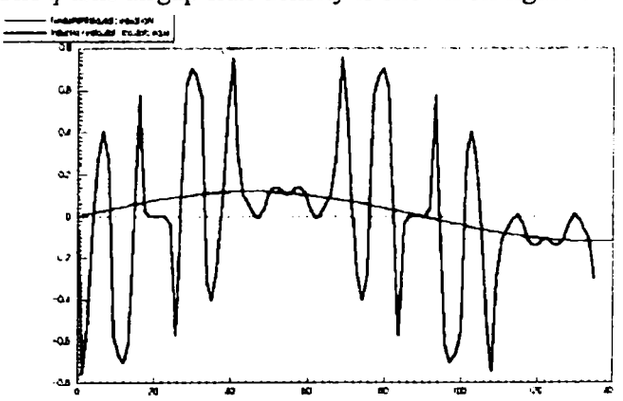

Fig. 5. Total aigap flux density in axis q versus position for $I_s = I_q =$ (rated value)

It is evident that is possible to provide a negative flux linkage in axis q (for zero airgap flux).

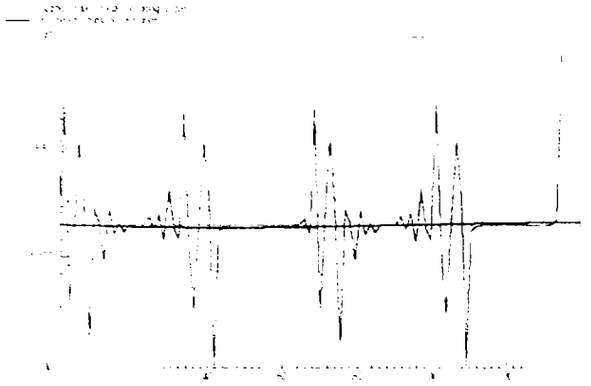

Fig. 6. The cogging torque versus position.

The cogging torque is moderate as the rotor surface looks rather smooth, figure 6. As shown on figure 5, the fundamental of flux density in the airgap along axis q is small but notable harmonics are present. Carefull design of rotor/stator slotting/flux barriers geometries should reduce these harmonics notably.

4. The circuit model equations

The dq model equations may be written as:

$$\overline{V_s} = R_s \bar{i}_s + \frac{\overline{d\lambda_s}}{dt} + j\omega_r \overline{\lambda_s} \qquad (11)$$

with:

$\overline{\lambda_s}$, $\overline{i_s}$ as of (5) – (6) and

$$\overline{V_s} = V_d + jV_q \qquad (12)$$

The speed versus time $\omega_r(t)$ is given for generator mode.

The core loss may be considered to be produced by the stator flux linkage λ_s in a parallel resistance R_{core}.

$$R_{core} = \frac{3}{2}\frac{(\omega_r \lambda_s)^2}{p_{core}}; \quad i_{core} = \frac{\omega_r \lambda_s}{R_{core}} \qquad (13)$$

with p_{core} measured or calculated through analytical or FEM methods.

Finally for unity power factor the voltage equation (4) becomes (for steady state):

$$V_1 = \omega_r \lambda_s - R_s\left(i_s + \frac{\omega_r \lambda_s}{R_{core}}\right) = \omega_r \lambda_s \left(1 - \frac{R_s}{R_{core}}\right) - R_s i_s \qquad (14)$$

This way the electrical efficiency can be easily calculated. Notice that the core loss produces an apparent reduction of stator flux linkage while in reality it causes an additional resistive voltage drop.

5. The block diagram

The block diagram of the BEGA system is shown on figure 7.

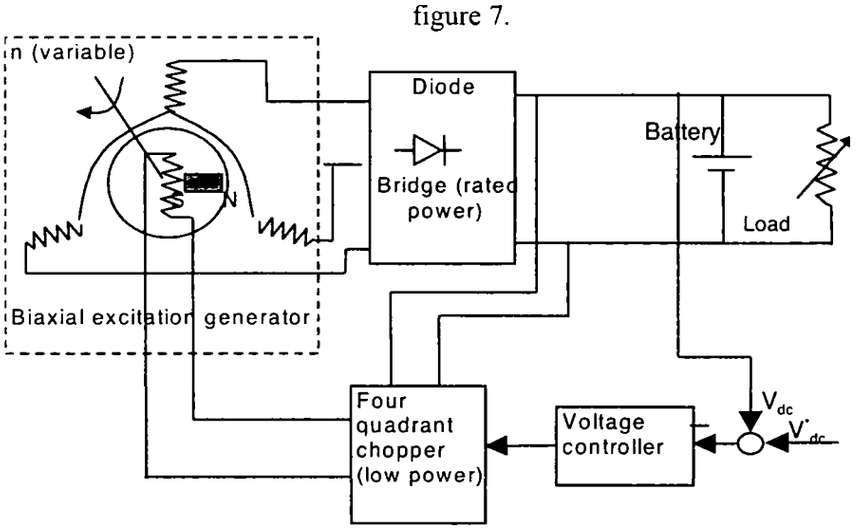

Fig. 7. The control system for BEGA

6. Conceptual design (summary)

A conceptual design should start from initial specifications:

Rated d.c. output voltage: V_{dc}= 42 V
Rated d.c. current: I_{dc}= 75 A (above 2 n_{min})
Idle engine speed: n_{min}= 1500 rpm
D.c. current at n_{min}: I_{dcm} = 75/2 A
Maximum speed: n_{max}= 9000 rpm

Additional data is required to start the dimensioning process.

The following data are considered (as a example):

- no load airgap flux density: B_{g0}= 0.65 T
- rated tangential force density: f_r = 2.0 N/cm^2
- rated stator current density: j_{cos}= 12 A/mm^2
- rated field current density: j_{cof}= 9 A/mm^2
- number of poles: $2p$ = 4
- stack length / bore diameter: $\lambda = L_s / ID$ = 0.6

Based on the above data, we may start by calculating the stator bore diameter ID through computing first the electromagnetic torque T_{ek}, with an assigned value of maximum efficiency at idle engine speed:

$$T_{ek} = \frac{V_{dc} I_{dcm}}{\eta_{nmin} 2\pi n_{min}} = \frac{42(75/2)}{0.8x2\pi 2(1500/60)} = 12.54 \text{ Nm} \quad (15)$$

Now the ID is:

$$ID = \sqrt[3]{\frac{2T_{ek}}{f_1 \pi \lambda}} = 0.09 \text{ m} \quad (16)$$

The stack length L_s is:

$$L_s = \lambda \cdot ID = 0.054 \text{ m} \quad (17)$$

We will assume that unity power factor is met through the use of the diode rectifier and battery back-up d.c. load. The designing of the BEGA rotor should be an iterative process and FE analysis is required for refinements but for start let us suppose that the Ferrite PMs, with B_r = 0.39 T with flux barrier/iron thickness of 0.6, and with the presence of an airgap g = 0.5 mm, produce an airgap flux density $B_{PMg} = (3/4)B_r$ = 0.3 T.

Let us consider that this suffices to provide the condition for zero q axis airgap flux at half rated current and $L_q i_{rated}/2 = \lambda_{PMq}$ ($L_{qm} \approx L_q/2$).

At idle engine speed half of rated current is delivered and thus the $L_q i_{nmin} = \lambda_{PMq}$.

Consequently the q axis airgap flux density in such conditions is $B_{PMg}/2$ = 0.15 T.

Notice that the field current (no load) airgap flux density is 0.65 T and the d axis current contribution (not yet known) should add more (though not much) to it.

The relationship between the phase RMS current I_1 and the output d.c. current I_{dc} is [2].

$$I_{dc} = \frac{3}{\pi}\sqrt{2}\cos\varphi_1 I_1 = K_i I_1 \quad (18)$$

$$K_i = 1.347$$

Also the relationship between the d.c. voltage and the phase RMS voltage is:

$$V_1 = \frac{V_{dc} I_{dc} + 3(V_D + R_D I_{dc}/K_i) I_{dc}/K_i}{3\left(\frac{I_{dc}}{K_i}\right)\cos\varphi_1} = \frac{V_{dc}}{K_V} \quad (19)$$

where V_D is the residual diode voltage drop and R_D is the equivalent diode resistance.

In general V_D= 0.6 - 0.8 V and $R_D I_{DC}/K_i < 1$ V.

To simplify the calculations for V_{dc}= 42 V we may consider $V_D + R_D I_{DC}/K_i$ = 1.8 V (constant).

Thus:

$$V_1 \approx \frac{V_{dc} I_{dc} + 3x1.8 I_{dc}/K_i}{3 I_{dc}/K_i \cos\varphi_1} \quad (20)$$

Now, with given efficiency η_{nmin}, the voltage equation (12) may be applied ($V_1 = V_s$):

$$3V_1(I_{rated}/2) = -(p_{copper} + p_{core})_{nmin} + 3(2\pi n_{min} \lambda_s I_{rated}/2$$

with: $\eta_{nmin} = 0.8$ (21)

$$\frac{3V_1}{\eta_{nmin}} = 3x2\pi n_{min} P \lambda_s \quad (22)$$

With (18) and (20) and I_{Dcmin} = 75/2;

$$I_{rated}/2 = 75/2/1.347 = 27.84 \text{ A} \quad (23)$$

Also: $V_s = V_1$ = 20.658 V.

From (22)

$$\lambda_s = \frac{V_1}{\eta_{nmin} 2\pi n_{min} P} \quad (24)$$

Now: $$\lambda_s = B_{g1}(2/\pi) L_s \cdot \tau \cdot K_W \cdot W_1 \quad (25)$$

The winding coefficient K_{W1} (for q = 2, Y/Y = 6/6) is:

$$K_{W1} = \frac{\sin\frac{\pi}{6}}{q\sin\frac{\pi}{6q}} \quad (26)$$

The pole pitch τ is:

$$\tau = \frac{\pi ID}{2P} \quad (27)$$

To figure out a value for the fundamental airgap flux density we should first estimate its value produced by the field current alone, B_{gF1}:

$$B_{gF1} = B_{gF}\frac{4}{\pi}\sin\frac{\pi}{2}\frac{\tau_p}{\tau} \quad (28)$$

where τ_p is the pole shoe span in the rotor.

For τ_p/τ = 0.8 we obtain:

$$B_{gF1} = 0.75\text{T} \quad (29)$$

Now the augmentation of B_{gF1} through the armature reaction at $I_{rated}/2$ (1500 rpm) could be considered to be of 0.05 T only, with B_{g1} = 0.8 T.

Consequently the member of turns per path (two paths in parallel are considered) is:

$$W_1 = \frac{\pi \lambda_s}{2 B_{g1} L_s \tau K_{W1}} \quad (30)$$

The number of turns per slot W_c is:

$$W_c = 2W_1/Pq \quad (31)$$

with I_{rated} = 55.6 A, j_{cos} = 12 A/mm^2, the stator winding wire diameter d_{cos} is:

$$d_{cos} = \sqrt{\frac{4}{\pi} x \frac{55.x6}{2x12}} = 1.717mm \quad (32)$$

With a slot filling factor K_{fill} = 0.45, the slot useful area A_{slot} is:

$$A_{slot} = \frac{W_c(I_{rated}/2)}{K_{fill} j_{cos}} = \frac{22x55.6}{0.45x12x2} = 113.26mm^2 \quad (33)$$

The slot pitch τ_s is:

$$\tau_s = \tau / 3q \quad (34)$$

The base slot width b_{s1} = 6 mm. The trapezoidal slot is shown on figure 8.

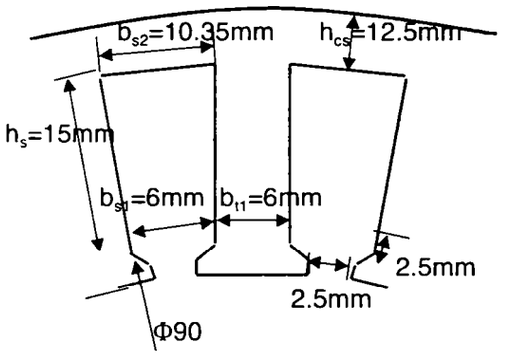

Fig. 8. The stator slot

Finally with the slot height h_{su} = 15 mm, b_{s2} = 10.35 mm we obtain a useful slot area very closed to the required one (120 mm).

The stator yoke h_{cs} is

$$h_{cs} = \frac{1}{\pi} \frac{B_{g1}\tau}{B_{cs}} \quad (35)$$

Finally the outer stator diameter OD is :

$$OD = ID + 2 \cdot 2.5 \cdot 10^{-3} + 2h_s + 2h_{cs} = $$
$$= (90 + 5 + 30 + 25)10^{-3} = 0.150 \text{ m} \quad (36)$$

Now basically we have the main data to calculate the machine inductances and resistance.

The field winding

Still essential is the sizing of the field winding.

With a given airgap flux density B_{gF} and a saturation coefficient (which has to be verified) K_s:

$$W_F i_F = (B_{gF}/\mu_0) g K_c (1 + K_S) \quad (37)$$

with K_c = 1.15 and K_s = 0.40, g = 0.5x10^{-3} m

$$W_F i_F = \frac{0.65x0.5x10^{-3}x1.15x1.4}{1.256x10^{-6}} = 416Aturns \quad (38)$$

with a design current density j_{cof} = 9 A/mm^2 and K_f = 0.45, the pole window half-area A_W is:

$$A_W = \frac{W_F i_F}{K_{fill} j_{cof}} = \frac{416}{0.45x9.0} = 102.72 \text{ mm}^2 \quad (39)$$

This room is available, as evident in figure 2.

The field coil main turn length l_{cF} is:

$$l_{cF} = 2L_s + 1.5\tau + 4\pi W_{coil}/2 =$$
$$= 2 \cdot 0.054 + 1.5 \cdot 0.07065 + 4\pi \cdot 0.001/2 = 0.276\text{m} \quad (40)$$

The voltage equation for the field circuit is:

$$V_{dc} K_D = \rho_{co} 2P W_F \cdot l_{cF} \cdot j_{coF} =$$
$$= 42 \cdot 0.92 = 2.3 \cdot 10^{-8} \cdot 4 \cdot W_F \cdot 0.276 \cdot 9 \cdot 10^{-6} \quad (41)$$

$$W_F = 169 \text{ turns/coil}; \; i_F = W_F \cdot i_F / W_F = 416.6 / 169 =$$
$$= 2.465 \text{ A} \quad (42)$$

The power in the field winding p_{cof} is:

$$p_{cof} = V_{dc} i_F = 42 \cdot 2.465 = 103.5 \text{ W} \quad (43)$$

The coefficient K_D = 0.92 accounts for the losses in the low power d.c.-d.c. converter used to control the field current.

The wire gauge d_F is:

$$d_F = \sqrt{\frac{4}{\pi} \frac{i_F}{j_{cof}}} = \sqrt{\frac{4}{\pi} x \frac{2.465}{9}} = 0.59mm \quad (44)$$

So each field coil has 169 turns made of 0.59 mm diameter wire (class F).

Machine parameters

In a rather straightforward manner we obtain the machine parameters.

The stator phase resistance R_s (two current paths in parallel) is:

$$R_S = 0.05775\Omega$$

The d and q axis inductance:

$$L_d \approx 3.483 \cdot 10^{-3} \text{ H}$$
$$L_q \approx 0.66 \cdot 10^{-3} \text{ H}$$

l_{cs} - the stator turn length:

$$l_{cs} = 2l_s + 0.02 + 2.5y = 2 \cdot 0.054 + 0.02 + 2.5 \cdot$$
$$\cdot 0.07065 = 0.268 \quad (45)$$

y- coil span

The PM flux:

$$\Lambda_{PMq} = 1.7608 \cdot 10^{-2} \text{ Vs}$$

The mutual inductance:

$$L_{mf} = 31.287 \cdot 10^{-3} \text{ H}$$

Thus the rated power loss p_{cos} will be:

$$p_{cos} = 3R_s i^2_{rated} = 3 \cdot 0.0577 \cdot (55.6)^2 = 540 \text{ W} \quad (46)$$

Finnaly the field winding inductance:

$$L_F = 0.598 \text{ H}$$

The field winding resistance (4 coils in series) R_F is:

$$R_F = V_{dc}/i_F = 42/2.465 = 17.0385\ \Omega \quad (47)$$

Tentative total electrical efficiency at 1500 rpm.

After estimating the core loss, we finally obtain at 1500rpm and 1.575W output, an efficiency of 80%

Active material weights

The copper, iron and PM weights together make 7.35Kg.

It can be said that the even in torque/weight BEGA is slightly better than existing claw-pole generators while the efficiency is notably higher (above 80% at all speeds).

The price of the system (generator + controller) will be (probably) at most 20% higher because the generator costs will be higher by 25% or so due to the ferrite PM rotor added complexity and excitation four quadrant chopper controller.

$V_s = 20.658 \text{ V} \approx \text{ct}$

$R_s = 0.0577\ \Omega$

$L_{mF} = 31.287\text{x}10^{-3}$ H

$L_d = 3.33\text{x}10^{-3}$ H

$L_q = 0.48\text{x}10^{-3}$ H

$\lambda_{PMq} = 0.017608$ Vs

$i_s = 55.6$ A

We will explain the steady state operation domains for 1500 rpm (when half full power is to be produced already) 3000rpm and for 9000 rpm (maximum speed) when the control is lost from a fraction of rated power downward. Fortunately at highest speed there is some load all the time.

From (4)-(6) we obtain:

$$\lambda_s = (V_s - R_s i_s) / 2\pi Pn \quad (48)$$

$$K_d = i_d/i_s = \frac{\lambda_s \lambda_{PM} \pm L_q i_s \sqrt{\lambda_s^2 - \lambda_{PM}^2 + L_q^2 i_s^2}}{\lambda_s^2 + L_q^2 i_s^2} \quad (49)$$

$$I_q = i_s \sqrt{1 - \left(\frac{i_d}{i_s}\right)^2}\ ;\ P = 3V_s i_s \quad (50)$$

The results are shown on figure 9, for 1500, 3000, 9000 rpm.

Steady state operation domains

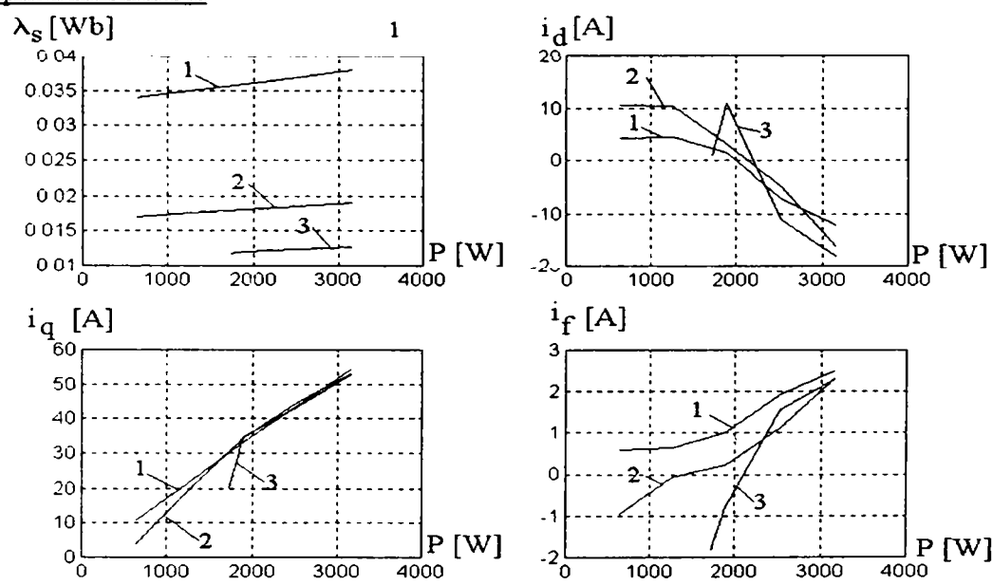

Fig. 9. Simulation results for:
Stator flux (λ_s) vs. power
d axis current (i_d) vs. power
q axis current (i_q) vs. power
Excitation current (i_F) vs. power (where: 1-50Hz; 2-100Hz; 3-300Hz)

Pspice complete simulations not shown here from lack of space show that while for 1500rpm 1.5kW at 42Vd.c. is available, from 1650 rpm forward (already) full power (3kW, at 42Vd.c.) is available which is much better than in claw pole generators.

Notice the negative field current values at high speeds and lower loads.

7. The prototype and very preliminary test results

The prototype has the following main data:

Rated d.c. output voltage:	V_{dc}= 42 V
Rated d.c. current:	I_{dc}= 75 A
Speed ratio:	n_{max}/n_{min}= 1/6
Maximum speed:	n_{max}= 9000 rpm
Power:	P_n=1,5...3 kW
Airgap:	g = 0,5mm
Rotor external diameter:	D_{rext} = 0.085m
Stator external diameter:	D_{sext} = 0.15m
Rotor stack length:	L_r = 0.07m.

The very preliminary tests are shown as follows:

No load test results

For different values of excitation currrent the induced voltage given by the generator was measured (figure 10).

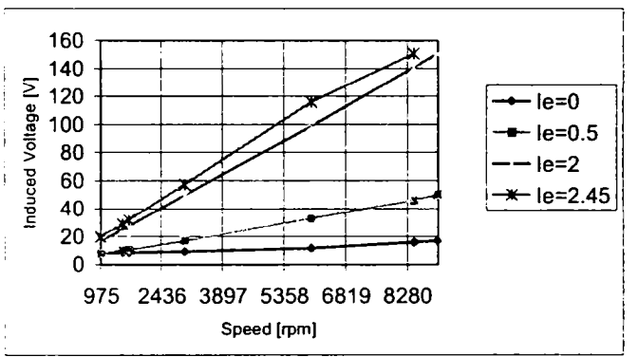

Fig. 10. The induced voltage vs. speed for different excitation currents

The d axis and q axis inductances have been measured in a.c. standstill tests (figure 11).

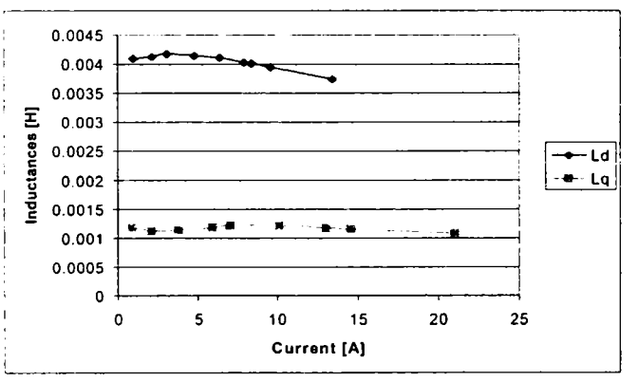

Fig. 11. The d axis and q axis inductances vs. current

Short-circuit tests

The short-circuit test have been performed without excitation current and for a I_e=1.9A excitation current (figure12).

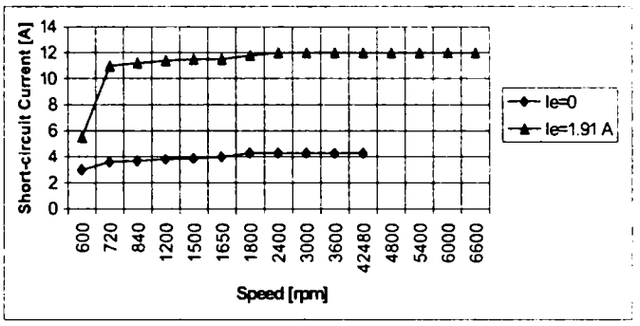

Fig. 12. The short-circuit current vs. speed at different excitation currents

8. Conclusion

It should be noted that :

- Full power range controll is available up to 6000 rpm and higher, but at 9000 rpm even with negative field current (figure 7) not less than 54% rated power can be delivered.
- The excitation current should be controlled for positive and negative values through a 4 quadrant chopper.
- The values of i_q remain positive but i_d could be ei..e. p..i.i e .. neg..i e .epen.ing .n .pee. and load.
- Half rated power is delivered at 1500 rpm but full power is already available from 1650 rpm.
- More work is needed to fully establish the BEGA system.

References:

1. I.G. Kassakian, H.C. Wolf, I.H.Miller, C.H.I. Hurton: *"Automotive electrical system circa 2005"* In: IEEE Spectrum, August 1996, p. 22-27
2. S. Kueppers: *"Numerische Verfahren zur Berechnung und Ausle von Drehstrom Klauenpolgeneratoren"* In: Ph. D. Thesis, Shaker Verlag, Aachen Germany, 1996
3. M. Naidu, M. Boules, R. Henry: *"A high efficiency, high power generation system for automobiles"* In: Proceedings of IEEE- IAS 1995 -Annual Meeting, p. 709- 716
4. H.I.Gutt, I. Mueller: *"New aspects for analysing and optimizing modern motorcar generators"* In: Proceedings of IEEE-IAS 1994 - Annual Meeting, vol.1, p. 3-8
5. I. Boldea *"Automotive electric generator systems. A review."* In: Proceedings of ELECTROMOTION 1999, vol. 1, pp.7-19, July 1999, Patras, Greece
6. C.D. Syverson et all *"Hybrid alternator with voltage regulator"* - U.S. Patent (5502368, March 26, 1996)
7. Mizuno, Takyuki, C/O Kabushiki, Kaisha Meidensha *"Hybrid excitation type permanent magnet synchronous motor"* European Patent Application (941056335, 12.04.1994)
8. Mutter Albert *"Elektrische maschine und deren anwendung zum fahrzeugbetrieb"* Patentschrift DE (413943C2, 03.12.1991)
9. T.M. Jahns: *"Uncontrolled generator operation of interior PM synchronnes machines following high speed inventer shut down"* In: Proceedings of IEEE-IAS 1998 - Annual Meeting, vol.1.

CHARACTERIZATION OF BIAXIAL EXCITATION GENERATOR FOR AUTOMOBILES

Ion BOLDEA – Fellow Member IEEE, Ewen RITCHIE*, Frede BLAABJERG* - Senior Member IEEE, Sever SCRIDON, Lucian TUTELEA
Department of Electrical Engineering, *Politehnica* University of Timisoara,
2, V. Parvan Blvd., RO-1900 Timisoara, Romania
Phone/Fax: +40 56 204402, E-mail: boldea@lselinux.utt.ro
*Department of Electrical Energy Conversion, Institute of Energy Technology,
Aalborg University
101 Pontoppidanstraede, DK-9200 Aalborg East, Denmark,
Phone: +45 96359254, Fax: +45 98151411, E-mail: fbl@iet.auc.dk

Abstract – **This paper presents the d-q model, operational direct and quadrature axis inductances by means of locked-rotor tests, together with other characteristics for a 3 kW, 9000 rpm, 42 V d.c. prototype of biaxial excitation generator for automobiles (BEGA).**
Despite the good power/volume ratio and low costs but due of their low efficiency, the actual exclusively used automotive alternators, the claw-poles generators, will be replaced in the near future by new types of electrical generators which has to generate more power by keeping the approximately the same volume as before.
In order, new improvements were made by inserting PM's in various ways or by changing the number of poles but those solutions has not solved the efficiency problems and neither system dynamic behave for consumer voltage recovery.
The biaxial excitation generator for automobiles (BEGA) has a three-phase stator and a salient pole excited hetero-polar rotor with multiple flux-barriers filled with low cost permanent magnets. Its configuration, operation principle, d-q model equations, operational parameters and some promising performance characteristics results consitute the core of the paper.

Index terms – **High Speed permanent magnet synchronous generator, operational parameters.**

I. INTRODUCTION

In today's vehicles, the combustion engine directly drives many of the accessories. When the engine is cut off, during driving, also these accessories stop to operate. But systems like power steering, vacuum brake or air conditioning compressor must be available permanently. So it is mandatory to find alternatives to power these components.
To ensure a sufficient charging balance engine-driven alternator has to produce this increased average during vehicle running time and the batteries for the vehicle operation time.
An increased power demand for the alternator by a factor of about 4 compared to today's design is required, as long as no additional consumers are introduced.
Anyway, additional electrical consumers are expected to be introduced for safety (like on-board diagnosis systems) and comfort reasons (air conditioning). Improving alternators efficiency will allow producing more electric power with limited increase of the engine load and with minimal increase of their weight.
Today's 14 V electrical systems cannot cover the demands of these consumers, which often exceed 50 or 100 A. For this, 42 V electrical power generation and distribution systems are on their way to replace the existing 14 V systems in automobiles.
A 42 V power system would allow at least some of the functions provided now by propulsion engine, through a variety of belts and chain drives, to be driven by independent electric motors. Eliminating the need for belts and pulleys would bring some benefits in terms of saving space and simpler mechanical design.
The real gain would be the greater overall efficiency; in terms of energy efficiency a good example is to provide steering assistance with an electric motor that operates only as and when required.
To use the claw-pole generator for a large speed bandwidth, field-weakening domain, with effective conditions, some constructive changes were made, the result is the Rice-Lundell modified alternator.[3, 4]
Other constructive topologies, like switched reluctance, reluctance or doubly salient stator PM's have been suggested to be considered in automobile industry [5], but no full-scale competitive prototypes were demonstrated.
A new generator, the biaxial excitation generator for automobiles (BEGA), which blends the advantages of field current electronic control (so, at low power) with unity power factor, zero (and negative) q axis flux linkage operation of a multiple flux barrier salient pole rotor with low cost PM's in axis q is proposed. Together

with the principle equations, the conceptual design and performance characteristics have been presented for an existing prototype. [10]

The BEGA uses a laminated salient pole rotor with hetero-polar electromagnetic excitation (2p = 4, 6, 8 poles) to eliminate the large addition losses in the existing claw-pole solid-iron rotor.

Using a simple 4 quadrant low power chopper, placed in the field circuit (figure 10), the field current is controlled and so the output power of the generator.

The stator is a standard three-phase induction machine stator, with 24 slots. Through a reduction in the number of poles, from 12 (14) for claw-pole rotor generators (CPRG) with ring-shape single coil excitation, to 4 (6, 8) poles BEGA suggests increased excitation copper losses and larger yokes.

Another feature of BEGA rotor is the presence on the rotor of multiple flux barriers filled with low cost (ferrite) PM's designed to fully destroy the q axis stator produced flux linkage ($(\lambda_q)_{I_{rated}}/2=0$ – figure 1).

Now as the diode rectifier produces unity power factor, for, say, half rated load , $\lambda_q = 0$. It follows that $I_d = 0$. Thus the d axis armature reaction is forced to zero.

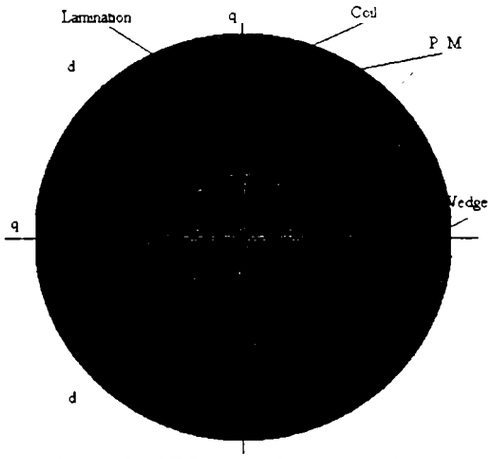

Fig. 1. The BEGA rotor has the flux barriers filled with low cost PM's.

The frequency (for given or higher speeds) is however smaller. At half load, the total e.m.f. E_{tl} is equal to no load (excitation) e.m.f. E_{0l} and thus the voltage equation (per phase) became similar to the case of a d.c. generator:

$$V_l = E_{0l} - R_s I_{qr} \; ; \; I_{qr} = I_{rated}/2 \tag{1}$$

with $$E_{0l} = 2\pi n P L_{mf} I_f \tag{2}$$

where P – pole pairs;
n – speed in rps;
L_{mf} – mutual inductance;
R_s – stator phase resistance;
i_f - field current.

As expected the stator winding should be of single layer three phase type to simplify its manufacturing.

For lower loads (lower I_q)

$$\lambda_q = L_q I_q - \lambda_{PMq} < 0 \tag{3}$$

With: L_q – q axis inductance; λ_{PMq} – q axis PM flux linkage.

Still the power factor remains unity. Equation (1) is now to be slightly modified to:

$$V_l = E_l - R_s I_s \; ; \quad I_s < I_{rated} \tag{4}$$

$$I_s = I_d + \mathrm{j}\, I_q \tag{5}$$

$$E_l = 2\pi p n \lambda_s \; ; \quad \lambda_s = l\,\lambda_d + \mathrm{j}\,\lambda_q\, l \; ; \tag{6}$$

$$\lambda_d = L_{mf} I_f + L_d I_d > 0;$$

$$\lambda_q = L_q I_q - \lambda_{PMq} < 0 \tag{7}$$

with $\lambda_q < 0$ and $\cos\varphi_1 = 1$.

Similary for $i_q > I_{rated}/2$; $\lambda_q > 0$.

To avoid PM demagnetization fac:

$$L_{qm} i_{rated} = \lambda_{PMq}. \tag{8}$$

In our case I_d is small in general and, when the load decreases, the value of field current has to be reduced to zero, or even to negative values for high speeds.

The large voltage regulation is thus reduced notably with BEGA by adequate design.

II. The Circuit Model Equations

Since the BEGA machine is a type of salient pole synchronous machine, a different value of stator inductance Ld and respectively Lq characterize each of the d and q axis equivalent circuits.

The d-q model equations may be written as:

$$\overline{V_s} = R_s \bar{i}_s + \frac{\overline{d\lambda_s}}{dt} + j\omega_r \overline{\lambda_s} \tag{9}$$

with:

$\overline{\lambda_s}$, $\bar{i}_s$ as of (5) – (6) and

$$\overline{V_s} = V_d + \mathrm{j} V_q \tag{10}$$

The speed versus time $\omega_r(t)$ is given for generator mode. The core loss may be considered to be produced by the stator flux linkage λ_s in a parallel resistance R_{core}.

$$R_{core} = \frac{3}{2}\frac{(\omega_r \lambda_s)^2}{p_{core}} \; ; \quad i_{core} = \frac{\omega_r \lambda_s}{R_{core}} \tag{11}$$

with p_{core} measured or calculated through analytical or FEM methods.

Finally, for unity power factor, the voltage equation (4) became (for steady state):

$$V_s = \omega \lambda_s - R_s\left(i_s + \frac{\omega \lambda_s}{R_{core}}\right) = \omega \lambda_s\left(1 - \frac{R_s}{R_{core}}\right) - R_s i_s \quad (12)$$

This way the electrical efficiency can be easily calculated. Notice that the core loss produces an apparent reduction of stator flux linkage while in reality it causes an additional resistive voltage drop.

III. The Prototype and Test Results

The prototype under test is presented in figure 2 and has the following main data:

Fig. 2. The BEGA prototype used for tests

Generator technical data:
Idle engine speed (minimum speed – n min): 1500 rpm
Maximum speed (n max): 9000 rpm
Max. Speed / min. Speed ratio: 1/6
Electrical power: 1,5 – 3 kW
Generating system data (including the rectifier)
Rated d.c. output voltage: Vdc = 42 V d.c.
Rated d.c current: Idc = 75 A (above 2 x n min)
D.c. current at n min: Idc min = 75/2 A
The stator:
Stator lamination material: DK 66 50 silicon sheet lamination steel
Sheet width: 0,5 mm
Stator outer diameter: SOD = 150 mm
Stator inner diameter: SID = 92 mm
Stack length: Lc = 94 mm
Number of slots: 24
Number of stator poles: 2p = 4
Number of phase: m = 3
Number of turns on stator phase: N1 = 24
Parallel current path: p = 2
Layers: 1
Number of stator slots per pole per phase: q = 3
Stator coils – Cu – Y connection:
Number of conductors per slot: 8
Insulated conductors dimension: 2x1,608 (2x1,5 without insulation)
The rotor:
Lamination material: DK 66 50 silicon sheet lamination steel for ABB Motors Odense
Sheet outer diameter: ROD = 91 mm
Sheet inner diameter: RID = 29 mm
Sheet width: 0,5mm
Number of sheets: 175 pcs.
The Permanent Magnet:
Material: Ferrite
HcB = 260 kA/m max.
Hcj = kO kA/m max.
Br = 0,36 T
Heig t: = ,8 ± ,1 mm
Length: L = 92 mm
Width: w = 15 mm
The field coil:
Four Copper coils in serial connection:
Number of conductors per coil: 116
Insulated conductor dimension:1x0,79 (1x0,71 without insulation)
Frame
Aluminium : Size 90, for ABB motor type QU 90L

IV. The Results

From static transient tests, the direct axis reactance and quadrature axis reactance were calculated.
The most used method to determine the direct axis reactance is using the results from the ideal no load and symmetrical three phase short circuit permanent operations. From the first one, the e.m.f., V_s, is measured and from the second, the short circuit current, I_{sc}, both measurements are made at the same excitation level resulting the direct axis synchronous reactance as follow:

$$X_d = V_s / I_{sc} \quad (13)$$

This relative simple method, requires two separate tests and implies mechanical coupling between the machine under tests and a driving motor.
Another method is the standstill frequency method that requires a complex test stand with a variable frequency power generator.
A more simple method is the d.c. decay (transient) method [12] which is a standstill method and consist of applying a step voltage into the stator winding of the machine by closing the breaker K and recording the corresponding current waveforms.
In this case the direct axis reactance is:

$$X_d = \frac{R_s \omega_n}{I_{d0}} \int_0^\infty i_d(t)dt \quad (14)$$

The quadrature reactance is:

$$X_q = \frac{R_s \omega_n}{I_{q0}} \int_0^{\infty} i_q(t)dt \qquad (15)$$

The phase resistance, R_s, measured value is 0.17Ω. With the rotor locked in d axis position, and than in q axis position (rotating with 90^0 electrical degrees), the operational reactance were measured using a performant oscilloscope monitoring the direct and quadrature currents waveforms.

The R_f resistance is for protection of the d.c. source when K is closed.

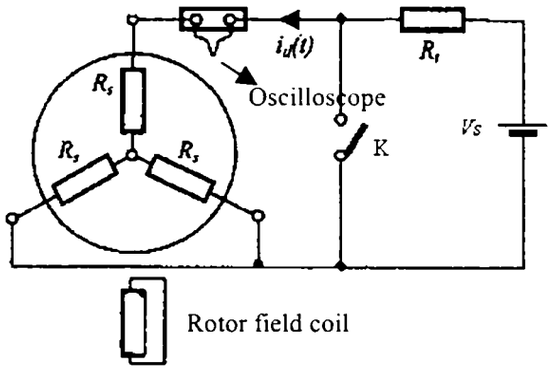

Fig. 3. The setup for direct axis reactance measurement

The recordings of current waveforms for both axes are presented in figures 4 and 5.

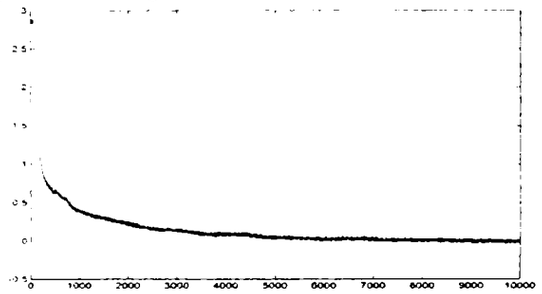

Fig. 4. Direct axis transient current from d.c. decay test

In figure 4, the presented current waveform is obtained through data acquisition and numerical analysis using MATLAB software program.

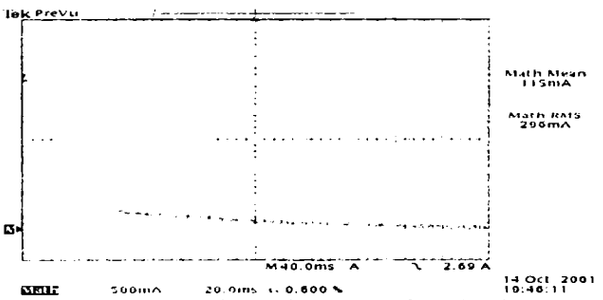

Fig. 5. Quadrature axis transient current from d.c. decay test

The current waveform from figure 5 was obtained using an oscilloscope.

Knowing the stator phase resistance, the rated speed, the initial currents and having the current waveforms, the direct axis reactance and quadrature reactance were calculated and compared with the values predicted.

Next figures (from figure 6 to figure 9) show us the measured impedances (inductances and resistances) in the direct and quadrature axis as a function of the frequency.

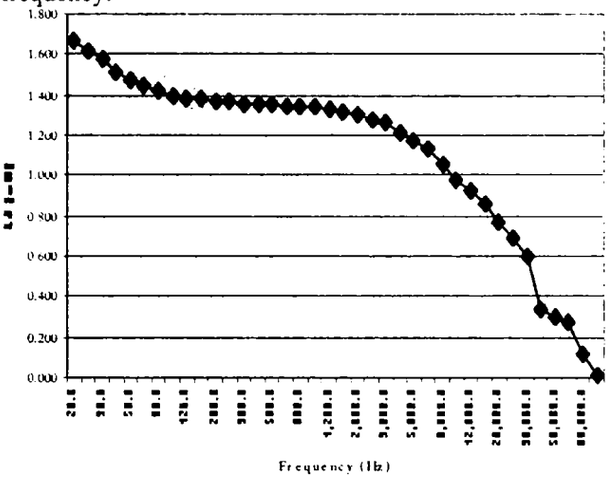

Fig. 6. Direct axis inductance versus frequency

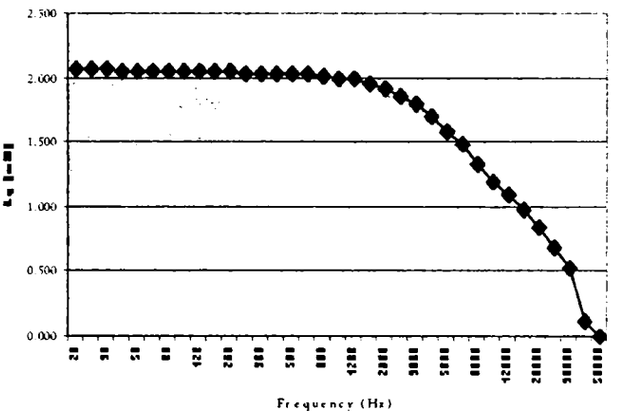

Fig. 7. Quadrature axis inductance versus frequency

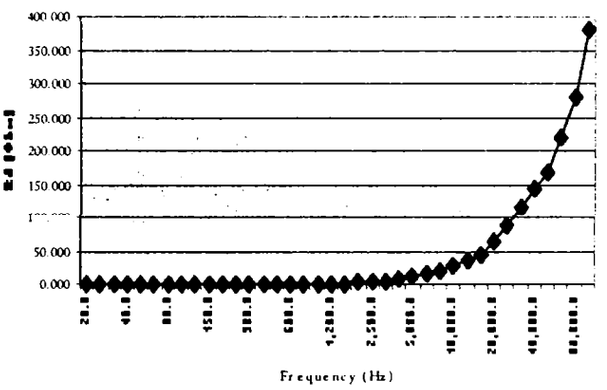

Fig. 8. Direct axis resistance versus frequency

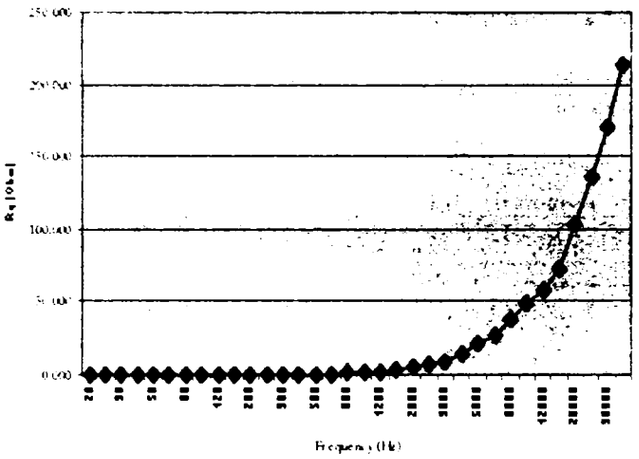

Fig. 9. Quadrature axis resistance versus frequency

As was predicted by analytical design equations, the d.rec. ax.s operat.onal .nduc.ance has a larger value than the quadrature axis operational inductance. The difference between the direct axis operational inductance and the quadrature axis operational inductance it is not very big and this because the machine rotor saliency is not very high and of the influence of permanent magnets from the inside of flux barriers.

In both, design and optimization using the finite element analysis procedures, the content of harmonics for the output voltage has been carefully treated.

From the no load tests we can evaluate the THF (telephonic harmonic factor) and so the output voltage distortion. The THF factor is important because all electrical consumers like on-board electronic diagnosis systems, board computer and air conditioning electric and electronic circuits, are placed near the generator, so, both the harmonic amplitudes and order are important.

We can determine this factor using the formula:

$$THF=\frac{100}{V}\sqrt{V_1^2\lambda_1^2+V_2^2\lambda_2^2+\ldots+V_n^2\lambda_n^2} \qquad (16)$$

where: V – the measured output voltage of the generator;

V_n – the value of the n - order harmonic;

λ_n – the share factor for the frequency corresponding to the n - order harmonic.

The experimental setup used for the no load test is presented in figure 10.

The driving motor is a two poles ABB squirrel cage motor of 7.5kW and the frequency converter is a VLT 5000 series, 7.5.kW Danfoss frequency converter.

To determine the *THF*, the BEGA generator was driven at rated speed with a field current that produced the .ate_ o_tp_t voltage.

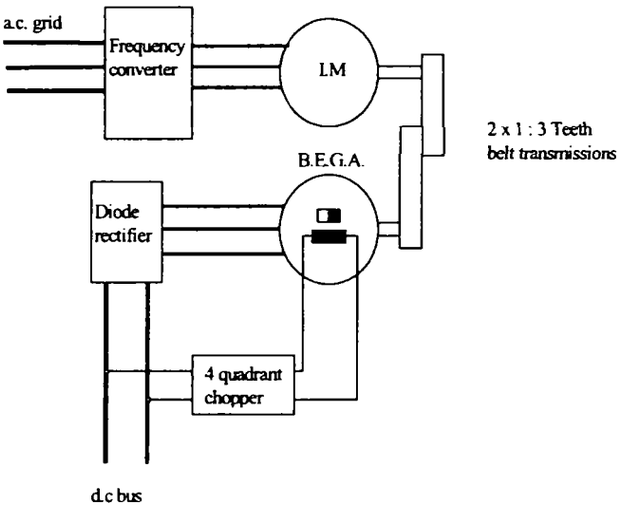

Fig. 10. The setup for the no load tests

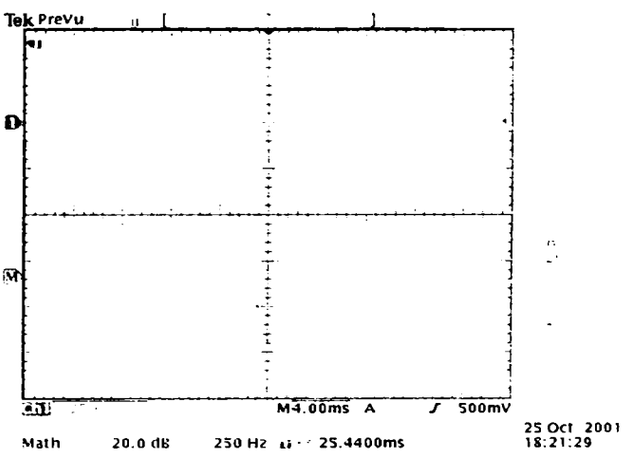

Fig. 11. The output voltage and FFT for from no load tests (n=3000rpm, I_f=0.5A)

The output voltage waveform is recorded and with help of a power analyzer and using the FFT (Fast Fourier Transformed) for the voltage waveform, the content of harmonics and the values were determined.

The value obtained for *THF* was *THF* = 5.3%.

In parallel with the power analyzer, an oscilloscope was used to visualize the output voltage waveform.

Figure 11 presents the BEGA output voltage for a field current of I_f = 0.5A and a rotational speed of 3000 rpm (100Hz). To complete the no-load tests, the output voltage was measured for the entire range of the field current (-3A to +3A). The results are presented in figure 12.

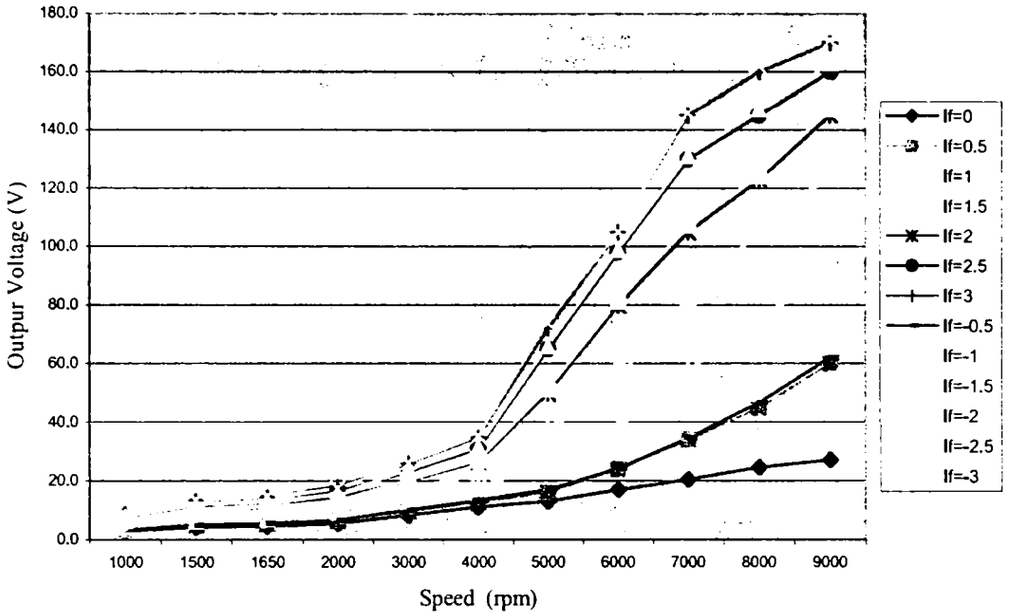

Fig. 12. The output voltage vs. speed for different field currents

V. CONCLUSION

The d.c transient tests gives us information regarding the operational reactance on both direct and quadrature axis.

From no-load tests, the calculated *THF* has a large value but the influence is reduced because this type of electrical generator is designed to work on automobiles so on isolated equipments, where the influence of high order harmonics is small.

Anyway, considering the presence of many electronic devices on automobile board, the generator geometry has to be optimized using the finite element method, in order to reduce the slots influence.

ACKNOWLEDGMENT

For the financial and technical support from the Institute of Energy Technology, University of Aalborg – Denmark, for help in making the prototype and offering the laboratory facilities for accurate tests.

REFERENCES

[1] I.G. Kassakian, H.C. Wolf, I.H.Miller, C.H.I. Hurton: "Automotive electrical system circa 2005" *in: IEEE Spectrum*, August 1996, p. 22-27.

[2] S. Kueppers: *"Numerische Verfahren zur Berechnung und Ausle von Drehstrom Klauenpolgeneratoren"* in: Ph. D. Thesis, Shaker Verlag, Aachen Germany, 1996.

[3] M. Naidu, M. Boules, R. Henry: "A high efficiency, high power generation system for automobiles" *in: Proceedings of IEEE- IAS 1995 -Annual Meeting*, p. 709-716.

[4] H.I.Gutt, I. Mueller: "New aspects for analyzing and optimizing modern motorcar generators" *in: Proceedings of IEEE-IAS 1994 - Annual Meeting*, vol.1, p. 3-8.

[5] I. Boldea "Automotive electric generator systems. A review." *in: Proceedings of ELECTROMOTION 1999*, vol. 1, pp.7-19, July 1999, Patras, Greece.

[6] C.D. Syverson et all *"Hybrid alternator with voltage regulator"* - U.S. Patent (5502368, March 26, 1996).

[7] Mizuno, Takyuki, C/O Kabushiki, Kaisha Meidensha *"Hybrid excitation type permanent magnet synchronous motor"* European Patent Application (941056335, 12.04.1994).

[8] Mutter Albert *"Elektrische maschine und deren anwendung zum fahrzeugbetrieb"* Patentschrift DE (413943C2, 03.12.1991).

[9] T.M. Jahns: "Uncontrolled generator operation of interior PM synchronnes machines following high speed inventer shut down" *in: Proceedings of IEEE-IAS 1998 - Annual Meeting*, vol.1.

[10] I.Boldea, S. Scridon, L. Tutelea: "BEGA – a biaxial excitation generator for automobiles" *in Proceedings of the 7th International Conference OPTIM 2000*, Brasov , May 10-11 2000, pp.345-352.

[11] E.C.Lovelace, T.M.Jahns, J.T.Kirtley Jr., J.H.Lang – "An interior PM starter/generator for automobile applications" *Record from IEE* 1998.

[12] V. Z. Groza, M. Biriescu – "Measurement of Reactance of SynchronousMmachine at Standstill" – *Record from IEEE*, 1999.

APPENDIX B.

BEGAProject – the formulas from the design program - the listing of: "Formule.h" source file

```
#include <stdio.h>
#include <stdlib.h>
#include <string.h>
#include <math.h>
#include "ProgDlg.h"

#define PI 3.1415926536

void ReadInitialData();
void CommonDesign();
void OptimalDesign();
double SUMT(int,double*);
double findmin(int,double,double*);
int readdata(char *,char **,double **,int);
int writedata(char *,char **,double **,int);
int readXY(char *,float *,float *,int);
double interpol(double,float *,float *,int);


/* Design data files */
char initfile[]="initial.dat",magfile[]="magnet.dat";        /* input files */
char
optfile[]="optimal.dat",resfile[]="result.dat",randament[]="randament.dat",totalweight[]="totalwei
ght.dat",totalcost[]="totalcost.dat";        /* output files */


const int initnr=63,resnr=56,altnr=29, magnr=41;
double Vdc,p,Bg0,fr,Idc,Idem,jcof,jcos,lamda,nmax,nmin,cosfi,Br0,g,Vd,RD,effmin;
double q,Bg1,Kfill,Irated,Bgf,Kc,Ks,Kdm,m,bs1,hsu,Clam,Ccop,Cpm,Wcoil,KD,Kfillfe;
double kbr,khc,TPM,Hc0,miu0,hfbt,roco,giron,gcopper,alphac,dutycy,Dshaft,Nps,Tamb;

/* Design data */
double etaerror=0.01,kserror=0.01;

double Tek,ID,Ls,Bpmg,Bpmq,Ki,I1,V1,P,lambdas,Kw1,tau,taup,W1,Wc,dcos,Aslot,f;
double taus,WFiF,AW,lcF,WF,iF,Pcof,pcof,dF,lcs,RS,pcos,RF,Ldm,Lm,Lqm,KF1,LmF,LF,Pout;
double
pcore,pdiode,nel,bs2,hcs,OD,Wcs,Wcos,Wcr,Wcof,Wta,TClam,TCcop,Hc,miur,hm,lambdaPMq;
double
Uair,alpha1,Kfix,Br,lamPM,wps,lwi,Dinfs,fff,hps,Dpe,Dse,hpr,bcr,bcs,Bcr,Bpr,Hps,Hcs,Hpr,Hcr;
double Ucore,hps0,hps1,Kfrige,Kurel,Kurels,gampm,hfbtlim,hfbtcost,hfbtstep;
double TCpm,Wpm,nbar,Kpm,a,sratio,Bcs,pFe50,how,bts,Aslotp,TC,Hts,Bts,hcr,lcr,Klcr,Poutmin;


float Bmag[magnr],Hmag[magnr];
/* Input data */
```

```
char *initname[initnr]={"Vdc","Idc","nmin","Idem","nmax","Bg0","fr","jcos","jcof","p","lamda",

        "cosfi","g","Vd","RD","effmin","q","Bg1","Kfill","Irated","Bgf","Kc","Ks","Kdm",

        "m","bs1","hsu","Clam","Ccop","Cpm","Wcoil","KD","Kfillfe","kbr","khc","TPM","Br0",
"Hc0","miu0","hfbt",

        "roco","giron","gcopper","alphac","dutycy","Tamb","Kfrige","Kurel","Kurels","gampm","
Dshaft","Nps","nbar","Kpm","a",
                "sratio","Bcr","Bts","pFe50","how", "hfbtlim", "hfbtcost","hfbtstep"};

double *initaddr[initnr]={&Vdc,&Idc,&nmin,&Idem,&nmax,&Bg0,&fr,&jcos,&jcof,&p,&lamda,
                &cosfi,&g,&Vd,&RD,&effmin,&q,&Bg1,&Kfill,&Irated,&Bgf,&Kc,&Ks,&Kdm,

        &m,&bs1,&hsu,&Clam,&Ccop,&Cpm,&Wcoil,&KD,&Kfillfe,&kbr,&khc,&TPM,&Br0,
&Hc0,&miu0,&hfbt,

        &roco,&giron,&gcopper,&alphac,&dutycy,&Tamb,&Kfrige,&Kurel,&Kurels,&gampm,&
Dshaft,&Nps,&nbar,&Kpm,
                &a,&sratio,&Bcr,&Bts,&pFe50,&how,&hfbtlim,&hfbtcost,&hfbtstep};


char *randamentname[1] = {"eff"};
double *randamentadd[1] = {&nel};
char *totalweightname[1] = {"tw"};
double *totalweightadd[1] = {&Wta};
char *totalcostname[1] = {"tc"};
double *totalcostadd[1] = {&TC};

double
jcoblim,Bcslim,fxlim,lamlim,etalim,Glim,jcobcost,Bcscost,fxcost,lamcost,etacost,Gcost,jcobstep,B
csstep,fxstep,lamstep;

/* Output data */
char *resname[]={
        "\t\t\tBEGA Project\n\t\t\tGeneral & Optimal Design\n\n\nElectromagnetic torque\t\t Tek
=",
   "Stator bore diameter ID =",
   "Stack length Ls =",
        "PM remanent flux density Br =",
        "PM coercive force Hc =",
        "PM relative recoil permeability miur =",
        "PM radial thickness hm =",
        "Airgap PM flux density Bpmg =",
        "q axis flux density Bpmq =",
        "Phase current I1 =",
        "Line voltage V1 =",
        "Generator rated power P =",
        "Stator flux (lambdas) =",
        "Winding coefficient Kw1 =",
        "Pole pitch (tau) =",
        "Pole shoe span (taup) =",
        "Number of turns per path W1 =",
        "Number of turns per slot Wc =",
```

```
        "Winding wire diameter dcos =" ,
        "Stator useful area Aslotp =",
        "Slot pitch (taus) =",
        "Outer stator diameter OD [m] =",
        "Field winding mmf per pole (WFiF) =",
        "Pole window half-area AW =",
        "Field coil main turn length lcF =",
        "Numbers of field turns/coil WF =",
        "Field current iF =",
        "Field winding power Pcof =",
        "Field winding losses pcof =",
        "Field wire gauge dF =",
        "Stator turn length lcs =",
        "Stator phase resistance RS =",
        "Rated power loss pcos =",
        "Field winding resistence RF =",
        "Magnetizing inductance along axis d Ldm =",
        "Magnetizing inductance Lm =",
        "Magnetizing inductance along axis q Lqm =",
        "Mutual inductance LmF =",
        "KF1 =",
        "Field winding inductance LF =",
        "Core loss pcore =" ,
        "Electrical efficiency (etab)=",
        "Stator core weight Wcs =",
        "Stator copper weight Wcos =",
        "Rotor core weight Wcr =",
        "Field winding copper weight Wcof =",
        "Permanent Magnets total weight WPM =",
        "Total active weight of the machine Wta =",
        "Total lamination costs TClam =",
        "Total copper costs TCcop =",
        "Total PM costs TCPM =",
        "Total costs TC =",
        "Airgap flux in axis q at full current lambdaPMq=",
        "Air speed with selfventilation Uair=",
        "Convection coefficient with air speed alpha1=",
        "Stator area overtemperature increasing Kfix="};

double
*resaddr[]={&Tek,&ID,&Ls,&Br,&Hc,&miur,&hm,&Bpmg,&Bpmq,&I1,&V1,&P,&lambdas,&K
w1,&tau,&taup,

        &W1,&Wc,&dcos,&Aslotp,&taus,&OD,&WFiF,&AW,&lcF,&WF,&iF,&Pcof,&pcof,&d
F,&lcs,&RS,&pcos,

        &RF,&Ldm,&Lm,&Lqm,&LmF,&KF1,&LF,&pcore,&nel,&Wcs,&Wcos,&Wcr,&Wcof,
&Wpm,&Wta,
                        &TClam,&TCcop,&TCpm,&TC,&lambdaPMq,&Uair,&alpha1,&Kfix};

const int optimnr=5,optnr=17;

char *optname[optnr]={"jcoblim","Bcslim","fxlim","lamlim","etalim","Glim",
        "jcobcost","Bcscost","fxcost","lamcost","etacost","Gcost",
        "jcobstep","Bcsstep","fxstep","lamstep","hfbtstep"};
```

```
double *optaddr[optnr]={&jcoblim,&Bcslim,&fxlim,&lamlim,&etalim,&Glim,
        &jcobcost,&Bcscost,&fxcost,&lamcost,&etacost,&Gcost,
        &jcobstep,&Bcsstep,&fxstep,&lamstep,&hfbtstep};


double *point[optimnr]={&jcos,&Bpmq,&fr,&lamda,&hfbt};
double *limit1[optimnr]={&jcoblim,&Bcslim,&fxlim,&lamlim,&hfbtlim}, limit[optimnr];
double *cost1[optimnr]={&jcobcost,&fxcost,&Bcscost,&lamcost,&hfbtcost}, cost[optimnr];
double *step1[optimnr]={&jcobstep,&Bcsstep,&fxstep,&lamstep,&hfbtstep}, step[optimnr];
double start[optimnr],actual[optimnr],minim[optimnr];
double oldFunc,minFunc,newFunc,moded;
enum {weight=0,effic=1};

int mode, move=1,desnr=6,error=0;



CString out(double in)
{
        CString out1;
        out1.Format("%.10f",in);
        return out1;
}

void ReadInitialData()
{

        readdata(initfile,initname,initaddr,initnr);
        readdata(initfile,optname,optaddr,optnr);
        readXY(magfile,Bmag,Hmag,magnr);

}


void OptimalDesign()
 {
  int i,k;
        CProgressDlg   prog;


  for(i=0;i<optimnr;i++){
                start[i]=actual[i]=*point[i];
                step[i]=*step1[i];
                limit[i]=*limit1[i];
                cost[i]=*cost1[i];

        }

        oldFunc=minFunc=newFunc=SUMT(mode,start);
  //AfxMessageBox("oldFunc "+ out(oldFunc));

        prog.Create();
        prog.SetStep(1);
```

```
for(k=0,move=1;move;k++)
        {
         move=0;

         for(i=0;i<optimnr;i++)
                {
                 //AfxMessageBox("i"+ out(i));
                 actual[i]=start[i]-step[i];
                // AfxMessageBox("actual "+ out(actual[i]));

                 minFunc=findmin(mode,minFunc,actual);
                // AfxMessageBox("minFunc "+ out(minFunc));

                 actual[i]=start[i]+step[i];
                // AfxMessageBox("actual 2 "+ out(actual[i]));

                 minFunc=findmin(mode,minFunc,actual);
                // AfxMessageBox("minFunc 2 "+ out(minFunc));
                 actual[i]=start[i];
                // AfxMessageBox("actual 3 "+ out(actual[i]));

                 prog.StepIt();

                 writedata(randament,randamentname,randamentadd,1);
                 writedata(totalweight,totalweightname,totalweightadd,1);
                 writedata(totalcost,totalcostname,totalcostadd,1);


                }

         // AfxMessageBox("k "+ out(k));
         // AfxMessageBox("minFunc " + out(minFunc));

         if(minFunc<oldFunc)
                {
                  //AfxMessageBox("minFunc < oldFunc ");
                 oldFunc=minFunc;
                 for(i=0;i<optimnr;i++) start[i]=minim[i];
                 move=1;
                }
         minFunc=SUMT(mode,start);


        }

  minFunc=SUMT(mode,start);
       //AfxMessageBox(out(lamda));

  //Write optimal result's

  writedata(optfile,resname,resaddr,resnr);
}
```

```
/* User defined functions */
/* Objective function calculation */
double SUMT(int mode,double *crt)
 {
  int i;
  double Func;

  for(i=0;i<optimnr;i++) *point[i]=crt[i];
  for(i=0;i<desnr;i++) CommonDesign();



  switch(mode) {
       case weight:

            if(nel<etalim){  //etab<etalim

                                    Func=Wta+etacost*pow(etalim-nel,2);


                 }
                      else Func=Wta;
                      break;
       case effic:

            if(Wta>Glim){
            //       AfxMessageBox("GCost"+out(Gcost));
                      Func=1.0/nel+Gcost*pow(Wta-Glim,2);
            }else{
                      Func=1.0/nel;
                      break;
            }
        //case cost :
        default:    Func=0;
        }

  for(i=0;i<optimnr;i++)
       if(crt[i]>limit[i])
        Func=Func+cost[i]*pow(crt[i]-limit[i],2);

  return Func;
 }

/* Mininum objective function evaluation */
double findmin(int mode,double minF,double *curent)
 {
  int i;
  double newF;
  //AfxMessageBox("minF"+out(minF));
       newF=SUMT(mode,curent);

       //AfxMessageBox("newF"+out(newF));

       if(newF<minF)
        {
```

```
            minF=newF;
            for(i=0;i<optimnr;i++) minim[i]=curent[i];
           }
  return minF;
 }

//BEGA Common Design
void CommonDesign()
  {

        CString szout;
        int i=0,j=0,k=0;

        double etab1=nel=0.70, Ks1=Ks;


 while (j==0 || fabs((etab1-nel)/nel)>etaerror)
        {
                nel = (nel+(etab1-nel))*Kurel;
                j++;



                //AfxMessageBox("gamp="+out(gampm));
                // Core design

                f=p*nmin/60;//Hz
                Tek = (Vdc*(Idem))/(effmin*PI*2*(nmin/60)); //Nm
                ID= pow((2*Tek)/(fr*pow(10,4)*PI*lamda),1.0/3.0); //m
                Ls = lamda * ID * Kfillfe; //m
                Br = Br0*(1+kbr*(TPM-25)/100); //T
                Hc = Hc0*(1+khc*(TPM-25)/100); //A/m
                miur = (Br/Hc)/miu0;
                hm = (g*hfbt)/nbar; //m
                //AfxMessageBox("hm="+out(hm));

                // Saturation
        while (k==0 || fabs(Ks1-Ks)>kserror)
        {

                Ks=Ks+((Ks1-Ks)*Kurels); //Saturation factor

                k++;

                Bpmg = Br/((1+miur*g/hm*(nbar/Kpm))/(1+Ks)); //T
                Bpmq = Bpmg/2;//T
                Ki = ((3/PI)* sqrt(2) * cosfi); //current coefficient
                I1 = Idc/Ki; //A
                RD = (1.5 - Vd)/Idc; //Ohm
                V1 = (Vdc + ((Vd + (RD*Idc)/Ki)*3)/(3*(Idc/Ki)*cosfi)); //V
                P = sqrt(3) * V1 * I1; //W
                lambdas = V1*60/(effmin*2*PI*nmin*p); //
                Kw1 = (sin(PI/6)/(q*sin(PI/(6*q)))); //
                tau = (PI * ID)/(2*p); //m
                taup = 0.8 * tau; //m
```

```
                W1 = (PI * lambdas)/(2*Bg1*Ls*tau*Kw1); //turns
                W1 = (int)W1;
                Wc = a*W1/(p*q); //turns
                Wc = (int)Wc;
                dcos = sqrt((4/PI)*(I1/(a*jcos*pow(10,6))));  //m
                Aslot = (Wc*(I1/a))/(Kfill*jcos*pow(10,6)); //sqm
                taus = tau/(3*q);//m
                hsu = sratio*taus/2; //m
                bts=taus/2;
                bs1 = (PI*(ID+2*how)/Nps)-bts; //m
                bs2 = (PI*(ID+2*how+2*hsu)/Nps)-bs1; //m
                Bcs = Bg1; //T
                hcs = (1/PI)*((Bg1*tau)/Bcs); //m
        OD = ID+2*how+2*hsu+2*hcs; //m
                lcs = (2*Ls)+0.02+(2.5*tau); //m
                RS = ((roco*lcs*W1)/(((PI*pow(dcos,2))/4)))/a;  //Ohm
                pcos = 3*RS*pow(I1,2); //W

                // The field winding
                WFiF = (Bgf/miu0)*g*Kc*(1+Ks); //Aturns
                AW= WFiF/(Kfill*jcof*pow(10,6)); //sqm
                Wcoil=sqrt(AW);//m
                lcF = (2*Ls)+(1.5*tau)+(4*PI*(Wcoil/2)); //m
                lcr = (tau*sqrt(2)*Klcr)/2; //m??
                hcr = (ID-Dshaft)/2-nbar*hm; //m??
                WF = (Vdc*KD)/(2*p*lcF*jcof*pow(10,6)*roco); //turns
                WF = (int)WF;

                if(WF<0.0) {error=1;break;AfxMessageBox("Error");}
                iF = WFiF/WF; //A
                Pcof = Vdc*iF; //W
                dF = sqrt((4/PI)*(iF/jcof*pow(10,-6))); //mm
                RF = Vdc/iF; //Ohm
                Lm = ((m/a) * miu0 * pow(W1*Kdm,2)*tau*Ls)/(pow(PI,2)*p*Kc*g*(1+Ks));
//H
                Ldm = Kdm * Lm; //H
                Lqm = Ldm/(1+hfbt);//
                lambdaPMq = Lqm * I1; //Wb
                KF1 = (4/PI) * sin((PI/2) * (taup/tau));
                LmF = ((miu0*WF*KF1)/(g*Kc*(1+Ks)))*(2/PI)*tau*Ls*Kw1*W1; //H
                LF = (1.1*p*miu0*pow(WF,2)*taup*Ls)/(g*Kc*(1+Ks)); //H
                Pout = Vdc*Idc; //W
                Poutmin = Pout/2; //W
                pcore = (pFe50*pow(Bcs,2)*pow(f/50,2)*0.5*PI*(pow(OD,2)-
pow(ID,2))*Ls*giron)/4; //W
                pdiode = 2*Vd*Idc; //W
                pcof = RF*pow(iF,2)*(0.9); //W

                nel = Pout/(Pout+(pcos/4)+pcore+pdiode+pcof); //%

    Aslotp = ((bs1+bs2)*hsu)/2; //mp
                //AfxMessageBox("Aslotp= "+ out(Aslotp));
                if (fabs((Aslotp-Aslot)/Aslotp) > 0.01) {

                        if ((sratio <= 12.0) && (sratio >= 2.0)){
```

```
                    sratio = sratio *(1- (((Aslotp-Aslot)/Aslotp)*0.3));
                        //AfxMessageBox("sratio="+out(sratio));
                }else
                  break;
            }


            //Weights
            Wcs = (0.5*PI*(pow(OD,2)+pow(ID,2)*Ls*giron)/4); //kg
            Wcos = (6*W1*lcs*PI*pow(dcos,2)*gcopper)/4; //kg
            Wcr = (PI*pow(ID,2)*Ls*0.7*giron)/4; //kg
            Wcof = (2*p*WF*iF*lcF*gcopper)/(jcof*pow(10,6)); //kg
            Wpm = 2*p*nbar*hm*Kpm*(tau/2)*Ls*gampm; // kg
            Wta = Wcs+Wcos+Wcr+Wcof+Wpm; //kg

            //Costs
            TClam = (Wcs+Wcr)*Clam; //$
            TCcop = (Wcos+Wcof)*Ccop; //$
            TCpm = Wpm * Cpm; //$
            TC = TClam+TCcop+TCpm; //$

            //Cooling
            Uair = (PI*nmin*(ID+OD))/120; //m/s
            alpha1 = alphac*(1+(3/2)*sqrt(Uair));
            Kfix = ((pcore + pcos + pcof)*dutycy)/(alpha1*PI*OD*Ls*(TPM-Tamb));

            // Ks verification
            Hts=interpol(Bts,Bmag,Hmag,magnr); //
            Hcs=interpol(Bcs,Bmag,Hmag,magnr); //
            Hcr=interpol(Bcr,Bmag,Hmag,magnr); //

            Ucore = Hts*hsu+Hcs*PI*(Dse-hcs)/(2*p)+Hcr*lcr; //??
            Ks1=Ucore*miu0/Bg1/g/(1+hm/miur*g); //??

            }

   if (error) break;
        etab1=nel;
  }
}

/* Read data file - float values */
int readdata(char *name,char **var,double **adr,int datanr)
 {
 register FILE *fis;
 register int i=0,k=0;
 float val;
 char text[17];
 CString szout;

 if (!(fis=fopen(name,"rt")))
  {
        printf("\nCannot open the file %s\n",name);
        return 0;
```

```
  }
 while ((i=fscanf(fis,"%15s %f",text,&val))!=EOF)
        //AfxMessageBox(out((double)val));
  if (i==2)
        for (i=0;i<datanr;i++){

         if (!strcmp(text,var[i]))
         {
                if(text == "pFe50")
            AfxMessageBox(var[i]);

              *adr[i]=val;
              k++;break;
         }
              }
 fclose(fis);
 return k;
}

/* Write result file - float values */
int writedata(char *name,char **var,double **adr,int datanr)
 {
 register FILE *fis;
 int i=0;

 if (!(fis=fopen(name,"a")))
  {
        printf("\nCannot open the file %s\n",name);
        return 0;
  }
 for(i=0;i<datanr;i++)
  if (fprintf(fis,"%s\t%e\n",var[i],*adr[i])==EOF)
        printf("\nError writing file %s\n",name);
 fclose(fis);
 return i;
}

/* Read the magnetization file - float values */
int readXY(char *name,float *X,float *Y,int datanr)
 {
  register FILE *fis;
  register int i=0,k=0;

  if (!(fis=fopen(name,"rt")))
        {
         printf("\nCannot open the file %s\n",name);
         return 0;
        }
  for(i=0;i<datanr;i++)
         if((k=fscanf(fis,"%f %f",X+i,Y+i))==EOF) break;
         else if(k!=2) printf("\nError reading file %s\n",name);
  return i;
 }

/* Linear interpolation for X-Y space */
```

```
double interpol(double x,float *X,float *Y,int datanr)
 {
  register int i;

  for(i=1;i<datanr;i++)
        if(x<=X[i]) return Y[i-1]+(Y[i]-Y[i-1])*(x-X[i-1])/(X[i]-X[i-1]);
  return Y[i-2]+(Y[i-1]-Y[i-2])*(x-X[i-2])/(X[i-1]-X[i-2]);
 }
```

APPENDIX C.

Prototype drawings

THE BEGA PROTOTYPE MAIN TECHNICAL DATA

1. Generator technical data:
   Idle engine speed (minimum speed – n min): 1500 rpm
   Maximum speed (n max): 9000 rpm
   Max. Speed / min. Speed ratio: 1/6
   Electrical power: 1,5 – 3 kW
   Rated d.c. output voltage: Vdc = 42 V d.c.
   Rated d.c current: Idc = 75 A (above 2 x n min)
   D.c. current at n min: Idc min = 75/2 A
2. Stator:
   Stator lamination material: DK 66 50 silicon sheet lamination steel for ABB Motors Odense
   Sheet width: 0,5 mm
   Stator outer diameter: SOD = 150 mm
   Stator inner diameter: SID = 92 mm
   Stator length: Lc = 94 mm
   Number of slots: 24
   Number of stator poles: 2p = 4
   Number of phase: m = 3
   Number of turns on stator phase: N1 = 24

Parallel current path: p = 2

   Layers: 1
   Number of stator slots per pole per phase: q = 3

3. Stator coils – Cu – Y connection:
   Number of conductors per slot: 8
   Insulated conductors dimension: 2x1,608 (2x1,5 without insulation)

4. Rotor:
   Lamination material: DK 66 50 silicon sheet lamination steel for ABB Motors Odense
   Sheet outer diameter: ROD = 91 mm
   Sheet inner diameter: RID = 29 mm
   Sheet width: 0,5mm
   Number of sheets: 175 pcs.

5. Permanent Magnet:
   Material: Ferrite
   HcB = 260 kA/m max.
   Hcj = kO kA/m max.
   Br = 0,36 T
   Height: h = 2,8 ± 0,1 mm

Length: L = 92 mm
Width: w = 15 mm

6. Frame – Aluminium :
   Size 90, for ABB motor type QU 90L
   Weight: 17 kg

7. Bearings (ball bearings) SKF type:
   at D-end: 6205 2RS C3
   at N-end: 6205 2RS C3

8. Field coil – Cu – 4 coils in serial connection:
   Number of conductors per coil: 116
   Insulated conductor dimension: 1x0,79mm (1x0,71mm without insulation)

9. Shaft:
   Material: Steel
   Dimensions: Φ 29/L mm

The stator

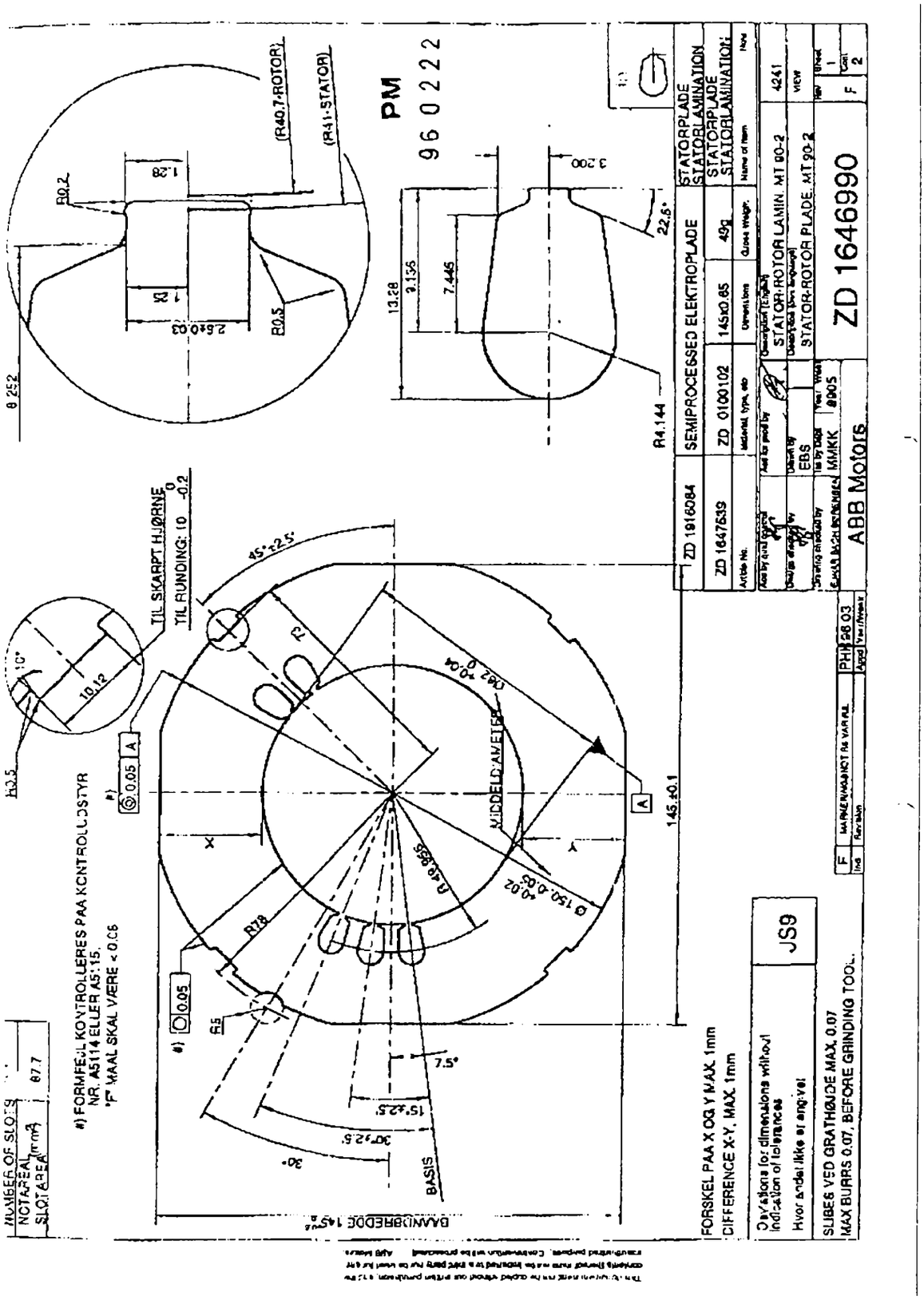

The rotor

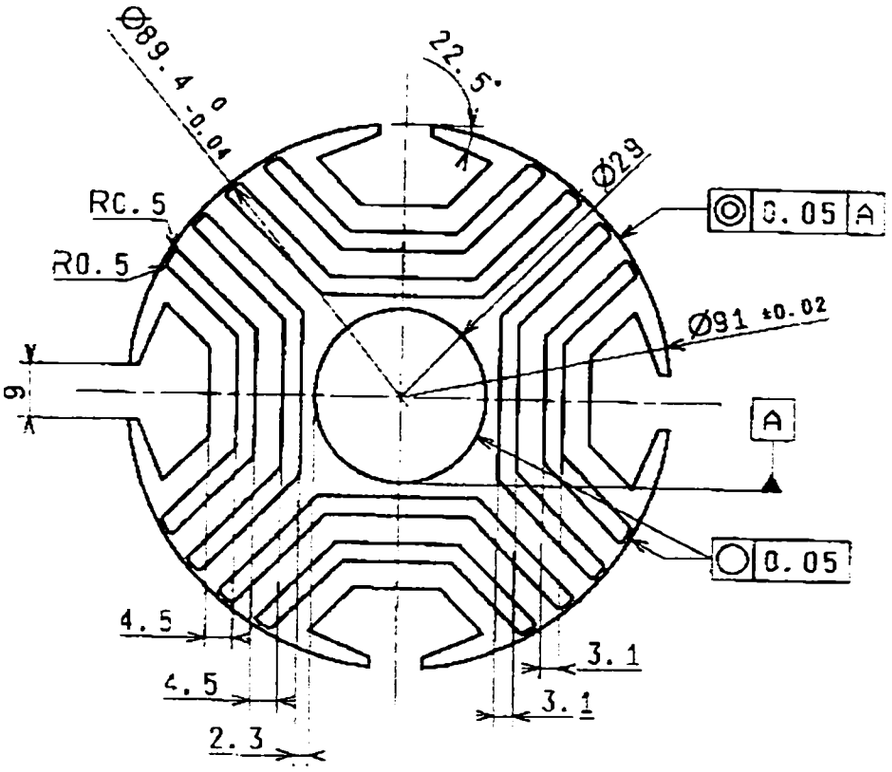

Length of cutting line	
I.D.	91.11
O.D.	493.79
Slots	1052.48
Total	1637.38

Finally annealed EN 10106 A
M400-50A (EN10027-1).

		Drawing type: Part Drawing	GRUNDFOS DK-8850 BJERRINGBRO DENMARK	Scale: 1:1	Drawn: BPE/PP 99-09-13
		Related drawings:			Approved: Date:
		Projection:		Replaced:	
		Basic material no:		Replaced by:	
		Dimension of basic material: 8.50 ± 0.05, 12.74g	Part name: Rotor lamination Ø 29/91x0.50	Drawing no: 88.24 68	
1300	990316 BPE	Type of basic material:		Page 1 of 1	
Org. no.	Date - init.				

The bearings

APPENDIX D.

Matlab & PSpice™ program listings

D.1. Flux Reversal Generator

D.1.1. FRG generating system for 42 V d.c.

```
* -the generator
.param pi=3.1415927
.param n=300
.param fi={2*pi/3}
E1 10 11  VALUE={n*(1.6*sin(16*pi*n*time)+0.3*sin(48*pi*n*time))}
E2 10 12  VALUE={n*(1.6*sin(16*pi*n*time-fi)+0.3*sin(48*pi*n*time))}
E3 10 13  VALUE={n*(1.6*sin(16*pi*n*time+fi)+0.3*sin(48*pi*n*time))}
*
Ls1 11 14 670u
Ls2 12 15 670u
Ls3 13 16 670u
Rs1 14 17 0.119
Rs2 15 18 0.119
Rs3 16 19 0.119
*
* -the  rectifier
D1 17 1 D_redres
D2 0 17 D_redres
D3 18 1 D_redres
D4 0 18 D_redres
D5 19 1 D_redres
D6 0 19 D_redres
Rd1 17 1 10MEG
Rd2 0 17 10MEG
Rd3 18 1 10MEG
```

```
Rd4 0 18 10MEG
Rd5 19 1 10MEG
Rd6 0 19 10MEG
.model D_redres D
Cf 1 0 500u
*
*-the regulator
Smos 1 2 105 0 comut
.MODEL comut VSWITCH(RON=0.02 ROFF=10MEG VON=10 VOFF=1)
x1 101 102 103 0 105 LM139
Vcc 103 0 15
Vref 104 0 7.5
Ri 104 101 1k
Rr 101 105 1MEG
Rdiv1 3 102 34.5k
*Cderv 3 102 50n
RwwÓdiv2 102 0 7.5k
Rcolect 103 105 5k
Lfc 2 3 .002
Df 0 2 D_redres
Rdf 0 2 10MEG
Cfc 3 0 10u
Rc 3 0 0.58
* -the simmetrical load
*R1 17 0 100
*R2 18 0 100
*R3 19 0 100
*R0 10 0 1MEG
.lib linear.lib
.tran 5u 30m
.PROBE
```

```
.end
```

D.1.2. Digital simulation of the generating system, including the load resistance

```
* -the generator
.param pi=3.1415927
.param n={18000/60}
.param fi={2*pi/3}
.lib pwr_elec.lib

E1 10 11  VALUE={n*(1.6*sin(16*pi*n*time)+0.3*sin(48*pi*n*time))}
E2 10 12  VALUE={n*(1.6*sin(16*pi*n*time-fi)+0.3*sin(48*pi*n*time))}
E3 10 13  VALUE={n*(1.6*sin(16*pi*n*time+fi)+0.3*sin(48*pi*n*time))}
*
Ls1 11 14 670u
Ls2 12 15 670u
Ls3 13 16 670u
Rs1 14 17 0.119
Rs2 15 18 0.119
Rs3 16 19 0.119
*
* -the rectifier
D1 17 1 D_redres
D2 4 17 D_redres
D3 18 1 D_redres
D4 4 18 D_redres
D5 19 1 D_redres
D6 4 19 D_redres
Rd1 17 1 10MEG
Rd2 4 17 10MEG
Rd3 18 1 10MEG
Rd4 4 18 10MEG
Rd5 19 1 10MEG
Rd6 4 19 10MEG
```

```
.model D_redres D
Cf 1 4 500u Ic={2.5*n}
*
* the chopper
Smos1 1 2 100 0 comut
D7 4 2 D_redres
Rd7 4 2 10MEG
Lf1 2 3 0.002 IC=72
*
* Voltages balance
Smos2 1 5 101 0 comut
Smos3 5 4 102 0 comut
D8 5 1 D_redres
D9 4 5 D_redres
*
* Output filter
Lf2 5 0 0.002 IC=-72
Cf1 3 0 10u IC=-14
Cf2 4 0 10u IC=-42
*
*Load
Rload1 3 0 .19
Rload2 4 0 116
*
* 0 difference -div rezistiv
Rdiv1 3 6 100k
Rdiv2 6 4 300k
*
.MODEL comut VSWITCH(RON=0.02 ROFF=10MEG VON=5 VOFF=1)
*
* -Regulators
```

```
* Hysteresis Regulator
ecomp1 200 0 value={(V(3)-V(4)-56)*10}
xlogic1 200 100 COMPHYS PARAMS: VHYS=.1V ic_sw=-11V
*
ecomp2 300 0 value={(-V(6)+.2)*10}
xlogic2 300 101 COMPHYS PARAMS: VHYS=.1V ic_sw=-11V
*
ecomp3 400 0 value={(V(6)+.2)*10}
xlogic3 400 102 COMPHYS PARAMS: VHYS=.1V ic_sw=-11V
*
.tran 5u 5m UIC
.PROBE
.end
```

D.2. Biaxial Electrical Generator for Automobiles

D.2.1. Digital simulation for: generator -rectifier – load system

```
* - generator
.param pi=3.1415927
.param w={400*pi}
.param ld=.00314
.param lq=.00055
.param lmf={.032*1.2247}
.param lsig=.0003
.param r1=.02925
*.param lpm={.026*1.2247}
.param lpm={.017*1.2247}
.param fi={2*pi/3}
.param park=.8164965
.lib pwr_elec.lib

*d-axis modeling
G_Ie 0 111 VALUE={2.75*lmf/ld}
V_Id0 111 112 0
L_ld 112 0 {ld} Ic={2.75*lmf/ld}
E_rotd 111 113 VALUE={-w*lq*I(V_Iq0)}
G_Id 113 0 VALUE={park*(I(Ea)*cos(w*time)+I(Eb)*cos(w*time-fi)+I(Ec)*cos(w*time+fi))}
R_D 113 0 1000

* q-axis modeling
G_lpm 0 121 VALUE={-lpm/lq}
V_Iq0 121 122 0
L_lq 122 0 {lq} IC={-lpm/lq}
E_rotq 121 123 VALUE={w*ld*I(V_Id0)}
G_Iq 123 0 VALUE={park*(-I(Ea)*sin(w*time)-I(Eb)*sin(w*time-fi)-I(Ec)*sin(w*time+fi))}
R_Q 123 0 1000
```

```
*Park inverse, phase coordinates
Ea 1 131 VALUE={-park*(V(113)*cos(w*time)-V(123)*sin(w*time))}
Eb 1 132 VALUE={-park*(V(113)*cos(w*time-fi)-V(123)*sin(w*time-fi))}
Ec 1 133 VALUE={-park*(V(113)*cos(w*time+fi)-V(123)*sin(w*time+fi))}
R_nul 1 0 1MEG

La 131 134 {lsig}
Lb 132 135 {lsig}
Lc 133 136 {lsig}

Ra 134 137 {r1}
Rb 135 138 {r1}
Rc 136 139 {r1}

*Load ( on a. c.)
*Rsa 137 0 1
*Rsb 138 0 1
*Rsc 139 0 1

*rectifier
 D1 137 2 D_redres
D2 0 137 D_redres
D3 138 2 D_redres
D4 0 138 D_redres
D5 139 2 D_redres
D6 0 139 D_redres
Rd1 137 2 10MEG
Rd2 0 137 10MEG
Rd3 138 2 10MEG
```

```
Rd4 0 138 10MEG
Rd5 139 2 10MEG
Rd6 0 139 10MEG

*Batteries
Cf 2 0 100u
Rs 2 0 1MEG
Rbat 2 3 .05
Ecc 3 0 VALUE={42}
.model D_redres D

*Resistive load
Rsarc 4 0 0.7
*Switch
S1 4 2 200 0 comut
.Model comut VSWITCH (RON=0.002 ROFF=10MEG VON=5 VOFF=4.99)
V_comanda 200 0 PULSE (0 10 0 200m 0 200m 200m )

.tran 2u 200m 0 20u UIC
.PROBE
.end
```

D.2.2. Digital simulation for generator steady-state characteristics

```
auto=0;
new=0;
if auto==1
   if(new==1)
   Rs=sR;
   Rex=rex;
   lpmq=lambda_pm/sqrt(2);
   Lmf=Lmf/sqrt(2);

   end
else
   Rs=.03328;
   Lq=.00021;
   Ld=.00101;
   Lmf=.0321/sqrt(2);
   lpmq=.0148/sqrt(2);
   Vex=42;
   Rex=13.53;
   pp=2;
end

Ifn=Vex/Rex;

n_max=1000;

w1=314;

% No load characteristics at 50,100,300Hz - fig.1

for I=1: n_max, If(I)=2*I*Ifn/n_max;
      Uf1(I)=w1*sqrt((lpmq)^2+(If(I)*Lmf)^2); end;
Uf2=2*Uf1; Uf3=6*Uf1;
figure(1);
plot(If,Uf1,'r',If,Uf2,'b',If,Uf3,'m'), grid;
legend(' 50Hz','100Hz','300Hz');
title('No load voltage');
xlabel('Excitation current (A)');
ylabel('(V)');

%Short-circuit characteristics at f=50,100,300Hz, infinite - fig.2

w=w1;
Id=(w*Rs*lpmq-w^2*Lmf*Lq*If)/(w^2*Ld*Lq+Rs^2);
Iq=(w*Rs*Lmf*If+w^2*Ld*lpmq)/(w^2*Ld*Lq+Rs^2);
Is1=sqrt(Id.^2+Iq.^2);

w=2*w1;
Id=(w*Rs*lpmq-w^2*Lmf*Lq*If)/(w^2*Ld*Lq+Rs^2);
Iq=(w*Rs*Lmf*If+w^2*Ld*lpmq)/(w^2*Ld*Lq+Rs^2);
Is2=sqrt(Id.^2+Iq.^2);

w=6*w1;
Id=(w*Rs*lpmq-w^2*Lmf*Lq*If)/(w^2*Ld*Lq+Rs^2);
Iq=(w*Rs*Lmf*If+w^2*Ld*lpmq)/(w^2*Ld*Lq+Rs^2);
Is3=sqrt(Id.^2+Iq.^2);

Is0=sqrt((lpmq/Lq)^2+((Lmf/Ld).*If).^2);
```

```
figure(2);
plot(If,Is1,'r',If,Is2,'b',If,Is3,'m',If,Is0,'g'), grid;
legend(' 50Hz','100Hz','300Hz', '  R<<XL ');
title('Short circuit current');
xlabel('Excitation current (A)');
ylabel('(A)');


%External characteristics pure resistive f=50,100,300Hz, If=Ifn and If=0
-fig.3
w=w1;
for I=1:n_max, R_load(I)=200*(I/n_max)^2; R(I)=Rs+R_load(I);
   Id(I)=(w*lpmq*R(I)-w^2*Lmf*Lq*Ifn)/(w^2*Ld*Lq+R(I)^2);
   Iq(I)=(w*Lmf*Ifn*R(I)+w^2*Ld*lpmq)/(w^2*Ld*Lq+R(I)^2); end;

Is1=sqrt(Id.^2+Iq.^2);
Us1=Is1.*R_load;

w=2*w1;
for I=1:n_max, R_load(I)=200*(I/n_max)^2; R(I)=Rs+R_load(I);
   Id(I)=(w*lpmq*R(I)-w^2*Lmf*Lq*Ifn)/(w^2*Ld*Lq+R(I)^2);
   Iq(I)=(w*Lmf*Ifn*R(I)+w^2*Ld*lpmq)/(w^2*Ld*Lq+R(I)^2); end;

Is2=sqrt(Id.^2+Iq.^2);
Us2=Is2.*R_load;

w=6*w1;
for I=1:n_max, R_load(I)=200*(I/n_max)^2; R(I)=Rs+R_load(I);
   Id(I)=(w*lpmq*R(I)-w^2*Lmf*Lq*Ifn)/(w^2*Ld*Lq+R(I)^2);
   Iq(I)=(w*Lmf*Ifn*R(I)+w^2*Ld*lpmq)/(w^2*Ld*Lq+R(I)^2); end;

Is3=sqrt(Id.^2+Iq.^2);
Us3=Is3.*R_load;

%Electromagnetic torque
w=w1;
for I=1:n_max, R_load(I)=200*(I/n_max)^2; R(I)=Rs+R_load(I);
   Id(I)=w*lpmq*R(I)/(w^2*Ld*Lq+R(I)^2);
   Iq(I)=(w^2*Ld*lpmq)/(w^2*Ld*Lq+R(I)^2); end;

Is10=sqrt(Id.^2+Iq.^2);
Us10=Is10.*R_load;

w=2*w1;
for I=1:n_max, R_load(I)=200*(I/n_max)^2; R(I)=Rs+R_load(I);
   Id(I)=w*lpmq*R(I)/(w^2*Ld*Lq+R(I)^2);
   Iq(I)=(w^2*Ld*lpmq)/(w^2*Ld*Lq+R(I)^2); end;

Is20=sqrt(Id.^2+Iq.^2);
Us20=Is20.*R_load;

w=6*w1;
for I=1:n_max, R_load(I)=200*(I/n_max)^2; R(I)=Rs+R_load(I);
   Id(I)=w*lpmq*R(I)/(w^2*Ld*Lq+R(I)^2);
   Iq(I)=(w^2*Ld*lpmq)/(w^2*Ld*Lq+R(I)^2); end;

Is30=sqrt(Id.^2+Iq.^2);
Us30=Is30.*R_load;

figure(3);
```

```
plot(Is1,Us1,'r',Is2,Us2,'b',Is3,Us3,'m',Is10,Us10,'r',Is20,Us20,'b',Is30
,Us30,'m'), grid;
legend(' 50Hz','100Hz','300Hz');
title('Phase voltage');
xlabel('Phase current (A)');
ylabel('(V)');

Pem1=3*Is1.^2.*(R_load+Rs);
Pem10=3*Is10.^2.*(R_load+Rs);
Pem2=3*Is2.^2.*(R_load+Rs);
Pem20=3*Is20.^2.*(R_load+Rs);
Pem3=3*Is3.^2.*(R_load+Rs);
Pem30=3*Is30.^2.*(R_load+Rs);

Mem1=pp*Pem1/w1;
Mem10=pp*Pem10/w1;
Mem2=pp*Pem2/(2*w1);
Mem20=pp*Pem20/(2*w1);
Mem3=pp*Pem3/(6*w1);
Mem30=pp*Pem30/(6*w1);


figure(4);
plot(Is1,Mem1,'r',Is2,Mem2,'b',Is3,Mem3,'m',Is10,Mem10,'r',Is20,Mem20,'b'
,Is30,Mem30,'m'), grid;
% Electromagnetic torque (' 50Hz','100Hz','300Hz');
title('Electromagnetic torque');
xlabel('Phase current (A)');
ylabel('(Nm)');

zoom on
```

D.3. The Program for Integral Calculus for the d.c.Decay Test of the Biaxial Electrical Generator for Automobiles

```
clear all
close all

R1=1.5*0.17;

M=load('TEK00001.DAT');
np=M(1);
dt=M(2);

t1=dt*(0:np-1)';
I1=M(5:end);
plot(t1,I1);
grid;

Isort=sort(I1);
df=abs(diff(Isort));
dfnz=df(find(df>0));
qi=min(dfnz);
Imax=max(I1);
Imin=min(I1);
nqi=(Imax-Imin)/qi;
[N1,X1]=hist(I1,nqi);
figure
bar(X1,N1)
[np1 ip1]=max(N1(1:floor(nqi/2)));
[np2 ip2]=max(N1((1+floor(nqi/2)):end));
Ibase=X1(ip1);
Itop=X1(floor(nqi/2)+ip2);
Idc=Itop-Ibase;
I1c=I1-Ibase;
I1c1=0.9*Idc;
I1c2=0.85*Idc;
k1=min(find(I1c1>I1c));
k2=min(find(I1c2>I1c));

t2=t1(k1:k2);
x2=I1c(k1:k2);
p1=polyfit(t2,x2,1);
t3=(Idc-p1(2))/p1(1);
k3=min(find(t1>t3));

figure
plot(t1,I1c);
grid
hold on
plot([0 t3],[Idc Idc],'r');
hold off;

IntI=dt*(sum(I1c(k3:end))-(I1c(k2)+I1c(end))/2)+0.5*(t1(k3)-
t3)*(Idc+I1c(k3));

L1=R1*IntI/Idc
```

APPENDIX E.

E.1. The output data from the general design - the input data are the same as for the analytical design example

BEGA Project

General Design

Electromagnetic torque Tek = 1.253345e+001
Stator bore diameter ID = 8.728170e-002
Stack length Ls = 4.975057e-002
PM remanent flux density Br = 9.325000e-001
PM coercive force Hc = 4.235000e+005
PM relative recoil permeability miur = 1.834908e+000
PM radial thickness hm = 2.000000e-003
Airgap PM flux density Bpmg = 4.883013e-001
q axis flux density Bpmq = 2.441506e-001
Phase current I1 = 5.553604e+001
Line voltage V1 = 4.202280e+001
Generator rated power P = 4.042225e+003
Stator flux (lambdas) = 1.672034e-001
Winding coefficient Kw1 = 9.597951e-001
Pole pitch (tau) = 6.855088e-002
Pole shoe span (taup) = 5.484071e-002
Number of turns per path W1 = 6.600000e+001
Number of turns per slot Wc = 2.200000e+001
Winding wire diameter dcos = 1.716473e-003
Stator useful area Aslotp = 1.140399e-004
Slot pitch (taus) = 7.616765e-003
Outer stator diameter OD [m] = 1.687718e-001
Field winding mmf per pole (WFiF) = 5.773402e+002
Pole window half-area AW = 1.603723e-004
Field coil main turn length lcF = 2.818966e-001
Numbers of field turns/coil WF = 1.860000e+002
Field current iF = 3.103980e+000
Field winding power Pcof = 1.303671e+002
Field winding losses pcof = 1.173304e+002
Field wire gauge dF = 7.028611e-004
Stator turn length lcs = 2.908783e-001
Stator phase resistance RS = 8.296438e-002
Rated power loss pcos = 7.676490e+002
Field winding resistence RF = 1.353102e+001
Magnetizing inductance along axis d Ldm = 1.070768e-003
Magnetizing inductance Lm = 1.103884e-003
Magnetizing inductance along axis q Lqm = 2.141535e-004
Mutual inductance LmF = 3.219308e-002
KF1 = 1.210923e+000
Field winding inductance LF = 2.158088e-001
Core loss pcore = 2.535945e+001
Electrical efficiency (etab)= 8.812170e-001
Stator core weight Wcs = 1.082796e+000
Stator copper weight Wcos = 2.372249e+000

Rotor core weight Wcr = 1.500254e+000
Field winding copper weight Wcof = 7.242385e-001
Permanent Magnets total weight WPM = 3.655998e-001
Total active weight of the machine Wta = 6.045137e+000
Total lamination costs TClam = 6.457625e+000
Total copper costs TCcop = 1.238595e+001
Total PM costs TCPM = 3.655998e+001
Total costs TC = 5.540355e+001
Airgap flux in axis q at full current lambdaPMq= 1.189324e-002
Air speed with selfventilation Uair= 1.005520e+001
Convection coefficient with air speed alpha1= 4.170993e+001
Stator area overtemperature increasing Kfix= 1.103201e+003

E.2. The output data from the optimisation design following the maximum efficiency - the input data are the same as for the analytical design example

BEGA Project

Optimal Design

Electromagnetic torque Tek = 1.253345e+001
Stator bore diameter ID = 9.991260e-002
Stack length Ls = 3.796679e-002
PM remanent flux density Br = 9.325000e-001
PM coercive force Hc = 4.235000e+005
PM relative recoil permeability miur = 1.834908e+000
PM radial thickness hm = 1.500000e-003
Airgap PM flux density Bpmg = 4.211339e-001
q axis flux density Bpmq = 2.105670e-001
Phase current I1 = 5.553604e+001
Line voltage V1 = 4.202280e+001
Generator rated power P = 4.042225e+003
Stator flux (lambdas) = 1.672034e-001
Winding coefficient Kw1 = 9.597951e-001
Pole pitch (tau) = 7.847117e-002
Pole shoe span (taup) = 6.277694e-002
Number of turns per path W1 = 7.600000e+001
Number of turns per slot Wc = 2.500000e+001
Winding wire diameter dcos = 1.716473e-003
Stator useful area Aslotp = 1.296932e-004
Slot pitch (taus) = 8.719019e-003
Outer stator diameter OD [m] = 1.884789e-001
Field winding mmf per pole (WFiF) = 5.773402e+002
Pole window half-area AW = 1.603723e-004
Field coil main turn length lcF = 2.732095e-001
Numbers of field turns/coil WF = 1.920000e+002
Field current iF = 3.006980e+000
Field winding power Pcof = 1.223932e+002
Field winding losses pcof = 1.136639e+002
Field wire gauge dF = 6.917917e-004
Stator turn length lcs = 2.921115e-001
Stator phase resistance RS = 9.593976e-002
Rated power loss pcos = 8.700070e+002
Field winding resistence RF = 1.396750e+001
Magnetizing inductance along axis d Ldm = 1.240331e-003
Magnetizing inductance Lm = 1.278691e-003
Magnetizing inductance along axis q Lqm = 3.100826e-004
Mutual inductance LmF = 3.342900e-002
KF1 = 1.210923e+000
Field winding inductance LF = 2.008855e-001
Core loss pcore = 2.368978e+001
Electrical efficiency (etab)= 8.921749e-001
Stator core weight Wcs = 1.085560e+000
Stator copper weight Wcos = 2.743261e+000
Rotor core weight Wcr = 1.500254e+000
Field winding copper weight Wcof = 7.019199e-001
Permanent Magnets total weight WPM = 2.395356e-001

Total active weight of the machine Wta = 6.270531e+000
Total lamination costs TClam = 6.464536e+000
Total copper costs TCcop = 1.378072e+001
Total PM costs TCPM = 2.395356e+001
Total costs TC = 4.419882e+001
Airgap flux in axis q at full current lambdaPMq= 1.722076e-002
Air speed with selfventilation Uair= 1.132511e+001
Convection coefficient with air speed alpha1= 4.365280e+001
Stator area overtemperature increasing Kfix= 1.392707e+003

E.3. The output data from the optimisation design following the minimum weight - the input data are the same as for the analytical design example

BEGA Project

Optimal Design

Electromagnetic torque Tek = 1.253345e+001
Stator bore diameter ID = 6.430970e-002
Stack length Ls = 6.109422e-002
PM remanent flux density Br = 9.325000e-001
PM coercive force Hc = 4.235000e+005
PM relative recoil permeability miur = 1.834908e+000
PM radial thickness hm = 2.000000e-003
Airgap PM flux density Bpmg = 4.883013e-001
q axis flux density Bpmq = 2.441506e-001
Phase current I1 = 5.553604e+001
Line voltage V1 = 4.202280e+001
Generator rated power P = 4.042225e+003
Stator flux (lambdas) = 1.672034e-001
Winding coefficient Kw1 = 9.597951e-001
Pole pitch (tau) = 5.050872e-002
Pole shoe span (taup) = 4.040698e-002
Number of turns per path W1 = 7.300000e+001
Number of turns per slot Wc = 2.400000e+001
Winding wire diameter dcos = 1.716473e-003
Stator useful area Aslotp = 1.246427e-004
Slot pitch (taus) = 5.612080e-003
Outer stator diameter OD [m] = 1.413464e-001
Field winding mmf per pole (WFiF) = 5.773402e+002
Pole window half-area AW = 1.603723e-004
Field coil main turn length lcF = 2.775206e-001
Numbers of field turns/coil WF = 1.890000e+002
Field current iF = 3.054710e+000
Field winding power Pcof = 1.282978e+002
Field winding losses pcof = 1.154680e+002
Field wire gauge dF = 6.972605e-004
Stator turn length lcs = 2.684602e-001
Stator phase resistance RS = 8.469138e-002
Rated power loss pcos = 7.836285e+002
Field winding resistence RF = 1.374926e+001
Magnetizing inductance along axis d Ldm = 1.185246e-003
Magnetizing inductance Lm = 1.221903e-003
Magnetizing inductance along axis q Lqm = 2.370492e-004
Mutual inductance LmF = 3.273752e-002
KF1 = 1.210923e+000
Field winding inductance LF = 2.016147e-001
Core loss pcore = 2.364534e+001
Electrical efficiency (etab)= 8.811138e-001
Stator core weight Wcs = 7.222524e-001
Stator copper weight Wcos = 2.421630e+000
Rotor core weight Wcr = 1.000169e+000
Field winding copper weight Wcof = 7.129960e-001
Permanent Magnets total weight WPM = 3.307968e-001
Total active weight of the machine Wta = 5.187844e+000
Total lamination costs TClam = 4.306055e+000

Total copper costs TCcop = 1.253850e+001
Total PM costs TCPM = 3.307968e+001
Total costs TC = 4.992424e+001
Airgap flux in axis q at full current lambdaPMq= 1.316477e-002
Air speed with selfventilation Uair= 8.076096e+000
Convection coefficient with air speed alpha1= 3.841847e+001
Stator area overtemperature increasing Kfix= 1.180441e+003

APPENDIX F.

Other Test Results

F.1. The a.c. standstill tests using an a.c. power source

F.1.1. The d-axis measurements, when the stator coils of the prototype is supplied through the a.c. power source, the rotor winding is open

F	Ud	Id	P	S	Q	PF	Uf	UfTHD
Hz	V	A	W	VA	VAr		V	%
20,000	3,000	8,800	6,165	26,660	25,940	0,230	36,550	7,200
25,000	3,000	7,190	4,403	21,720	21,270	0,203	36,770	6,500
30,000	3,000	6,110	3,456	18,728	18,407	0,850	37,300	6,780
40,000	3,000	4,700	2,277	13,948	13,761	0,163	36,800	4,530
50,000	3,000	3,780	1,710	11,365	11,231	0,151	36,700	4,372
60,000	3,000	3,230	1,384	9,768	9,669	0,142	37,040	4,100
80,000	3,000	2,500	0,981	7,496	7,430	0,131	36,800	3,820
100,000	3,000	2,020	0,770	6,154	6,104	0,125	36,800	3,440
120,000	3,000	1,740	0,636	5,271	5,232	0,121	36,900	3,610
150,000	3,000	1,420	0,514	4,295	4,263	0,120	36,730	3,100
200,000	3,000	1,090	0,396	3,307	3,283	0,119	36,500	3,020
250,000	3,000	0,903	0,330	2,690	2,674	0,121	36,500	2,470
300,000	3,000	0,772	0,287	2,314	2,296	0,124	36,700	2,530
400,000	3,000	0,596	0,237	1,780	1,767	0,132	36,200	2,240
500,000	3,000	0,473	0,196	1,380	1,370	0,141	35,300	1,950

F.1.2. The d-axis measurements, when the stator winding of the prototype is supplied through the a.c. power source, the rotor is short-circuited

f	Ud	Id	W	VA	VAr	PF	If	IfTHD
Hz	V	A					A	%
20	1	9,000	7,902	9,610	5,458	0,823	0,581	0,500
25	1	8,290	6,585	8,581	5,488	0,769	0,530	0,370
30	1	7,600	5,654	7,890	5,500	0,717	0,490	0,390
40	1	6,470	4,101	6,586	5,139	0,626	0,416	0,400
50	1	5,600	3,098	5,612	4,678	0,553	0,359	0,270
60	1	4,920	2,438	4,945	4,301	0,493	0,316	0,190
80	1	3,930	1,610	3,980	3,642	0,405	0,254	0,210
100	1	3,280	1,148	3,314	3,109	0,346	0,212	0,220
120	1	2,860	0,887	2,926	2,788	0,304	0,183	0,340
150	1	2,380	0,658	2,551	2,466	0,258	0,155	0,340
200	1	1,820	0,417	1,938	1,894	0,215	0,118	0,280
250	1	1,490	0,308	1,644	1,614	0,188	0,098	0,200
300	1	1,240	0,206	1,234	1,215	0,169	0,078	0,300
400	1	0,925	0,134	0,923	0,912	0,146	0,059	0,480
500	1	0,780	0,109	0,808	0,802	0,135	0,050	0,570

F.1.3. The d-axis measurements, when the field coil of the prototype is supplied through the a.c. power source, the stator windings are open.

F	Uf	If	P	VA	VAR	PF	Uf THD	Ud	Ud THD
Hz	V	A	W						
500	30	0,031	0,111	0,940	0,930	0,118	0,070	1,938	0,150
400	30	0,035	0,121	1,051	1,044	0,116	0,120	1,938	0,210
300	30	0,040	0,135	1,145	1,135	0,117	0,119	1,938	0,220
250	30	0,049	0,177	1,492	1,479	0,119	0,257	1,937	0,150
200	30	0,060	0,211	1,800	1,794	0,115	0,139	1,935	0,150
150	30	0,077	0,249	2,319	2,310	0,106	0,310	1,933	0,170
120	30	0,094	0,317	2,833	2,814	0,113	0,120	1,930	0,250
100	30	0,111	0,383	3,340	3,316	0,115	0,100	1,931	0,140
80	30	0,135	0,469	4,060	4,030	0,116	0,200	1,931	0,170
60	30	0,174	0,641	5,245	5,205	0,122	0,250	1,932	0,250
80	30	0,205	0,790	6,180	6,130	0,127	0,200	1,932	0,270
40	30	0,251	1,013	7,540	7,470	0,134	0,160	1,932	0,340
30	30	0,326	1,434	9,790	9,680	0,143	0,180	1,934	0,370
25	30	0,386	1,816	11,590	11,440	0,157	0,070	1,934	0,420
20	30	0,475	2,466	14,270	14,050	0,173	0,100	1,932	0,500

F.1.4. The d-axis measurements, when the field coil of the prototype is supplied through the a.c. power source, the stator windings are short-circuited.

F	Uf	If	P	S	Q	PF	Uf THD	Id	Id THD
Hz	V	A	W	VA	VAr		%	A	%
500	30	0,114	0,683	3,459	3,385	0,198	0,210	1,370	0,480
400	30	0,139	0,928	4,196	4,090	0,221	0,150	1,683	0,520
300	30	0,179	1,394	5,380	5,200	0,259	0,170	2,175	0,520
250	30	0,209	1,830	6,280	6,010	0,291	0,230	2,544	0,480
200	30	0,252	2,544	7,578	7,137	0,336	0,180	3,077	0,530
150	30	0,318	3,839	9,547	8,735	0,404	0,120	3,875	0,520
120	30	0,376	5,194	11,284	10,020	0,460	0,220	4,580	0,530
100	30	0,428	6,544	12,814	11,014	0,511	0,320	5,190	0,550
80	30	0,491	8,462	14,713	12,037	0,575	0,200	5,930	0,460
60	30	0,570	11,040	17,190	13,080	0,649	0,260	6,870	0,504
50	30	0,620	12,870	18,610	13,440	0,691	0,100	7,400	0,420
40	30	0,671	14,745	20,070	13,620	0,734	0,130	7,830	0,480
30	30	0,741	17,010	22,170	14,220	0,767	0,099	8,480	0,560
25	30	0,779	18,161	23,320	14,630	0,779	0,070	8,630	0,700
20	30	0,834	19,524	24,960	15,550	0,782	0,200	8,860	0,900

F.2. The load current and voltage when the load resistance changes, for an excitation current of I_f=2.5A

	25Hz		50Hz	
Is	Us	Rs	Is	Us
A	V	Ohm	A	V
21,5	21	1,1	25,8	25
15,4	31,9	2,2	20,5	42,2
11,8	37,8	3,2	17,2	54,6
9,5	41,1	4,3	14,9	62,9
8	43,3	5,3	13	69
6,8	44,7	6,3	11,6	73,3
5,9	45,8	7,5	10,3	76,9
5,2	46,7	8,6	9,3	79,6
4,7	47,3	9,6	8,5	81,8
4,3	47,9	10,7	7,8	83,7